UNIVERSITÀ DEGLI STUDI DI PADOVA

FACOLTÀ DI SCIENZE MM.FF.NN.

DIPARTIMENTO DI SCIENZE CHIMICHE

SCUOLA DI DOTTORATO IN SCIENZE MOLECOLARI

INDIRIZZO: SCIENZE CHIMICHE

CICLO XXIII

PORPHYRIN DERIVATIVES AS OPTICAL MOLECULAR SENSORS

Direttore della Scuola: Ch.mo Prof. Maurizio Casarin

Coordinatore Indirizzo: Ch.mo Prof. Maurizio Casarin

Supervisore: Dr. Tommaso Carofiglio

Dottoranda: Elisa Lubian

2008 - 2010

INDEX

Chapter I
Synthesis and Host-Guest Properties of Melamine-Bridge Bis(Porphyrin-Zn^{II}) Receptors: Recognition of Diamines

Introduction

Results and Discussion

Chapter II

Novel Sterically Encumbered and CD Sensitive Zn-Porphyrin Tweezer as a Probe for Molecular Chirality

Introduction

Results and Discussion

Experimental Section

Chapter III
Supramolecular Self-Assembly of Porphyrin Derivatives onto Conductors and Semiconductors Surfaces

Introduction

Results and Discussion

Experimental Section

RIASSUNTO

Il progetto di ricerca di questa Tesi di Dottorato ha riguardato la sintesi, la caratterizzazione e lo studio delle proprietà di ricognizione molecolare di nuovi derivati bis-porfirinici contenenti un ponte triazinico. Studi di spettroscopia UV-vis hanno permesso di determinare l'affinità di tali recettori nei confronti delle diammine lineari di formula generale $H_2N(CH_2)_nNH_2$, con n = 4-8. Le costanti di formazione dei complessi host-guest sono molto grandi, fino a 10^7 M^{-1}, grazie all'effetto ditopico realizzato dai due centri porfirinici. La coordinazione delle diammine al dimero porfirinico è associata ad una variazione marcata del colore e questo fatto ha favorito l'impiego di tali derivati in ambito sensoristico. A tal proposito, è stata messa a punto una procedura per supportare i dimeri porfirinici su materiali polimerici per la costruzione di sensori da utilizzare per l'analisi in flusso continuo.

Questi derivati sono stati anche utilizzati come pinze molecolari (*tweezers*) per la determinazione della configurazione assoluta di molecole chirali (diammine, α-ammino esteri, α-ammino ammidi e α-amminoalcoli, monoalcoli secondari) mediante l'impiego della spettroscopia di dicroismo circolare (CD), in collaborazione con la Prof. Berova della Columbia University.

Parallelamente, sono stati realizzati studi di deposizione di derivati porfirinici su superfici in vista di applicazioni di tipo sensoristico e in campo energetico (fotovoltaico). La caratterizzazione dei substrati è stata condotta mediante misure di microscopia elettronica a scansione (SEM), microscopia a forza atomica (AFM) e microscopia a scansione ad effetto tunnel (STM). Questi studi di deposizione hanno dimostrato come, scegliendo le opportune condizioni di deposizione, sia possibile costruire dei sistemi ordinati a lungo raggio, su superfici di diversa natura, rendendo questi sistemi candidati ideali per lo sviluppo di nuovi materiali ad alto contenuto tecnologico.

ABSTRACT

In this Doctorate Thesis project, a small library of four structurally related melamine-bridge bis(porphyrin-Zn^{II}) receptors, was synthesized The coordination properties of these porphyrin derivatives has been investigated by UV-vis spectroscopy for a series of aliphatic α,ω-diamines of general formula $H_2N\text{-}(CH_2)_n\text{-}NH_2$ (n = 4-8). A marked colour variation occours due to a favourable host-guest ditopic interaction. The binding constants, higher than 10^7 M^{-1}, make these receptors excellent candidates for the development of sensor devices for continuous flow analyses, in which the porphyrin derivatives are covalently supported onto appropriate solid materials.

These dimeric metalloporphyrin hosts (molecular tweezers), have also been successfully exploited as chirality probes for determination of the absolute configuration (AC) for a wide variety of chiral molecules (diamines, α-amino-esters, α-amino-amides, α-amino alcohols and secondary monoalcohols) by using circular dichroism spectroscopy, in collaboration with Prof. Nina Berova of Columbia University.

The deposition of porphyrin derivatives on different matrices was also investigated. Characterizations of substrates were carried out by scanning electron microscopy (SEM), atomic force microscopy (AFM) and scanning tunneling microscopy. These results show promising potential in the synthesis of highly ordered networks of surface-supported functional materials for sensing and solar energy applications.

List of Publications

1 T. Carofiglio, E. Lubian, I. Menegazzo, G. Saielli, A. Varotto, "Melamine-Bridged Bis (Porphyrin-Zn^{II}) Receptors: Molecular Recognition Properties", *Journal of Organic Chemistry*, **2009**, *74*, 9034-9043.

2 M. Di Marino, F. Sedona, M. Sambi, T. Carofiglio, E. Lubian, M. Casarin, E. Tondello; "STM Investigation of Temperature-Dependent Two-Dimensional Supramolecular Architectures of C_{60} and Amino-Tetraphenylporphyrin on Ag(110)" *Langmuir*, **2010**, *26*, 2466-2472.

3 M. Sambi, F. Sedona, M. Di Marino, T. Carofiglio, E. Lubian, M. Casarin, E. Tondello, "Fullerene/porphyrin multicomponent nanostructures on Ag(110): from supramolecular self-assembly to extended copolymers", *ACS Nano*, **2010**, *4*, 5147-5154.

4 T. Carofiglio, E. Comini, A. Gasparotto, E. Lubian, C. Maccato, G. Sberveglieri; "Surface-driven porphyrin self-assembly on pre-activated Si substrates", *Journal of Nanoscience and Nanotechnology*, **2010**, manuscript in press.

5 S. Trupp, M. Alberti, T. Carofiglio, E. Lubian, H. Lehmann, R. Heuermann, E. Yacoub-George, K. Bock, G.J. Mohr, "Development of pH sensitive indicator dyes for the preparation of micro-patterned optical sensor films", *Sensors and Actuators B- Chemical*, **2010**, *150*, 206-210.

6 E. Lubian, F. Baldini, A. Giannetti, C. Trono, T. Carofiglio, "Solid-supported Zn(II) porphyrin tweezers as optical sensor for diamines", *Chemical Communications*, **2010**, *46*, 3678-3680.

7 T. Carofiglio, E. Lubian, A. Varotto, "Synthesis, heterogeneization and sensing properties of melanine-bridged bis-porphyrin dimers", *Journal of Porphyrin and Phthalocyanine*, **2010**, *14*, 701-707.

Chapter I

Synthesis and Host-Guest Properties of Melamine-Bridge Bis(Porphyrin-Zn^{II}) Receptors: Recognition of Diamines

INTRODUCTION

1.1 Supramolecular Chemistry

For over 100 years, chemistry has focused primarily on understanding the behavior of molecules and their construction from constituent atoms. Our current level of understanding of molecules and chemical building techniques has given us the confidence to tackle the construction of virtually any molecule, be it biological or designed, organic or inorganic, monomeric or macromolecular in origin. During the last few decades, chemists have extended their investigations beyond atomic and molecular chemistry into the realm of the so called *supramolecular chemistry*.[1]

Supramolecular chemistry is one of the topical chemical fields of the 21st century,[2,3] and has first been defined in 1978 by Jean-Marie Lehn as the *chemistry of molecular assemblies and of the intermolecular bonds*.[4] Supramolecular chemistry is a vast interdisciplinary field of research and technology, where noncovalent bonding interactions may be a common ground.[5] It is no coincidence that already six Nobel prizes were attributed to research topics related to this field. Although their striking and fascinating self-assembly architectures are a sufficient motivation to carry out fundamental investigations, the applications of supramolecular compounds or materials remain the central objective of the contemporary supramolecular chemist.

In covalent chemistry, atoms are held together by covalent bonds to form molecules. In supramolecular chemistry, the components are held together by noncovalent intermolecular interactions to build a supramolecular system (Figure 1.1).

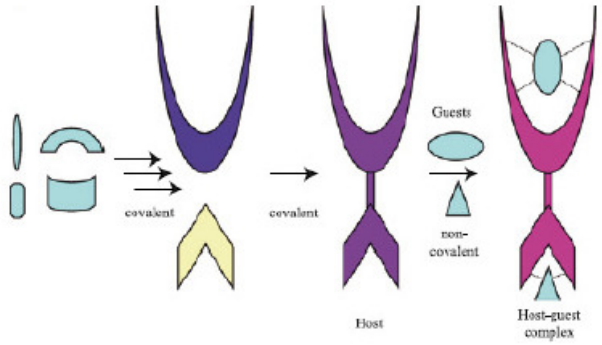

Figure 1.1: scheme of the use of covalent chemistry to build up host molecules, and noncovalent chemistry lead to host-guest complex.

Now, it has paved the way toward apprehending chemistry as an information science through the implementation of the concept of molecular information with the aim of gaining progressive control over the spatial (structural) and temporal (dynamic) features of matter and over its complexification through self-organization, the drive to life.[6,7] Its roots extend into organic chemistry and the synthetic procedures for molecular construction, into coordination chemistry and metal ion-ligand complexes, into physical chemistry and the experimental and theoretical studies of interactions, into biochemistry and the biological processes that all start with substrate binding and recognition, into materials science and the mechanical properties of solids.

Synthetic approaches to supramolecular chemistry can be categorized based on the nature of the molecular building blocks, *i.e.*, whether they are organic or inorganic in nature, or whether they are small molecules or macromolecules. Small-molecule organic building blocks include molecular liquid crystals, hydrogen bonding molecules, catenanes, and rotaxanes.[8] These have been used to create supramolecular ensembles ranging from nanostructured catalytic reactors to electrochemically switched molecular shuttles. Macromolecular organic building blocks include phase-separated block copolymers and, more recently, dendrimers. These have been used to generate sophisticated ordered composites and to allow nanopatterning on surfaces. Self-assembling coordination compounds featuring ligand-functionalized porphyrins and related components have been a mainstay of inorganic supramolecular chemistry.[4] More recently, semiconductor or metal nanoparticles have been used as macromolecular inorganic components for supramolecular arrays with interesting electronic properties.

1.1.1 Noncovalent Interactions: the Glue of Supramolecular Chemistry

Supramolecular systems are formed thanks to noncovalent intermolecular interactions, including electrostatic interactions (*e.g.*, ion-ion, ion-dipole, and dipole-dipole), hydrogen bonding,[9] metal-to-ligand bonding,[10] π-π interactions,[11] cation-π interactions,[12] van der Waals forces,[13] hydrophobic effects,[14] *etc*. These interactions are much weaker than covalent bonds (5-30 kJ mol^{-1} for a typical hydrogen bond; 350 kJ mol^{-1} for a C-C single bond), but they become significant when considered in numbers.

Supramolecular complex systems are the result of additive and cooperative interactions and, due to their feeble nature, they are easily disrupted.

These noncovalent intermolecular forces have fundamentally an electrostatic character and are described below.

- Hydrogen bonds: are attractive interactions between a hydrogen atom transferred to an electronegative atom, like oxygen, nitrogen, or fluorine (that causing the hydrogen to acquire a significant amount of positive charge), and a second species bearing a lone pair. The hydrogen bond (5-30 kJ/mole) is stronger than a van der Waals interaction, but weaker than covalent or ionic bonds;
- Ionic bonds: one or more electrons from one atom are removed and attached to another atom, resulting in positive (cation) and negative (anion) ions that attract each other. These are similar in strength to covalent bonds (*e.g.*, lattice energy of sodium chloride is −411 kJ/mol);
- Van der Waals forces: are the sums of the attractive or repulsive forces between molecules or parts of the same molecule with one another or with neutral molecules. The term includes force between two permanent dipoles (Keesom force), a permanent dipole and a corresponding induced dipole (Debye force), and two instantaneously induced dipoles (London dispersion force). These forces are nondirectional and relatively weak (< 5 kJ/mol) compared to normal chemical bonds, but play a fundamental role for binding;
- Ion-dipole interactions: involve interactions between a charged ion and a polar molecule and are usually in the range of 50-200 kJ/mol in strength. The magnitude of the interaction energy depends upon the charge of the ion, the dipole moment of the molecule and the distance from the center of the ion to the midpoint of the dipole. They are important in solutions of ionic substances in polar solvents (*e.g.*, a salt in aqueous solvent);
- Dipole-dipole interactions: exist between neutral polar molecules with permanent dipoles. Polar molecules attract one another when the partial positive charge on one molecule is near the partial negative charge on the other molecule. These interactions are much weaker (5-20 kJ/mol) than ionic or covalent bonds and have a significant effect only when the molecules involved are close together (touching or almost touching). The strength of these interactions decreases drastically with increases in distance;

- π-π interactions: are noncovalent interactions between organic compounds containing aromatic moieties and are caused by intermolecular overlapping of π-orbitals in π-conjugated systems, so they become stronger as the number of π-electrons increases (2-50 kJ/mol). The most common examples of a stacked system are found for consecutive base pairs in DNA, and in proteins where two relatively non-polar rings overlap;
- Metal-to-ligand bonds: are generally considered to be the strongest of the directional noncovalent interactions. The energies of these bonds are on the same order as those of covalent bonds. Several supramolecular coordination cage compounds have been prepared using these directional metal-ligand dative bonds with various applications;
- Cation-π interactions: involve molecular interactions between the face of an electron-rich π system (*e.g.*, benzene, ethylene) with an adjacent cation (*e.g.*, Li^+, Na^+). Cation-π interaction energies are of the same order of magnitude as hydrogen bonds or salt bridges (5-80 kJ/mol) and play an important role in molecular recognition;
- Hydrophobic binding: described as the association of non-polar regions belonging to individual host and guest molecules in aqueous or other protic media. Hydrophobic molecules tend to be non-polar and thus prefer other neutral molecules and they often form in water cluster and micelles. At the molecular level, the hydrophobic binding effect is an important force that drives protein folding, formation of the lipid bilayer, insertion of membrane proteins to the non-polar lipid environment and protein-small molecule interactions;
- Charge-transfer (CT) interactions: also termed electron donor acceptor (EDA) interactions, result from the mixing of the ground and excited charge-separated states (for example AB and A^+ B^- states). These are very weak intermolecular forces. Charge-transfer complexes may form when good electron donors and acceptors lie in close proximity. This situation is typically associated with charge-transfer transitions in the UV-vis spectral region.

In Figure 1.2 are summarized some of the above forces related to their interactions energies.

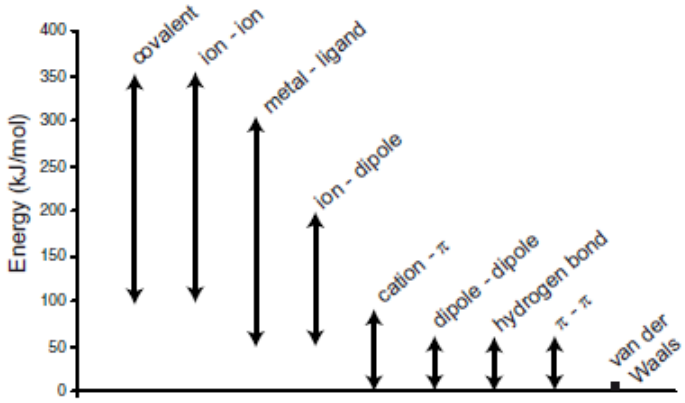

Figure 1.2: energies values of covalent and noncovalent interactions.

1.1.2 Concept of Host-Guest Chemistry

Supramolecular chemistry involves the formation of supermolecule or host-guest complex that arise from binding between a molecule, the host, with another molecule, the guest. The host-guest relationship has been defined by Donald Cram, who shared the 1987 Nobel Prize in Chemistry with Jean-Marie Lehn and Charles J. Pedersen for their development and use of molecules with structure-specific interactions of high selectivity. Cram defined the host as a molecule possensing *convergent* binding sites and the guest as a molecular entity in which the binding sites are *divergent*.[15]

Commonly, hosts are large molecules or aggregates containing a cavity, as cyclodextrins, calixarenes, cucurbiturils, porphyrins, metallacrowns, crown ethers, zeolites, cyclotriveratrylenes, cryptophanes and carcerands. The guests generally are cations, anions, ion pair, neutral molecules or other complex compounds.[4]

1.1.3 Molecular Recognition and Self-Organization

The essential elements of life, self-replication, information processing, and metabolism, arise by specific interactions between biological molecules. Understanding how molecules recognize each other and in which way molecular recognition works is also an important issue in applied biochemistry because it determines whether a compound possesses useful clinical properties.[16]

The dutch chemist Emil Fisher proposed in the 1894 the idea that the enzyme and substrate fit together like "lock and key". On consequence, also molecular recognition could be explained as the complementarity of interacting surfaces. A modern view on molecular recognition is that the interacting molecules are flexible and can change their shape during the recognition process in order to maximize the interaction energy. The induced fit has been observed experimentally for many protein-ligand interactions. At the molecular level, the factors that contribute to the complementarity between two molecules are:

- shape of the two molecular surfaces;
- hydrogen bonding between molecules;
- ion-ion interactions and London forces, as ion-dipole and dipole-dipole interactions;
- dispersion forces, as van der Waals attraction;
- π-π interactions;
- unfavorable solvation of non-polar groups by water gives rise to hydrophobic interaction.

The weak forces that act over short distances (hydrogen bonds, van der Waals interactions, and aryl stacking) provide most of the selectivity observed in biological chemistry and permit molecular recognition. The strength of binding of a ligand to macromolecules is governed by the free energy change in the binding process. The binding free energies can be determined experimentally but this requires availability of both the ligand and the macromolecule. An alternative method of obtaining binding free energies is a computer simulation.[17]

Beyond molecular recognition lies the preorganization of supramolecular system for the design of tailor-made molecular receptors effecting molecular recognition, catalysis, and transport on a variety of substrates, from metal ions to anions and chiral molecular substrates.[4,8] It also opened new way to chemical synthesis, establishing procedures for the construction of supramolecular entities and providing supramolecular assistance to synthesis in which noncovalent positioning of the components is followed by covalent bond formation.[9,18] Preorganization of system give rise to the self-organization of host and guest molecules through explicit manipulation of molecular recognition features, which governed the build up to supramolecular species and devices.[19,20] Understanding,

inducing, and directing such self-assembly are the keys to straighten out the progressive emergence of complex matter.

Self-organization is the driving force that led to the evolution of the biological world from inanimate matter.[21,22] The inclusion of dissipative non equilibrium processes, like those present in the living world, constitutes a major goal and challenge for supramolecular chemistry. More or less strict programming of the output species may be achieved depending on the robustness of a given directing code (such as hydrogen bonding or metal coordination); that is, on how sensitive it is to internal factors (such as secondary metal coordination or van der Waals stacking) or external factors (such as concentrations and stoichiometries of the components or the presence of foreign species). Sensitivity to perturbations limits the operation range but introduces diversity and adaptability into the self-organization process.[8]

1.2 Porphyrins and their Properties

Porphyrins are an important class of organic molecules largely found in biological compounds. The word porphyrin is derived from the Greek *porphura* meaning purple, and all porphyrins are intensely coloured. They are a large class of deeply coloured red or purple, fluorescent crystalline pigment, of natural or synthetic origin, having in common a substituted aromatic macrocycle ring consisting of four pyrrole molecules, linked together with four methine bridging units.[23]

The metalloporphyrin ring is found in a variety of important biological system where it is the active component of the system or, in some ways, intimately connected with the activity of the system and whose functions range from oxygen transfer and storage (hemoglobin and myoglobin), to electron transfer (cytochrome c, cytochrome oxidase), to energy conversion (chlorophyll). They also have been proven to be efficient sensitizers and catalysts in a number of chemical and photochemical processes, especially in photodynamic therapy (PDT). The diversity of their functions is due in part to the variety of metals that bind into the "pocket" of the porphyrin ring system (Figure 1.3).

Porphyrin macrocycle is an aromatic heterocyclic system containing 22 π-electrons, but only 18 of them are delocalized according to the Hückel's rule of aromaticity (4n+2 delocalized π-electrons, where n = 4). Double bonds 7-8 (Δ^7) and 17-18 (Δ^{17}) could be

easily reduced because they aren't involved in aromatic conjunction and thus producing the so-called chlorin compounds.

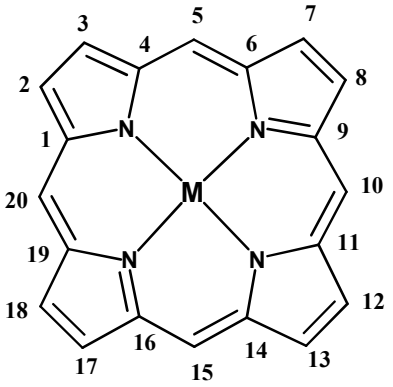

Figure 1.3: porphyrin skeleton**.**

The size of the macrocycle is perfectly suited to bind almost all metal ions and indeed a large number of metals (*e.g.*, Fe, Zn, Cu, Ni, Hg, Co, *etc.*) can be inserted in the center of the macrocycle forming metalloporphyrins.

Given the capabilities of porphyrins to bind and release gases and to act as active center in catalytic reactions in biological systems, porphyrin-based films on metal or semiconductor surfaces are extremely appealing as chemical and gas sensors as well as nanoporous catalytic materials in novel synthetic biomimetic devices. Moreover, the role of porphyrins in photosynthetic mechanisms indicates a good attitude of these molecules to mediate visible photon–electron energy transfer processes.[24,25]

The involvement of porphyrins in many biological processes and the possibility to tailor their physical and chemical properties at the molecular level, including very large dipole moments, polarizability, non-linear optical response, absorption spectrum, energy transfer and catalytic properties, make porphyrins and metalloporphyrins extremely versatile synthetic base materials for research projects in many disciplines of chemistry and physics, like electronics, opto-electronics, electrochemistry, catalysis and photophysics.

1.2.1 General Synthetic Methodology

The synthetic world of porphyrins is extremely rich and its history began in the middle of 1930s. An enormous number of synthetic procedures have been reported until now, and the reason can be easily understood analysing the porphyrin skeleton. In principle, there are many chemical strategies to construct it, involving different building

blocks, like pyrroles, aldehydes, dipyrromethanes, dipyrromethenes, tripyrranes and linear tetrapyrroles.

The most famous monopyrrole polymerization route to obtain porphyrins involves the synthesis of tetraphenyl porphyrins, from reaction between pyrrole and benzaldehyde.[26] This procedure was first developed by Rothemund[27] and, after modification by Adler, Longo and colleagues,[28] was finally optimized by Lindsey's group.[29] In the Rothemund and Adler/Longo methodology the crude product contains between 5 and 10% of a by-product, discovered later to be the *meso*-tetraphenylchlorin which is converted in the product under oxidative conditions (Figure 1.4).

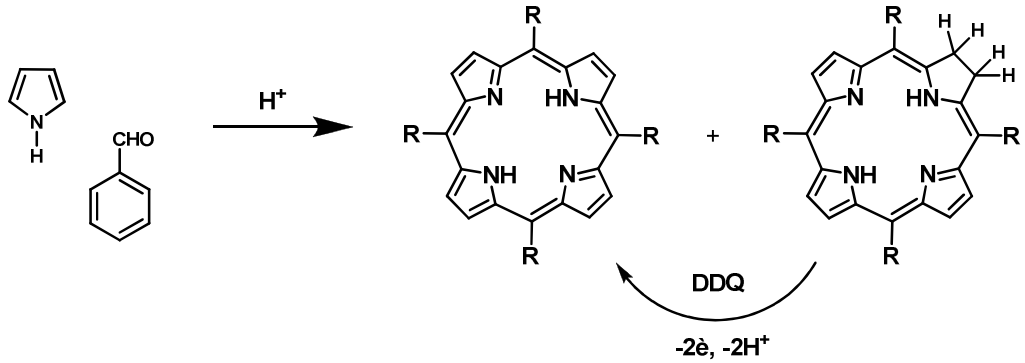

Figure 1.4: synthesis of 5,10,15,20-tetraphenyl porphyrin with the reaction conversion of *meso*-substituted chlorin to the porphyrin.

Rothemund, in 1935 set up the synthesis of porphyrins in one step by reaction of benzaldehyde and pyrrole in pyridine in a sealed flask at 150 °C for 24 h. The yields were low, only 7-9%, and the conditions so severe (high concentration of reagents, about 3 M, and high temperature, 150-220 °C) that few benzaldehydes could be converted to the corresponding substituted porphyrin.[30,31] The Rothemund conditions were obviously based on the premise that the porphyrin is aromatic, aromatic compounds are stable, and therefore merely cracking the initially formed adducts of benzaldehyde and pyrrole at high temperatures should give the porphyrin.[32]

The reason in the low yield is that the main by-product of reaction was *meso*-substituted chlorin and in understanding the nature of its formation, Calvin and coworkers discovered that the addition of metal salts to the reaction mixture, such as zinc acetate, increases the yield of porphyrin from 4-5% for the free-base derivative, and decreases the amount of chlorin compound.[33] This is the first example that describes how the presence of metals could affect the condensation reaction. Others improvement were obtained by

changing opportunely the reaction conditions and substituents in benzaldehyde molecule framework.

Adler, Longo and coworkers, in the 1960s, re-examined the synthesis of *meso*-substituted porphyrins and developed an alternative approach (Figure 1.5). This method involves an acid catalyzed pyrrole aldehyde condensation in glassware open to the atmosphere in the presence of air. The role of acid is to activate aldehyde with protonation of carbonyl group.

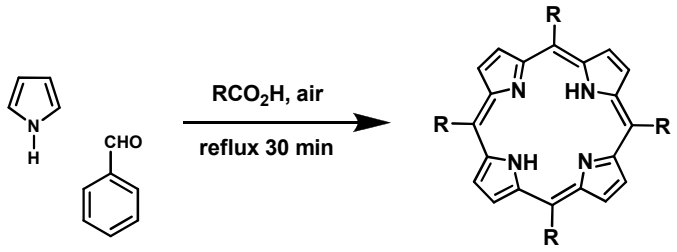

Figure 1.5: Adler-Longo method for preparing *meso*-substituted porphyrins.

The reactions were carried out at high temperature, in different solvents and in the concentrations range of reactants from 0.01 M to 0.2 M. The solvents investigated were organic acids, such as acetic acid, trifluoroacetic acid, butyric acid, propionic acid and benzene containing chloroacetic acid.[8] The yields obtained were of 30-40%, which tend to decrease in the presence of metal salts. The chlorin contamination was often around 10%, which is lower than that obtained with the Rothemund synthesis (20%).

Over the period 1979-1986, Lindsey developed a new and innovative two-step room temperature method to synthesize porphyrins, motivated by the need for more gentle conditions for the condensation of aldehydes and pyrrole, in order to enlarge the number of the aldehydes utilizable and then the porphyrins available. The method was inspired from few simple considerations:

a. pyrrole and benzaldehyde are reactive molecules; so they don't need strong conditions for condensation;[34,35]

b. biosynthesis of porphyrin-like structures proceed under the condensation of porphobilinogen, peripheral modification of side chains and finally oxidation of protoporphyrinogen IX to gave protoporphyrin IX, the

precursor of heme and chlorophylls molecules (Figure 1.6);[36,37] as in nature, the synthesis of porphyrin could be performed in the same way;

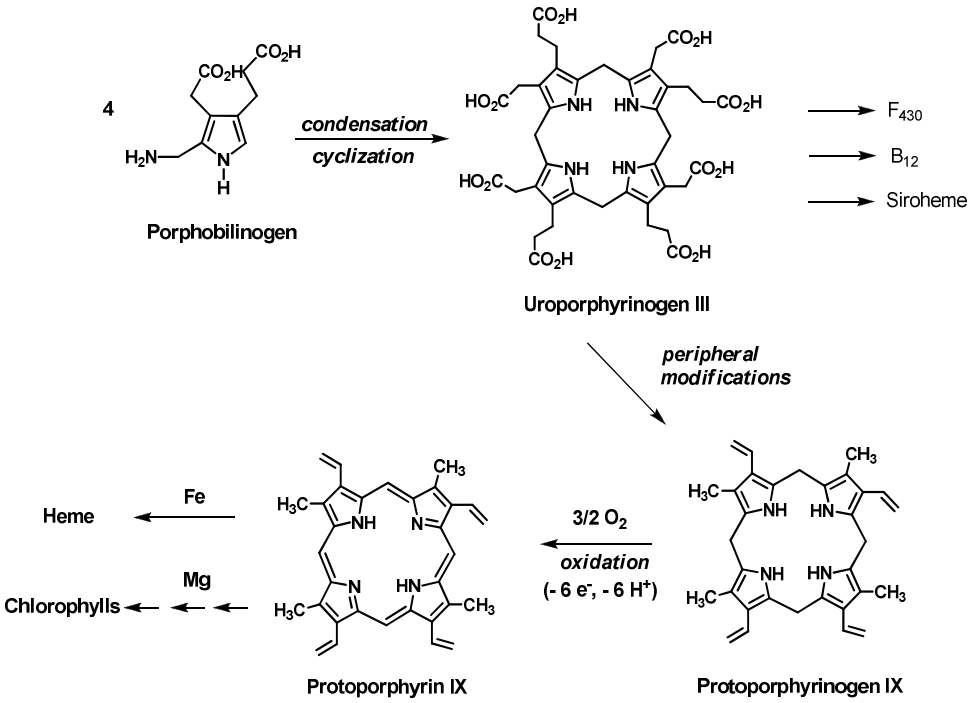

Figure 1.6: outline for the biosynthesis of naturally occurring porphyrins.

c. biosynthesis of porphyrins is mediated by enzyme, but condensation undergoes without its presence;[38]

d. it was demonstrated that a mixture of isomers could be obtained starting from porphobilinogen under mild condition (85 °C) in aqueous acid solution followed by oxidation with iodine. The ratio of these isomers change with the modification of peripheral side chains.

These considerations gave the basis for planning a new strategy for the synthesis of porphyrins, using a sequential process of condensation and oxidation steps. The reactions were carried out under mild conditions in an attempt to achieve equilibrium during condensation, and to avoid side reactions in all steps of the porphyrin-forming process (Figure 1.7).

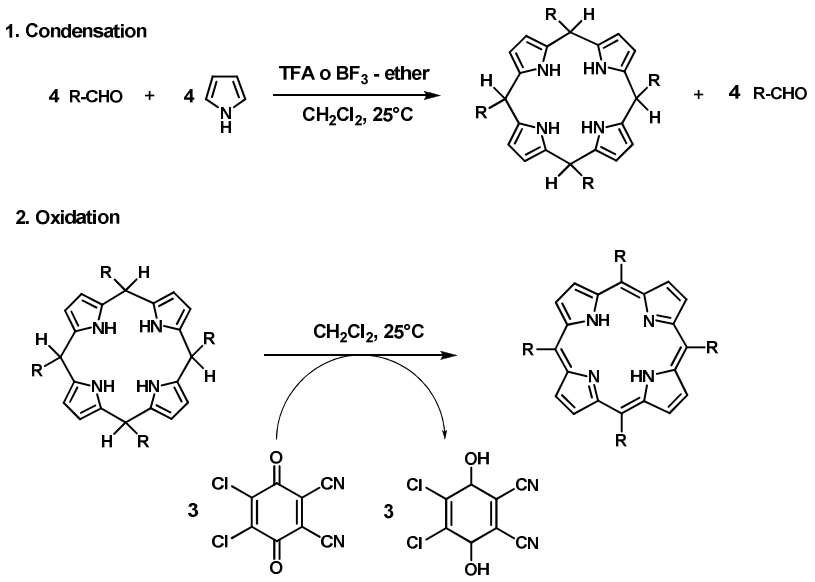

Figure 1.7: two-step one-flask room-temperature synthesis of porphyrins.

The maximum yield of tetraphenyl porphyrin is obtained when a solution of dry methylene chloride is charged with benzaldehyde and pyrrole at equimolar concentrations of 10^{-2} M. To this solution is added an aliquot of trifluoroacetic acid or BF_3-etherate (10^{-3} M). The ensuing condensation was found to level off after 30-60 minutes at room temperature. Then in a second step, the oxidant 2,3-dichloro-5,6-dicyanobenzoquinone (DDQ) is added in stoichiometric amount and the solution is stirred for 1 h at room temperature. Oxidant causes conversion of the porphyrinogen to the porphyrin. The reaction progress can be monitored by removal of aliquots and analysis by absorption spectroscopy around 420 nm that indicates the formation of tetraphenyl porphyrin in yields which typically range around 50%. Evaporation of the solvent followed by flash chromatography affords tetraphenyl porphyrin that is pure in yields of 45-50%. The yields scale linearly throughout the 25 mL to 1 L range.

The yield of porphyrin depends on a variety of factors, including choice of oxidant and acid catalyst, condensation time, concentrations of acid, pyrrole, and benzaldehyde, and the presence of water in the solvent. The oxidation of porphyrinogen to porphyrin can be performed with either DDQ or 2,3,5,6-tetrachlorobenzoquinone (*p*-chloranil). This latter is a much milder oxidant, requires an exposure time larger than 1 hour for complete reaction, and affords yields uniformly higher than those obtained with DDQ. Neutralization of the acid catalyst (by addition of K_2CO_3 or triethylamine) prior to the addition of *p*-chloranil caused no effect on the porphyrin yield. *p*-Chloranil was used in

preparative work when a maximal yield was the chief objective. DDQ was employed to provide rapid quenching during exploratory studies of reaction conditions.

The optimal duration of the condensation period was determined by reacting benzaldehyde and pyrrole at equimolar concentrations of 10^{-2} M. Consistent yields of tetraphenyl porphyrin in the 35-40% range were obtained with several acid catalysts, including BF_3 (10^{-3} M, 1 h), trifluoroacetic acid (TFA, 1-2.5 x 10^{-2} M, 1-2 h), and BCl_3 (3 x 10^{-3} M, 30 min). The rate of porphyrinogen formation is proportional to the acid concentration.

Several attempts have been made to use metal salts to facilitate porphyrin macrocycle formation in the Adler-Longo and Rothemund reaction. However, porphyrinogen and pyrrole do not ligate to metals. A higher isolated yield of metalloporphyrin can result from different mechanisms but does not alone implicate either a kinetic or thermodynamic template effect in the cyclization process.[29]

1.2.2 Reactivity

As previously explained, the porphyrin macrocycle is a highly-conjugated molecule. Its structure supports a highly stable configuration of single and double bonds, called an aromatic π-system. The simplest and archetypal aromatic π-system is benzene, and like it, porphyrins undergo the characteristic reactions of aromatic compounds, with the difference of having two different sites on the macrocycle where electrophilic substitution can take place with different reactivities: positions 5, 10, 15 e 20, called *meso*, and 2, 3, 7, 8, 12, 13, 17 and 18, called β-pyrrole positions. The first kind of compounds are widely present in natural products, while the second have no counterpart in nature and were developed as functional artificial models.

The activation of these sites depends in which extent a porphyrin is electron-rich or electron-poor. The influence on it could be the choice of coordination metal in the macrocycle center. Indeed, the introduction of the proper divalent metal can change the reactivity of porphyrin from β-positions to *meso* positions, and *vice versa*. Thus, these complexes in the order MgP > ZnP > CuP > NiP > PdP (P represent porphyrin), gave substitutions only on *meso* carbons. On the other hand, metals in high oxidation state, like Sn^{IV} or porphyrin in the free-base form deactivated the *meso* positions and activated the β-pyrrole positions to electrophilic attack.

Like benzene derivatives, porphyrins can undergo *meso* substitutions in the Vilsmeier formylation, when the metal center M is Cu, and alogenation in the case in which M = Mg or in a free-base form. Also nitration occurs unexpectedly at the *meso* carbons, even when the less electrophilic β-pyrrole positions are vacant. Electron-deficient species, like carbenes and nitrenes, react with porphyrins but in different ways: carbenes tend to attack at the β-pyrrole positions to give mainly cyclopropane derivatives, while nitrenes attack at the *meso*-carbons to give ring expanded compounds called homoazaporphyrins, which readily extrudes the nitrogen atom on heating or by metal chelation.[39]

1.2.3 UV-visible Spectra of Porphyrins

Porphyrins typically have very intense absorption bands in the visible region and may be deeply coloured. As it is shown in Figure 1.8, the electronic absorption spectrum of a typical porphyrin consists of two distinct regions. The first involve the transition from the ground state to the second excited state (S0 → S2) and the corresponding band is called the Soret or B band. The range of absorption is between 395-425 nm depending on whether the porphyrin is β- or *meso*-substituted. The second region consists of a weak transition to the first excited state (S0 → S1) in the range between 480-700 nm (the Q bands). These favourable spectroscopic features of porphyrins are due to the conjugation of 18 π-electrons and provide the advantage of easy and precise monitoring of guest-binding processes by spectroscopic methods (*e.g.*, UV-visible,[40] CD,[41] fluorescence,[42] and NMR spectroscopy[43]).

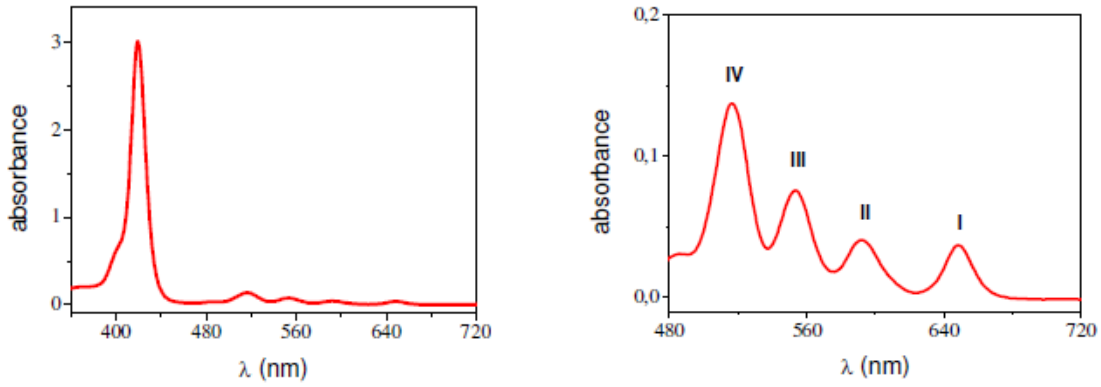

Figure 1.8: left. UV-vis spectrum of porphyrin in $CHCl_3$. Right. Enlargement of region between 480-720 nm.

While variations of the peripheral substituents on the porphyrin ring often cause minor changes to the intensity and wavelength of the absorption features, protonation of two of the inner nitrogen atoms or the insertion/change of metal atoms into the macrocycle usually strongly change the visible absorption spectrum. For this reason, in recent years, metal porphyrins and porphyrin-metal interfaces have become of major interest for applications in opto-electronics, data storage and solar cells and a still increasing number of covalently linked donor-acceptor supramolecular porphyrin based assemblies have been studied for these purposes.[25,44]

When porphyrinic macrocycle is protonated or coordinated with any metal, there is a more symmetrical situation than in the porphyrin free base and this produces a simplification of Q bands pattern (the four Q bands collapse to two) that can eventually result in marked colour changes.

The relative intensity of Q bands is due to the kind and the position of substituents on the macrocycle ring. Basing on this latter consideration, porphyrins could be classified as *etio*, *rhodo*, *oxo-rhodo* e *phyllo*.[9] When the relative intensities of Q bands are such that IV > III > II > I, the spectrum is said *etio-type* and porphyrins called *etioporphyrins*. This kind of spectrum is found in all porphyrins in which six or more of the β-positions are substituted with groups without π-electrons, *e.g.*, alkyl groups. Substituent with π-electrons, as carbonyl or vinyl groups, attached directly to the β-positions gave a change in the relative intensities of the Q bands, such that III > IV > II > I. This is called *rhodo-type* spectrum (*rhodoporphyrin*) because these groups have a "reddening" effect on the spectrum by shifting it to longer wavelengths. However, when these groups are on opposite pyrrole units, the reddening is intensified to give an *oxo-rhodo-type* spectrum in which III > II > IV > I. on the other hand, when *meso*-positions are occupied, the *phyllo-type* spectrum is obtained, in which the intensity of Q bands is IV > II > III > I.[39]

1.2.4 NMR Spectra of Porphyrins

Nuclear magnetic resonance (NMR) spectroscopy is a very powerful tool for exploring molecular structure, and gives important information about aromatic structures. Before starting to consider porphyrins, it's important to explore the property of aromatic molecules, like benzene and their relatives.

Benzene has six π-electrons and when it is exposed to an external magnetic field perpendicular to the plane of the aromatic system, a ring current is induced in the delocalized π-electrons of the aromatic ring (Figure 1.9).[45]

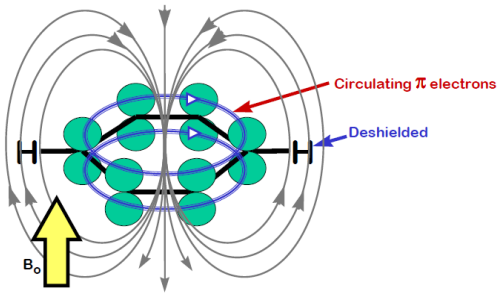

Figure 1.9: ring current in benzene ring.

Aromatic ring currents are relevant to NMR spectroscopy and influence the chemical shifts of ^{13}C and ^{1}H nuclei in aromatic molecules, as well as in any organic or inorganic aromatic molecule.[46] In benzene, the ring protons experience deshielding because the induced magnetic field has the same direction as the external field and their chemical shift is around 7.0 ppm compared to 5.6 ppm of the vinylic protons in cyclohexene. In contrast any proton inside the aromatic ring experiences shielding because fields are in opposite direction. This effect can be observed in cyclooctadecanonaene ([18] annulene) with 6 inner protons moving at −3.0 ppm.

In porphyrins, ring current deshields the protons on the macrocycle. In particular, β-pyrrole protons shift upfield more than *meso*-protons because the latters are attached to electron-deficient carbons. Also, the inner N-H protons are shifted upfield because the ring current has the opposite direction with respect to the applied field B_0. Figure 1.10 reports the NMR spectrum of a substituted porphyrin 5-(4-aminophenyl)-10,15,20-triphenyl porphyrin, **$TPPNH_2$**.

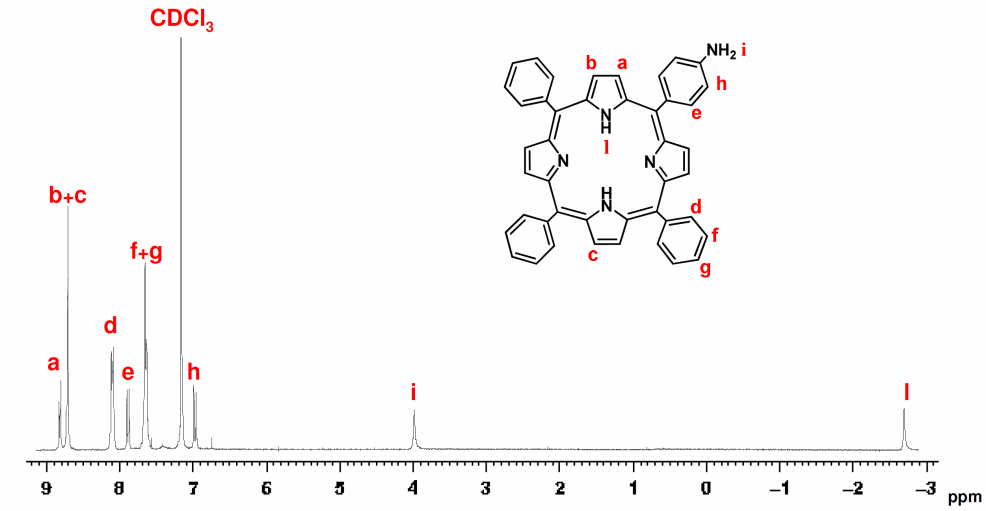

Figure 1.10: ^{1}H-NMR spectrum of **TPPNH$_2$** in $CDCl_3$.

Characteristic peaks of β-pyrrolic protons (*a, b, c*) are found around 9.0 ppm, while the inner protons (*l*) are at -2.8 ppm. The aryl protons of four *meso*-phenyl groups falls in the range of 7.5-8.5 ppm: *orto*-protons (*d*) are at 8.2 ppm, while *meta*- and *para*-protons (*f*, *g*) are around 7.8 ppm. Aromatic protons in *orto*-position (*h*) and *meta*-position (*e*) respect to the amino group are found around 7.0 ppm and 8.0 ppm, respectively. Singlet peak at 4.0 ppm is ascribable to the NH_2 protons (*i*).

1.3 Sensors Array: a Briefly History

There are three sensory systems in humans which contribute to the sensation of flavour. These three chemical senses are olfaction (the sense of smell), gustation (the sense of taste) and the trigeminal sense (responsive to irritant chemical species). However, smell is the dominant factor in our sensation of flavour and so can often be used alone to profile the flavour of various products.

The human nose is still the primary instrument used in many industries to evaluate the smell or flavour of products such as perfumes (cosmetics, soaps), foodstuffs (fish, meat, cheese) and beverages (beer, whisky, coffee). This is a costly process, because trained panels of experts are required who can only work for relatively short periods of time.[47]

The physical-chemical properties of the products are also measured using conventional analytical equipment, such as gas chromatography and gas chromatography-

mass spectrometry. These (mechanical) methods are not only time-consuming but the results are often inadequate. For example, there are some key flavour constituents of beer that are below the detection limits of most gas chromatographs.[48]

The relationship between the physicochemical properties of the odorant molecules and their sensory impact is still unclear, in spite of a considerable amount of research effort.[49] Consequently there is enormous demand for an electronic instrument that can mimic the human sense of smell and provide low-cost and rapid sensory information.

The earliest work on the development of a specific instrument to detect odours probably dates back to Moncrieff in 1961.[50] This was really a mechanical nose. The first electronic noses were reported by Wilkens and Hatman in 1964 (redox reactions of odorants at an electrode),[51] Buck *et al*. (modulation of conductivity by odorants)[52] and Dravieks and Trotter (modulation of contact potential by odorants),[53] both in 1965. However, the concept of an electronic nose as an intelligent chemical array sensor system for odour classification did not really emerge until nearly 20 years later from publications by Persaud and Dodd (1982) at Warwick University in UK and Ikegami *et al*. (1985)[54] at Hitachi in Japan.[55] Later, at the end of 1990s, Suslick gave an important contribute for the accomplishment of electronic nose system, based on porphyrin and metalloporphyrin derivatives in the detection of volatile organic compounds (VOCs).[56]

Generally, the definition of electronic nose is *an instrument, which comprises an array of electronic chemical sensors with partial specificity and an appropriate pattern-recognition system, capable of recognising simple or complex odours.*[57] Electronic noses are thus identified as types of intelligent chemical array sensor systems or chemical sensor array devices (ChemSADs) that are specifically used to sense odorant molecules as in analogue to the human nose. However, the architecture of electronic nose is also applied in the field of gas sensing for the detection of individual components or mixtures of gases, to afford the fingerprint of the system.

1.3.1 Electronic Nose Technology and Applications

Odorant molecules are typically hydrophobic and polar with molecular masses of up to about 300 Dalton. A simple odour is a single molecule and some examples are listed in Table 1, together with the type of odour and its olfactory threshold.[58] In reality most natural smells, perfumes and flavours are complex mixtures of chemical species and so

contain hundreds of constituents. Often subtle differences in the relative amounts of these constituents determine the smell of the product.[57]

Chemical Structure	Characteristic Odour	Odour Threshold (ppb in water)
Diacetyl	off-flavour of beer	500
Trans-2-hexenal	green leaves	316
Geraniol	rose	290
5-isopropyl-2-methylphenol	thyme	86
Limonene	lemons	10
Ethyl mercaptan	decayed cabbage	0.19
Thiocresol	skunk, rancid	0.062
Allyl mercaptan	garlic	0.05
Cis-4-heptenal	off-flavour of white fish	0.04
Octa-1,5-diene-3-one	off-flavour of butter	0.01
2-isobutyl-3-methoxypyrazine	green peppers	0.002
α-terphinethiol	grapefruit	0.00002

Table 1.1: some common simple odours.

Obviously, an ideal sensor should respond to only one compound and provide a unique output. However, with an electronic nose, like the human nose, we are able to identify many odours that may contain hundreds of individual chemical components. In this way, should be possible to obtain the specific fingerprinting, unique for any complex system.

An odour stimulus generates a characteristic response from an array of sensors. Patterns or fingerprints from known odours are used to construct a database and train a pattern recognition system so that unknown odours can subsequently be classified and/or identified.[58]

Typically an electronic nose consists of three elements: a sensor array which is exposed to the volatiles, conversion of the sensor signals to a readable format, and software analysis of the data to produce characteristic outputs related to the odour encountered (Figure 1.11). The output from the sensor array may be interpreted via a variety of methods such as pattern recognition algorithms, principal component analysis (PCA), cluster analysis and artificial neural networks to discriminate between samples. This technology is a user-friendly, inexpensive and intelligent laboratory diagnostic device.[59]

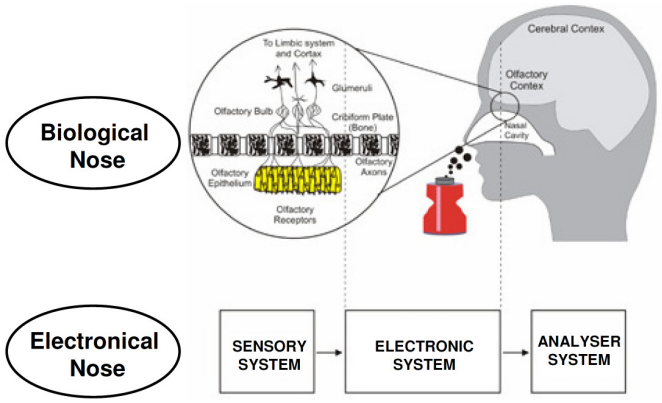

Figure 1.11: schematic representation of human and artificial olfactory system.

The potential applications for the electronic nose technology are very extensive. This technology has been applied to a range of food science,[60,61,62] medical,[59,63] and environmental applications.[64,65] In addition, offers great potential for the detection of different microbial species. Some chemical products are specific to fungal and bacterial species and are commonly used as a useful diagnostic tool. The advantage of the electronic nose technology is that it can be used for effective monitoring in a storage situation, especially if linked to a real time analyser network which has information on the volatile patterns from non-spoiled material. It could then be used to effectively provide a warning of when conditions may become compromised and effective management could be then employed for preventing loss of valuable cultural material. This has already been successfully demonstrated for detection of mouldy grain and growth of moulds in libraries, archives and museums.[61] The field of sensor technology is also advancing rapidly and other sensor arrays are now commercially available with better sensitivity and stability in different abiotic environments.

1.3.2 Importance in the Detection of Biogenic Amines, Diamines and Polyamines

In the last few years, there was increasing society awareness for improving welfare and well-being through healthy eating. In this light, and with respect to the priorities for the future of the food chain, the European Technological Platform (ETP) called “Food for Life” has pointed out several key challenges with a special emphasis on food safety and quality control. ETP provides a framework for stakeholders, led by industry, to define

research and development priorities, timeframes and action plans on a number of strategically important issues where achieving Europe's future growth, competitiveness and sustainability objectives is dependent upon major research and technological advances in the medium to long term. Noteworthy, monitoring the spoilage degree of foodstuff susceptible to microbial degradation during aging and storage is one of some priority issue. In particular, it has been established that the production of specific amines by bacteria may be directly linked to the freshness and quality of foods such as fish, meat, cheese, and wine. In virtually all foods that contain proteins or free aminoacids and are subject to conditions enabling microbial or biochemical activity biogenic amines can be expected.[66,67]

Biogenic amines are basic nitrogenous compounds with low molecular weight formed mainly by decarboxylation of amino acids or by amination and transamination of aldehydes and ketones.[68] They possess a distinctive smell and can be found in relatively large amounts in some fermented foodstuffs as a consequence of microbial activity (enzymatic decarboxylation of the corresponding amino acids). The chemical structure of biogenic amines can either be: aliphatic (putrescine, cadaverine, spermine, and spermidine); aromatic (tyramine, phenylethylamine); heterocyclic (histamine, tryptamine). Amines such as polyamines, putrescine, spermidine, spermine and also cadaverine are indispensable components of living cells and are important in the regulation of nucleic acid function and protein synthesis and probably also in the stabilization of membranes.[69] Few examples of biogenic amines and their pharmacological effects are reported in Table 1.2.

Amine	**Precursor**	**Pharmacological Effects**
Histamine	Histidine	Liberates adrenaline and noradrenaline; excites the smooth muscles of the uterus, the intenstine, and the respiratory tract; stimulates both sensory and motor neurons; controls gastric acid secretion.
Tyramine	Tyrosine	Peripheral vasocostriction; increases the cardiac output; causes lacrimation and salivation; increases respiration; increases blood sugar level; releases noradrenaline from the sympathetic nervous system; causes migraine.
Putrescine and Cadaverine	Ornithine and Lysine	Hypotension; bradycardia; lockjaw; paresis of the extremities; potentiate the toxicity of other amines.
β-Phenylethylamine	Phenylalanine	Releases noradrenaline fro the sympathetic nervous system; increases the blood pressure; causes migraine.
Tryptamine	Tryptophane	Increases the blood pressure.

Table 1.2: biogenic amines in foode and their pharmacological effects.

Determination of the biogenic amines, in particular histamine, tyramine, agmantine, putrescine, cadaverine, spermine and spermidine are important not only as indicators of the degree of freshness or spoilage of food but also for the point of view of their toxicity. Nitrosable secondary amines (*e.g.*, agmatine, spermine, and spermidine) can form nitrosamines by reaction with nitrite and produce carcinogenic compounds. N-nitroso compounds can be formed by the interaction of amino compounds with nitrosating reagents such as nitrite and nitrogen oxides during the storage, conservation and cooking of foods. The reaction of nitrosating agents with primary amines produces short-lived alkylating species that react with other components in the food matrix to generate products, mainly alcohols, devoid of toxic activity in the relevant concentrations. The nitrosation of secondary amines leads to the formation of stable N-nitroso compounds, while that of tertiary amines produces a range of labile N-nitroso products.[70]

Putrescine (1,4-diamino butane) and cadaverine (1,5-diamino pentane) are commonly used by trained inspectors and individual consumers for a qualitative evaluation of food freshness. Furthermore, they are used as tumoral markers due to their presence in high concentration in diseased tissue. However, the quantitative analysis of polyamines via chromatographic techniques is complicated by the lack of natural chromophoric or electrophoric groups and by the high polarity of these compounds. Hence, extensive chemical derivatisation is indispensable to assist the chromatographic separation and to enhance the detection sensitivity of biogenic amines.[71] Such derivatisation protocol is usually performed off-line, prior to the chromatographic analysis, thus increasing the risk of analyte loss, contamination, and prolongs the overall analysis duration. Thus, there is the need for a sensing device which accurately and rapidly detects the presence of biogenic amines in their pristine form and in different matrices.[72] From an applicative point of view, such device would prompt analysis automation thus enhancing the efficiency of food processing and giving to the manufacture real-time and online information on their products.

According to such interesting target, the development of ditopic tweezer-like structures, combined ligand to metal coordination and cage effect motif, could be an important issue for the detection of bidentate ligands such as diamines and alike.

1.4 Porphyrins and Metalloporphyrins as Ditopic Optical Sensors

Porphyrin and metalloporphyrins are excellents candidates for a variety of sensing material applications. They offer a unique combination of structural and electronic features that can leverage important improvements in the construction of synthetic molecular receptors.[73] In particular, the metal center at the porphyrin core exhibits an open coordination site that can be tailored for specific binding according to the hard-soft acid-base paradigm.[74] In addition, well established synthetic methodologies allow the modifications of the outer-porphyrin scaffold with proper exocyclic substituents in order to tune both the electronic and sterical properties of the receptor. Due to the extended aromatic framework of the porphyrin ring, the binding event often traslates in a remarkable variation of its spectroscopic behavior, thus fostering detection of the host-guest complexation by a number of techniques such as UV-visible, circular dichroism, fluorescence, NMR, and resonance Raman spectroscopy. As a result, a great variety of porphyrin-based sensors have been developed for the recognition of simple, monofunctional molecules including alcohols,[75] amines,[76] and carbohydrates.[77] However, a single porphyrin unit might be a fairly inadequate host for multifunctional molecules. In this case, enhanced binding stability can be achieved with receptors containing more than one porphryin unit.

Dimeric metalloporphyrin hosts with tweezer-like structures, called *optodes*, have been designed to effectively complex bifunctional guests through a ditopic interaction. A prominent example are the dimeric metalloporphyrin hosts made of two achiral zinc- or magnesium-porphyrins linked by a flexible covalent tether (Figure 1.12).[78] These constructs have been exploited to assess the absolute stereochemical configuration of chiral amines, alcohols, and carboxylic acids through the sign of the exciton-coupled circular dichroism in the porphyrin spectral region.

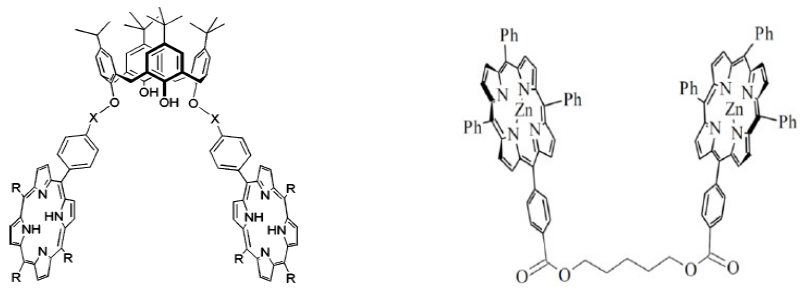

Figure 1.12: left: lower rim calixarene bisporphyrin, with different **X** linker; right: pentandiol-bridge bis(porphyrin-Zn^{II}) tweezer.

Another prosperous field of application for bis-porphyrin hosts deals with the self-assembly of donor-acceptor (D-A) systems promoted by the π–π stacking between the curved surface of a fullerene and a porphyrin macrocycle. Such fullerene–porphyrin recognition motif has been successfully employed for selective extraction of higher fullerenes (*e.g.*, C_{70}),[79] and to build photovoltaic devices.[80]

The other side of the coin is that the synthesis of porphyrin dimers or oligomers in high yield and purity generally entails multistep procedures, involving also protection/deprotection strategies, and extensive purification steps. Synthesis can be even more challeging when the multiporhyrinic constructs have to be covalently attached to a solid support with the valuable purpose of fabricating a sensing device. Examples include the functionalization of electroactive surfaces with redox active molecular triggers[81] or the immobilization of porphyrin based receptors onto transparent substrates in order to be interrogated with light for sensing purposes.[82] This general approach is also applied to the construction of arrays of sensors on micro/nano patterned surfaces, and so on. However, many grafting procedures involve several chemical steps to modify both the active molecule and the support matrix before performing the actual coupling reaction. Thus, the development of new approaches to synthesize multiporphyrin assemblies and support them by using simple and reliable chemistry still represents a major challenge.[83,84]

1.4.1 Solid Materials for Supported Melamine-Bridge Bis(Porphyrin) Derivatives

As described before, determination of the biogenic amines is important not only as indicators of the degree of freshness or spoilage of food but also for the point of view of their toxicity. Accordingly, there is a need for a sensing device which accurately and rapidly detects the presence of these compounds in their pristine form and in different matrices.[72]

Solid support in organic synthesis relies the opportunity to use filtration as a separation technique to purify the final compound. Analogously, immobilization of porphyrin-based sensors on appropriate solid material affords a convenient way for the construction of recyclable optical sensors, for their miniaturization and arraying, as well as for the development of multi-analyte detection systems.[85,86,87]

In solid phase synthesis, the solid support is generally based on a polystyrene resin. The most commonly used resin supports include spherical beads of lightly cross linked gel type polystyrene with 1–2% divinylbenzene and polystyrene-oxyethylene graft copolymers (*e.g.*, TentaGel® Rapp Polymere Gmbh) which are functionalised to allow attachment of linkers and substrate molecules. Consequently, a large number of new macroporous polymers were designed with different linkers and rigidity of the open pores. Besides polymer resin, there was an increasing development in the use of controlled pore glass, a rigid, glass-derived bead material, compatible with any type of solvent, stable to aggressive reagents and extreme conditions of pressure and temperature, which has occasionally been used for the combinatorial synthesis of peptides and oligonucleotides.

- *TentaGel Resins*

Poly (styrene-oxyethylene) graft copolymers, first reported by Bayer and Rapp in 1985, are a class of widely used supports for organic synthesis. The most pre-eminent of these is TentaGel (TG) resin which consists of polyethylene glycol attached to cross-linked polystyrene through an ether link, and combines the benefits of the soluble polyethylene glycol support with the insolubility and handling characteristics of the polystyrene bead (Scheme 1.1).

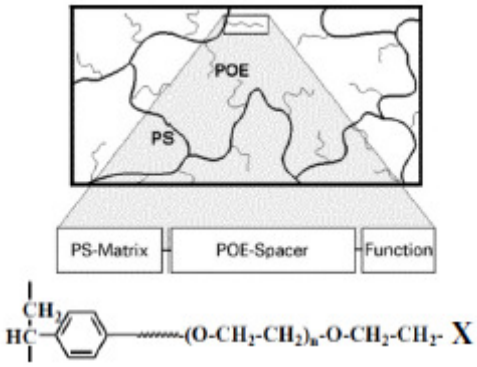

Scheme 1.1: schematic representation of TG resin.

The polymers are produced by grafting ethylene oxide from the polystyrene backbone creating long flexible chains that terminate with a reactive site spatially separated from the more rigid polystyrene backbone. This resin offers several advantages such as (i) uniform swelling in a variety of solvents from medium to high polarity ranging from toluene to

water; (ii) optical transparency; (iii) a variety of available functional groups; (iv) sizes of beads ranging from 5 to 400 mm with narrow size dispersion.

- *Glass-Derived Beads*

Controlled pore glass (CPG) is extremely used as a stationary phase in size-exclusion chromatography, and occasionally in solid phase synthesis. CPG's have excellent mechanical properties, and can be prepared with a wide range of porosities, and attached with a variety of functional groups. They possess extreme rigidity and high chemical stability.

The glass is produced from a ternary system consisting of silica (50-75%) sodium oxide (l-10%) and boric acid (to 100%). For special purposes, *e.g.*, with higher hydrolytic stability or larger pore sizes, substances such as alumina can be also added. The homogeneous molten glass is phase separated by heat treatment between 500 and 750 °C. The phase-separated glass is then crushed and screened, resulting in a glass powder of the desired grain dimensions.

1.5 One-Pot Synthesis: Triazine Derivatives as Scaffolds

In chemistry a one-pot synthesis is a strategy to improve the efficiency of a chemical reaction whereby a reactant is subjected to successive chemical reactions in just one reactor. This is much desired by chemists because avoiding a lengthy separation process and purification of the intermediate chemical compounds would save time and resources while increasing chemical yield. The development of simple, efficient and environmentally benign chemical processes or methodologies for widely used organic compounds from readily available reagents is one of the major challenges for chemists in organic synthesis.[88]

Cyanuric chloride (2,4,6-trichloro-1,3,5-triazine), has been extensively used in analytical chemistry as complexation agent, in electrochemistry as multi-step redox system and as pesticide or herbicide component in agriculture.[89] In recent years, owing to its high reactivity and trifunctionality that allows easy and controlled sequential replacement of the halogens by nucleophiles, cyanuric chloride has attracted increasing attention for potential use in the synthesis of fluorescent labeling compounds and dendrimer.[90,91] This compound has also been used to prepare porphyrin dimers and oligomers (Figure 1.13).[92]

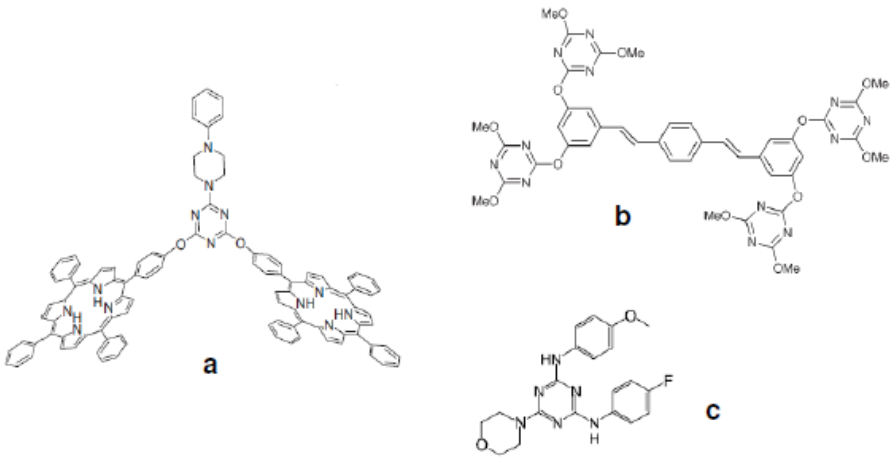

Figure 1.13: few examples of the triazine use in literature: a) ref. [89]; b) ref. [90]; c) ref. [92].

Sophisticated triazine derivatives can be easily prepared from the cheap and readily available 2,4,6-trichloro-1,3,5-triazine.[93] Cyanuric chloride is definitely an excellent starting compound for the straightforward preparation of highly structured multitopic receptors. Indeed, each chlorine atom of 2,4,6- trichloro-1,3,5-triazine can be substituted by any nucleophilic reactant. The first substitution is exothermic and, therefore, the temperature of the reaction mixture has to be maintained to 0 °C. The substitution of the second chloride can be performed at room temperature. Finally, the third position is functionalized under reflux of the solvent. As a result, a careful control of the temperature during the substitution reactions will allow the synthesis of 2,4,6-trisubstituted-triazines by sequential and very selective addition of amines, alcohols, thiols or Grignard reagents (Figure 1.14).[94]

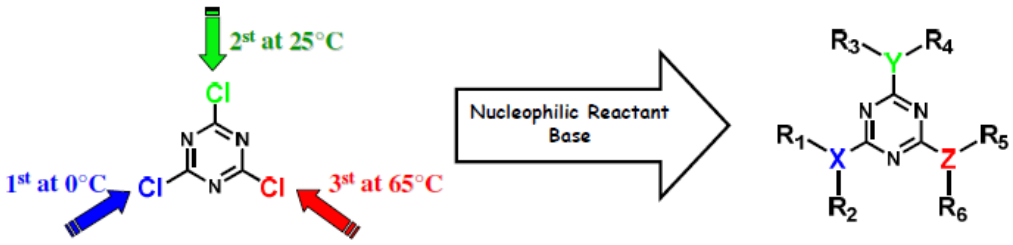

Figure 1.14: preparation of polyfunctional triazine derivatives taking advantage of the differential reactivity of 2,4,6-trichloro-1,3,5-triazine. **X**, **Y**, **Z** = C, N, O, S. $\mathbf{R_1}$....$\mathbf{R_6}$ = alkyl, alkenyl, aryl.

The yield of each substitution often exceeds 95%,[95] and the symmetric trisubstituted derivatives can even be obtained in a one-pot synthesis. Various solvents can

be used such as tetrahydrofuran, 1,2-dimethoxy ethane, acetonitrile, and diethyl ether. Numerous **R** substituents, such as carboxylate,[96] 4-pyridyl,[97] phenyl,[98] azacrown,[99] and dipyridylamine,[94] have been successfully incorporated following this flexible and straightforward synthetic pathway. In addition to the synthetic versatility aforementioned, the triazine ring exhibits an excellent potential for the formation of noncovalent bonds, which involve either its nitrogen lone-pairs (coordination and hydrogen bonds), its heteroaromatic π-electrons (π–π stacking and cationic π interactions) or its σ backbone (anionic–σ and electronrich σ interactions).

REFERENCES

[1] Nguyen, S.T.; Gin, D.L.; Hupp, J.T.; Zhang, X., *PNAS*, **2001**, *98*, 11849.

[2] Steed, W.W.; Atwood, J.L, *Supramolecular Chemistry*, John Wiley & Sons Ltd, West Sussex, **2002**.

[3] Hoog, P.; Gamez, I.; Mutikainen, U.; Turpeinen, J.; Reedijk, J, *Angew. Chem., Int. Ed. Engl.*, **2004**, *43*, 5815.

[4] Lehn, J.-M., *Supramolecular Chemistry: Concepts and Perspectives*, VCH, Weinheim, **1995**.

[5] Nobel prizes for research investigations in relation to supramolecular chemistry: **1953**, Hermann Staudinger (Germany) For: Discoveries in the Area of Macromolecular Chemistry; **1973**, Ernst Otto Fischer (Germany), Geoffrey Wilkinson (United Kingdom) For: Chemistry of Metal-Organic Sandwich Compounds; **1974**, Paul J. Flory (USA) For: Physical Chemistry of Macromolecules; **1987**, Donald J. Cram (USA), Charles J. Pedersen (USA), Jean-Marie Lehn (France) For: Development of Molecules with Structurally Specific Interaction of High Selectivity; **2000**, Alan J. Heeger (USA), Alan G. MacDiarmid (USA), Hideki Shirakawa (Japan) For: Discovery and Development of Conductive Polymers; **2003**, Peter Agre (USA), For: Discovery of Water Channels in Cell Membranes & Roderick MacKinnon (USA) For: For Structural and Mechanistic Studies of Ion Channels in Cell Membranes.

[6] Eigen, M., *Naturwissenschaften*, **1971**, *58*, 465.

[7] Yates, F.E., *Self-Organizing Systems*, Ed. Plenum, New York, **1987**.

[8] Atwood, J.L.; Lehn, J.-M.; Gokel, G. W.; Vogtle, F.; Osa, T.; Szejtli, J.; Murakami, Y.; Suslick, K.S.; MacNicol, D.D.; Toda, F., et al., *Comprehensive Supramolecular Chemistry*, Eds. Pergamon, New York, **1996**.

[9] Prins, L. J.; Reinhoudt, D. N.; Timmerman, P., *Angew. Chem. Int. Ed.*, **2001**, *40*, 2382.

[10] Seidel, S.R.; Stang, P.J., *Acc. Chem. Res*., **2002**, *35*, 972.

[11] (a) Hunter, C.A.; Lawson, K.R.; Perkins, J.; Urch, C.J., *J. Chem. Soc., Perkin Trans*., **2001**, *2*, 651. (b) Meyer, E. A.; Castellano, R. K.; Diederich, F., *Angew. Chem. Int. Ed.*, **2003**, *42*, 1210.

[12] Ma, J. C.; Dougherty, D. A., *Chem. Rev*., **1997**, *97*, 1303.

[13] Autumn, K.; Liang, Y.A.; Hsieh, S.T.; Zesch, W.; Chan, W.-P.; Kenny, W.T.; Fearing, R.; Full, R.J., *Nature*, **2000**, *405*, 681.

[14] (a) Jaenicke, R., *Angew. Chem. Int. Ed.*, **1984**, *23*, 395. (b) Schneider, G.; Wrede, P., *Angew. Chem. Int. Ed.*, **1993**, *32*, 1141.

[15] Cram, D.J.; Cram, J.M., *Container Molecules and Their Guests*, The Royal Society of Chemistry, Cambridge, UK, **1994**.

[16] Kahn, K.; Bruice, T.C., *J. Phys. Chem. B*, **2003**, *107*, 6876.

[17] Lehn, J.-M., *Science*, **2002**, *295*, 2400.

[18] (a) Whitesides, G. M.; *et al.*, *Acc. Chem. Res.*, **1995**, *28*, 37. (b) Fyfe, M.C.T.; Stoddart, J.F., *Acc. Chem. Res.*, **1997**, *30*, 393.

[19] J.M. Lehn, *Angew. Chem. Int. Ed.*, **1990**, *29*, 1304

[20] (a) Whitesides, G.M.; Mathias, J.P.; Seto, C.T., *Science*, **1991**, *254*, 1312. (b) Philp, D.; Stoddart, J.F., *Angew. Chem. Int. Ed.*, **1996**, *35*, 1154. (c) Lawrence, D.S.; Jiang, T.; Levett, M., *Chem. Rev.*, **1995**, *95*,

2229. (d) Leinninger, S.; Olenyuk, B.; Stang, P.J., *Chem. Rev.*, **2000**, *100*, 853. (e) Swiegers, G.F.; Malefetse, T.J., *Chem Rev.*, **2000**, *100*, 3483.

[21] Eigen, M., *Naturwissenschaften*, **1971**, *58*, 465.

[22] Yates, F.E., *Self-Organizing Systems*, Ed. Plenum, New York, **1987**.

[23] Milgrom, L.R., *The Colours of Life*, OUP, Oxford, **1997**; *The Porphyrins*, ed. D. Dolphin, Academic Press, New York, **1978**.

[24] Collman, J.P., *et al.*, *Metal Ions in Biology*, Vol. 2, T.G. Spiro Ed., Wiley, NY, 1 (**1980**), Schiavon, M.A.; *et al.*, *J. Molecular Catalysis A,* **2001**, *174*, 213. Richardson, T.H.; *et al.*, *Thin Solid Films*, **2001**, *393*, 259.

[25] (a) Suslick, K.S.; *et al.*, *Shape Selective Oxidation Catalysis in Comprehensive Supramolecular Chemistry*, Vol. 5, K.S. Suslick Ed., Elsevier, Oxford, 141 (**1996**). (b) Bhyrappa, P. ; *et al.*, *J. Am. Chem. Soc.*, **1996**, *118*, 5708. (c) Elemans, J.A.A. ; *et al.*, *Org. Chem.*, **1999**, *64*, 7009.

[26] Atwood, J.L.; Davies, J.E.D. ; MacNicol, D.D. ; Vogtle, F. ; Lehn, J.-M., Eds., *Handbook : Comprehensive Supramolecular Chemistry*, Pergamon, Oxford, **1996**.

[27] Rothemund, P., *J. Am. Chem. Soc.*, **1935**, *57*, 2010.

[28] Adler, A.D.; Longo, F.R.; Finarelli, J.D.; Goldmacher, J.; Assour, J.; Karsakoff, L., *J. Org. Chem.*, **1967**, *32*, 476.

[29] Lindsey, J. S.; Schreiman, I.C.; Hsu, H.C.; Kearney, P.C.; Marguerettaz, A.M., *J. Org. Chem.*, **1987**, *52*, 827.

[30] Rothemund, P., *J. Am. Chem. Soc.*, **1936**, *58*, 625.

[31] Menotti, A. R., *J. Am. Chem. Soc.*, **1941**, *63*, 267.

[32] Lindsey, J. S.; Schreiman, I.C.; Hsu, H.C.; Kearney, P.C.; Marguerettaz, A.M., *J. Org. Chem.*, **1987**, *52*, 827.

[33] Calvin, M.; Ball, R. H.; Arnoff, S., *J. Am. Chem. Soc.*, **1943**, *65*, 2259. Ball, R.H.; Dorough, G.D.; Calvin, M., *J. Am. Chem. Soc.*, **1946**, *68*, 2278.

[34] Anderson, H.J.; Loader, C.E.; Jackson, A.H., In *Pyrrole*, Part 1; Jones, R. A.; Ed.; *The Chemistry of Heterocyclic Compounds*, Vol. 48, John Wiley & Sons: New York, **1990**; p 295-397.

[35] Acheson, R.M. *An Introduction to the Chemistry of Heterocyclic Compounds*, 3rd ed; John Wiley & Sons: New York, **1976**. Albert, A. *Heterocyclic Chemistry*, 2nd ed; Oxford University Press: New York, **1976**.

[36] Dailey, H.A., Ed. *Biosynthesis of Heme and Chlorophylls*, McGrawHill, Inc.: New York, **1990**.

[37] Porra, R.J., *Photochem. Photobiol.*, **1997**, *65*, 492.

[38] Mauzarall, D., *J. Am. Chem. Soc.***1960**, *82*, 2605.

[39] Milgron, L.R., *The Colours of Life*, Oxford University Press, **1997**.

[40] (a) Yang, R.; Wang, K.; Long, L.; Xiao, D.; Xiaohai Yang, X.; Tan, W., *Anal. Chem.*, **2002**, *74*, 1088. (b) Gulino, A.; Mineo, P.; Bazzano, S.; Vitalini, D.; Fragalà, I., *Chem. Mater.*, **2005**, *17*, 4043. (c) Di Natale, C.; Salimbeni, D.; Paolesse, R.; Macagnano, A.; D'Amico, A., *Sens. Actuators, B*, **2000**, *65*, 220. (d) Di Natale, C.; Paolesse, R.; D'Amico, A., *Sens. Actuators, B*, **2007**, *121*, 238.

[41] (a) Scolaro, L.M.; Andrea Romeo, A.; Pasternack, R.F., *J. Am. Chem. Soc.*, **2004**, *126*, 7178. (b) Balaz, M.; Holmes, A.E.; Benedetti, M.; Rodriguez, P.C.; Berova, N.; Nakanishi, K.; Proni, G., *J. Am. Chem. Soc.*, **2005**, *127*, 4172.

[42] (a) Zhang, Y.; Yang, R. H.; Liu, F.; Li, K.A., *Anal. Chem.*, **2004**, *76*, 7336. (b) Zhou, H.; Baldini, L.; Hong, J.; Wilson, A. J.; Hamilton, A.D., *J. Am. Chem. Soc.*, **2006**, *128*, 2421.

[43] (a) Shundo, A.; Labuta, J.; Hill, J.P.; Ishihara, S.; Ariga, K., *J. Am. Chem. Soc.*, **2009**, *131*, 9494. (b) Tong, Y.; Hamilton, D.G.; Meillon, J.-C.; Sanders, J.K.M., *Org. Lett.*, **1999**, *1*, 1343.

[44] (a) Collman J.P.; *et al.*, *Metal Ions in Biology*, Vol. 2, T.G. Spiro Ed., Wiley, NY, 1 (**1980**), Schiavon, M.A.; *et al.*, *J. Molecular Catalysis A*, **2001**, *174*, 213. (b) Richardson T.H.; *et al.*, *Thin Solid Films*, **2001**, *393*, 259.

[45] Merino, G.; Heine, T.; Seifert, G., *Chem. Eur. J.*, **2004**, *10*, 4367.

[46] Mallion, R.B., *Chem. Rev.*, **2001**, *101*, 1349.

[47] Gardner, G. W.; Bartlett, P. N., *Sensors and Actuators B*, **1994**, *19*, 211.

[48] Meilgaard, M.C., *MBAA Tech. Q.*, **1975**, *12*, 151.

[49] Beets, M.G.J., *Structure-Activity Relationships in Human Chemoreception*, Allied Science Publishers, London, **1978**.

[50] Moncrieff, R.W., *J. Appl. Physiol.*, **1961**, *16*, 742.

[51] Wilkens, W.F.; Hatman, A.D., *Ann. NY Acad. Sci.*, **1964**, *116*, 608.

[52] Buck, T.M.; Allen, F.G.; Dalton, M., *Detection of Chemical Species by Surface Effects on Metals and Semiconductors*, in T. Bregman and A. Dtavnieks (eds.), *Surface Effects in Detection*, Spartan Books Inc., USA, **1965**.

[53] Dravnieks, A.; Trotter, P.J., *J. Set Instnrm.*, **1965**, *42*, 624 .

[54] Persaud, K.; Dodd, G.H., *Nature*, **1982**, *299*, 352.

[55] Ikegami, A.; Kaneyasu, M., *Olfactory detection using integrated sensors, Proc. 3rd Int. Conf Solid-State Sensors and Actuators (Transducers 85)*, Philadelphia, PA USA, June 7-11, **1985**, pp. 136-139.

[56] Suslick, B. A,; Feng, L., Suslick, K. S., *Anal. Chem*, **2010**, *82*, 2067.

[57] Gardner, G. W.; Bartlett, P. N., *Sensors and Actuators B*, **1994**, *19*, 211.

[58] Dodd, G.; Bartlett, P.N.; Gardner, J.W., *Odours-the stimulus for an electronic nose*, in J .W. Gardner and P.N. Bartlett (eds.), *Sensors and Sensory Systems for an Electronic Nose, NA TO ASI Series E: Applied Sciences*, Vol. 212, Kluwer, Dordrecht, **1992**.

[59] Turner, A. P. F.; Magan, N., *Nature Review in Microbiology*, **2004**, *2*, 161.

[60] Casalinuovo, I.A.; Di'Piero, D.; Coletta, M.; Di'Francesco, P., *Sensors*, **2006**, *6*, 1428.

[61] Paolesse, R.; Alimelli, A.; Martinelli, E.; Natale, C.D.; D'Amico, A.; D'Egidio, M.; G. Aureli, G.; Ricelli, A.; Fanelli, C., *Sensors and Actuators*, **2006**, *119*, 425.

[62] Vestergaard, J.S.; Martens, M.; Turkki, P., *LWT Food Science and Technology*, **2007**, *40*, 1095.

[63] Pavlou, A.K.; Turner, A.P.F., *Clinical Chemistry and Laboratory Medicine*, **2000**, *38*, 99.

[64] Bourgeois, W.; Burgess, J.E.; Stuetz, R.M., *Journal of Chemical Technology and Biotechnology*, **2001**, *76*, 337.

[65] Canhoto, O.; Magan, N., *Biosensor and Bioelectronics*, **2003**, *18*, 751.

[66] Santos, M.H.S., *Int. J. Food Microbiol.*, **1996**, *29*, 213.

[67] Moret, S.; Smela, D.; Populin, T.; Conte, L. S., *Food Chem.*, **2005**, *89*, 355.

[68] Askar and Treptow, **1986**; Maijala *et al.*, **1993**.

[69] Bardez, *et al.*, **1993**; Maijala *et al.*, **1993**; Halez *et al.*, **1994**.

[70] Ahmad, *et al.*, *Biogenic Amines in Food*, **1987**; Hotchkiss, **1987**; Smith, **1981**; Pfundstein, *et al.*, **1991**.

[71] Muresan, L.; Valera, R.R.; Frebort, I.; Popescu, I.C.; Csoregi, E.; Nistor, M., *Microchim. Acta*, **2008**, *163*, 219.

[72] (a) Reinert, S.; Mohr, G.J., *Chem. Commun.*, **2008**, 2272. (b) Acosta, B.G.; Comes, M.; Bricks, J.L.; Kudinova, M.A.; Kurdyukov, V.V.; Tolmachev, A.I.; Descalzo, A.B.; Marcos, M.D.; *et al.*, *Chem. Commun.*, **2006**, 2239. (c) Lu, G.; Grossman, J.E.; Lambert, J.B., *J. Org. Chem.*, **2006**, *71*, 1769. (d) DiNatale, C.; Olafsdottir, G.; Einarsson, S.; Martinelli, E.; Paolesse, R.; D'Amico, A., *Sens. Actuators, B*, **2001**, *77*, 572. (e) Macagnano, A.; Careche, M.; Herrero, A.; Paolesse, R.; Martinelli, E.; Pennazza, G.; Carmona, P.; D'Amico, A.; Di Natale, C., *Sens. Actuators, B*, **2005**, *111–112*, 293.

[73] (a) Drain, C. M.; Varotto, A.; Radivojevic, I., *Chem. Rev.*, **2009**, *109*, 1630. (b) Beletskaya, I.; Tyurin, V. S.; Tsivadze, Y. A.; Guilard, R.; Stern, C., *Chem. Rev.*, **2009**, *109*, 1659. (c) Ogoshi, H.; Kuroda, Y.; Mizutani, T.; Hayashi, T., *Pure Appl. Chem.*, **1996**, *68*, 1411.

[74] (a) Scolaro, M.L.; Romeo, A.; Pasternack, R.F., *J. Am. Chem. Soc.*, **2004**, *126*, 7178. (b) Balaz, M.; Holmes, A. E.; Benedetti, M.; Rodriguez, P. C.; Berova, N.; Nakanishi, K.; Proni, G., *J. Am. Chem. Soc.*, **2005**, *127*, 4172.

[75] (a) Neal, A.; Rakow, N.A.; Suslick, K.S., *Nature*, **2000**, *306*, 710. (b) Lvova, L.; Di Natale, C.; Paolesse, R.; D'Amico, A., *Sens. Actuators, B*, **2006**, *118*, 439.

[76] (a) Dunbar, A.D.F.; Richardson, T.H.; McNaughton, A.J.; Hutchinson, J.; Hunter, C.A., *J. Phys. Chem. B*, **2006**, *110*, 16646. (b) Bang, J.H.; Lim, S.H.; Park, E.; Suslick, K.S., *Langmuir*, **2008**, *24*, 13168. (c) Deviprasad, G. R.; D'Souza, F., *Chem. Commun.*, **2000**, 1915.

[77] Mizutani, T.; Kurahashi, T.; Murakami, T.; Noriyoshi Matsumi, N.; Ogoshi, H., *J. Am. Chem. Soc.*, **1997**, *119*, 8991.

[78] (a) Hosseini, A.; Taylor, S.; Accorsi, G.; Armaroli, N.; Reed, C.A.; Boyd, P.D.W., *J. Am. Chem. Soc.*, **2006**, *128*, 15903. (b) Yagi, S.; Ezoe, M.; Yonekura, I.; Takagishi, T.; Nakazumi, H., *J. Am. Chem. Soc.*, **2003**, *125*, 4068. (c) Kuroda, Y.; Kawashima, A.; Hayashi, Y.; Ogoshi, H., *J. Am. Chem. Soc.*, **1997**, *119*, 4929. (d) Phillips-McNaughton, K.; Groves, J.T., *Org. Lett.*, **2003**, *5*, 1829. (e) Kuramochi, Y.; Satake, A.; Kobuke, Y., *J. Am. Chem. Soc.*, **2004**, *126*, 8668.

[79] (a) Marois, J.-S.; Cantin, K.; Desmarais, A.; Morin, J.-F., *Org. Lett.*, **2008**, *10*, 33. (c) Shoji, Y.; Tashiro, K.; Aida, T., *J. Am. Chem. Soc.*, **2004**, *126*, 6570. (d) Boyd, P.D.W.; Reed, C.A., *Acc. Chem. Res.*, **2005**, *38*, 235.

[80] Nagata, N.; Kuramochi, Y.; Kobuke, Y., *J. Am. Chem. Soc.*, **2009**, *131*, 10.

[81] Gryko, D.T.; Clausen, C.; Lindsey J.S., *J. Org. Chem.*, **1999**, *64*, 8635.

[82] McDonagh, C.; Burke, C.S.; MacCraith B.D., *Chem. Rev.*, **2008**, *108*, 400.

[83] Rakow, N.A.; Suslick, K.S., *Nature*, **2000**, *406*, 710.

[84] Lim, S.H.; Feng, L.; Kemling, J.W.; Musto, C.J.; Suslick, K.S., *Nature*, **2009**, *1*, 562.

[85] Zhang, C.; Suslick, K.S., *J. Am. Chem. Soc.*, **2005**, *127*, 11548.

[86] Kocincova, A.S.; Borisov, S.M.; Krause, C.; Wolfbeis, O.S., *Anal. Chem.*, **2007**, *79*, 8486.

[87] Filippini, D.; Alimelli, A.; Di Natale, C.; Paolesse, R.; D'Amico, A.; Lundstrom, I., *Angew. Chem., Int. Ed.*, **2006**, *45*, 3800.

[88] Wang, K.; Fu, S. T.; Zhang, Z.; Li, Z. Y., *J. Braz. Chem. Soc.*, **2007**, *18*, 911.

[89] Giacomelli, G.; Porcheddu, A.; De Luca, L.; *Curr. Org. Chem.*, **2004**, *8*, 1497.

[90] Su, M. H.; Ma, H. M.; Ma, Q. L.; Wang, Z. H.; Xiong, S. X.; Liang, S. C.; *Anal. Chim. Acta.* **2001**, *426*, 51; Ma, H. M.; Nie, L.H.; Xiong, S. X.; *Supramol. Chem.* **2004,** *16*, 311.

[91] Lupton, J. M.; Hemingway, L. R.; Samuel, I. D. W.; Burn, P. L. J.; *J. Mater. Chem.* **2000,** *10*, 867.

[92] Lebreton, S.; Newcombe, N.; Bradley, M.; *Tetrahedron* **2003**, *59*, 10213.

[93] Carofiglio, T.; Varotto, A.;Tonellato, U., *J. Org. Chem.*, **2004**, *69*, 8121.

[94] Hoog, P.; Gamez, P.; Driessen, W.L., Reedijk, J., *Tetrahedron Lett.*, **2002**, *43*, 6783.

[95] Piguet, C.; Williams, A.F.; Bernardinelli, G.; Moret, E.; Bunzli, J.C.G.; *Helv. Chim. Acta*, **1992**, *75*, 1697.

[96] Galan-Mascaros, J.R.; Clemente-Juan, J.M.; Dunbar, K.R., *J. Chem. Soc., Dalton Trans.*, **2002**, 2710.

[97] Biradha, K.; Fujita, M., *Angew. Chem., Int. Ed. Engl.*, **2002**, *41*, 3392.

[98] Munakata, M.; Wen, M.; Suenaga, Y.; Kuroda-Sowa, T.; Maekawa, M.; Anahata, M., *Polyhedron*, **2001**, *20*, 2037.

[99] Comba, P.; Lampeka, Y.D.; Lotzbeyer, L.; Prikhod'ko, A.I., *Eur. J. Inorg. Chem.*, **2003**, 34.

RESULTS AND DISCUSSION

2.1 One-Pot Synthesis of Melamine-Bridge Bis(Porphyrin-Zn^{II}) Hosts

In the past few years, there has been remarkable progress in the synthesis of multiporphyrin oligomers.[1] Nevertheless, gaining access to the compounds needed in significant quantities often entails tremendous preparative efforts and reiterative purification steps. Thus, the development of new synthetic methodologies and/or the improvement of existing reactions in order to obtain target porphyrins in high yield and purity with minimal recourse to separation techniques still represents a challenging issue.

In our laboratories, a new synthetic methodology, called one-pot protocol, has been developed in order to synthesize porphyrin-porphyrin dyads in few steps. This procedure employs cyanuric chloride (**CC**) as essential building block and takes advantage of its temperature-dependent stepwise nucleophilic substitution at the chlorine atoms by an appropriate modified porphyrin.[2]

Typically, the first chlorine reacts rapidly at 0 °C, whereas room temperature or moderate heating (depending on the nucleophile strength) promotes the second substitution. The nucleophilic displacement of the third chlorine requires harsher conditions (T > 80 °C for multiple hours). Since quantitative yields are often achieved for these reactions, sequential, one-flask introduction of various substituents into a triazine ring is also feasible (Scheme 2.1).

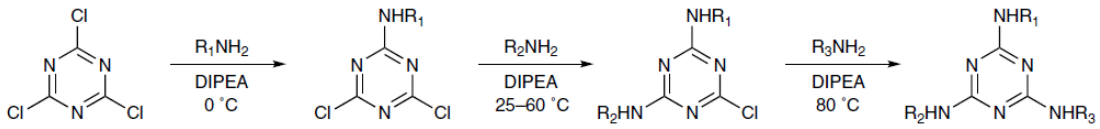

Scheme 2.1: temperature-dependent reactivity of cyanuric chloride.

The benefits of this synthetic methodology are readily envisaged in the design of porphyrin dyads where the overall stereo electronic diversity can be generated by a proper synthesis/selection of the isolated components in a homodimer arrangement, by the combination of these within an heterodimeric structure, and/or by differential metalation of the porphyrin units.[3] In particular, the steric constrains of the macrocycle components are expected to affect the conformational stability and binding geometry of the dyad whereby

the two porphyrin units are forced into close proximity as a consequence of the recognition event. To this aim, in this research work were used two amino-porphyrin building blocks **P**, and **M**, respectively, carrying phenyl and mesityl *meso*-subsituents, to yield the homoconjugates free bases **PP**, **MM**, and the hetero dyad **PM**. After metalation with Zn^{II}, a small library of three structurally related bis(porphyrin-Zn^{II}) receptors is readily obtained, namely **P(Zn)P(Zn)**, **P(Zn)M(Zn)**, and **M(Zn)M(Zn)** derivatives (Figure 2.1). The steric hindrance at the peripheral positions is supposed to govern the different strength of coordination towards bifunctional ligands.

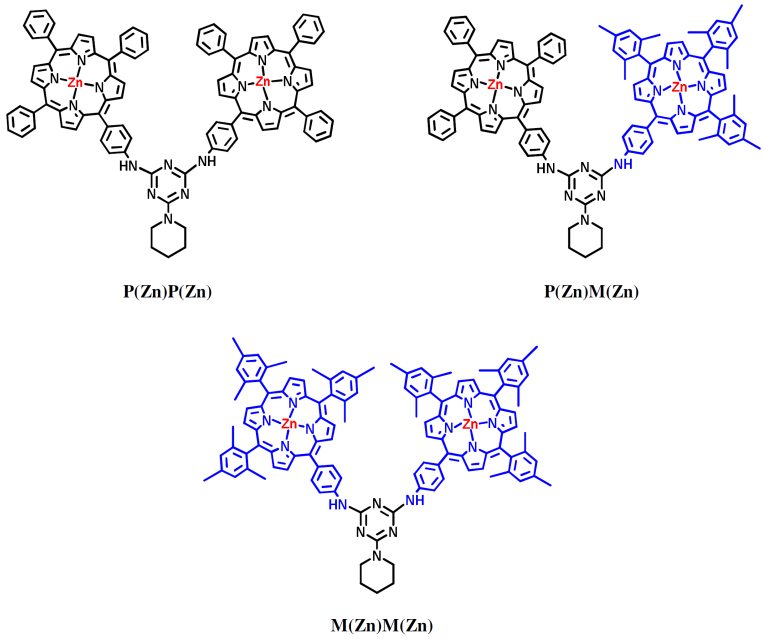

Figure 2.1: the three porphyrinZn^{II}-porphyrinZn^{II} hosts.

2.1.1 Synthesis of Porphyrins as Building Blocks

The preparation of melamine bridged bis(porphyrin) adducts required the preliminary synthesis of the two amino-porphyrins that then react with triazine molecule.

Synthesis of 5-(4-aminophenyl)-10,15,20-triphenyl porphyrin, **P**, can be conveniently prepared on a milligrams scale and in 80% yields, as reported by Kruper, by direct mononitration of tetraphenyl porphyrin followed by reduction with $SnCl_2$ in concentrated HCl.[4] On the other hand, 5-(4-aminophenyl)-10,15,20-trimesityl porphyrin, **M**, was synthesized in 78% yield following the Lindsey's method that comes from a modification of the Alder-Longo approach. Pyrrole reacts with a binary mixture of mesitylbenzaldehyde and 4-acetamidobenzaldehyde in the presence of BF_3-etherate as

catalyst. The desired monoamidoporphyrin was recovered by preparative column chromatography and hydrolyzed in acidic conditions to produce the corresponding amino-derivative.[5] These syntheses are reported in Figure 2.2.

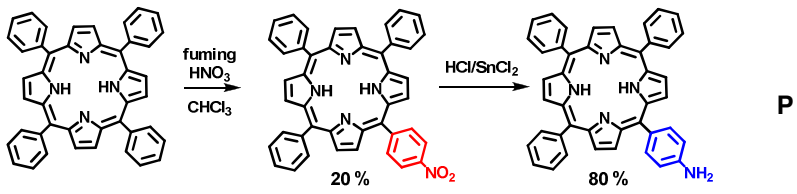

Kruper, W.J. Jr., et al., *JOC,* **1989**, *54*, 2753.

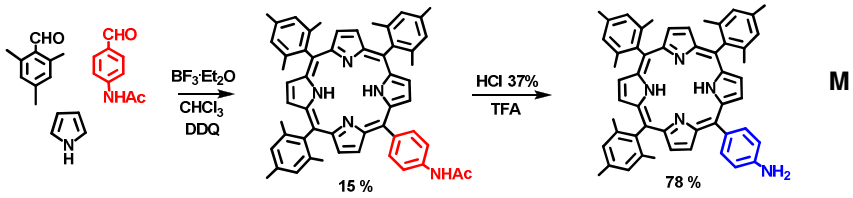

Lindsey, J.S., et al., *Inorg. Chem.*,**2003**, *42*, 6616.

Figure 2.2: synthesis of the amino-porphyrins **P**, and **M**.

2.1.2 Synthesis of Melamine-Bridge Bis(Porphyrin-Zn^{II}) Derivatives

Bis(porphyrin) receptors were prepared in our laboratories according to the one-flask synthetic protocol outlined in Scheme 2.2.[6] Briefly, the amino-porphyrin (**P** or **M**) was reacted with 1 equivalent of cyanuric chloride in tetrahydrofuran (THF) at 0 °C in the presence of diisopropylethylamine (DIPEA) as base. The reaction was stirred at room temperature until TLC analysis indicated the complete disappearance of the starting materials and the formation of the corresponding monoadduct. At this point, a second equivalent of amino-porphyrin derivative (**P** or **M** depending on whether the target molecule was a homodimer, **PP**, and **MM**, or a heterodimer, **PM**) was added to the solution and the reaction mixture was stirred at 60-70 °C to afford the corresponding bis(porphyrin) adduct. Finally, the third chlorine atom was reacted with piperidine at 80 °C, producing a soluble compound. Noticeably, the third substitution might also afford a convenient route for supporting such porphyrin dimers onto solid materials carrying amino-functionalities, such as TentaGel-amino resin beads, and amino-silanized porous glass particles. This strategy offers a very convenient route to supported catalysts or chemical sensors.[7]

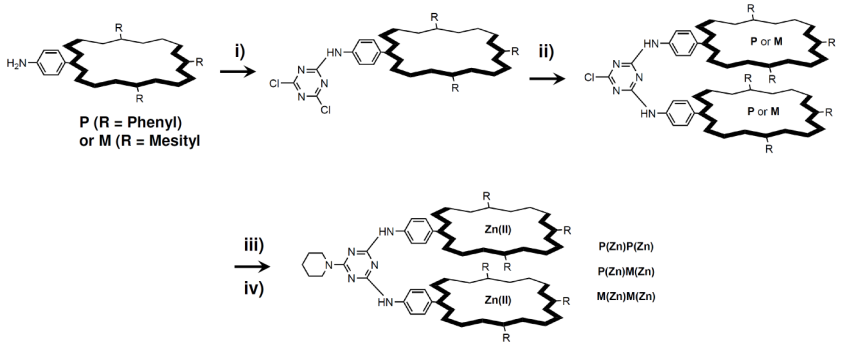

Scheme 2.2: synthesis of melamine-bridged bis(porphyrin) dimers. Reagents and conditions: (i) **CC**, THF, DIPEA, 0°C; (ii) **P** or **M**, THF, DIPEA, 60 °C; (iii) piperidine, THF, DIPEA, 80°C; (iv) $Zn(Ac)_2$ x $2H_2O$, MeOH/$CHCl_3$, reflux.

After standard workup, purification of the crude containing porphyrin-porphyrin derivatives was accomplished by preparative column chromatography. Identity and purity of the products were assessed by UV-vis and ^{1}H-NMR spectroscopy, ESI-MS, and HPLC analysis. The isolated yields for **PP**, **PM**, and **MM** dimers were about 90%. Metalation of the porphyrin units was accomplished in quantitative yield by reacting the dimers with an excess of $Zn(Ac)_2$ x $2H_2O$ in a MeOH/$CHCl_3$ solvent mixture. The reaction occurs smoothly under reflux conditions as witnessed by (i) the red-shift of the Soret band, (ii) collapse of the Q bands from four to two, and (iii) the disappearance of the pyrrolic proton signal in the up field region of ^{1}H-NMR spectra.

2.2 Binding Properties of Melamine-Bridged Bis(Porphyrin-Zn^{II}) Hosts

Zinc-porphyrins are known to coordinate nitrogenous bases to form five-coordinated complexes.[8] Hence, the melamine-bridged bis(porphyrin-Zn^{II}) derivatives are expected to behave as ditopic receptors suitable for binding of diamines ligands. Indeed, a marked colour variation from purple to blue was consistently observed upon adding aliphatic α,ω-diamines of general formula $H_2N(CH_2)_nNH_2$ (n = 4-8) to a dichloromethane solution of any of the three bis(porphyrin-Zn^{II}) receptors (Figure 2.3).

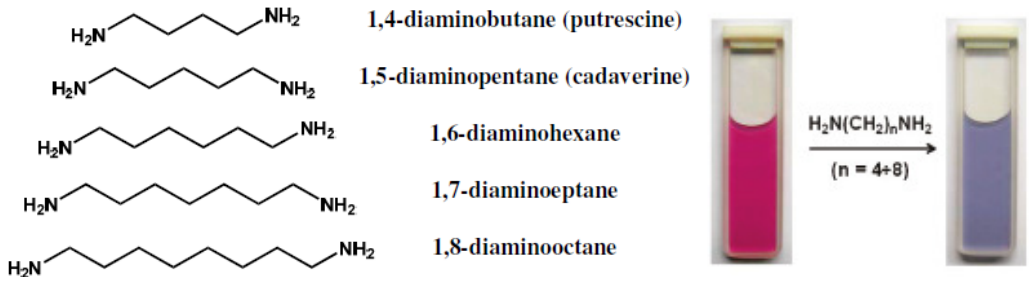

Figure 2.3: left: linear aliphatic diamines under investigation; right: colour change of the receptors.

2.2.1 UV-visible Characterization

Formation of a receptor-diamine host-guest complex could be studied in dichloromethane (DCM), at 298 K, by UV-visible monitoring the characteristic red-shift of the porphyrin Soret band upon diamine coordination. To this purpose, a solution of the bis(porphyrin-Zn^{II}) maintained at a constant micromolar concentration was titrated by adding incremental amounts of diamine in DCM. Figure 2.4 shows a typical spectral change observed for **P(Zn)P(Zn)** upon addition of cadaverine.

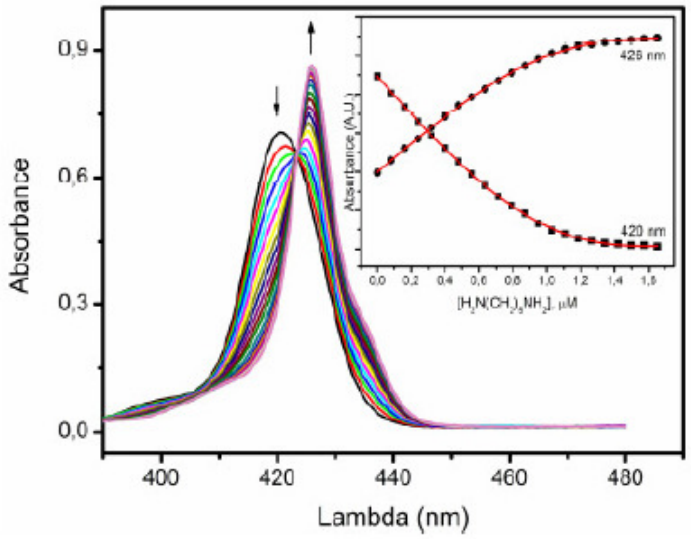

Figure 2.4: UV-vis spectra evolution in DCM at 298 K upon titration of **P(Zn)P(Zn)** (1.1 μM)with cadaverine (0-1.7 μM). **Inset**: titration plot at 420 nm and 426 nm and non-linear fitting curve using a 1:1 binding model.

Depletion of the Soret band at 420 nm was accompanied by the formation of a new absorption peak at 426 nm, ascribable to the host-guest complex formation. The

appearance of a sharp isosbestic point at 423 nm is suggestive of a 1:1 binding stoichiometry. The spectral data were analyzed in order to obtain the value of the binding constant by using the opportune fitting procedure.[9] The software allows a simultaneous fit of the absorbance values at all the wavelengths as a function of the analytical concentration of the diamine, thus yielding a binding constant calculation with higher precision compared to conventional methods based on a single wavelength monitoring.

The binding constant values for all the hosts with the diamines are collected in Table 2.1. For comparison purposes, are also reported the corresponding binding constants for the monodentate *n*-$BuNH_2$ with the three porphyrin dimers.

$H_2N(CH_2)_nNH_2$	Dimer (Binding constants in DCM, M^{-1})		
	P(Zn)P(Zn)	**P(Zn)M(Zn)**	**M(Zn)M(Zn)**
n = 4 putrescine	$4.8x10^6$	n.d.[a]	n.d.[a]
n = 5 cadaverine	$3.4x10^7$	$8.1x10^6$	$8.5x10^6$
n = 6	$1.3x10^7$	$2.8x10^7$	$9.0x10^6$
n = 7	$4.5x10^6$	$7.2x10^6$	$6.9x10^6$
n = 8	$4.2x10^6$	$5.3x10^6$	$5.2x10^6$
***n*-$BuNH_2$**	$3.2x10^4$	$2.7x10^4$	$1.9x10^4$

a) The binding constant was not determined due to slow binding.

Table 2.1: binding constants between **P(Zn)P(Zn)**, **P(Zn)M(Zn)**, **M(Zn)M(Zn)**, and $H_2N(CH_2)_nNH_2$ (n = 4-8) diamines and *n*-butylamine (for comparison purposes).

Scrutiny of data in Table 2.1 shows that bis(porphyrin-Zn^{II}) receptors display a high affinity toward the aliphatic diamines under examination, with binding constants in the range from $2.1x10^6$ M^{-1} to 3.4×10^7 M^{-1}. In contrast, the monodentate benchmark, *n*-$BuNH_2$, binds the ditopic hosts, with a 3 orders of magnitude smaller constants. This behavior is likely ascribed to the simultaneous binding of both amino groups of the aliphatic diamine to the two zinc recognition sites of the porphyrin dyad, acting as a molecular tweezer. Noteworthy, the association constants found here are 1 or 2 orders of magnitude smaller than those reported in literature (for the same series of diamines) with a porphyrin tweezer with a flexible pentandiol linker.[10] This is likely due to the interplay of both the rigidity of the melamine bridge and the bulky *meso*-substituents at the porphyrin periphery, which turns out to impart some conformational constrains to the receptors.

The differential binding affinity is ascribable both to steric effects on the porphyrinic macrocycles and to the conformational flexibility of the bound diamine. In particular, peak affinities are registered for the short-chain diamines (n = 5, 6) binding to the low hindered receptor **P(Zn)P(Zn)**. This latter displays the highest binding constants for the diamine with n = 5 ($K = 3.4x10^7\ M^{-1}$). On the other hand, increasing of the steric constrains in the **P(Zn)M(Zn)** dimer is responsible for its preferential binding to the diamine with n = 6 ($K = 2.8x10^7\ M^{-1}$), featuring an elongated alkyl chain and a consequent enhanced conformational flexibility with respect to lower homologues. The **M(Zn)M(Zn)** host forms remarkably stable host:guest adducts as well, but without any special preference for any of them.

Interestingly, the receptor rigidity seems to affect also the kinetics of the binding process. This is especially apparent in the titration of the **P(Zn)M(Zn)** and **M(Zn)M(Zn)** receptors with the shortest chain diamines (n = 4). Indeed, an immediate and pronounced red-shifting of the Soret band was observed upon addition of the first aliquots of the diamine, followed by a slow blue-shift evolution of the spectrum that required 5-10 minutes to reach equilibrium. The complexation is hampered by the mesityl substituents at the periphery of the porphyrin macrocycle. This behaviour might result from a fast formation under kinetic control of a 1:2 host/guest complex that then evolved to a thermodynamically more stable 1:1 complex. For such a reason, these data were considered inappropriate for an accurate determination of the corresponding binding constants.

As reported in literature for similar receptors, the red-shift of the Soret band changes almost linearly with the chain length of the diamine.[11] This fact is the result of two counteracting effects: (i) amine binding to the metalloporphyrin, which leads to a red-shift of the absorption bands and (ii) the proximity of the two chromophores due to the bridging diamine, causing an exciton coupling blue-shift. Figure 2.5 reports the Soret band shift ($\Delta\nu$, cm^{-1}) for the different porphyrin dimers upon diamine addition. The values have been calculated from the titration data, by evaluating the difference between the wavelength of the Soret band for the free receptor (ν_{free}) and that at the end of the titration ($\nu_{complex}$).

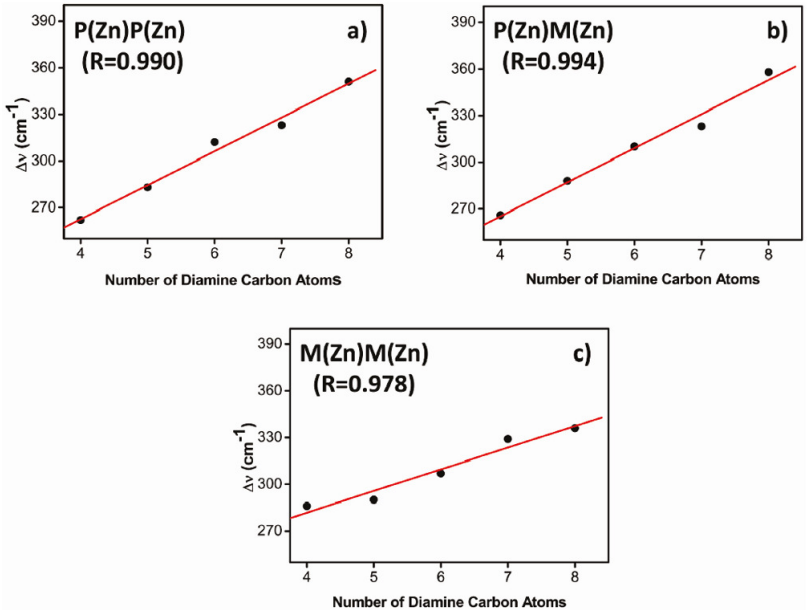

Figure 2.5: variation of the Soret band red-shift (Δν, cm-1) of **P(Zn)P(Zn)**, **P(Zn)M(Zn)**, and **M(Zn)M(Zn)** upon complexation with $H_2N(CH_2)_nNH_2$ (n = 4-8), as a function of the diamine chain length, in DCM at 298 K. Correlation parameters (slope and correlation coefficient, R) are as follows: (a) slope = 22 ± 2, R= 0.990; (b) slope = 22 ± 1, R = 0.994; and (c) slope = 14 ± 2, R = 0.978.

It is evident from the graphs that for all receptors, the Δν values change linearly with the number of carbon atoms of the aliphatic diamine. Furthermore, comparing the binding constants in Table 2.1 to the correlation graphs in Figure 2.5, the most hindered receptor **M(Zn)M(Zn)** exhibits a modest response to the diamine structural change, as it appears from the roughly halved slope of the linear fitting. This behavior depends on the mesityl substituents that limit the conformational freedom of the **M(Zn)M(Zn)** tweezer.

2.2.2 NMR Characterization

The solution structure of the supramolecular complex has been further addressed by NMR spectroscopy. My studies were focused on the solution behavior of the **P(Zn)P(Zn)** receptor and on the host-guest complexation with cadaverine, $H_2N(CH_2)_5NH_2$.

The ^{1}H-NMR spectrum of **P(Zn)P(Zn)** dimer freshly prepared in $CHCl_3$ at room temperature is shown in Figure 2.6, together with the resonance assignments obtained by the correlation spectroscopy (COSY) and the double-quantum filtered correlation spectroscopy technique (DQF-COSY).

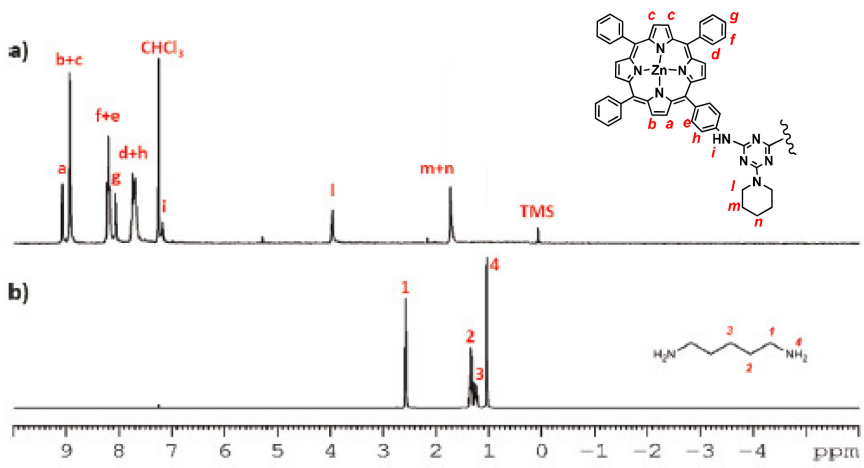

Figure 2.6: ^{1}H-NMR (400 MHz, $CDCl_3$) of (a) **P(Zn)P(Zn)** and (b) $H_2N(CH_2)_5NH_2$ together with the resonance assignments according to COSY and DQF-COSY.

The porphyrin spectrum *a* shows three main sets of signals: (i) the porphyrin β-pyrrolic protons, around 9 ppm, (ii) the porphyrin phenyl protons in the 8.5-7 ppm region, and (iii) the piperidine methylenic protons, at 3.94 and 1.75 ppm. The ^{1}H-NMR spectrum of free diamine in the same conditions is also reported in Figure 2.6b.

Noteworthy, at millimolar concentration, the **P(Zn)P(Zn)** dimer undergoes aggregation phenomena, which result in the progressive broadening of the NMR signal and ultimately yield a massive precipitation of a porphyrin-based material. On the other hand, addition of the diamine guest induces the reversible dissolution of this precipitate, by supramolecular complexation. This behaviour is reflected in the NMR titration experiments outlined in Figure 2.7. The evolution of the NMR spectrum during the titration experiments can be conveniently discussed by analyzing the two separate regions pertaining to the aromatic resonances of the receptor from 9.5 to 7.0 ppm, and to the bound diamine signals found between -1.0 and -6.0 ppm.

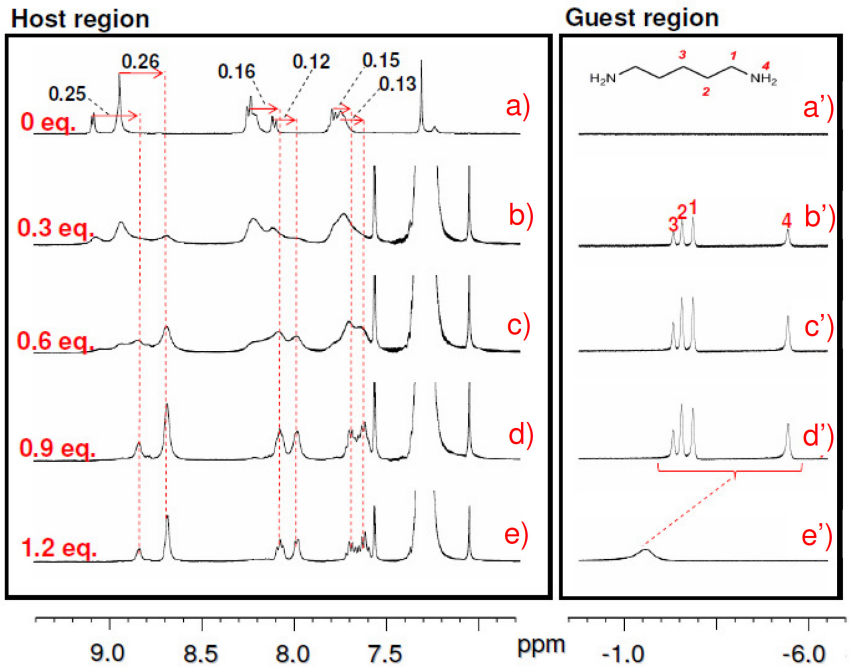

Figure 2.7: Signal changes in the host and guest region during the ^{1}H-NMR (400 MHz, $CDCl_3$) titration of **P(Zn)P(Zn)** (0.1 mM) with $H_2N(CH_2)_5NH_2$. Spectra a, b, c, d, and e respectively represent the ^{1}H-NMR spectra acquired after adding 0, 0.3, 0.6, 0.9, and 1.2 equivalents of diamine.

Upon incremental addition of the diamine, up to 1 equivalent, the aromatic host region shows two distinct sets of chemical shifts, corresponding to the protons of free host and to those of the host-guest assembly (Figure 2.7a-d). For the latter complex, the new resonances build up at significant upfield chemical shift. Precisely, the amount of shifting was about 0.25 ppm for the pyrrolic protons, whereas the aromatic protons shifted upfield to a smaller extent (0.12-0.16 ppm). This effect is associated with the proximity of the two porphyrin π-systems, upon diamine binding, causing the signals to experience a large ring current induced shift.[12] A further remark is that broadening of all the aromatic signals is observed as well. In this respect, speciation of the receptor may be complicated by aggregation phenomena, occurring in the time course of the titration experiments. A key observation is that upon reaching the 1:1 host-guest ratio, the resulting NMR spectrum contains just the aromatic signals ascribable to the supramolecular complex, where the *ortho* and *meta* protons of the *meso*-phenyl substituents become non equivalent, and give rise to sharp multiplets (Figure 2.7e). Similar splitting is often observed in porphyrin systems with non equivalent faces.[13] The signals of the diamine protons (Figure 2.7a'-e'), in turn, exhibit significant upfield shifts by effect of complexation, due to ring current anisotropy from porphyrin π-planes.[14] Indeed, with substoichiometric diamine, the guest

signals are found between -2 and -6 ppm chemical shift (Figure 2.7a'-d'). This evidence is consistent with the bidentate amine being bound within the **P(Zn)P(Zn)** concave, via ditopic interaction, and exposed to the ring current effects of porphyrin macrocycles.

The resonances of the diamine, while complexed within the host, could be assigned by DQF-COSY and TOCSY experiments. On the basis of these assignments, we could quantify the upfield shift of the methylene groups (Figure 2.8).

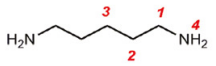

Protons	Experimental $\Delta\delta$	Calculated $\Delta\delta_{calc}$
1	-5.41	-5.06
2	-3.91	-3.47
3	-3.62	-3.58
4	-6.11	-5.09

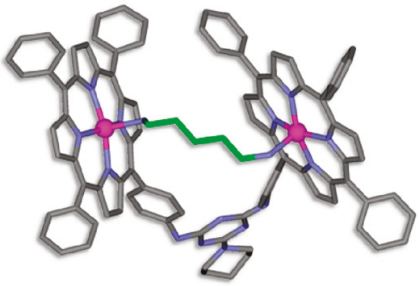

Figure 2.8: energy-minimized conformation obtained for the **P(Zn)P(Zn)**-$H_2N(CH_2)_5NH_2$ host-guest complex, and experimental versus calculated $\Delta\delta$ values evaluated for the free and bonded diamine ligand.

The order of shift found experimentally is $H_1 > H_2 > H_3$. Interestingly, above 1 equivalent of diamine, the guest signals coalesce due to fast exchange equilibrium and cannot be observed separately (Figure 2.7e'). We decided to investigate further, by computational methods in collaboration with Dr. Giacomo Saielli of the University of Padova, the strong high-field shift induced by the extended π-system of the porphyrin rings to the resonances of the diamine.[15] Shielding calculations require high level DFT methods and, in turn, considering the size of the complex, a high computational effort, especially if relativistic effects are considered.[16] Thus, we have first tested the effect of relativity on the proton chemical shifts by running zeroth-order regular approximation (ZORA) calculations at the Scalar and Spin-Orbit level (BLYP/TZ2P).[17,18] To this end, we have first considered a simplified model system made by a single Zn-porphyrin having an ethylamine bound to the Zn ion. Comparison of non relativistic results with those obtained at the Scalar and Spin-Orbit level reveals that relativistic effects can be safely ignored. Indeed, relativistic proton chemical shifts, even for the NH_2 protons, the closest to the heavy atoms, differ only by less than 0.1 ppm from the non relativistic results. We run shielding calculations for the most stable conformer resulting from the conformational analysis carried out with

MacroModel package.[19] Relative chemical shifts, Δδ, observed for the free and complexed diamine are then evaluated. Comparisons of calculated and experimental Δδ values stand in good agreement (Figure 2.8). Moreover the strong deshielding of the signals and the general trend as a function of the distance is correctly reproduced, although a somewhat larger error is found for the NH_2 protons.

2.3 Supported Melanine-Bridged Bis(Porphyrin-Zn^{II}) Derivatives: Synthesis and Characterization

Previously, the use of porphyrin-porphyrin dyads as optical molecular sensors towards bifunctional molecules like diamines was described. Also, widely technological applications of supported sensors devices, taking advantages from solid phase synthesis, were explained. Now, the importance to support these porphyrin receptors appears clearly.

In the one-pot protocol, it has been established that the third chlorine atom of triazine could be replaced either with a piperidine terminus, to give a classical dyad, or with surface amino-functions anchored on a solid material for supporting the porphyrin–porphyrin dyads (Scheme 2.3).

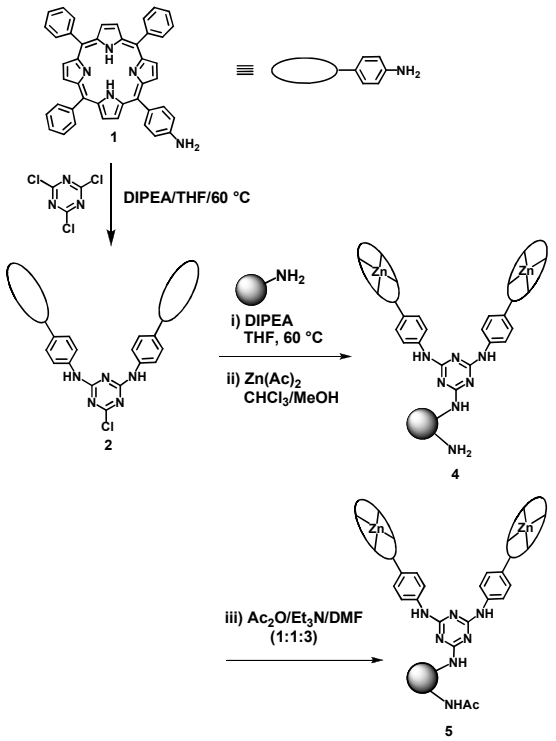

Scheme 2.3: supporting bis(porphyrin-Zn^{II}) dyads on aminated solid materials, TG-NH_2.

Monochloro dimer **2** formed upon reaction of the amino-porphyrin **1** with half an equivalent of cyanuric chloride in the presence of DIPEA. Then, it is readily scavenged by an appropriate amount of the TG-NH_2 resin added *in situ*. Heating of the mixture is prolonged until complete discoloration of the supernatant solution with formation of purple-coloured beads. The resin is collected by filtration and washed extensively with tetrahydrofuran in order to remove unreacted products. Metalation with $Zn(Ac)_2$ takes place smoothly affording the bis-Zn^{II} porphyrin adduct, **4**. According to the TG-NH_2/dimer stoichiometry adopted, the supported tweezer corresponds to 1% of the overall amino-functionalities of the beads. In order to avoid any competitive intra-bead Zn-coordination, the residual free-amino groups of the TG-NH_2 resin have been capped by acetylation reaction with acetic anhydride and triethylamine in dimethylformamide (DMF) to yield the corresponding acetamidate derivative **5** (Scheme 2.3).

Evolution of the TentaGel resin is conveniently monitored through single bead UV–vis spectroscopy by a *home-made* apparatus consisting of a confocal microscope (a) coupled to a diode-array spectrophotometer (b) connected through an optical-fiber to a computer (c) that in real-time elaborates and collects the spectra (Figure 2.9).

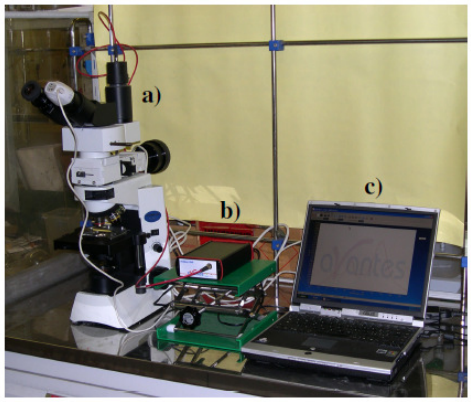

Figure 2.9: *home-made* equipment for UV-vis analysis.

The microscope allows to focalize one single functionalized bead as illustrated in Figure 2.10 right, in which the light beam spot is visible. In this way is possible to record the spectrum of a single bead (Figure 2.10 left).

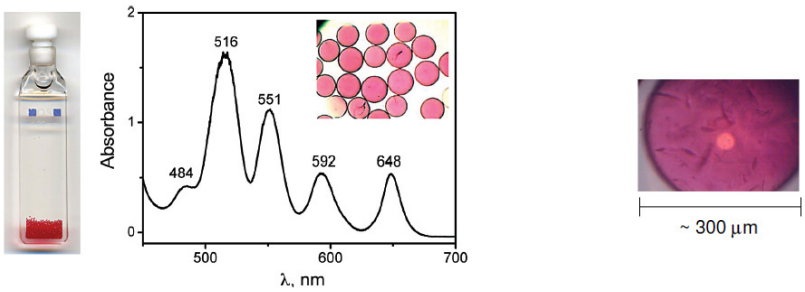

Figure 2.10: Left: single-bead UV-vis spectrum of **PP** dyad (free-base form) supported on TentaGel beads. Right: microphotograph of the TentaGel bead functionalized with a porphyrin dimer **PP**.

Due to the intense bead colour, recording of the Soret band around 420 nm is impracticable. On the contrary, the Q bands region, in the 500–650 nm wavelength range, gives a direct proof of the tweezer attachment to the substrate, of its metalation, and of the coordination status of the Zn^{II} centers. It is noteworthy that the Q bands pertaining to compound **4** (Scheme 2.3) are typical of a Zn^{II} porphyrin,[6] thus confirming the attachment of the metalated tweezer, but turn out to be more red-shifted than expected, with maxima at 564 and 606 nm, as a result of some adventitious binding to the Zn^{II} centers. This phenomenon is also evident from a visual analysis of the resulting bead colour that appears to be blue–green rather than purple, as generally obtained for uncomplexed Zn^{II} porphyrins (Fig. 2.11A).

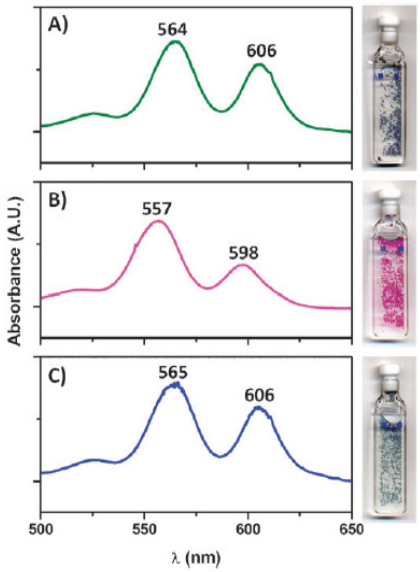

Figure 2.11: single-bead UV–vis spectra (Q bands region), monitoring the evolution of the TG-NH_2 resin in material **4** (spectrum A), **5** (spectrum B), and the spectral variation of **5** in the presence of an excess of cadaverine. All spectra are recorded in DCM at 25 °C.

The spectrum is recorded in a non-coordinating solvent (*e.g.*, dichloromethane) and the observed coordination can be uniquely ascribed to the residual amino groups of the beads which account for 99% of the total resin functionalization. Since such intra-bead coordination will prejudice the ability of material **4** to signal the coordination with an exogenous amine, the capped material **5** (Scheme 2.3) is the sensor of choice. The success of this approach is evident from the single bead UV–vis spectrum of **5** (Figure 2.11B) showing the Q bands with maxima at 557 and 598 nm. As a further remark, the capped beads show the expected purple colour, indicating the free- Zn^{II} state within the tweezer receptor. Finally, the ability of **5** to sense biogenic diamines is readily demonstrated upon its exposure to a solution of 1,5-diaminopentane (cadaverine) in DCM. The colour of the beads turns to blue–green, as a consequence of the spectral red-shift, which is observed for the Q bands with maxima at 565 and 606 nm (Figure 2.11C). These results confirm that the sensing properties of the melamine-bridged bis(porphyrin-Zn^{II}) tweezer are maintained upon immobilization on a solid support, as compared to the behaviour in homogeneous solution.[6]

2.3.1 Sensing Properties on TentaGel (TG) Resin and Controlled Pore Glass (CPG) Functionalized Materials

The response of the TentaGel-supported dyad to diamines has been analyzed under flow conditions by placing a sequence of two beads within a 400 μm square glass capillary, one bead carrying the **P(Zn)P(Zn)** dyad and a second one in the pristine form for zeroing purposes.[20] The flow cell (Scheme 2.4) is completed by inserting two fused silica capillaries that act both as inlet and outlet for the microfluidic circuit and as stoppers to keep the two beads in place.

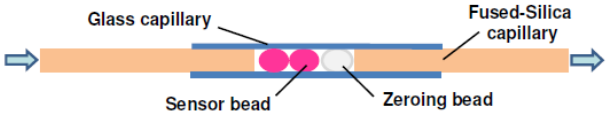

Scheme 2.4: *home-made* flow cell for continuous flow analyses.

Continuous monitoring of the sensing bead is performed at 565 nm while a solution of cadaverine (0.1 mM in toluene) or toluene are alternatively infused at 1 mL/min flow rate (Figure 2.12).

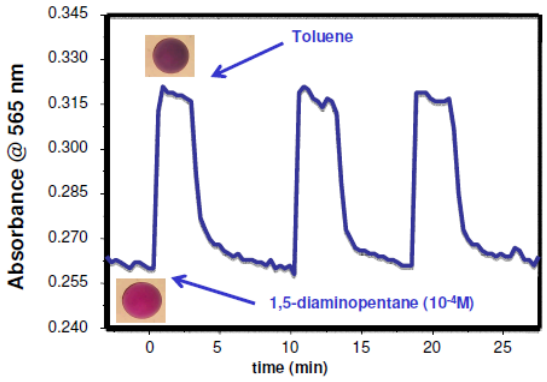

Figure 2.12: single-bead UV-vis analysis of cadaverine (0.1 mM) by **P(Zn)P(Zn)**, under flow conditions (1 mL/min) in toluene.

The time course of the flow analysis suggests that the sensing process by **P(Zn)P(Zn)** is reproducible, reversible and effective towards a submillimolar concentration of the analyte. In addition, the sensor response is rapid (less than a minute long) and complete recovery to the initial state upon solvent fluxing takes places in few minutes.

As a further upgrade, diamine sensing with the tweezer based sensor has been applied also in water, in order to evaluate its potential towards aqueous matrices typically found in food analysis. Unfortunately, the TentaGel beads become translucid when swollen in aqueous solution, thus hampering the UV-vis detection. On the other hand, this problem was not observed in the case of the controlled pore glass-supported dyad. This material, already tested with success for pH sensing in aqueous conditions,[21] is commercially available in different pore sizes and can be easily functionalized with amino groups by reacting the CPG with γ-APTES (3-aminopropyltrimethoxysilane) in dry toluene (Figure 2.13).

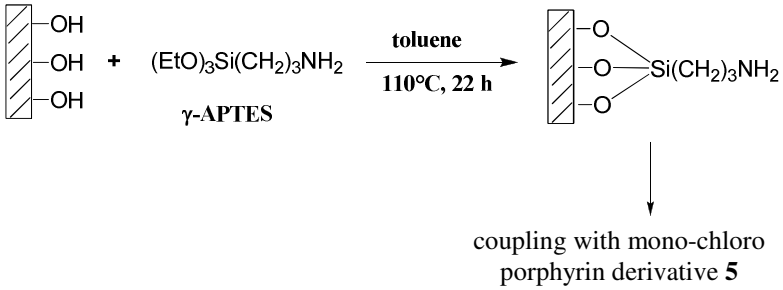

Figure 2.13: scheme of functionalization of CPG-OH to form aminated substrates that then reacts with mono-chloro derivatives **2**.

In turn, the CPG-NH_2 can be functionalized with the porphyrin dimer as accomplished for the TG-NH_2 resin (Scheme 2.3). Also in this case, the residual amino-groups of CPG-NH_2 have been capped by reaction with acetic anhydride. The response of the CPG-supported tweezer has been analyzed under flow conditions with a properly designed apparatus composed by a miniaturised polymer well filled with CPG and coupled to the common end of an optical fibre bifurcated bundle (Figure 2.14). The two branches of the bundle are connected with a halogen lamp and a spectrophotometer, respectively. The light coming from the source is scattered by the CPG and the portion of the light which is coupled back to the optical fibre bundle is clearly modulated by the absorption properties of the CPG. A peristaltic pump allows to flow the buffered solutions (phosphate buffered saline at pH 7.4) containing different concentrations of cadaverine inside the miniaturised well. The inlet and outlet are constituted by two glass capillaries having an internal diameter of 300 μm.

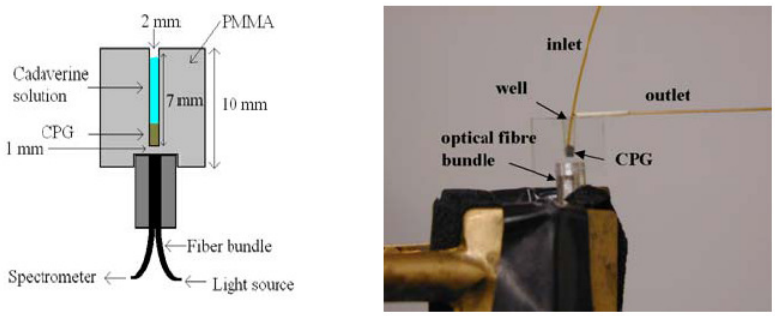

Figure 2.14: Left: sketch of the set-up for the optical characterisation of the CPG. Right: photo of the set-up with the inlet and outlet for the cadaverine solutions, constituted by two glass capillaries.

Figure 2.15 shows the absorption spectra achieved with CPG 1400 Å and CPG 700 Å when buffers at different concentrations of cadaverine (ranging from 10^{-5} to 10^{-2} M) flow through the well. As expected, the sensitivity toward cadaverine increases upon reducing the pore size of CPG, since a decreasing in the porosity corresponds to an increase of the surface available for the immobilisation. The spectrophotometer was zeroed on the porphyrin dyad in the absence of cadaverine, so the spectra collected during the analysis are difference spectra. In the presence of cadaverine in the sample solution, the diamine binds to both the Zn^{II} centers causing a red-shift of the absorption spectrum of the porphyrin dimer.

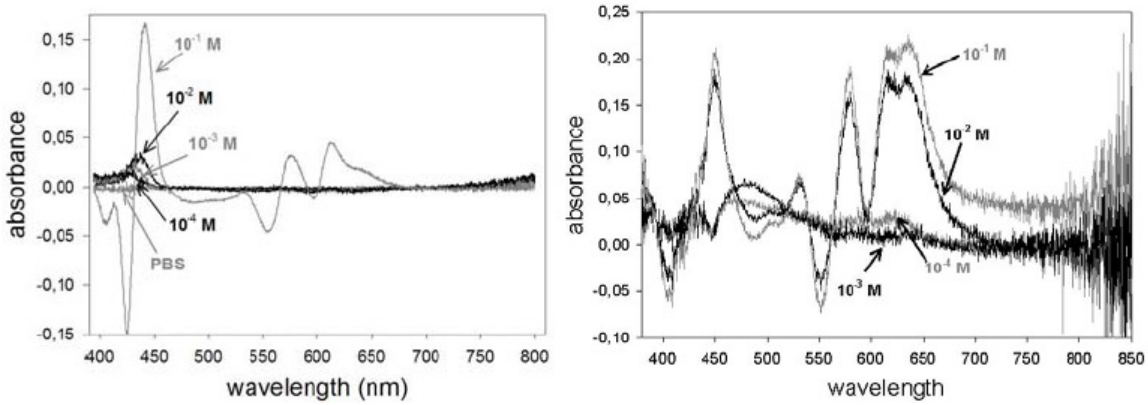

Figure 2.15: absorption spectra of CPG with pore size of 1400 Å (left) and 700 Å (right) for different concentrations of cadaverine in 40 mM phosphate buffer solution at pH 7.4.

The response time of the system is of the order of a few minutes. A much more interesting aspect is given by the reversibility of the interaction of the cadaverine with the dyad immobilized on the CPG. Indeed, upon flowing through the cell the solvent in the absence of cadaverine, the initial absorption is fully recovered. However, the reversibility is effective for a much higher concentration (range of sensitivity 10^{-2}–10^{-1} M) if compared to what is observed in non-aqueous environment for TG-NH_2 resin (in toluene the range of sensitivity is 10^{-4}–10^{-3} M). This is not surprising due to the strong competition of bulk water with diamine for the coordination to the Zn^{II} centers. Nevertheless, the final goal is to access the gas phase sensing of the biogenic amines by taking advantage of the analyte volatility in the head-space of the sample, where the interference of water is supposed to be less severe than in aqueous solution. In this light, the porphyrin-based sensing materials offer an unprecedented opportunity in terms of the variety of component assembly, the

consequent modulation of the molecular recognition properties, the resulting performance and the microfluidic applications.

REFERENCES

[1] (a) Speckbacher, M.; Yu, L.; Lindsey, J. S., *Inorg. Chem.* **2003**, *42*, 4322. (b) Li, F.; Yang, S. I.; Ciringh, Y.; Seth, J.; Martin, C. H., III; Singh, D. L.; Kim, D.; Birge, R. R.; Bocian, D. F.; Holten, D.; Lindsey, J. S., *J. Am. Chem. Soc.*, **1998**, *120*, 10001. (c) Mak, C.C.; Bampos, N.; Darling, S. L.; Montalti, M.; Prodi, L.; Sanders, J.K.M., *J. Org. Chem.*, **2001**, *66*, 4476. (d) Twyman, L.J.; Sanders, J.K.M., *Tetrahedron Lett.*, **1999**, *40*, 6681.

[2] Gamez, P.; de Hoog, P., *et al.*, *Tetrahedron Letters*, **2002,** *43,* 6783.

[3] Carofiglio, T.; Varotto, A.; Tonellato, U., *J. Org. Chem.*, **2004**, *69*, 8121.

[4] Kruper, W. J.; Chamberlin, T. A.; Kochanny, M.; Lang, K., *J. Org. Chem.*, **1989**, *54*, 2753

[5] Lindsey, J.S.; *et al.*, *Inorg. Chem.*, **2003**, *42*, 6616.

[6] Carofiglio, T.; Lubian, E.; Menegazzo, I.; Saielli, G.; Varotto, A., *J. Org. Chem.*, **2009**, *74*, 9034.

[7] Carofiglio, T.; Schiorlin, M.; Tonellato, U., *J. Porph. Phthal.*, **2007**, *11*, 749.

[8] Weiss J. J. Inclusion Phenom. Macrocyclic Chem. 2001; **40**: 1–22.

[9] Gans, P.; Sabatini, A.; Vacca, A., *Talanta*, **1996**, *43*, 1739.

[10] Huang, X.; Borhan, B.; Berova, N.; Nakanishi, K. J.; *Indian Chem. Soc.*, **1998**, *75*, 725.

[11] Hunter, C. A.; Meah, M. N.; Sanders, J. K. M., *J. Am. Chem. Soc.*, **1990**, *112*, 5773.

[12] Ballester, P.; Costa, A.; Deyà, P.M.; Frontera, A.; Gomila, R.M.; Oliva, A.I.; Sanders, J.K.M.; Hunter, C.A., *J. Org. Chem.*, **2005**, *70*, 6616.

[13] Ballester, P.; Costa, A.; Castilla, A. M.; Deyà, P.M.; Frontera, A.; Gomila, R.M.; Hunter, C.A., *Chem.;Eur. J.*, **2005**, *11*, 2196.

[14] Packer, M. J.; Zonta, C.; Hunter, C. A., *J. Magn. Reson.*, **2003**, *162*, 102.

[15] Gomila, R.M.; Garau, C.; Frontera, A.; Quinonero, D.; Ballester, P.; Costa, A.; Deyà, P.M., *Tetrahedron Lett.*, **2004**, *45*, 9387.

[16] Bagno, A.; Saielli, G., *Theor. Chem. Acc.*, **2007**, *117*, 603.

[17]de Velde, G.; Bikelhaupt, F.M.; Baerends, E.J.; Fonseca Guerra, C.; Van Gisbergen, S.J.A.; Snijders, J.G.; Ziegler, T., *J. Comput. Chem.*, **2001**, *22*, 931.

[18](a) Becke, A.D., *Phys. Rev. A*, **1998**, *38*, 3098. (b) Lee, C.; Yang, W.; Parr, G., *Phys. Rev. B*, **1988**, *37*, 785. (c) Miehlich, B.; Savin, A.; Stoll, H.; Preuss, H., *Chem. Phys. Lett.*, **1989**, *157*, 200.

[19] Mohamadi, F.; Richards, N.G.J.; Guida, W.C.; Liskamp, R.; Lipton, M.; Caufield, C.; Chang, G.; Hendrickson, T.; Still, W.C., *J. Comput. Chem.*, **1990**, *11*, 440.

[20] Lubian, E.; Baldini, F.; Giannetti, A.; Trono, C.; Carofiglio, T., *Chem. Commun*. **2010**, *46*, 3678.

[21] Bacci, M.; Baldini, F.; Bracci, S., *Appl. Spectrosc.*, **1991**, *45*, 1508.

EXPERIMENTAL SECTION

3.1 Materials and Reagents

Tetraphenyl porphyrin **TPP** was purchased from EGA-CHEMIE, Germany. All the dimers are prepared following the one-pot protocol.[1] Other reagents and solvents (Sigma-Aldrich, Fluka and Carlo Erba Reagenti) were of the highest grade available and were used without further purification. Solvents employed in the spectroscopic studies are of spectroscopic grade and used as received. Silica gel MN 60 (70–230 Mesh) by Macherey-Nagel and neutral alumina (Brockmann Grade III) were used for column chromatography. Analytical thin layer chromatography (TLC) was performed using a Polygram SilG/UV_{254} TLC plates with fluorescent indicator. TentaGel-NH_2 resin was purchased from Rapp Polymere GmbH Tübingen, Germany.

3.2 Instruments

^{1}H-NMR spectra were recorded with a spectrometer Bruker AC-F 250 operating at 250 MHz. Two-dimensional NMR spectra were acquired at 298 K, on a 400 MHz spectrometer equipped with a 5 mm multinuclear inverse z-field gradient probe-head. Data processing was performed on a workstation using the TOPSPIN 1.3 software. The proton chemical shifts were referenced to the residual ^{1}H $CDCl_3$ solvent signal (7.26 ppm). Proton resonance assignments were obtained using 2D homonuclear correlation spectroscopy (DQF-COSY for free guest and host, DQF-COSY and TOCSY for the host-guest assignments) with gradient coherence selection. ^{1}H one-dimensional spectra were acquired with 32 transients, 8022.6 Hz spectral width, 16K data points. Double-Quantum Filtered Correlation (DQF-COSY) and Total Correlation Spectroscopy (TOCSY) experiments were recorded using a repetition delay of 2 s; a total of 400 experiments of 32 scans were accumulated; 2K data points were recorded in the acquisition dimension (F2) and the spectral width was 20.05 ppm. Zero-filling in both F1 and F2 multiplication with a gaussian function in F2 and a squared sine function (in DQF-COSY) or a squared cosine function (in TOCSY) in F1, was performed prior to Fourier transformation. In the TOCSY experiments the spin-lock time period was 70 ms. The signals are describe as s (singlet), d (doublet), and m (multiplet). Routine UV-vis spectra were recorded in CH_2Cl_2 on a Varian Cary 50 Spectrophotometer, whereas more delicate measurements were performed on a Perkin Elmer λ-45 spectrophotometer equipped with a temperature-controlled cell holder.

Mass spectra (ESI-MS) were recorded on a LC-MSD-Trap-SL (Agilent Technologies, Palo Alto, USA). Samples were dissolved in acetonitrile (~10^{-5} M) and injected in a stream of the same solvent containing the 0.1% of formic acid, at 50 µl min^{-1} (nitrogen nebulizing gas pressure = 20 psi; flow = 5 L min^{-1}; T = 325 °C).

3.3 Methods

3.3.1 Determination of the binding constants in solution

A micromolar solution of the dimer in CH_2Cl_2 was introduced in a UV-vis cuvette and titrated by adding aliquots of a diamine stock solution in CH_2Cl_2 by using a 10 µL gas-tight microsyringe. After any addition the solution was equilibrated for 5 minutes inside the cell-holder (temperature: 298 K) of the UV-vis spectrophotometer then the corresponding UV-vis spectrum was acquired in the range 380-480 nm. All the data were corrected by a dilution factor and background subtraction of the solvents. The addition was continued until the recorded spectrum was super-imposable to the previous one. All the spectra were imported into the program HYPERQUAD program,[2] a suite of programs designed for analyzing chemical equilibria using the non-linear least-squares curve-fitting based on a desired host:guest model (in our case a 1:1 dimer:diamine model).

3.3.2 Spectroscopy characterization of TG-NH_2 resin and CPG-NH_2

Resin. Single bead UV–visible spectra were conveniently monitored through a *home-made* apparatus consisting of a confocal microscope Olympus CX41RF coupled to a diode-array AvaSpec-2048 spectrophotometer through an optical-fiber (Figure 3.1). To check the reversibility of the sensor beads a *home-made* flow cell was built up placing a sequence of two beads within a 400 mm square glass capillary.

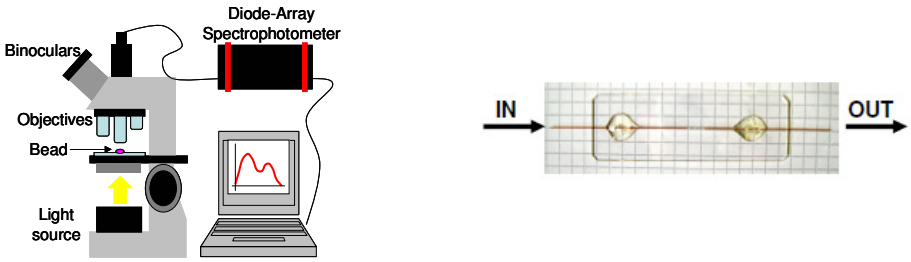

Figure 3.1: left. Schematic representation of the *home-made* apparatus used in the solid phase synthesis. Right. Photo of the *home-made* flow cell.

Glass CPG. A miniaturised poly methyl *meta* acrylic (PMMA) well was filled with CPG functionalized with the receptor. An Ocean Optics spectrophotometer and an halogen lamp (Zeiss) were connected to the cell used with optical fibre bifurcated bundle.

3.3.3 Bromophenol Blu test

All types of amines can be detected applying this test. A few resin beads are placed in a small test tube and 10-15 drops of reagent solution (0.05% bromophenol blue in dimethylformamide) are added. The beads are immediately inspected: blue beads are positive and colourless beads are negative.

3.3.4 Computational details

NMR shielding calculations were run using the ADF software package[3] at the non-relativistic level. The BLYP functional[4] and an all-electron, triple-ζ, double polarization, Slater-type basis set (TZ2P) were employed. Chemical shifts were calculated as $\delta = \sigma_{ref} - \sigma$ where σ_{ref} is the shielding constant of TMS ($\sigma H = 31.21$ ppm) and σ the shielding constants of interest. Chemical shifts of magnetically equivalent protons were obtained after averaging of the single resonances. Conformational searches were carried out in vacuum with MMFF94 force field as contained within Spartan 02 package for Windows (Wavefunction Inc., systematic method of search) and by using the OPLS-2005 force field implemented within MacroModel software (Schrödinger Inc., Monte Carlo Multiple Minimum searching method).

3.4 Synthesis of Compounds

3.4.1 Synthesis of 5-(4-aminophenyl)-10,15,20-triphenyl porphyrin, P

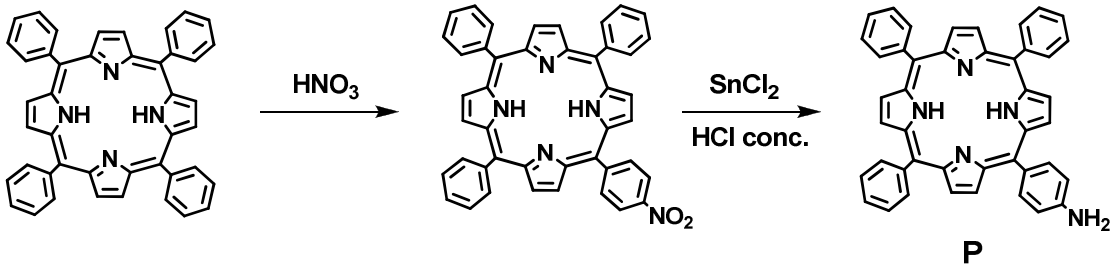

P

Following a general procedure,[5] tetraphenyl porphyrin (4 g, 6.51 mmol) was dissolved in 600 ml of pentene-stabilized chloroform under nitrogen. Red fuming nitric acid (6.8 g, 108 mmol) was added to the stirred solution of porphyrin at 0-5 °C through a pressure-equalizing dropping funnel over a 2 h period. The reaction was monitored at intervals by TLC to ensure total conversion of starting material (R_f = 0.88) to product (R_f = 0.78) by using chloroform/hexane (3:1) on silica plates. The dark green solution was extracted with 5 x 300 mL portions of water, dried over magnesium sulphate and sodium carbonate, filtered and concentrated under reduce pressure to give 4.5 g of nitro mixture. The reduction of nitro compound was conducted according to a modification of Hasegawa's procedure.[6] Raw material (2.5 g, 3.79 mmol) was dissolved in 80 mL of concentrated hydrochloric acid under nitrogen. Tin(II) chloride dehydrate (2.6 g, 11.5 mmol) was added to the solution and the reaction was heated to 65°C for 1 h. The porphyrin solution was cooled and added to 300 mL of cold water and was adjusted to pH 8 with concentrated ammonium hydroxide. The aqueous phase was extracted with 6 x 300 mL portions of chloroform, which were combined and dried over sodium sulphate. The organic phase was concentrated and this solution was separated on silica column with methylene chloride as an eluent. The product was obtained in 70% yield. ^{1}H-NMR ($CDCl_3$, 250 MHz) δ: 8.95 (d, 2H, β-pyrrole), 8.84 (d, 2H, β-pyrrole), 8.22 (m, 6H, ortho triphenyl), 8.00 (d, 2H, 4-aminophenyl), 7.76 (m, 9H, meta\para triphenyl), 7.06 (d, 2H, 4-aminophenyl), 4.02 (s, 2H, amino), -2.75 (s, 4H, pyrrole NH). ESI-MS $C_{44}H_{31}N_5$ (CH_3CN + 1% HCOOH as eluent) m/z: obsd 630.7 $[MH]^+$ (calcd 630.75), obsd 315.9 $[MH_2]^{2+}$ (calcd 315.88). UV-vis (CH_2Cl_2, nm): 419 (Soret band, ε = 337'000 $M^{-1}cm^{-1}$), 516 (ε = 9'300 $M^{-1}cm^{-1}$), 553 (ε = 5'300 $M^{-1}cm^{-1}$), 592 (ε = 3'000 $M^{-1}cm^{-1}$), 648 (ε = 2'800 $M^{-1}cm^{-1}$).

3.4.2 Synthesis of 5-(4-aminophenyl)-10,15,20-triphenyl porphyrin, M

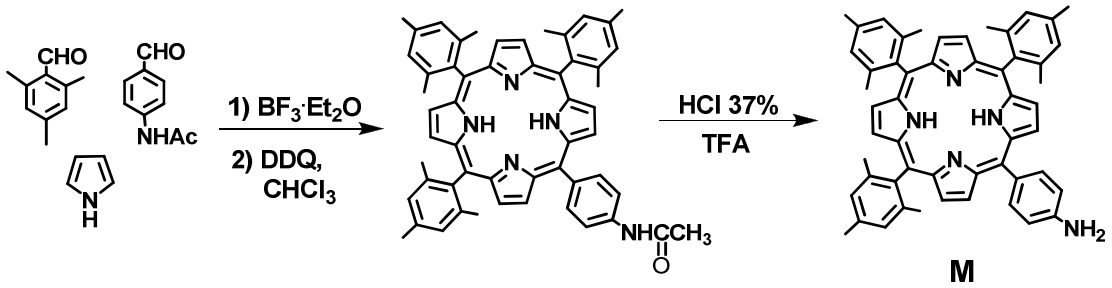

Following a literature method,[7] a mixture of mesitaldehyde (1.78 g, 12.0 mmol), 4-acetamidobenzaldehyde (0.652 g, 4.0 mmol) and pyrrole (1.10 mL, 16.0 mmol) in $CHCl_3$ (1.6 L) was treated with BF_3xOEt_2 (0.650 mL, 5.28 mmol, 3.3 mM). The mixture was stirred at room temperature for 1 h, then DDQ (2.72 g, 12.0 mmol) was added and stirring was continued for 1 h. The residue obtained was chromatographed on two silica column followed by an alumina column using $CHCl_3$ as eluent to afford a purple solid (142 mg, 4.6%). ^{1}H-NMR ($CDCl_3$, 250 MHz) δ: 8.81 (d, 2H), 8.70 (d, 2H), 8.68 (s, 4H), 8.16 (d, 2H), 7.87 (d, 2H), 7.68 (s, 1H), 2.61 (s, 9H), 2.29 (s, 3H), 1.85-1.87 (m, 18H), -2.54 (brs, 2H). ESI-MS $C_{55}H_{51}N_5O$ (CH_3CN + 1% HCOOH as eluent) m/z: obsd 799.0 $[MH]^+$ (calcd 799.03), obsd 399.8 $[MH_2]^{2+}$ (calcd 400.01). UV-vis (CH_2Cl_2, nm): 421, 515, 549, 594, 650.

A solution of amide intermediate (142 mg, 0.178 mmol) in 14 mL of TFA was treated with concentrated HCl (15 mL). The mixture was heated at 80 °C for 22 h. The mixture was cooled, diluited with water and extracted with CH_2Cl_2. The organic layer was washed with water and saturated aqueous $NaHCO_3$. The organic layer was dried (Na_2SO_4) and concentrated. The residue obtained was chromatographed (silica, CH_2Cl_2) to afford a purple solid (98.1 mg, 73%). ^{1}H-NMR ($CDCl_3$, 250 MHz) δ: 8.86 (d, 2H), 8.67 (d, 2H), 8.62 (s, 4H), 7.97 (d, 2H), 7.24-7.28 (m, 6H), 7.05 (d, 2H), 4.02 (brs, 2H), 2.60-2.64 (m, 9H), 1.83-1.87 (m, 18H), -2.55 (brs, 2H). ESI-MS $C_{53}H_{49}N_5$ (CH_3CN + 1% HCOOH as eluent) m/z: obsd 757.9 $[MH]^+$ (calcd 756.99), obsd 379.0 $[MH_2]^{2+}$ (calcd 378.99). UV-vis (CH_2Cl_2, nm): 422, 517, 552, 595, 652.

3.4.3 Synthesis of 5-(4-aminophenyl)-10,15,20-tri-(3,5-di-*tert*-butylphenyl) porphyrin, T

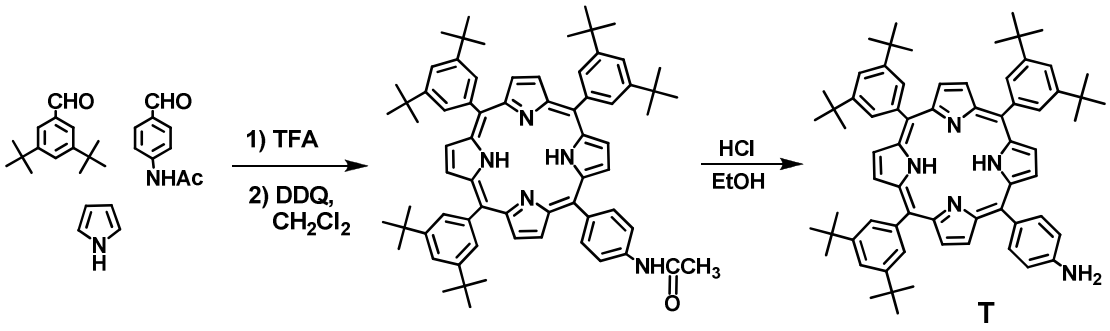

Following a literature method,[8] (1.637 g, 7.5 mmol) and *p*-acetamidobenzaldehyde (0.410 g, 2.5 mmol) were dissolved in 1 L of CH_2Cl_2 contained in a 2 L three-neck flask. The flask was covered with aluminium foil and purged with N_2 for 10 min before freshly-distilled pyrrole (700 μL, 10 mmol) was injected. The reaction was stirred for another 10 min, and the reaction was initiated by the injection of TFA (1.4 mL, 20 mmol). After stirring at room temperature for 1 h, DDQ (1.70 g, 7.5 mmol) was added. The reaction was stirred for 1 h at room temperature and was then neutralized with triethylamine (2.8 mL, 20 mmol). The crude mixture was purified with silica gel flash chromatography; elution with CH_2Cl_2 was able to remove tetraphenylporphyrin, and then with 20% EtOAc in CH_2Cl_2 to collect the desired mono-porphyrin product. Solvent was removed under vacuum, affording a purple solid in a yield of ~18 %. ^{1}H-NMR ($CDCl_3$, 250 MHz) δ: 8.8 ppm (m, 6H, βH), 8.5 ppm (d, 2H, βH), 8.0 ppm (m, 6H, Ar-meta-H), 7.9 ppm (d, 2H, ArH), 7.7 ppm (m, 3H, Ar-para-H), 7.4 ppm (d, 2H, ArH), 7.1 ppm (s, 1H, NH), 2.0 ppm (s, 3H, CH_3), 1.4 ppm (s, 54H, *tert*-BuH), -2.8 ppm (s, 2H, pyrrole H). ESI-MS $C_{70}H_{81}N_5O$ (CH_3CN + 1% HCOOH as eluent) m/z: obsd 1007.9 $[MH]^+$ (calcd 1008.64), obsd 504.2 $[MH_2]^{2+}$ (calcd 504.82). UV-Vis (CH_2Cl_2, nm): 421, 513, 548, 592, 647.

Porphyrin-amide (0.2067 g, 0.2 mmol) was dissolved in 60 mL EtOH in a 250 mL flask. Concentrated HCl (40 mL, 6 M) was added to the reaction mixture, which was heated at reflux for 13 h. The crude mixture was cooled, diluted with water and extracted with CH_2Cl_2 six times. The organic layer was washed with H_2O three times and with saturated $NaHCO_3$ solution twice. The pooled organic layer was dried over Na_2SO_4 and filtered. The solvent was removed under vacuum and flash chromatography with silica gel and CH_2Cl_2 afforded the desired porphyrin in quantitative yield. ^{1}H-NMR ($CDCl_3$, 250 MHz) δ: 8.8

ppm (m, 8H, βH), 8.0 ppm (m, 6H, Ar-meta-H), 7.9 ppm (d, 2H, ArH), 7.7 ppm (m, 3H, Ar-para-H), 6.9 ppm (d, 2H, ArH), 3.9 ppm (s, 2H, NH2), 1.4 ppm (d, 54H, tert-BuH), -2.7 ppm (s, 2H, pyrrole H). ESI-MS $C_{68}H_{79}N_5$ (CH_3CN + 1% HCOOH as eluent) m/z: obsd 966.8 $[MH]^+$ (calcd 966.63), obsd 483.5 $[MH_2]^{2+}$ (calcd 483.82). UV-vis (CH_2Cl_2, nm): 422, 515, 550, 593, 649.

3.4.4 Synthesis of Bis(Phenyl-Porphyrin) Homodimer, PP

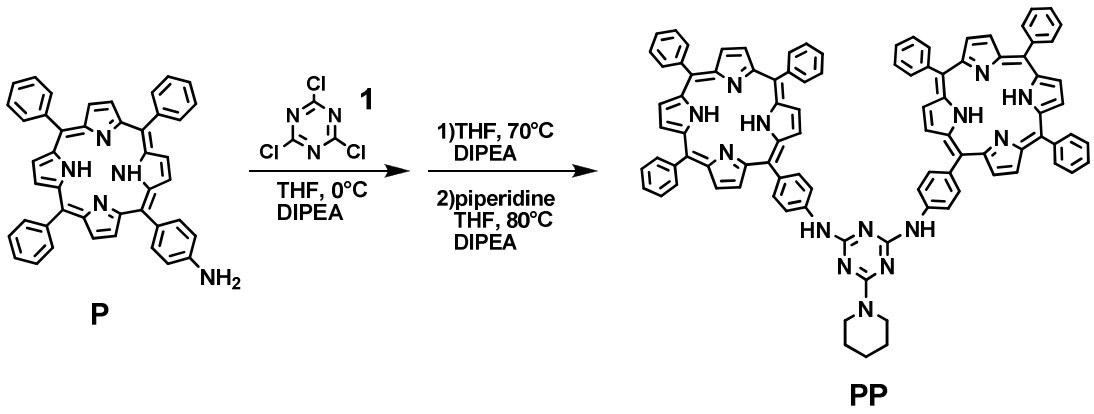

To a solution of porphyrin **P** (10 mg, 16 μmol) in THF (1.0 mL) cooled at 0 °C were added a THF solution of cyanuric chloride **1** (2.9 mg, 16 μmol) and DIPEA (2.5 mg, 19 μmol). After 10 minutes under stirring the solution was left to reach room temperature. The reaction was complete as witnessed by TLC analysis (silica gel, petroleum ether/ethyl acetate 3:2 v/v) showing the disappearance of porphyrin **P** (R_f = 0.33). More porphyrin **P** (10 mg, 16 μmol) was then added at room temperature together with 1.2 equivalents of DIPEA and the reaction was monitored by TLC (eluent: petroleum ether/ethyl acetate 3:2 v/v). ESI-MS $C_{91}H_{60}ClN_{13}$ (CH_3CN + 1% HCOOH as eluent) m/z: obsd $[MH]^+$ 1371.5 (calcd 1371.99), obsd $[MH_2]^{2+}$ 686.3 (calcd 686.50), obsd $[MH_3]^{3+}$ 457.8 (calcd 457.50), obsd $[MH_4]^{4+}$ 343.6 (calcd 343.75). After 24 h an excess of piperidine (4.1 mg, 48 μmol) was added together with 1.2 equivalents of DIPEA and the mixture was stirred at 80 °C. A purple solid formed. After 3 h the solvent was evaporated and the solid was subjected to flash column chromatography on silica-gel (eluent: petroleum ether/ethyl acetate 3:2 v/v) to give 16 mg of **PP** as a purple solid (71% yield). ^{1}H-NMR ($CDCl_3$, 250 MHz) δ: 8.98 (m, 4H, β-pyrrole), 8.96 (m, 12H, β-pyrrole), 8.23-7.68 (m, 38H, porphyrin phenyl aromatic protons), 7.07 (s, broad, 2H, NH), 3.99 (s, 4H, ortho piperidine), 1.75 (s, 6H, meta\para

piperidine), -2.75 (s, 4H, pyrrole NH). ESI-MS $C_{96}H_{70}N_{14}$ (CH_3CN + 1% HCOOH as eluent) m/z: obsd 1420.5 $[MH]^+$ (calcd 1420.68), obsd 710.5 $[MH_2]^{2+}$ (calcd 710.84), obsd 474.1 $[MH_3]^{3+}$ (calcd 474.23), obsd 355.8 $[MH_4]^{4+}$ (calcd 355.92). UV-vis (CH_2Cl_2, nm): 419, 512, 552, 592, 647.

3.4.5 Synthesis of Bis(Phenyl-Porphyrin-Zn^{II}) Homodimer, P(Zn)P(Zn)

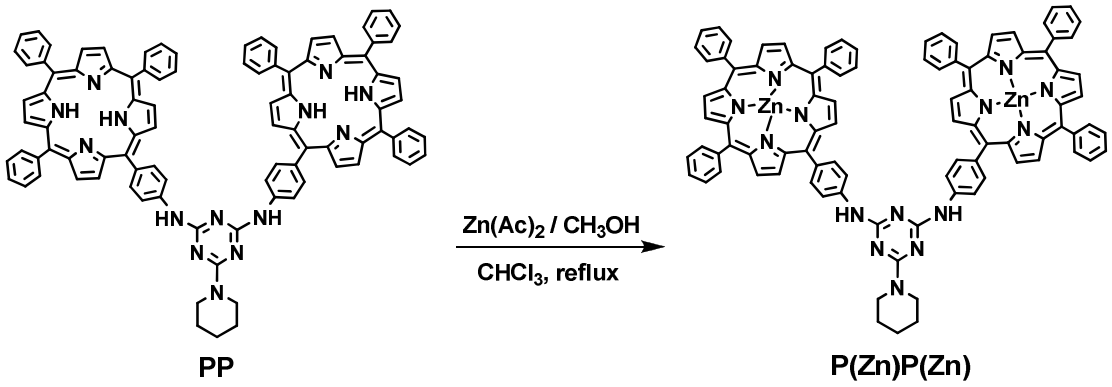

To a solution of **PP** (10 mg, 7 μmol) in $CHCl_3$ (5 mL) was added a saturated solution of zinc acetate (0.5 mL) in CH_3OH and refluxed for 1 h. The solvent was evaporated. The residue was dissolved with CH_2Cl_2 and washed with water in order to remove zinc acetate excess. The organic phases were combined, dried over Na_2SO_4, filtered and concentrated under reduced pressure to give a purple solid. Yield 97%. ^{1}H-NMR ($CDCl_3$, 250 MHz) δ: 9.08 (d, 2H, β-pyrrole), 8.94 (m, 6H, β-pyrrole), 8.24-7.74 (m, 19H, porphyrin phenyl aromatic protons), 7.07 (s, broad, 1H, NH), 3.84 (s, 4H, ortho piperidine), 1.67 (s, 6H, *m*-H and *p*-H piperidine). UV-vis (CH_2Cl_2, nm): 423 (Soret band, ε = 1'156'205 $M^{-1}cm^{-1}$), 551 (ε = 71'800 $M^{-1}cm^{-1}$), 592 (ε = 52'900 $M^{-1}cm^{-1}$).

3.4.6 Synthesis of (Phenyl-Porphyrin)(Mesityl-Porphyrin) Heterodimer, PM

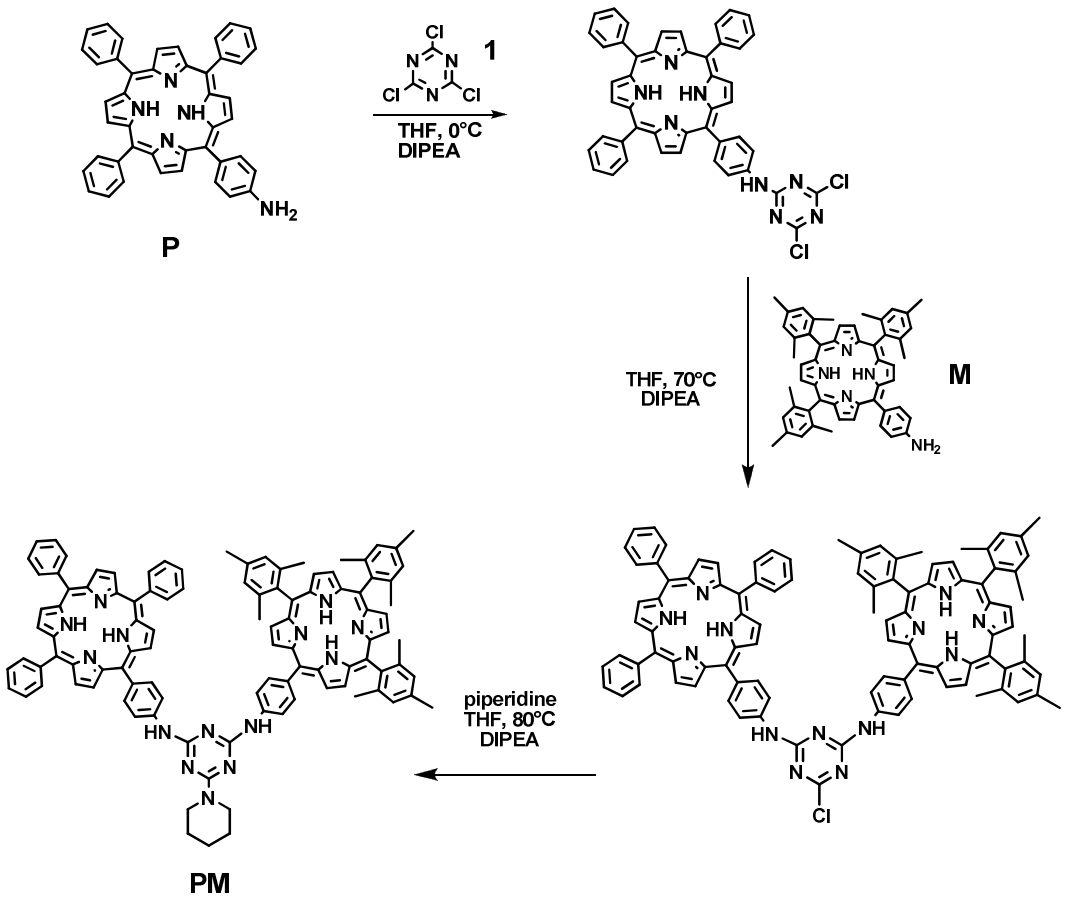

To a solution of porphyrin **P** (10 mg, 13 μmol) in THF (1.0 mL) cooled at 0 °C were added a THF solution of cyanuric chloride **1** (2.4 mg, 13 μmol) and DIPEA (2 mg, 16 μmol). After being stirred for 10 min at 0 °C, the solution was left to reach room temperature. TLC analysis (silica gel, petroleum ether/ethyl acetate 3:1 v/v) showed the disappearance of porphyrin **P** (R_f = 0.33) and the formation of a new TLC spot at R_f = 0.72 corresponding to the monoadduct derivative between **P** and cyanuric chloride. One equivalent of porphyrin **M** (8.3 mg, 13 μmol) was then added together with 1.2 equiv of DIPEA and the reaction was stirred at 80 °C for 24 h. After, an excess of piperidine (3.3 mg, 39 μmol) was added together with 1.2 equiv of DIPEA (6.2mg, 48 μmol) and the mixture was stirred at 80 °C for a further 3 h. The solvent was evaporated and the purple solid was purified by flash silica gel chromatography (silica gel, petroleum ether/ethyl acetate 3:1 v/v) to afford 18 mg of **PM** derivative (88% yield). ^{1}H-NMR ($CDCl_3$, 250 MHz) δ: 8.84 (m, 4H, β-pyrrole), 8.68-8.61 (m, 12H, β-pyrrole), 8.22-8.06 (m, 21H, phenyl aromatic protons), 7.77-7.67 (m, 8H, phenyl amino), 4.00 (br, s, 4H, piperidine), 2.62 (s, 9H, mesityl), 1.84

(br s, 18H, mesityl), 1.74 (s, 6H, piperidine), -2.54 (s, 2H, pyrrole mesitylporphyrin), -2.64 (s, 2H, pyrrole phenylporphyrin). ESI-MS $C_{105}H_{88}N_{14}$ (CH_3CN + 1% HCOOH as eluent) m/z: obsd 1546.8 $[MH]^+$ (calcd 1546.92), obsd 771.9 $[MH_2]^{2+}$ (calcd 773.96), obsd 516.1 $[MH_3]^{3+}$ (calcd 516.32), obsd 387.4 $[MH_4]^{4+}$ (calcd 387.49). UV-vis (CH_2Cl_2, nm): 420, 516, 552, 593, 647. Elem. Anal. calcd for $C_{105}H_{88}N_{14}$: C, 81.58; H, 5.74; N, 12.68. Found: C, 81.33; H, 5.90; N 12.70.

3.4.7 Synthesis of (Phenyl-Porphyrin-Zn^{II})(Mesityl-Porphyrin-Zn^{II}) Heterodimer, P(Zn)M(Zn)

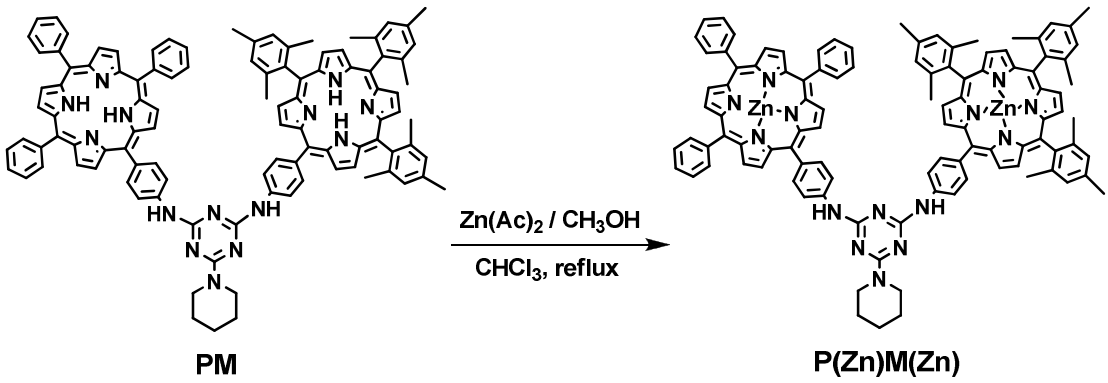

To a solution of **PM** (10 mg, 7 μmol) in 5 mL of $CHCl_3$ was added a saturated solution of zinc acetate in CH_3OH (0.5 mL) and then the mixture was refluxed for 1 h. After removing the solvent, the residue was dissolved with CH_2Cl_2 and washed with water in order to remove the excess of zinc salt. The organic phase was dried over Na_2SO_4 then filtered and the solvent was evaporated under reduced pressure to give a purple solid that was purified by short column chromatography on silica gel (eluent: $CHCl_3$). Yield: 93%. ^{1}H-NMR ($CDCl_3$, 250 MHz) δ: 8.84 (m, 4H, β-pyrrole), 8.68-8.61 (m, 12H, β-pyrrole), 8.22-8.06 (m, 21H, phenyl aromatic protons), 7.77-7.67 (m, 8H, phenyl amino), 4.00 (br s, 4H, ortho piperidine), 2.62 (s, 9H, *p*-methylphenyl), 1.84 (br s, 18H, *o*-methylphenyl), 1.74 (s, 6H, *m*-H and *p*-H piperidine). UV-vis (CH_2Cl_2, nm): 423 (ε = 1'168'000 M^{-1} cm^{-1}), 551, 592.

3.4.8 Synthesis of Bis(Mesityl-Porphyrin) Homodimer, MM

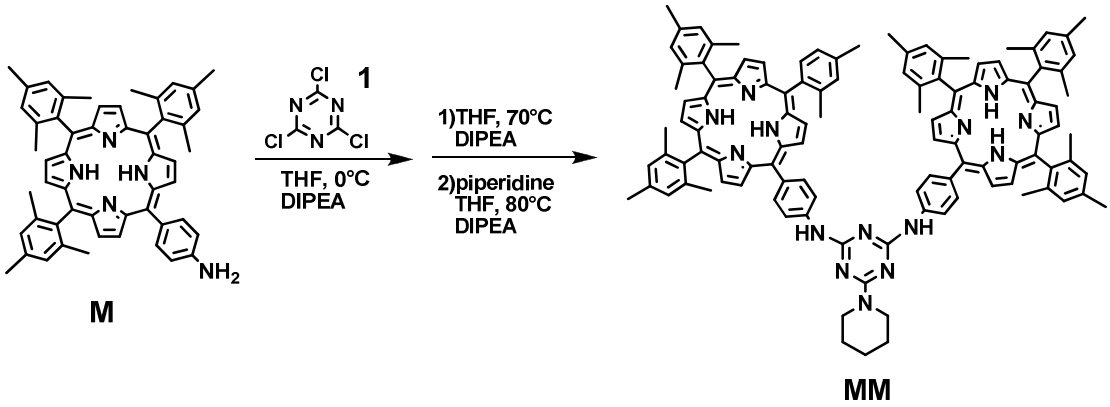

To a solution of porphyrin **M** (10 mg, 13 μmol) in THF (1.0 mL) cooled at 0 °C were added a THF solution of cyanuric chloride **1** (2.4 mg, 13 μmol) and DIPEA (2 mg, 16 μmol). After being stirred for 10 min at 0 °C, the solution was left to reach room temperature. The reaction was complete, as resulting from TLC analysis (silica gel, petroleum ether/ethyl acetate 5:1 v/v) showing the disappearance of porphyrin **M** (R_f = 0.38). A second equivalent of porphyrin **M** (10 mg, 13 μmol) was added together with 1.2 equiv of DIPEA and the reaction was stirred at 80 °C for 24 h. Then, an excess of piperidine (3.4 mg, 39 μmol) was added together with 1.2 equiv of DIPEA and the mixture was stirred at 80 °C for 3 h. After removal of the solvent, the residue was purified by flash silica gel chromatography (eluent: petroleum ether/ethyl acetate 5:1 v/v) affording 20mg of **MM** derivative. Yield: 90%. ^{1}H-NMR ($CDCl_3$, 250 MHz) δ: 8.88 (m, 4H, β-pyrrole), 8.69-8.62 (m, 12H,β-pyrrole), 8.21-8.04 (m, 20H, phenyl aromatic protons), 7.05 (br s, 2H, NH), 3.99 (br s, 4H, piperidine), 2.61 (s, 18H, mesityl), 1.84 (br s, 36H, mesityl), 1.74 (s, 6H, piperidine), -2.56 (s, 4H, pyrrole NH). ESI-MS $C_{113}H_{104}N_{14}$ (CH_3CN + 1% HCOOH as eluent) m/z: obsd 1672.9 $[MH]^+$ (calcd 1673.16), obsd 837.0 $[MH_2]^{2+}$ (calcd 837.08), obsd 558.3 $[MH_3]^{3+}$ (calcd 558.39), obsd 419.0 $[MH_4]^{4+}$ (calcd. 419.05). UV-vis (CH_2Cl_2, nm): 420, 516, 550, 593, 648. Elem. Anal. calcd for $C_{114}H_{106}N_{14}$: C, 81.88; H, 6.39; N, 11.73. Found: C, 82.10; H, 6.52; N 12.03.

3.4.9 Synthesis of Bis(Mesityl-Porphyrin-Zn^{II}) Homodimer, M(Zn)M(Zn)

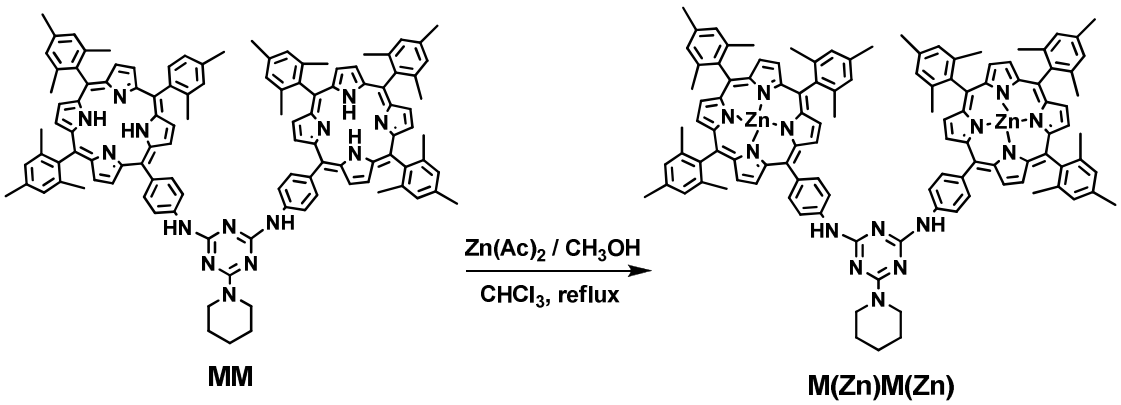

To a solution of **MM** (10 mg, x μmol) in 5 mL of $CHCl_3$ was added a saturated solution of zinc acetate (0.5 mL) in CH_3OH and refluxed for 1 h. The solvent was evaporated. The residue was dissolved with CH_2Cl_2 and washed with water in order to remove zinc acetate excess. The organic phases were combined, dried over Na_2SO_4, filtered and concentrated under reduced pressure to give a purple solid (97% yield). ^{1}H-NMR ($CDCl_3$, 250 MHz): δ 8.98 (m, 4H, β-pyrrole), 8.78-8.71 (m, 12H, β-pyrrole), 8.23-8.06 (m, 20H, phenyl aromatic protons), 7.07 (br s, 2H, NH), 4.00 (br s, 4H, piperidine), 2.63 (s, 18H, mesityl), 1.85 (br s, 36H, mesityl), 1.74 (s, 6H, piperidine). UV-vis (CH_2Cl_2, nm): 423 (ε = 1'121'000 M^{-1} cm^{-1}), 550, 593.

3.4.10 Synthesis of Bis(3,5-di-*tert*-Butylphenyl-Porphyrin) Homodimer, TT

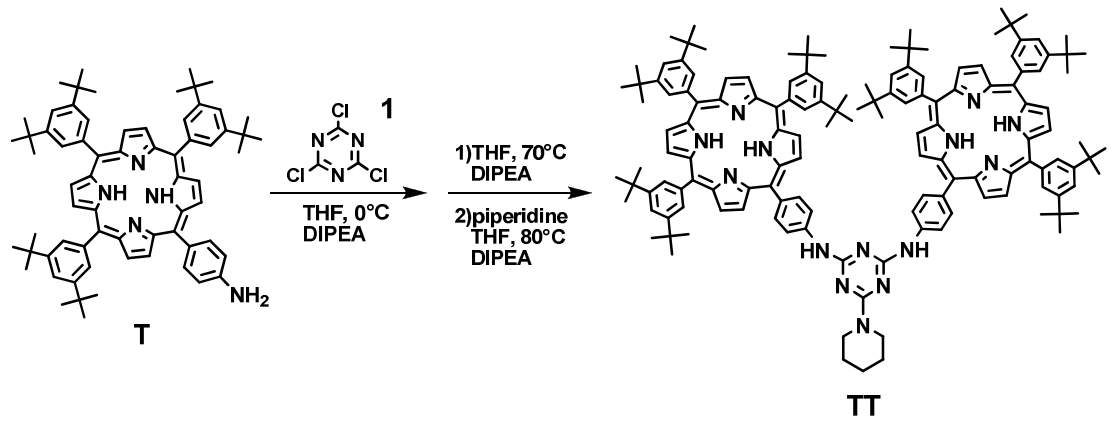

To a solution of porphyrin **T** (19.1 mg, 20 μmol) in THF (1.0 mL) cooled at 0 °C were added a THF solution of cyanuric chloride **1** (3.7 mg, 20 μmol) and DIPEA (3 mg, 24

μmol). After being stirred for 10 min at 0 °C, the solution was left to reach room temperature. The reaction was complete, as resulting from TLC analysis (silica gel, petroleum ether/ethyl acetate 3:2 v/v) showing the disappearance of porphyrin **T** (R_f = 0.31) and the formation of a new TLC spot at R_f = 0.63 corresponding to the monoadduct derivative between porphyrin **T** and cyanuric chloride. A second equivalent of porphyrin **T** (19.1 mg, 20 μmol) was then added together with 1.2 equiv of DIPEA and the reaction was stirred at 80 °C for 24 h then an excess of piperidine (5.0 mg, 60 μmol) was added together with 1.2 equiv of DIPEA and the mixture was stirred at 80 °C for 3h. After removal of the solvent, the residue was purified by flash silica gel chromatography (eluent: petroleum ether/ethyl acetate 3:2 v/v) affording 70 mg of **TT** derivative. Yield: 82%.^{1}H-NMR ($CDCl_3$, 250 MHz) δ: 9.09 (d, 4H, β-pyrrole), 9.02 (m, broad 12H,β-pyrrole), 8.04 (d, 4H, phenyl aromatic protons near triazine ring), 8.10-7.78 (m, 14H, phenyl aromatic protons) 7.19 (br s, 2H, NH), 3.99 (br s, 4H, piperidine), 1.74-1.68 (br s, 6H, piperidine), -2.46 (s, 4H, pyrrole NH). ESI-MS $C_{144}H_{166}N_{14}$ (CH_3CN + 1% HCOOH as eluent) m/z: obsd 2093.4 $[MH]^+$ (calcd 2093.95), obsd 1047.5 $[MH_2]^{2+}$ (calcd 1047.48), obsd 698.7 $[MH_3]^{3+}$ (calcd 698.65), obsd 524.4 $[MH_4]^{4+}$ (calcd. 524.24). UV-vis (CH_2Cl_2, nm): 421, 517, 551, 594, 649.

3.4.11 Synthesis of Bis(3,5-di-*tert*-butylphenyl-porphyrin-Zn^{II}) Homodimer, T(Zn)T(Zn)

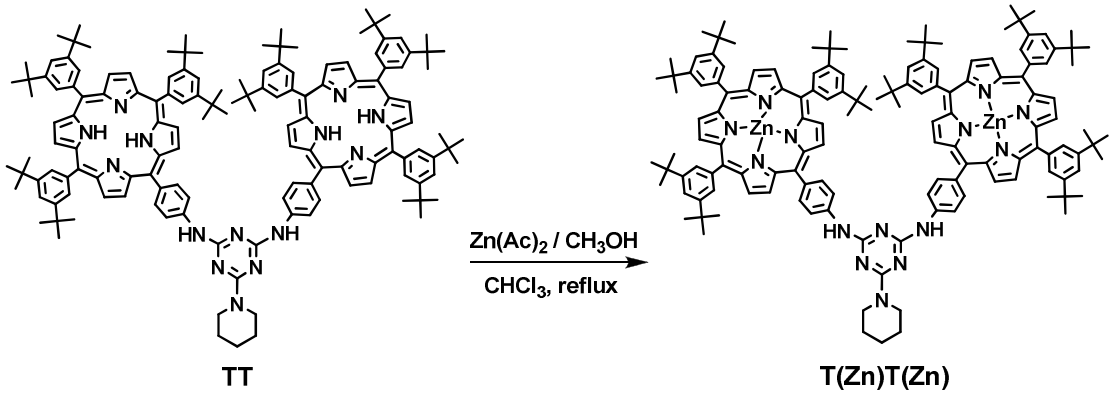

To a solution of **TT** (40 mg, 19 μmol) in 5 mL of $CHCl_3$ was added a saturated solution of zinc acetate (0.5 mL) in CH_3OH and refluxed for 1 h. The solvent was evaporated. The residue was dissolved with CH_2Cl_2 and washed with water in order to remove zinc acetate excess. The organic phases were combined, dried over Na_2SO_4, filtered and concentrated

under reduced pressure to give a purple solid (96% yield). ^{1}H-NMR ($CDCl_3$, 250 MHz) δ: 9.09 (d, 4H, β-pyrrole), 9.02 (m, broad 12H,β-pyrrole), 8.04 (d, 4H, phenyl aromatic protons near triazine ring), 8.10-7.78 (m, 14H, phenyl aromatic protons) 7.19 (br s, 2H, NH), 3.99 (br s, 4H, piperidine), 1.74-1.68 (br s, 6H, piperidine). UV-vis (CH_2Cl_2, nm): 425 (Soret band, ε = 1'055'830 $M^{-1}cm^{-1}$), 553, 596.

3.4.12 Synthesis of Supported Bis(Phenyl-Porphyrin-Zn^{II}) Homodimer P(Zn)P(Zn)

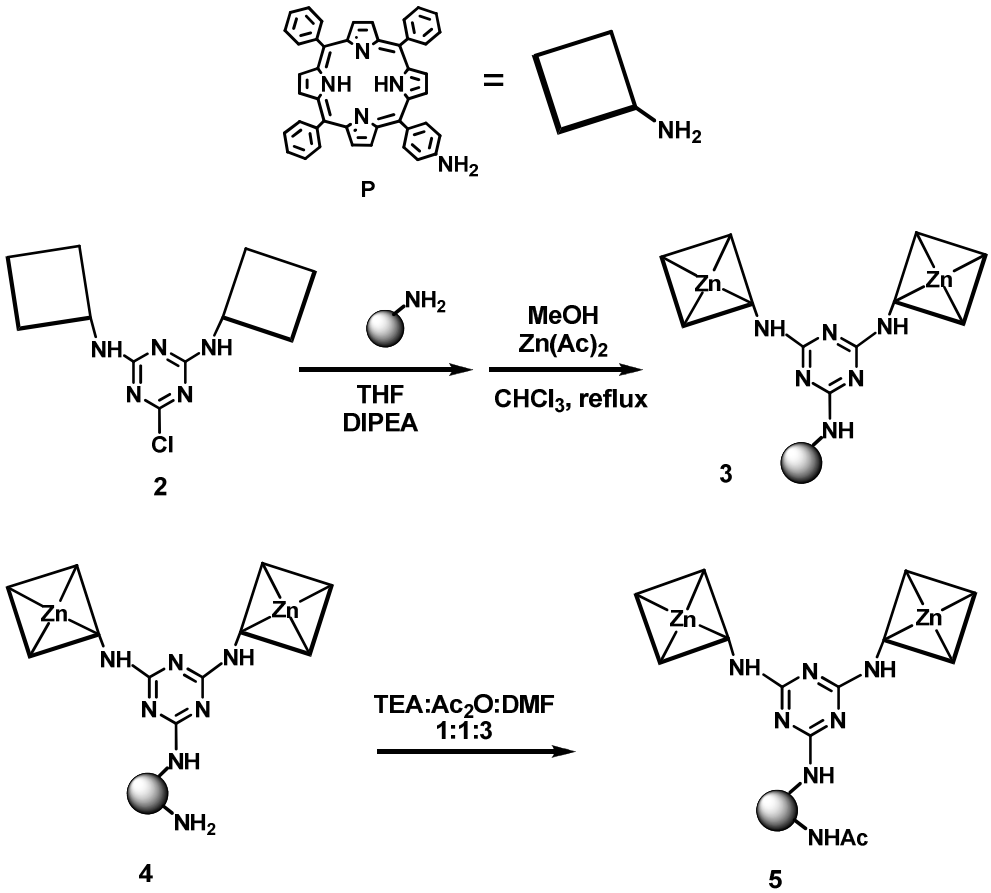

The monochloro dimer **2** was formed upon reaction of the amino-porphyrin **P** with cyanuric chloride in the presence of DIPEA, following the one-pot protocol used to prepare all the previous described dyads. The resin was left to swell for 1 h before reacting in the same solvent used for reaction (tetrahydrofuran). To a solution of monochloro dimer **2** (8.5 mg, 6 μmol) and DIPEA (1 mg, 7 μmol) in 1 mL of THF was added TG-NH_2 resin (110 mg, 23 μmol NH_2). The mixture was stirred and heated at 80 °C until complete discoloration of the supernatant solution with formation of purple-coloured beads, compound **3**. Then, the functionalized resin was collected by filtration and washed

extensively with THF in order to remove unreacted and adsorbed products. Metalation with $Zn(Ac)_2$ takes place smoothly in MeOH/$CHCl_3$ mixture affording the bis(porphyrin-Zn^{II}) adduct **4**. According to the TG-NH_2/dimer stoichiometry adopted, the supported tweezer corresponds to 1% of the overall amino functionalities of the beads.
In order to avoid any competitive intra-bead Zn-coordination, free-amino metalated beads (**4**) were immersed in 2 mL of a solution containing triethylamine, acetic anhydride and dimethylformamide in 1:1:3 ratios. The mixture was stirred for 1 h at 80 °C, following the reaction with bromophenol blu test. Then, the beads were washed with DMFx3, MeOHx3, $CHCl_3$x3, EtOHx3, CH_2Cl_2x3 and THFx3 to give the desired capped resin **5**.

The same protocol was used to synthesize CPG-sensor materials, previous functionalization illustrated in the discussion part.[9]

REFERENCES

[1] Carofiglio, T.; Lubian, E.; Menegazzo, I.; Saielli, G.; Varotto, A., *J. Org. Chem.*, **2009**, *74*, 9034.

[2] Gans, P.; Sabatini, A.; Vacca, A., *Talanta*, **1996**, *43*, 1739.

[3] G. de Velde, F. M.; Bikelhaupt, E. J.; Baerends, C.; Fonseca Guerra, S. J. A.; van Gisbergen, J. G.; Snijders, T. Ziegler, *J. Comput. Chem.*, **2001**, *22*, 931.

[4] (a) Becke, A. D., *Phys. Rev. A*, **1998**, *38*, 3098. (b) Lee, C.; Yang, W.; Parr, G., *Phys. Rev. B*, **1988**, *37*, 785. c) Miehlich, B.; Savin, A.; Stoll, H.; Preuss, H., *Chem. Phys. Lett.*, **1989**, *157*, 200.

[5] Kruper, W. J.; Chamberlin, T. A.; Kochanny, M.; Lang, K. *J. Org. Chem*. **1989**, *54*, 2753.

[6] (a)Hasegawa, E., et al, *Eur.Poly.J.* **1978**, *14*,123. b)Tsuchida, E., *J.Macromol.Sci.***1979**, *(4)*, 545.

[7] (a) Lindsey, J. S.; Schreiman, I. C.; Hsu, H. C.; Kearney, P. C.; Marguerettaz, A. M., *J. Org. Chem.*, **1987**, *52*, 827. (b) Speckbacher, M.; Yu, L.; Lindsey, J. S., *Inorg. Chem.* **2003**, *42*, 4322.

[8] Fazio, M.A.; Lee, O.P.; Schuster, D.I., *Org. Lett.,* **2008**, *10*, 4979.

[9] Lubian, E.; Baldini, F.; Giannetti, A.; Trono, C.; Carofiglio, T., *Chem. Commun*. **2010**, *46*, 3678.

Chapter II

Novel Sterically Encumbered and CD Sensitive Zn-Porphyrin Tweezer as a Probe for Molecular Chirality

INTRODUCTION

1.1 Supramolecular Chirogenesis

Thus far, supramolecular chirogenesis has attracted much attention in the scientific community and has become a fast growing interdisciplinary field of chemistry based on the principles of supramolecular chemistry and molecular chirality due to its vital importance in many natural and artificial systems, its requirement for addressing many fundamental science issues, and as a basis for numerous modern molecular technologies.[1] Therefore, understanding the mechanisms and various influencing factors is of particular significance for smart control and further effective application of supramolecular chirogenesis.

Supramolecular chirality forms an integral part of natural systems, examples of which include the DNA double helix and the secondary helical structure of proteins assembled by noncovalent interactions.[2] Furthermore, it plays an important role in the fields of asymmetric catalysis and autocatalysis,[3] non-linear optics,[4] polymer science,[5] molecular recognition, and self-assembly[6] and in design of molecular devices.[7] In addition, this phenomenon has proved to be a useful tool in the determination of the absolute configuration of chiral compounds through the *chirality induction* mechanism.[8] This is a symmetry breaking of achiral multi- or unimolecular systems upon noncovalent interactions with chiral environments. This phenomenon is associated with the processes of chirality information transfer and can be produced through direct synthetic modifications and/or by external asymmetric induction via self-assembly, axial ligation, or aggregation processes.

Since noncovalent interactions are the key elements in chirality induction, there are several internal (steric and electronic) and external (temperature, pH, polarity, viscosity) factors which may affect these supramolecular interactions and as a result the chirality induction in these systems.[9,10]

1.1.1 Chiral Compounds

Chiral molecules are characterized by three-dimensional handedness and can exist in two enantiomeric forms of opposite absolute configuration (AC). Most natural products and biologically active compounds are chiral and their biological and molecular functions

are closely related to their chirality, that is, AC and conformation. Furthermore, many drugs derived from natural products or of purely synthetic origin are currently used in enantiopure form. Therefore, the unambiguous determination of the AC of chiral compounds is critical for the studies of natural products and biomolecular systems.[11]

The characterization of chiral natural products could be investigated using different spectroscopy techniques, like circular dichroism (CD) spectroscopy in the UV-visible region as well as optical rotation (OR), which are fundamental constants for chiral compounds. In particular, CD is a very sensitive diagnostic tool for determining not only AC and conformation, but also for monitoring intermolecular interactions where chiral systems are involved.

1.1.2 Properties of Light and Circular Dichroism Spectroscopy

Linearly polarized light is composed of left- and right-circularly polarized light (l-CPL and r-CPL) with equal intensity, and the electromagnetic fields of these circularly polarized lights are mirror images of each other. When these components pass through a chiral medium the interaction of chiral material with l-CPL is not equal to that with r-CPL. As consequence, these interactions generated differences in light velocity and refractive index. This phenomenon is called optical rotation and the instrument for OR measurement is called polarimeter. Another phenomenon is that the absorption intensity of l-CPL with a chiral material is unequal to that of r-CPL, and this phenomenon generates circular dichroism, CD. In the latter case, the polarization plane of the transmitted light is rotated by an angle α compared to that of the incident light. At the same time the transmitted light is no longer linearly polarized but is ellipsoidally polarized (Figure 1.1).

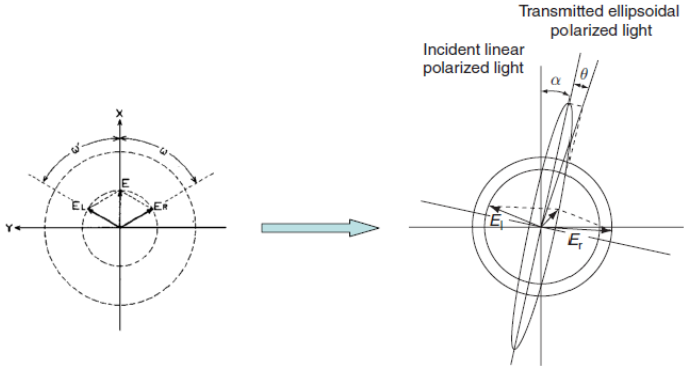

Figure 1.1: definition of optical rotation and circular dichroism. α, rotation angle; θ, ellipticity angle; E_l and E_r, electric field vectors of left- and right-circularly polarized lights, respectively.

The absorption coefficients (ε) of these two components change and become unequal and the angle θ of the ellipsoidally polarized transmitted light is defined as the ellipticity angle.[12,13]

Usually, circular dichroism is expressed in term of molar ellipticity, [θ]:

$$[\theta] = \frac{\theta M}{lc}$$

where θ is the observed ellipticity angle (degree = °), *M* the molecular or formula weight, *l* the cell length (dm = 10 cm), and *c* the concentration (g solute/100 cm^3 solution).

In the case of organic compounds, molar circular dichroism, Δε, is preferentially used and it is defined as the difference between the absorption coefficient ε_l for l-CPL and coefficient ε_r for r-CPL:

$$\Delta\varepsilon = \varepsilon_l - \varepsilon_r$$

where Δε is expressed $dm^3\ mol^{-1}\ cm^{-1}$).

Molar circular dichroism and molar ellipticity, [θ], are readily interconverted by the equation:

$$[\theta] = 3298\ \Delta\varepsilon$$

The intensity scale (or sensitivity) of a CD spectropolarimeter is generally expressed in millidegrees (m°)/cm, and therefore molar CD (Δε) is calculated as follows:

$$\frac{sensitivity\ (m°/cm) \times CD\ signal\ (cm)}{33000} = \Delta A = \Delta\varepsilon \times c' \times l'$$

A curve plotting Δε or [θ] against wavelength λ (nm) is called the CD spectrum, which generally shows a positive or negative band at the region of the corresponding UV-vis absorption band (Figure 1.2). These bands are called Cotton effects. A positive CD band is named a positive Cotton effect while a negative CD band is called a negative Cotton effect.

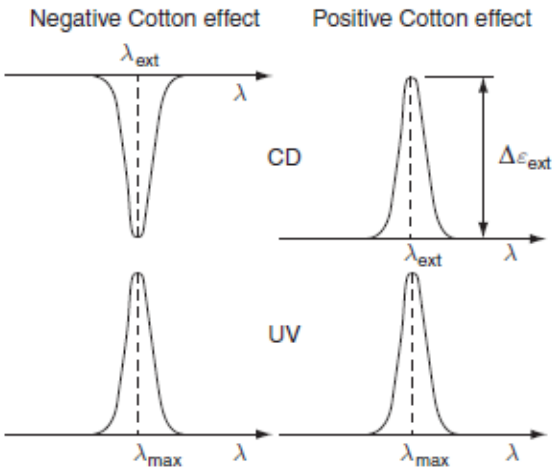

Figure 1.2: The general pattern of CD and UV spectra.

The sign and strength of CD Cotton effect is experimentally obtainable from the observed CD spectra and is formulated as the rotational strength R,[13,14,15]

$$R = k \int \frac{\Delta\varepsilon(\sigma)}{\sigma} d\sigma$$

where σ is wavenumber (cm^{-1}), k is a constant (2.296×10^{-39})

The rotational strength R is a function of the scalar product of electric (μ) and magnetic (M) transition moments:

$$\langle 0|\boldsymbol{\mu}|a\rangle \cdot \langle a|\boldsymbol{M}|0\rangle$$

The electric and magnetic moments are based on the linear and angular momentum of electrons involved in the transition. The angular momentum corresponds to the rotational motion of an electron, while the linear momentum corresponds to the linear motion of the electron. If the electric and magnetic moment vectors are parallel to each other in one enantiomer, they should be antiparallel in the other one. In particular, in the former case the rotational strength R is positive leading to a positive Cotton effect, while when the rotational strength R is negative, a negative CD Cotton effect is observed. Therefore, the rotational strength R, and CD spectra of enantiomers are opposite in sign but of equal intensity.

The problem of how to determine the absolutes configurations of chiral compounds in a theoretical manner is to calculate the rotational strength R by the use of equation

reported above. For this purpose, several theoretical methods have been developed and only one will be described in the following section.

If the CD Cotton effect is approximated by a Gaussian distribution, the CD curve is formulated as

$$\Delta\varepsilon(\sigma) = \Delta\varepsilon_{ext}\, exp\left\{-\left(\frac{\sigma-\sigma_0}{\Delta\sigma}\right)^2\right\}$$

where $\Delta\varepsilon_{ext}$ is the extremum value of the Cotton effect, σ_0 the central wavenumber of the Cotton effect, and $\Delta\sigma$ half the bandwidth at $1/e$ peak height of the Gaussian curve (Figure 1.3).

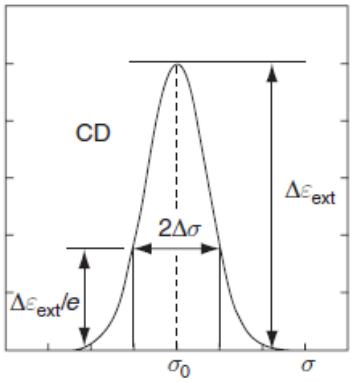

Figure 1.3: CD Cotton effect curve approximated by the Gaussian distribution, where $2\Delta\sigma$ is the bandwidth at 1/e peak height, e = 2.71828, and 1/e = 0.36788.

By substitution of this last equation on the relation that represents the rotational strength *R* and rearranging, the calculated CD curve results formulated as

$$\Delta\varepsilon(\sigma) = \left(\frac{\sigma_0}{2.296\times10^{-39}\sqrt{\pi}\,\Delta\sigma}\right)Rexp\left\{-\left(\frac{\sigma-\sigma_0}{\Delta\sigma}\right)^2\right\}$$

where $\Delta\sigma$ can be evaluated from the corresponding observed UV–vis spectra. Thus, if the rotational strength *R* is theoretically calculated by the reported equation, the CD spectral curve is reproducible by theoretical calculation.

1.2 CD Exciton Chirality Method: Basic Principles

For the calculation of rotational strength *R*, there are several theoretical method, such as CD exciton chirality,[13,16] De Voe[17,18] calculation, π-electron SCF-CI-DV MO (*Self-Consistent Field-Configuration Interaction-Dipole Velocity-Molecular Orbital*),[13,19] and *Ab Initio* Molecular Orbital calculations,[20] but the most widely used is the *CD exciton chirality* method. This method allows to deduce the absolute configuration (AC) of a variety of natural products without any reference compound.

The basic principles of the CD exciton chirality method could be explained considering two chromophores (*j* and *k*) within a molecule, that show an intense absorption in the range of UV-vis region due to their π-π* transition between the ground state and the excited state. The electric transition moments of the two chromophores *j* and *k* interact with each other causing the split of the excited state in two energy levels, α and β states (Figure 1.4), whereas the ground states remain unsplit.[13] This phenomenon is called *exciton coupling* or *exciton interaction*.[13,21] Thus the transitions between the ground state and the excited state will be two, 0 → α and 0 → β. Usually, the α-state is lower in energy than the β-state.

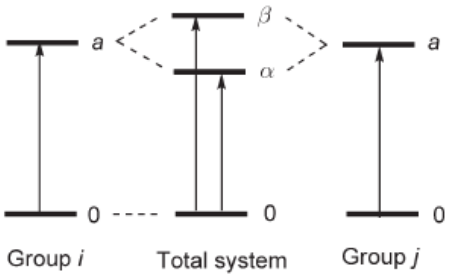

Figure 1.4: CD exciton chirality method.

The α-state corresponds to the transitions at longer wavelength, while the β-state corresponds to the transitions at shorter wavelength, called first and second Cotton effect respectively. In the bisignate CD spectrum these two bands are equal in intensity and opposite in sign (Figure 1.5).

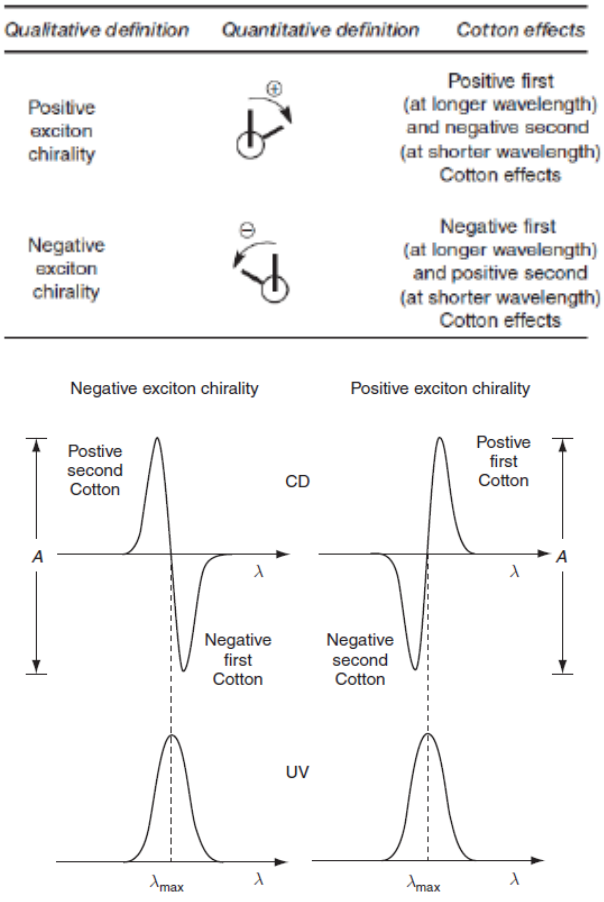

Figure 1.5: Top. Definition of exciton chirality. Down. Typical pattern of exciton-coupled CD Cotton effects and absorption band.

As shown in Figure 1.5, if two transition moments have a clockwise screw sense, CD shows positive first and negative second Cotton effects. On the other hand, if they describe a counterclockwise screw sense, negative first and positive second Cotton effects are observed. In general, the CD zero crossing point corresponds to λ_{max} of the absorption band in the UV-visible region. These exciton-coupled observed in the CD spectrum reflects the absolute configuration of the two electric transition moments, that is, two chromophores.

1.3 Chirality Induction

The configurational assignment of chiral substrates containing primary or secondary functional groups, like alcohols and amines, linked to a single stereogenic center is a challenging task. Since many of these substrates exhibit important biological activities

and often are available only in limited amounts, determination of their absolute configurations is of academic as well as of practical importance.[22]

The most widely available chiroptical method for establishing the AC of chiral molecules is Circular Dichroism (CD) spectroscopy, yet its use is sometimes hampered by the prerequisite for chiral species to contain UV-active chromophores. To bypass this challenge, over a decade ago, Berova *et al.* has developed a *tweezer methodology* based on the CD exciton chirality method, using a porphyrin tweezer as host and opportune derivatized substrates as a guest.[22,23]

Porphyrins and related chromophores have been shown to be well-suited host molecules for studying the processes involved in supramolecular chirality induction. Porphyrinoids have many desirable attributes for acting as effective host molecules of supramolecular systems.[24,25,26] They possess well-resolved and intense absorption spectra which are in the red-shifted spectral region where the majority of the prospective chiral guest molecules do not absorb. Also their synthetic modifications are both facile and versatile, particularly formation of various metal complexes that expand significantly the possible range of guest compounds, utilizing the well-known coordination properties of metalloporphyrins. These attractive features prompted us to apply porphyrin compounds as achiral host molecules for studying the processes of supramolecular chirality induction.[27]

1.3.1 Tweezer Methodology

As describe before, many important biological molecules are not UV-visible active due to the lack of chromophores groups within their skeleton. In order to overcome these constrains, complexation by porphyrin-porphyrin dimer could be convenient: so-formed complexes posses indeed strong absorption bands in the visible region due to the π-π^* transitions of the porphyrin macrocycle. Furthermore, their large extinction coefficients allow the detection of submicromolar amounts of analyte. The host-guest ditopic coordination is required to give rise to the exciton coupling mechanism, previously described in above paragraph. The lack of coordinating groups on the guest could be easily resolved through the introduction of suitable moieties by the so-called *derivatisation* procedure.[22]

The substrate derivatisation is carried out by the reaction with a carrier that gives an ester or an amide as product. Then, treatment of this chiral conjugated with a CD sensitive

dimeric zinc porphyrin host (*e.g.*, the commercial tweezer **A**, shown in Figure 1.6) yields a supramolecular complex which exhibits intense exciton coupled CD reflecting the absolute configurations of the original substrate.[22,23]

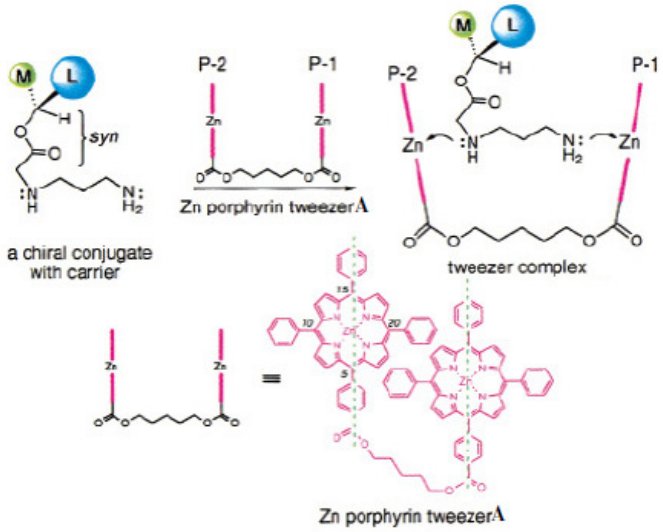

Figure 1.6: complexation of a chiral conjugate of carrier with zinc porphyrin tweezer **A**; the broken dashed lines in tweezer **A** depict the orientation of the electric transition moments. Upon treatment of tweezer **A** with the conjugate, the primary amino group of the carrier moiety coordinates with the zinc in P-1, and this is followed by coordination of the *sec*-amino group to the zinc in P-2 to yield the supramolecular complex; the helicity between the two porphyrin rings is dictated by the absolute configuration of the substrate and affords an exciton-coupled CD.

The search for a different type of carrier molecule has highlighted some important attributes to be considered. First, it should be an achiral molecule containing two amino nitrogens with sufficient Lewis basicity to bind to the tweezer zinc atoms and an additional carboxyl group to couple to alcohols or amines belonging to the guest molecule. Second, when linked to the substrate, the carrier molecule should lead to a bidentate conjugate where the stereogenic center is in close proximity to the nitrogen of the secondary amine, which upon coordination to zinc adopts a chirality controlled by the absolute configuration of the stereogenic center in the substrate.

The opportunely adopted carrier molecule **17** (Scheme 1.1) was synthesized from 1,3-diaminopropane (**13**) in four steps, via intermediates **14**, **15**, and **16** in 85% overall yield.

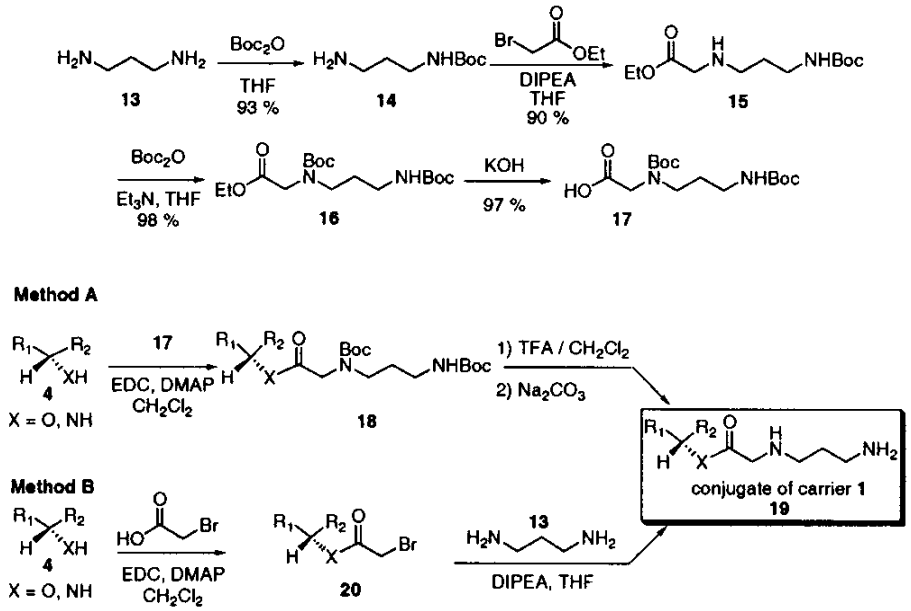

Scheme 1.1: synthesis of diBoc protected carrier molecule **17**. Methods A and B: derivatisation of chiral alcohols/amines with (3-aminopropylamino) acetic acid (Berova method).

The formation of a bidentate conjugate between carrier **17** and a chiral monoalcohol or monoamine prior to complexation with the zinc porphyrin tweezer **A** was performed by two independent routes (Scheme 1.1, bottom). Method A involved the use of the diBoc protected carrier molecule **17**, via carbodiimide condensation in the presence of 1-(3-dimethylaminopropyl)-3-ethylcarbodiimide (EDC) and 4-(dimethylamino)pyridine (DMAP). This was followed by removal of the Boc protecting groups with trifluoroacetic acid in dichloromethane to afford the TFA salt of conjugate **19**. The latter was converted to its free amine with Na_2CO_3 before complexation to tweezer **A**. In method B, conjugate **19** was prepared in two steps with no protecting groups to yield the product as the free amine, ready for complexation with the porphyrin tweezer. The chiral alcohol or amine **4** is first reacted with bromoacetic acid in the presence of EDC/DMAP, and then the resultant bromoester **20** is treated with an excess of 1,3-diaminopropane (**13**) to afford the free amine of conjugate **19**. While method A gives conjugates in excellent yields and it is applicable to most chiral alcohols, it is not suited for some benzylic alcohols where deprotection by TFA can also cleave the ester bond. Method B is thus preferred for benzylic monoalcohols. In the case of chiral amines, both methods can be used to yield amine conjugates in quantitative yields.

1.3.2 Chirality Determination

The tweezer methodology is based on the formation of a CD-active host/guest complex between an achiral dimeric metalloporphyrin host and the chiral guest under study. In the process of stereocontrolled formation of the 1:1 host/guest complex through the bidentate metal coordination, chirality is transferred from a chiral guest molecule to an achiral host (the tweezer) resulting in a preferential twist between the two porphyrins. This preferred interporphyrin helicity is dictated by the AC of a guest.[28,29,30] Chiral induction is empirically manifested in the CD spectrum through development of a red-shifted exciton CD couplet[29] in the porphyrin Soret band region (~ 420 nm). The sign of the couplet is a direct consequence of the absolute sense of twist between the electric transition moments of the interacting porphyrins within the tweezer. Its intensity is related to the overall geometry (conformation) of the host/guest complex, including the interporphyrin distance, the extent of interporphyrin twist as well as the steric size of the substituents around the stereogenic center of the guest (Figure 1.7).

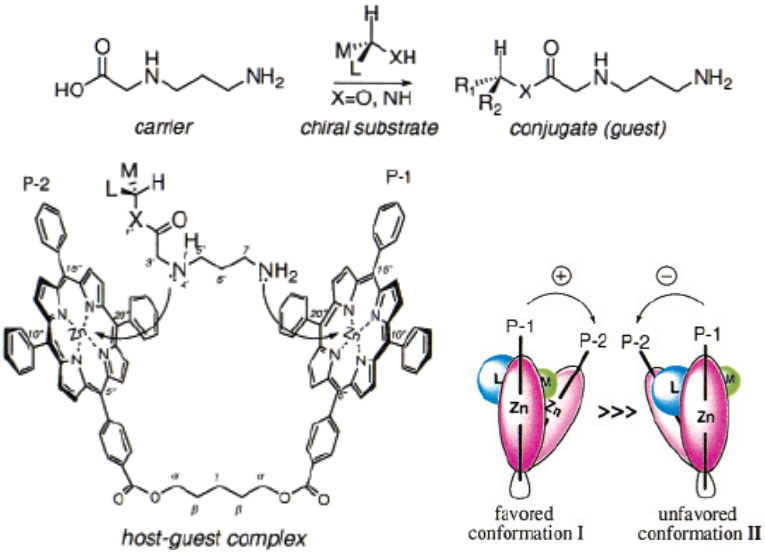

Figure 1.7: top. Carrier is linked to the chiral alcohol or amine substrate to provide conjugate that becomes the guest. The guest is then treated with the host, *e.g.*, zinc porphyrin tweezer **A**, yielding the host-guest complex. Two conformers are conceivable for the sandwich complex. In favored conformation **I** the larger group L protrudes from the sandwich while the medium group M is clamped between the two porphyrin rings. In the unfavored conformation **II** the M group protrudes out from the sandwich while L is within the tweezer. Upon complex formation, the *primary* amine of the conjugate coordinates with the Zn in one of the porphyrin rings P-1, and this is followed by coordination of the *secondary* amine with the other porphyrin ring P-2 in a manner that reflects the absolute configuration at the stereogenic center.

In order to reliably correlate the observed exciton split CD, which is a direct manifestation of the interporphyrin helicity, with the absolute configuration of the chiral guest, it was more recently established[31,32] that a prediction of preferred porphyrin helicity of the complex could be made by molecular mechanics calculations using the Monte Carlo (MC) algorithm, implemented in MacroModel package.[33] Molecular Modeling (MM) investigations of conformational search are now carried out with the support of the recently developed force field OPLS-2005.[34] The use of OPLS-2005 allows for a more meaningful consideration of the relatives energies and Boltzmann populations of conformations obtained via MC searches, which opens a window for a more detailed structural analysis of tweezer complexes.[31]

REFERENCES

[1] Examples of supramolecular chirogenesis in various systems: (a) Borovkov, V.V.; Harada, T.; Hembury, G.A.; Inoue, Y.; Kuroda, R., *Angew. Chem., Int. Ed.*, **2003**, *42*, 1746. (b) Ishikawa, M.; Maeda, K.; Yashima, E., *J. Am. Chem. Soc.*, **2002**, *124*, 7448. (c) Nabeshima, T.; Hashiguchi, A.; Saiki, T.; Akine, S., *Angew. Chem., Int. Ed.*, **2002**, *41*, 481. (d) Ribò, J.M.; Crusats, J.; Sagues, F.; Claret, J.; Rubires, R., *Science*, **2001**, *292*, 2063. (e) Nakashima, H.; Koe, J.R.; Torimitsu, K.; Fujiki, M., *J. Am. Chem. Soc.*, **2001**, *123*, 4847. (f) Iarossi, D.; Mucci, A.; Parenti, F.; Schenetti, L.; Seeber, R.; Zanardi, C.; Forni, A.; Tonelli, M., *Chem. Eur. J.*, **2001**, *7*, 676. (g) de Loos, M.; van Esch, J.; Kellogg, R.M.; Feringa, B.L., *Angew. Chem., Int. Ed.*, **2001**, *40*, 613. (h) Steffen, W.; Kohler, B.; Altmann, M.; Scherf, U.; Stitzer, K.; zur Loye, H.-C.; Bunz, U.H.F., *Chem. Eur. J.*, **2001**, *7*, 117. (i) Jung, J.H.; Kobayashi, H.; Masuda, M.; Shimizu, T.; Shinkai, S., *J. Am. Chem. Soc.*, **2001**, *123*, 8785. (j) Brunsveld, L.; Meijer, E.W.; Prince, R.B.; Moore, J.S., *J. Am. Chem. Soc.*, **2001**, *123*, 7978. (k) Zahn, S.; Proni, G.; Spada, G.P.; Canary, J.W., *Chem. Eur. J.*, **2001**, *7*, 88. (l) Rivera, J.M.; Martìn, T.; Rebek, J., Jr., *Science*, **2000**, *289*, 606. (m) Wang, M.; Silva, G.L.; Armitage, B.A., *J. Am. Chem. Soc.*, **2000**, *122*, 9977.

[2] Victor V. Borovkov, Juha M. Lintuluoto, Guy A. Hembury,† Makiko Sugiura,§ Ryuichi Arakawa,| and Yoshihisa Inoue , *J. Org. Chem.*, **2003**, *68*, 7176.

[3] Catalysis and autocatalysis: (a) Montanari, F.; Casella, L., *Metalloporphyrin Catalyzed Oxidations*; Kluwer: Dordrecht, **1994**. (b) Lee, D.H.; Granja, J.R.; Martinez, J.A.; Severin, K.; Ghadiri, M.R., *Nature*, **1996**, *382*, 525.

[4] Non-linear optics: Verbiest, T.; Van Elshocht, S.; Kauranen, M.; Hellemans, L.; Snauwaert, J.; Nuckolls, C.; Katz, T. J.; Persoons, A., *Science*, **1998**, *282*, 913.

[5] Polymer science: (a) Jha, S.K.; Cheon, K.-S.; Green, M.M.; Selinger, J.V., *J. Am. Chem. Soc.*, **1999**, *121*, 1665. (b) Akagi, K.; Piao, G.; Kaneko, S.; Sakamaki, K.; Shirakawa, H.; Kyotani, M., *Science*, **1998**, *282*, 1683. (c) Yashima, E.; Maeda, K.; Okamoto, Y., *Nature*, **1999**, *399*, 449.

[6] Molecular recognition and self-assembly: (a) Ogoshi, H.; Mizutani, T. *Acc. Chem. Res.* **1998**, *31*, 81-89. (b) James, T. D.; Sandanayake, K. R. A. S.; Shinkai, S. *Angew. Chem., Int. Ed. Engl.* **1996**, *35*, 1910-. (c) Prins, L. J.; Huskens, J.; de Jong, F.; Timmerman, P.; Reinhoudt, D. N. *Nature* **1999**, *398*, 498.

[7] Molecular device: Furusho, Y.; Kimura, T.; Mizuno, Y.; Aida, T., *J. Am. Chem. Soc.*, **1997**, *119*, 5267.

[8] (a) Baum, G.; Constable, E. C.; Fenske, D.; Housecroft, C. E.; Kulke, T. *Chem. Eur. J.* **1999**, *5*, 1862. (b) Huang, X.; Rickman, B.H.; Borhan, B.; Berova, N.; Nakanishi, K. *J. Am. Chem. Soc.* **1998**, *120*, 6185. (c) Yashima, E.; Matsushima, T.; Okamoto, Y. *J. Am. Chem. Soc.* **1997**, *119*, 6345. (d) Kikuchi, Y.; Kobayashi, K.; Aoyama, Y. *J. Am. Chem. Soc.* **1992**, *114*, 1351.

[9] Borovkov, V.V.; Lintuluoto, M.J.; Inoue, Y., *Organic Letters*, **2000**, *2*, 1568.

[10] Borovkov, V.V.; Lintuluoto, M.J.; Fujiki, M.; Inoue*J. Am. Chem. Soc.*, **2000**, *122*, 1134.

[11] Mason, S.F., *Molecular Optical Activity and the Chiral Discrimination*; Cambridge University Press: Cambridge, **1982**.

[12] Eliel; E.L.; Wilen, S.H.; Mander, L.N., *Stereochemistry of Organic Compounds*; John Wiley & Sons Inc.: New York, **1994**; Chapter 13, pp 991–1118.

[13] Harada, N.; Nakanishi, K., *Circular Dichroic Spectroscopy – Exciton Coupling in Organic Stereochemistry*; University Science Books: Mill Valley, CA, and Oxford University Press: Oxford, **1983**.

[14] Berova, N.; Di Bari, L.; Pescitelli, G., *Chem. Soc. Rev.*, **2007**, *36*, 914.

[15] Lightner, D.A.; Gurst, J.E., *Organic Conformational Analysis and Stereochemistry from Circular Dichroism Spectroscopy*; Wiley-VCH: New York, **2000**.

[16] Berova, N.; Nakanishi, K., *Exciton Chirality Method: Principles and Application. In Circular Dichroism: Principles and Applications, 2nd ed.*; N. Berova, K. Nakanishi, R. W. Woody, Eds.; Wiley-VCH: New York, **2000**; Chapter 12, pp 337–382.

[17] De Voe, H., *J. Chem. Phys.*, **1964**, *41*, 393; **1965**, *43*, 3199.

[18] Superchi, S.; Giorgio, E.; Rosini, C., *Chirality*, **2005**, *16*, 422.

[19] Kemp, C.M.; Mason, S.F., *Tetrahedron*, **1966**, *22*, 629.

[20] Crawford, T.D., *Theor. Chem. Acc.*, **2006**, *115*, 227.

[21] Berova N, Nakanishi K, Woody RW, editors. *Circular dichroism: principles and applications*; New York: John Wiley; **2000**.

[22] Kurtàn, T.; Nesnas, N.; Li, Y.-Q.; Huang, X.; Nakanishi, K.; Berova, N., *J. Am. Chem. Soc.* **2001,** *123,* 5962.

[23] Kurtàn, T.; Nesnas, N.; Koehn, F.E; Li, Y.-Q.; Nakanishi, K.; Berova, N., *J. Am. Chem. Soc.* **2001,** *123,* 5974.

[24] Ogoshi, H.; Mizutani, T., *Acc. Chem. Res.*, **1998**, *31*, 81.

[25] Furusho, Y.; Kimura, T.; Mizuno, Y.; Aida, T., *J. Am. Chem. Soc.*, **1997**, *119*, 5267.

[26] Huang, X.; Rickman, B. H.; Borhan, B.; Berova, N.; Nakanishi, K. *J. Am. Chem. Soc.* **1998**, *120*, 6185.

[27] Borovkov, V.V.; Lintuluoto, M.J.; Fujiki, M.; Inoue, Y., *J. Am. Chem. Soc.*, **2000**, *122*, 4403.

[28] Berova N, Di Bari L, Pescitelli G., *Chem. Soc. Rev.*, **2007**, 36, 914.

[29] Berova N, Nakanishi K, Woody R. *Circular Dichroism: Principles and applications, New York*; Wiley-VCH; 2nd ed., **2000.**

[30] Berova, N.; Pescitelli, G.; Petrovic, A., G.; Proni, G., *Chem. Comm.*, **2009**, 5958.

[31] Petrovic, A.; Chen, Y.; Pescitelli, G.; Berova, N.; Proni, G., *Chirality*, **2010**, *22*, 129.

[32] Chen, Y.; Petrovic, A.; Roje, M.; Pescitelli, G.; Kayser, M.M.; Yang, Y.; Berova, N.; Proni, G., *Chirality*, **2010**, *22*, 140.

[33] Mohamadi, F.; Richards, N.G.J.; Guida, W.C.; Liskamp, R.; Lipton, M.; Caufield, C.; Chang, G.; Hendrickson, T.; Still, W.C. J., *Comput. Chem.*, **1990**, *11*, 440.

[34] (a) Jorgensen, W.L.; Maxwell, D.S.; Tirado-Rives, J., *J. Am. Chem. Soc.*, **1996**, *118*, 11225. (b) Damm, W.; Frontera. A.; Tirado-Rives, J.; Jorgensen, W.L., *J. Comp. Chem.*, **1997**, *18*, 1955. (c) Jorgensen, W.L.; McDonald, N.A., *Theor. Chem.*, **1998**, *424*, 145. (d) McDonald, N.A.; Jorgensen, W.L., *J. Phys. Chem. B*, **1998**, *102*, 8049. (e) Rizzo, R.C.; Jorgensen, W.L., *J. Am. Chem. Soc.*, **1999**, *121*, 4827. (f) Watkins, E.K.; Jorgensen. W.L., *J. Phys. Chem. A*, **2001**, *105*, 4118. (g) Kaminski, G.A.; Friesner, R.A.; Tirado-Rives, J.; Jorgensen, W.L., *J. Phys. Chem. B*, **2001**, *105*, 6474.

RESULTS AND DISCUSSION

2.1 Porphyrin Tweezers used for Probing Molecular Chirality

For more than a decade, dimeric Zn- and Mg-porphyrin hosts (tweezers) have been successfully applied as chirality probes for determination of the absolute configuration (AC) for a wide variety of chiral synthetic compounds and natural products.[1] Since the originally developed pentanediol-bridged bis(porphyrin-Zn^{II}) tweezer (the commercial tweezer **A** in Figure 2.1), other types of porphyrin tweezers have been introduced by B. Borhan,[2] V.V. Borovkov[3] and coworkers that can provide better molecular recognition, a stronger CD response and a broader utility so that AC can be reliably determined for more complex chiral structures.

In my research work, a novel melamine-bridged Zn-based porphyrin tweezer, namely **B/TT**, was synthesized referring to the one-pot strategy used for the three analogues illustrated in the previous chapter (*results and discussion* part). Its properties as sensitive AC reporter were investigated and compared to the commercial tweezer **A** (Figure 2.1). Combined approach based on experimental circular dichroism response and theoretical predictions of the prevailing interporphyrin helicity demonstrates that this tweezer displays favourable properties for chiral recognition. The class of chiral guests investigated involved diamines, α-amino-esters, α-amino-amides, α-amino alcohols and secondary monoalcohols. The applicability of the **B/TT** tweezer as AC reporter is based on the following criteria:

- correct assignment of the AC based on the agreement between the observed sign of the CD couplet and the predicted interporphyrin helicity of the host-guest complex with the investigated guests;

- the sensitivity of the tweezer host gauged by the minimum number of equivalents of chiral guest needed to reach the maximum CD response;

- the univocal sign of the CD couplet regardless to solvent polarity.

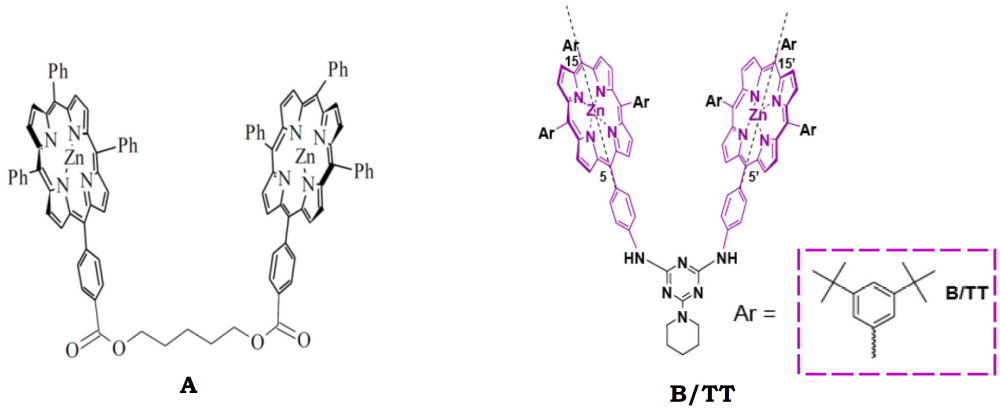

Figure 2.1: structure of the commercial tweezer **A** and the melamine-bridged **B/TT** used in this work.

The new derivative **B/TT** is characterized by two distinctive structural features:

a) a melamine-bridge incorporated between the two porphyrins, which represents a more rigid bridging unit than that found in the commercial tweezer **A**.

b) **B/TT** tweezer contains sterically encumbered substituents, *e.g.*, (*meta tert*-butyl)phenyl groups.

Preliminary studies on chiral diamines have shown that **B/TT** tweezer is more promising than **P(Zn)P(Zn)**, **M(Zn)M(Zn)** and **P(Zn)M(Zn)** in determining the absolute configuration of several classes of chiral compounds due to the increasing in the CD signal and, as consequence, a reduced amounts of potentially precious substrates required to carry out a chiroptical analysis. Therefore, we restricted our studies only to **B/TT** tweezer.

2.1.1 Synthesis and Characterization of B/TT tweezer

The preparation of **B/TT** tweezer required the preliminary synthesis of 5-(4-aminophenyl)-10,15,20-(3,5-*tert*-butylphenyl)porphyrin, **T**.[4] This synthesis was achieved starting from pyrrole, 3,5-di-*tert*-butylbenzaldehyde and *p*-acetamidobenzaldehyde; the mixture undergoes sequentially an acid-catalyzed condensation reaction in TFA at room temperature, followed by oxidation of porphyrinogen by 2,3-dichloro-5,6-

dicyanobenzoquinone (DDQ). After chromatographic separation and hydrolysis reaction, the desired mono amino product was obtained (Figure 2.2).

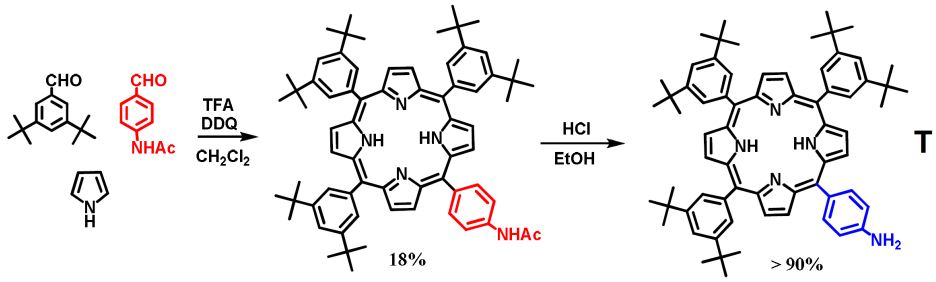

Fazio, M.A.; Lee, O.P.; Schuster, D.I., *Org.Lett.*,**2008**, *10*, 4979.

Figure 2.2: synthesis of the amino-porphyrin **T**.

Bis(porphyrin) receptor **B/TT** was prepared according to the one-flask synthetic protocol outlined in Scheme 2.1.[5]

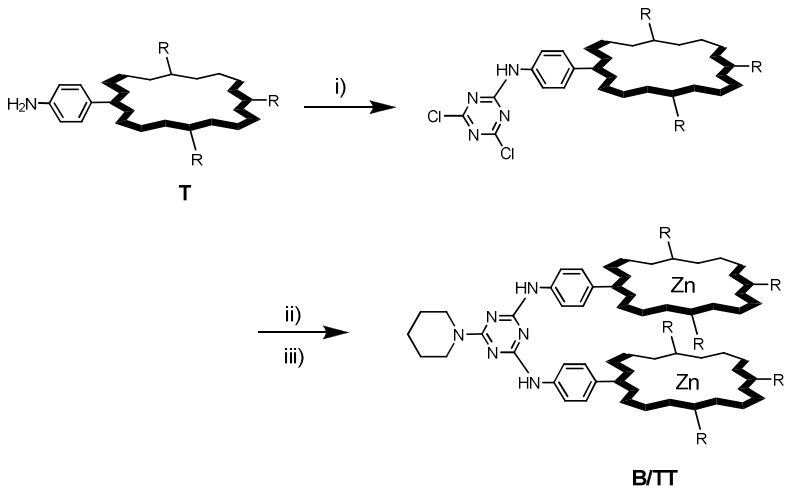

Scheme 2.1: experimental conditions: i) cyanuric chloride, DIPEA, THF, 0 °C; ii) **T**, DIPEA, THF, 60 °C; iii) excess of piperidine, DIPEA, THF, 80 °C, then, after chromatographic purification, treatment with a saturated solution of $Zn(Ac)_2$ x $2H_2O$ in $MeOH/CHCl_3$, reflux.

Briefly, the amino-porphyrin **T** was reacted with one equivalent of cyanuric chloride in tetrahydrofuran (THF) at 0 °C in the presence of diisopropylethylamine (DIPEA). The reaction was stirred at room temperature until TLC (Thin Layer Chromatography) analysis indicated the complete disappearance of the starting materials and the formation of the corresponding mono-adduct. At this point, a second equivalent of amino-porphyrin **T** was added to the solution and reaction mixture was stirred at 60-70 °C to afford the corresponding bis(porphyrin) adduct. Finally, the third chlorine atom was

reacted with piperidine at 80 °C. After standard work-up on the crude reaction mixture, final purification was accomplished by preparative column chromatography on silica-gel. Finally, metalation with $Zn(Ac)_2$ produced the **B/TT** molecular receptor.

The structure of **B/TT** was confirmed in $CDCl_3$ solution by a combined use of mono- and bi-dimensional NMR techniques (the spectra and ^1H and ^{13}C assignments are reported in the experimental section of this chapter). The NMR peaks were quite sharp thus suggesting that no aggregation takes places in $CDCl_3$ solution even at mM concentration. This is likely due to the presence of *tert*-butyl substituents that hinder intermolecular π–π stacking between porphyrin units.

2.1.2 Binding Properties of B/TT tweezer towards Diamines

The previous chapter (paragraph 2.2) reports the binding properties of the melamine-bridged bis(porphyrin-Zn^{II}) dimers, *e.g.*, **P(Zn)P(Zn)**, **M(Zn)M(Zn)** and **P(Zn)M(Zn)**, with a family α,ω-aliphatic diamine homologues of general formula $H_2N(CH_2)_nNH_2$ (n = 4-8). We have also established that the presence of two porphyrin receptors provides an enhanced binding interaction with diamine ligands, thus resulting in supramolecular complexes having stability constants in the range $10^6 \div 10^7$ M^{-1}, thus more than 3-orders of magnitude higher as compared to a monodentate reference amine (*e.g.*, *n*-butylamine). The influence of the porphyrin substituents on the conformational mobility of the resulting dimeric receptor and on their recognition capabilities has been demonstrated by structure-reactivity correlation, and NMR solution speciation. As expected, the increasing of sterical hinder at periphery of the porphyrin macrocycle leads to a diminished binding ability, especially for the shortest diamines of the series since they require the closest proximity between the coordination centers. In order to compare the binding properties of **B/TT** with our previous receptors, we determined the binding constants of the same diamine family with **B/TT** by UV-vis, monitoring the characteristic red-shift of the porphyrin Soret and Q bands upon diamine complexation in dichloromethane (DCM) at 298K. To this purpose, a solution of **B/TT** maintained at a constant micromolar concentration was titrated by adding incremental amounts of diamine. Figure 2.2, left, shows a typical spectral change observed for **B/TT** upon addition of cadaverine, $H_2N(CH_2)_5NH_2$. Depletion of the Soret band at 425 nm was accompanied by the formation of a new absorption peak at 428 nm, ascribable to

the host-guest complex. In addition, the appearance of sharp isosbestic point at 426 nm is suggestive of a 1:1 binding stoichiometry.

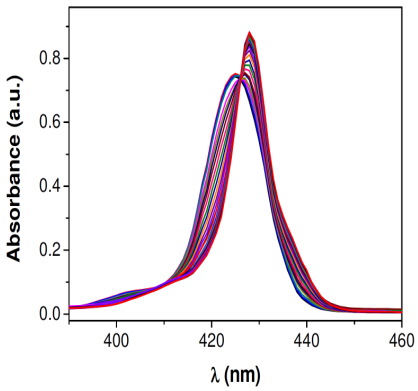

Amine	Tweezer, K (M^{-1})	
$H_2N(CH_2)_nNH_2$	**P(Zn)P(Zn)**	**B/TT**
n = 4	$4.8x10^6$	$3.8x10^6$
n = 5	$3.4x10^7$	$3.3x10^7$
n = 6	$1.3x10^7$	$2.1x10^6$
n = 7	$4.5x10^6$	$2.2x10^6$
n = 8	$4.2x10^6$	$2.1x10^6$
n-$BuNH_2$	$3.2x10^4$	$1.6x10^4$

Figure 2.2: left. UV-vis spectra evolution in DCM at 298 K upon titration of **B/TT** (1.0 μM) with $H_2N(CH_2)_5NH_2$ (0-1.6 μM). Right. Binding constants of the complexes between the different guests with **B/TT** tweezer compared to **P(Zn)P(Zn)** dimers.

The binding constant values for all the hosts with the diamines and the reference monodentate *n*-$BuNH_2$ are collected in Figure 2.2, right.[6] For comparison purposes, the figure also reports the corresponding binding constants for **P(Zn)P(Zn)** tweezer. Not surprising, the binding constants for the **B/TT** receptor are systematically lower that those observed for the less hindered **P(Zn)P(Zn)**. However, the binding constants are quite high, in the range $2.1x10^{-6} \div 3.3x10^{-7}$ M^{-1} and that guarantees for the complete formation of the supramolecular receptor-substrate complex in the presence of only few equivalents of diamine, even for a receptor at micromolar concentration.

Since **B/TT** receptor has been designed for chiral recognition purposes, we preliminary tested the affinity of the tweezer for a chiral substrate such as the (L)-Lysine-O-methylester, a natural occurring chiral aminoacid that possess a diamine functionality well suited to act as a bidentate ligand for the two Zn^{II} centers of the receptor. The binding constant determined by UV-vis spectroscopy was $5.4x10^5$ M^{-1}, so one or two orders of magnitude lower than in the case of the linear diamines examined before. This is likely due to the sterical effect of the ester group of the aminoacid.

2.1.3 NMR Studies of B/TT-(L)-lysine Methyl Ester Complex

The solution structure of the supramolecular complex between **B/TT** and L-lysine ester has been further addressed by NMR spectroscopy. The ^{1}H-NMR spectrum of free **B/TT** dimer, freshly prepared in $CHCl_3$ at 298 K is shown in Figure 2.3. The spectrum shows four main sets of signals: i) the porphyrin β-pyrrolic protons, around 9 ppm, ii) the porphyrin phenyl protons, in the 8.5-7 ppm region, iii) the piperidine methylenic protons, at 3.94 and 1.75 ppm and iv) the *tert*-butyl protons around 1.54 ppm. The ^{1}H-NMR spectrum of free L-lysine-O-Me ester in $CHCl_3$ at 298 K is also reported. The resonance assignments have been carried out by ^{1}H-^{1}H COSY, DQF-COSY and TOCSY techniques.

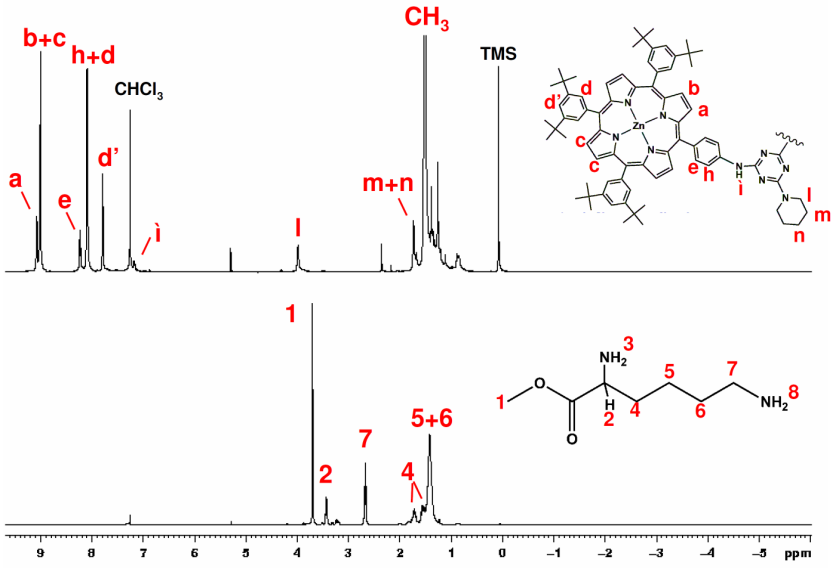

Figure 2.3: ^{1}H-NMR (400 MHz, $CDCl_3$) of **B/TT** tweezer (top) and lysine-O-methylester (bottom) together with the resonance assignments according ^{1}H-^{1}H COSY and DQF-COSY.

The NMR titration experiments have been carried out by adding increasing amounts of L-lysine-O-methylester guest to **B/TT** tweezer (Figure 2.4).

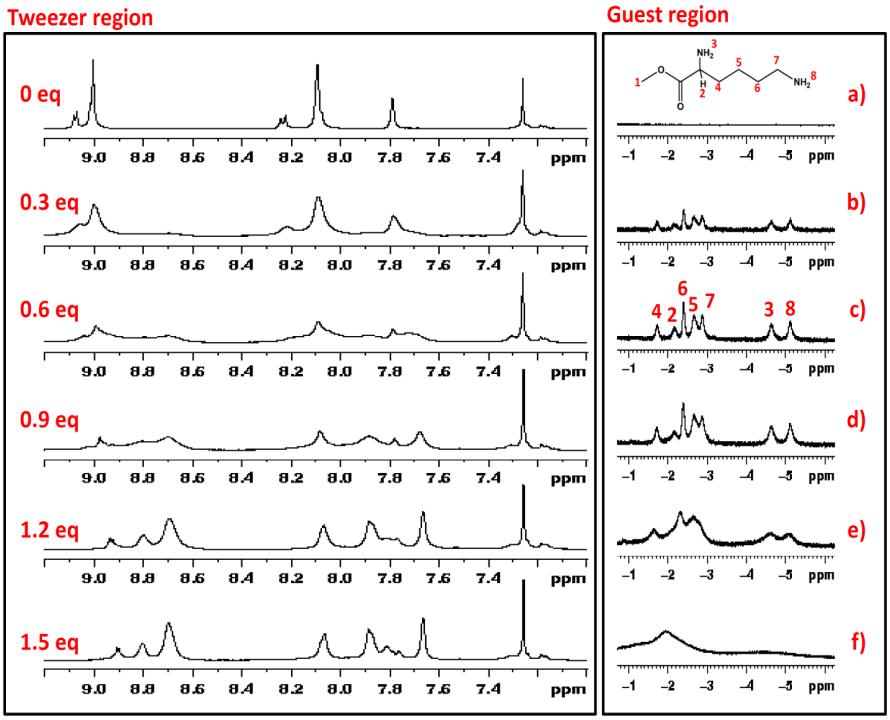

Figure 2.4: signal changes in the host- and guest-region during the ^{1}H-NMR (400 MHz, $CDCl_3$) titration of **B/TT** with lysine-O-methylester. a, b, c d, e and f, respectively, represent the ^{1}H-NMR spectra acquired after adding 0.0, 0.3, 0.6, 0.9, 1.2, and 1.5 equivalents of lysine-O-methylester.

Upon incremental addition of the L-lysine-O-methylester, the aromatic host region show a gradual broadening of the signals together with an upfield chemical shift that stops around to 1.2 equivalents of guest added due to the quantitative formation of the **B/TT**-lysine supramolecular complex. The signals of the guest, in turn, exhibit significant upfield shifts by effect of complexation, due to ring current anisotropy from porphyrin π-planes.[7] Indeed, with substoichiometric concentration of diamine, the guest signals are found between -1 and -5 ppm chemical shifts (Fig. 2.4a-e). This evidence is consistent with the bidentate guest being bound within the **B/TT** concave, via ditopic interaction, and exposed to the ring current effects of porphyrin rings. Interestingly, above 1 equivalent of diamine, the guest signals coalesce due to fast exchange equilibrium and cannot be observed separately (Fig. 2.4f).

We decided to investigate further, by computational methods, in collaboration with Dr. Giacomo Saielli of The University of Padova, the strong high-field shift induced by the extended π system of the porphyrin rings to the resonances of the guest.[8] Shielding calculations require high level DFT methods[9] and, in turn, considering the size of the

complexes, a high computational effort, especially if relativistic effects are considered. Previous comparison of non-relativistic results with those obtained at the Scalar and SpinOrbit level reveals that relativistic effects can be safely ignored. Indeed, relativistic proton chemical shifts, even for the NH_2 protons, the closest to the heavy atoms, differ only by less than 0.1 ppm from the non-relativistic results. We run shielding calculations for the four most stable conformers resulting from the conformational analysis carried out with MacroModel[10] and the corresponding calculated chemical shifts have been averaged in the hope to take in account the conformational flexibility of the host-guest complex.

Relative chemical shifts, $\Delta\delta$, observed for the free and complexed diamine are then evaluated. Comparison of calculated and experimental $\Delta\delta$ values stand in good agreement (Figure 2.5; calculated values are between square brackets). The strong deshielding of the signals and the general trend as a function of the distance is correctly reproduced, although a somewhat larger error is found for some of the protons of the lysine methylenic chain. As expected, protons belonging to the nitrogen atom involved in Zn^{II} coordination (*e.g.*, protons **3** and **8**) and the proton attached to the adjacent carbon atoms (*e.g.*, protons **7** and **2**) experience the largest shift. On the other hand, the fact that the central methylene protons (*e.g.*, **4**,**5** and **6**) does not experience the largest shift, speaks against a parallel arrangement of the porphyrin rings, which precludes an additive shielding effect converging in the middle of the receptor cavity.

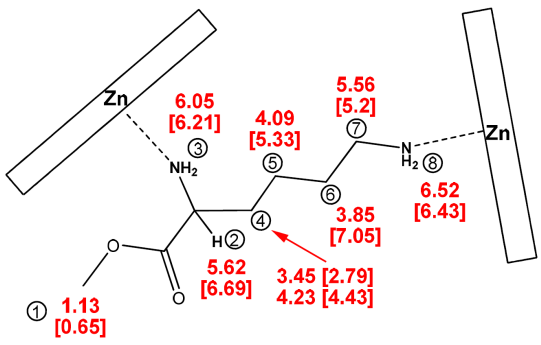

Figure 2.5: upfield shift of the diamine protons.

The conformational degree of freedom for the **B/TT** tweezer has been explored via MC/OPLS-2005[11,12] conformational search in collaboration with Prof. Nina Berova at the Columbia University (NY, USA). The energy profile for the **B/TT** conformers is reported in Figure 2.6, along with the model structures of four representative conformations.

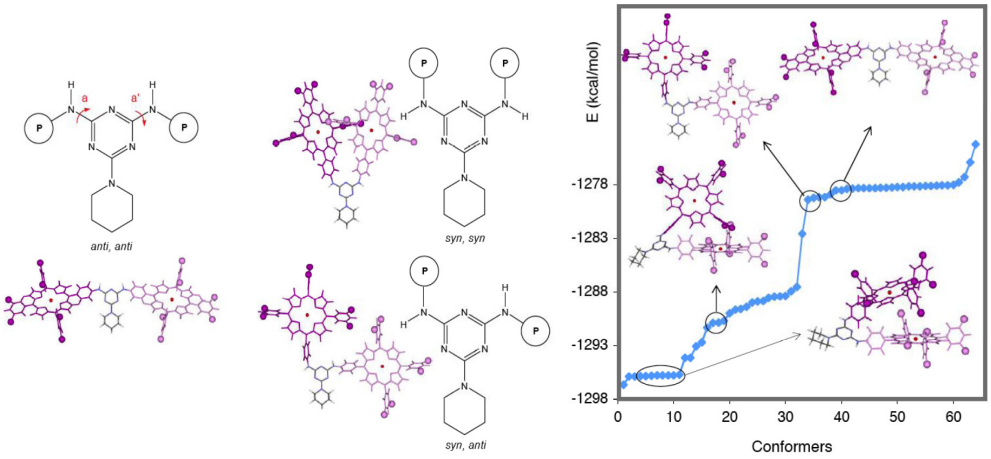

Figure 2.6: The energy profile for the **B/TT** conformers with the model structures of four representative conformations.

This analysis shows a preferential *syn-syn* arrangement in which the two porphyrin units are almost parallel to each other, displaying a small twist of + 2°. This conformer is almost 5.3 kcal/mol much stable than similar *syn-syn* arrangement with a V-shaped disposition of the two porphyrins, and a 17.2 kcal/mol more stable than the *syn-anti* and *anti-anti* conformers. Based on this theoretical analysis, the interporphyrin distance of the *syn-syn* arrangement is *ca.* 5.7 Å, which suggests that the *syn-syn* arrangement is stabilized by an attractive π-π interaction between the porphyrins.

2.2 Determination of the AC of Chiral Substrates

At this point, we have pointed out the ability of **B/TT** tweezer to coordinate bifunctional ligands. Since coordination properties of porphyrin tweezers towards diamines are well known (see chapter I, results and discussion part), in this research work we have investigated conformation of the tweezer with diaminic guests bearing additional functional moieties. In particular, we focused on aminoacidic derivatives, like α-amino-esters, α-amino-amides, α-amino-alcohols, for which the determination of AC is a topic issue for practical applications. Moreover, other monodentate ligands, as secondary monoalcohols, were investigated by using the derivatisation techniques already described in the introduction of this chapter (paragraph 1.3.1) and that will be also detailed in a following section. The guest chiral compounds studied are reported in Table 2.1.

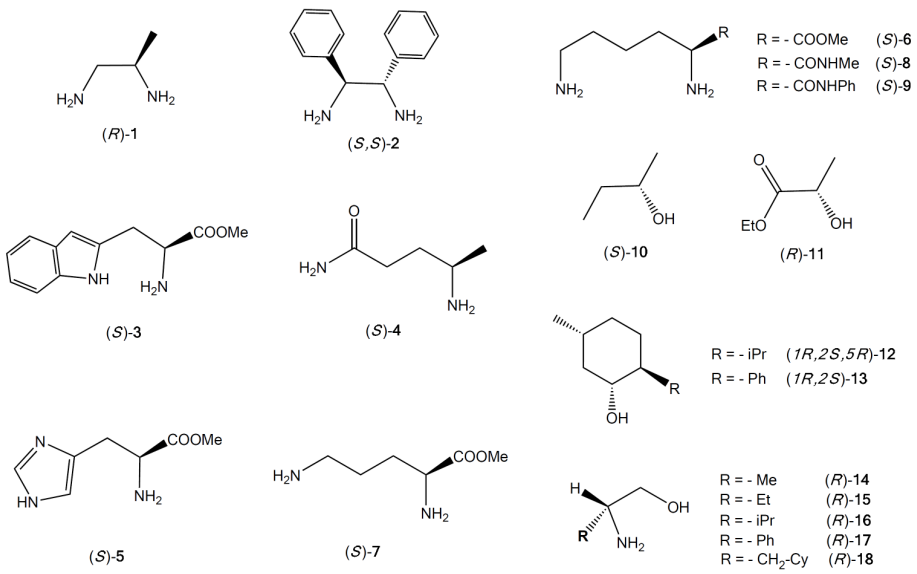

Table 2.1: chiral guests investigated.

2.2.1 α-Amino-Esters and α-Amino-Amides as Guests

Among the selected guests, some compounds contain ester or amide moieties. Such functional groups are able to give intramolecular interactions and also can act as Lewis bases, and therefore potentially compete with amine for zinc coordination. In order to resolve this issue, we have first performed CD studies on the **B/TT** tweezer with α-mono-amino-ester/amide (L-alanine methyl ester, and L-norleucine methyl amide and (S)-dimethyl-2-aminopentanedioate, Figure 2.7).

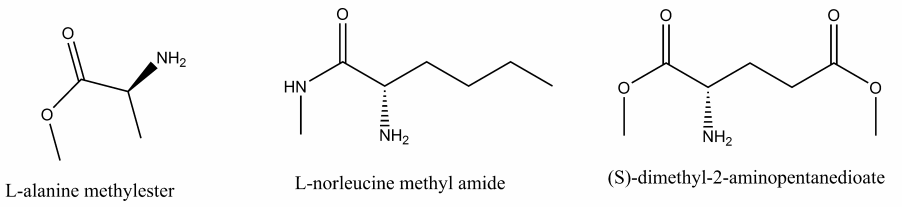

Figure 2.7: chemical structures of α-mono-amino-ester/amide investigated.

Monodentate binding of the amine with zinc is evidenced by observation of an absorbance shift in the UV-vis region and by the absence of a CD response. Nevertheless, molecules containing a longer carbon-chain between amine and amide coordinating groups could

possibly arise in a CD response due to a possible coordination of the amide to the **B/TT** tweezer, as in the case of derivative **4** (Figure 2.8).

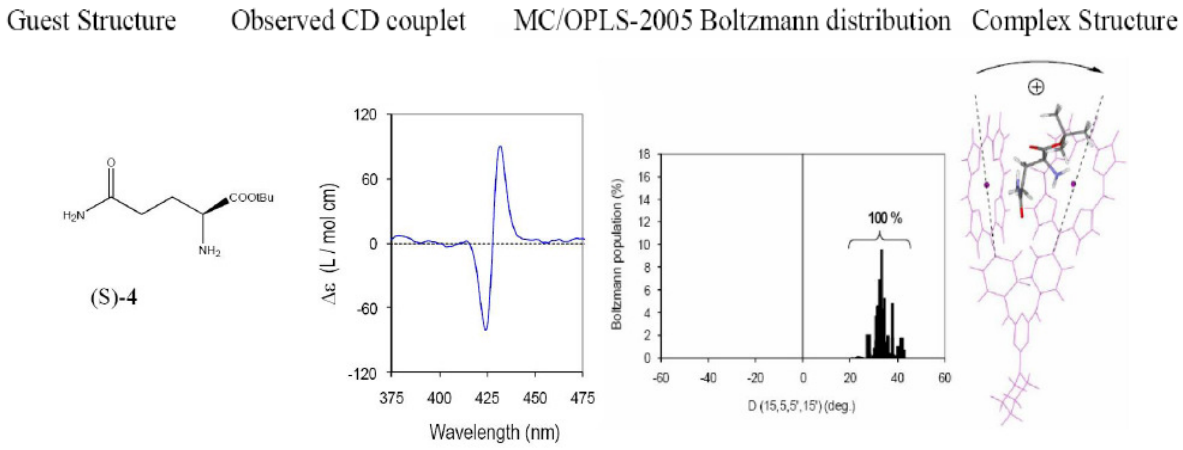

Figure 2.8: starting from the left: chemical structure of compound **4**, (S)-glutamine *tert*-butyl ester; experimentally CD response of the complex with **B/TT** tweezer; Boltzmann distribution of stable conformers in solution determined by MC/OPLS-2005; schematic representation of the two chromophores rotation in the complex with compound **4**.

Within the pool of α-amino-esters, the two challenging guests are **3** and **4** (Table 2.2, first coloumn) since the past investigations[13] with the traditional tweezer **A** have failed to provide chiral recognition of these molecules. As already mentioned, structural characteristics of the **B/TT** tweezer have been considered as potential means for enhancing the chiral recognition of these two challenging guests. In fact, **B/TT** host/guest complex provides a notable CD response in an apolar environment, as hexane and methylcyclohexane (Table 2.2, second column). Specifically, host/guest complex of α-amino-ester **3** displays a negative CD couplet with the maximum intensity of $\Delta\varepsilon = -71$ $Lmol^{-1}cm^{-1}$ developing at 6 equivalents of the α-amino-ester. This empirical response is in agreement with the MM study, which displays the dominance of negative interporphyrin helicity with a twist angle up to *ca.* -20º. On the other hand, α-amino-ester complex, **4-B/TT**, displays a positive CD couplet with a first distinguishable response appearing at 35 equivalents, which subsequently continues increasing to maximum intensity of + 170 L $mol^{-1}cm^{-1}$ until 230 equivalents. In this case, the outcome of molecular MM also agrees with the empirical data by providing a dominance of a positive interporphyrin helicity with a twist angle up to *ca.* + 30º (Table 2.2).

Structure of the guest	Solvent	Guests equivalents	λ / Δε (nm /L.mol^{-1}.cm^{-1})	A_{CD} amplitude observed (L.mol^{-1}.cm^{-1})	CD couplet *predicted*
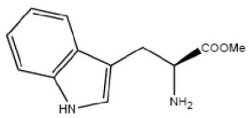 (S)-**3**	n-hexane	6 eq.	432 nm – 41 425 nm + 30	- 71	
	methylcyclohexane	20 eq.	433 nm – 52 423 nm + 25	- 77	negative
	dichloromethane		No distinctive CD		
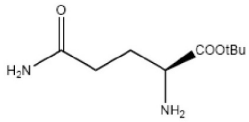 (S)-**4**	n-hexane	200 eq.	432 nm + 89 424 nm - 81	+ 170	
	methylcyclohexane	200 eq.	432 nm + 30 425 nm - 27	+ 52	positive
	dichloromethane		No distinctive CD		

Table 2.2: structures of chiral substrates ((S)-tryptophan methylester, **3**, (S)-glutamine *tert*-butylester, **4**) and CD data after complexation with tweezer in polar and apolar solvents.

In the case of L-histidine methyl ester **5**, the formation of the host-guest complex and the transfer of chirality to the **B/TT** tweezer have been investigated by taking into account two tautomeric forms **5-a** and **5-b** of the α-amino-ester (Figure 2.9).

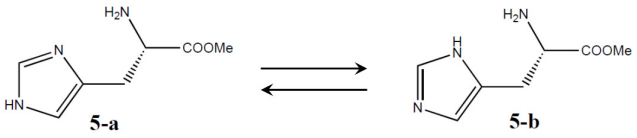

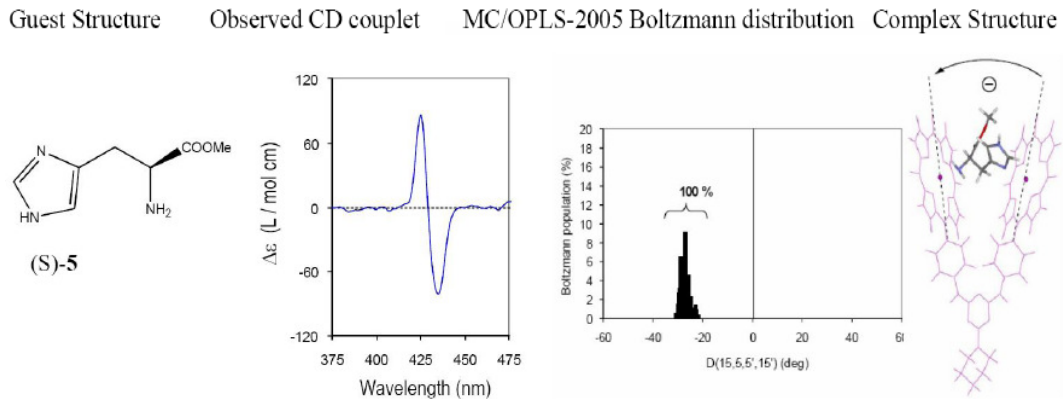

Figure 2.9: (top) tautomeric forms of L-histidine methyl ester and (bottom) starting from the left for L-histidine methyl ester **5**: chemical structure, experimentally CD response of the complex with **B/TT** tweezer; Boltzmann distribution of stable conformers in solution determined by MC/OPLS-2005; schematic representation of the two chromophores rotation in the supramolecular complex.

Both of these tautomers have been subjected to modeling studies with the **B/TT** tweezer in order to explain the origin of the empirically observed negative CD couplet for which a maximum intensity of $\Delta\varepsilon = 200$ $Lmol^{-1}cm^{-1}$ occurs at 10 equivalents. The MM of the host-guest complex associated with the both tautomers leads to a negative interporphyrin helicity, yet the more energetically stable form of the complex is given by tautomer **5-a**. The coordination leading to the negative twist is achieved through the more basic nitrogen of the histidine pentacycle and the primary amine. These results suggest that **B/TT** more optimally accommodates guests with a three atoms chain between the coordinating groups. Determination of binding constants that could confirm this hypothesis is underway.

As it can be seen in Figure 2.10, the absolute configuration of L-lysine esters derivatives **6**, **8** and **9** is reflected through a negative CD couplet, which is in an agreement with the MM study.

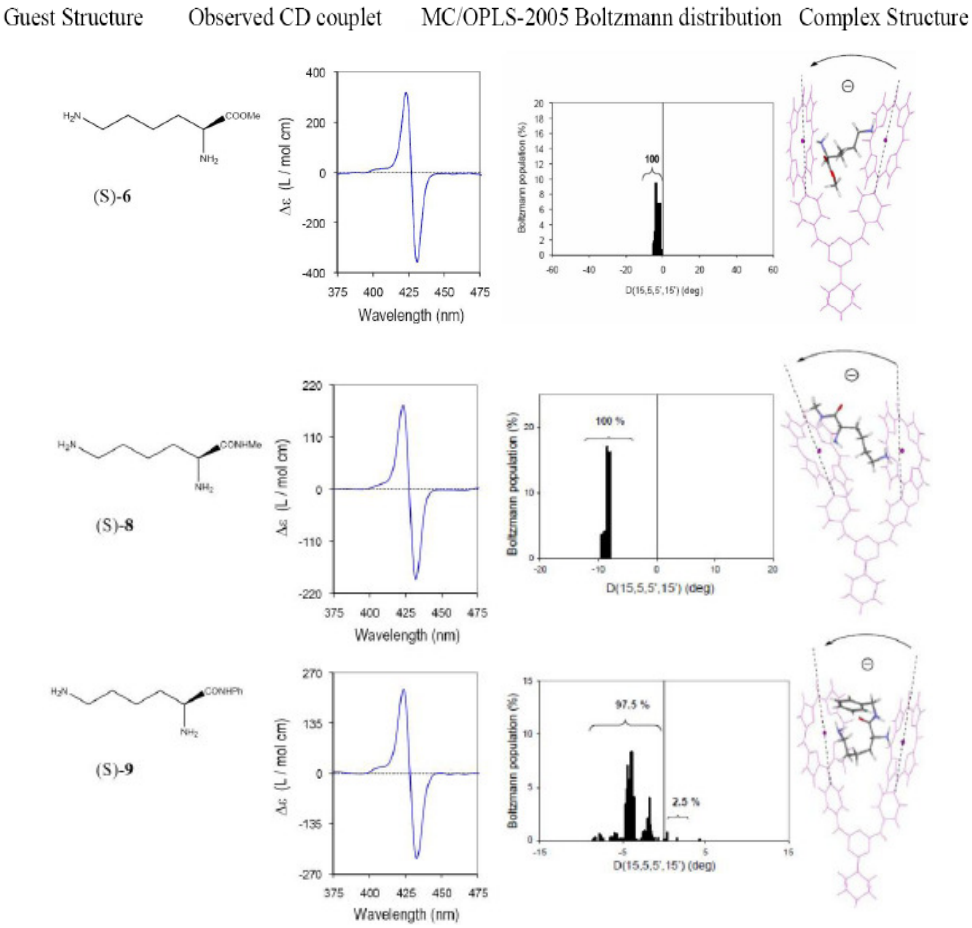

Figure 2.10: from left for L-lysine derivative **6** (methyl ester), **8** (methyl amide), **9** (phenyl amide): chemical structure, experimentally CD response of the complex with **B/TT** tweezer; Boltzmann distribution of stable conformers; schematic representation of rotation in the supramolecular complex.

Although L-lysine derivatives have provided consistency between the experimental and theoretical data, a very similar guest has provided an appealing challenge. Namely, L-ornithine methyl ester, compound **7**, which has the same absolute stereochemistry as lysine **6** which resulted in a positive rather than the negative CD exciton couplet. The sign of this CD couplet is also not in agreement with the most stable pool of conformers (open conformations), which exhibit a negative interporphyrin helicity. This result has been ambiguous especially because the L-lysine and L-ornithine differ only in one carbon atom. To explain this intriguing discrepancy, we engaged in two courses of further investigations: a) MM methodology to explore the possibility that, upon complexation, L-ornithine undergoes conformational change and binds to **B/TT** in a hydrogen bonded conformation; b) IR and NMR measurements to explore the possibility that the salt of ornithine methyl ester cyclizes after being treated with a base (*e.g.*, NaOH) in order to provide a free diamine. While MM results predict that **7** in an open conformation induce a negative interporphyrin helicity of the complex, the intramolecular H-bonded form of **7** induces a positive interporphyrin helicity (Figure 2.11).

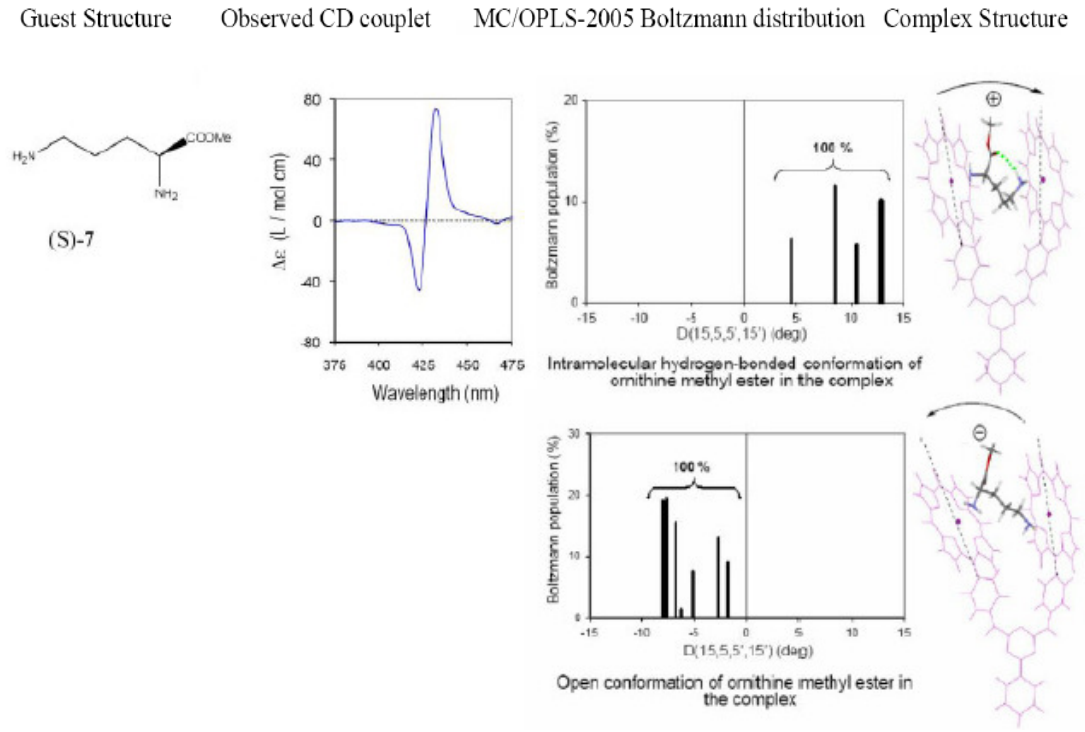

Figure 2.11: (top) from left for L-ornithine methyl ester **7** in hydrogen bonded conformation: chemical structure, experimentally CD response of the complex with **B/TT** tweezer; Boltzmann distribution of stable conformers; schematic representation of porphyrins rotation in the supramolecular complex; (bottom) Boltzmann distribution of conformers and its relative chromophores rotation in the complex.

Even more interestingly, the IR and NMR data shed light onto discrepancy in CD exciton couplet between L-lysine and L-ornithine methyl esters. Specifically, IR spectra show diagnostic differences between L-ornithine before and after the treatment with the base. Prior to the base treatment, L-ornithine methyl ester displays an IR band at ~1756 cm^{-1}, which is characteristic of an ester C=O stretching. On the other hand, after the base treatment, the spectrum displays a band at ~1651cm^{-1}, which is characteristic of an amide C=O stretching normal mode. These data clearly demonstrate that the compound that has been introduced within the **B/TT** is not ornithine methyl ester, yet the lactam analogue (Figure 2.12).

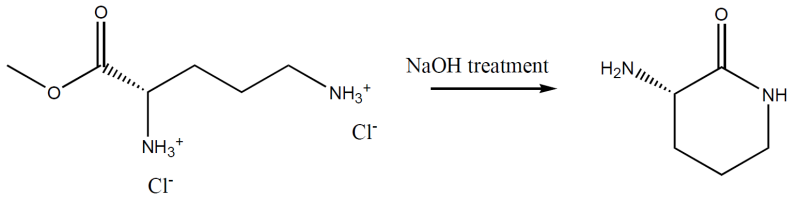

Figure 2.12: cyclization reaction of L-ornithine methyl ester under treatment with a base.

Considering that cyclization results in a stable six member ring, this fact justifies why this type of transformation takes place for ornithine methyl ester and doesn't take place in the case of lysine methyl ester, which would provide an unfavorable seven member ring. The IR based evidence for formation of the cyclic analogue has been confirmed with NMR. It is worth pointing out that molecular modeling of the ornithine methyl ester with intramolecular H-bonding, which most closely resembles the lactam analogue, does result in the prevailing positive interporphyrin helicity that matches with the sign of the experimentally observed CD couplet. Importantly, the molecular modeling simulations of **B/TT** complexed with the lactam analogue provide a prevalence of 55% towards the positive interporphyrin helicity (Figure 2.13), which matches the observed positive CD couplet.

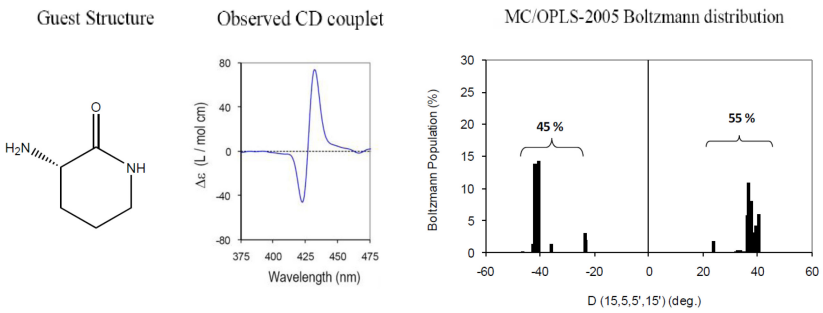

Figure 2.13: lactam analogue of L-ornithine methyl ester and Boltzmann distribution of conformers.

2.2.2 Derivatisation of the guest

As describe before (see introduction to this chapter) the *tweezer methodology* developed by Berova and coworkers[14] for the determination of absolute configuration of chiral compounds involved the derivatisation of the chiral guests under investigation. This method broadens the number of determinable chiral molecules by introducing diamine functionalities in order to allow formation of complexes between porphyrin dimers and molecules lacking coordination capability.

The synthesis of monodentate guest **18** (called carrier) is achieved in four steps as shown below, starting from 1,3-diaminopropane with an overall yield of 85% (Scheme 2.2).

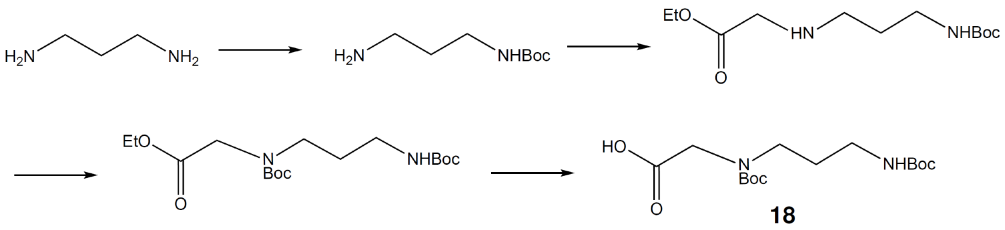

Scheme 2.2: schematic representation of the synthesis of carrier.

Thus, derivatisation is performed by linkage of the chiral guest (*e.g.*, a secondary monoalcohol like compound **10** in scheme 2.3) with the diBoc protected carrier molecule **18** via carbodiimide condensation (EDC/DMAP). Protecting groups cleavage with 10% TFA in dichloromethane affords the TFA salt of conjugate **10'**. The latter is converted to its free amine with Na_2CO_3 before complexation to **B/TT** tweezer (Scheme 2.3).

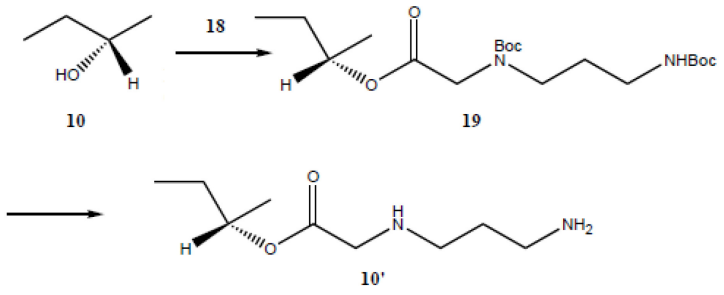

Scheme 2.3: example of derivatisation for *sec*-butanol (compound **10**).

Derivatisation has been applied to secondary monoalcohol and α-amino alcohols; although these latter have two nucleophilic functionalities (NH_2 and OH) chemical derivatisation was performed anyway to provide conjugates containing two amino moieties for achieving the coordination. Additionally, this derivatisation was considered beneficial in order to increase the distance between the two amino nucleophiles and avoid any strain during the binding between the **B/TT** tweezer and the guest.

2.2.3 Secondary Monoalcohols

Four monoalcohol chiral substrates **10**, **11**, **12** and **13** have been derivatized as described in the previous methodology section in order to obtain bidentate conjugates **10'**, **11'**, **12'** and **13'** that ensure the formation of the host-guest complex (Figure 2.14). In the past, these chiral guests have been successfully investigated with the traditional tweezer **A** via the steric size method[3]. We have chosen this class of guests to validate the applicability of **B/TT** tweezer as supported by the MM approach. These four monoalcohol derivatives differ in the steric size of substituents at the chiral center as well as in the propensity toward intramolecular hydrogen-bonding. In fact, complexes **10'-B/TT** and **11'-B/TT** exhibit weaker exciton CD couplets ($\Delta\varepsilon$ = 100 L mol^{-1} cm^{-1}) than complexes **12'-B/TT** and **13'-B/TT** ($\Delta\varepsilon$ = 400 L mol^{-1} cm^{-1}). This observation is intuitive considering that **10'** and **11'** involve small discrimination in the steric size of the substituents at the stereogenic center. For example, compound **10'** contains small ethyl and methyl functionalities, whereas compound **12'** contains bulky menthol substituents.

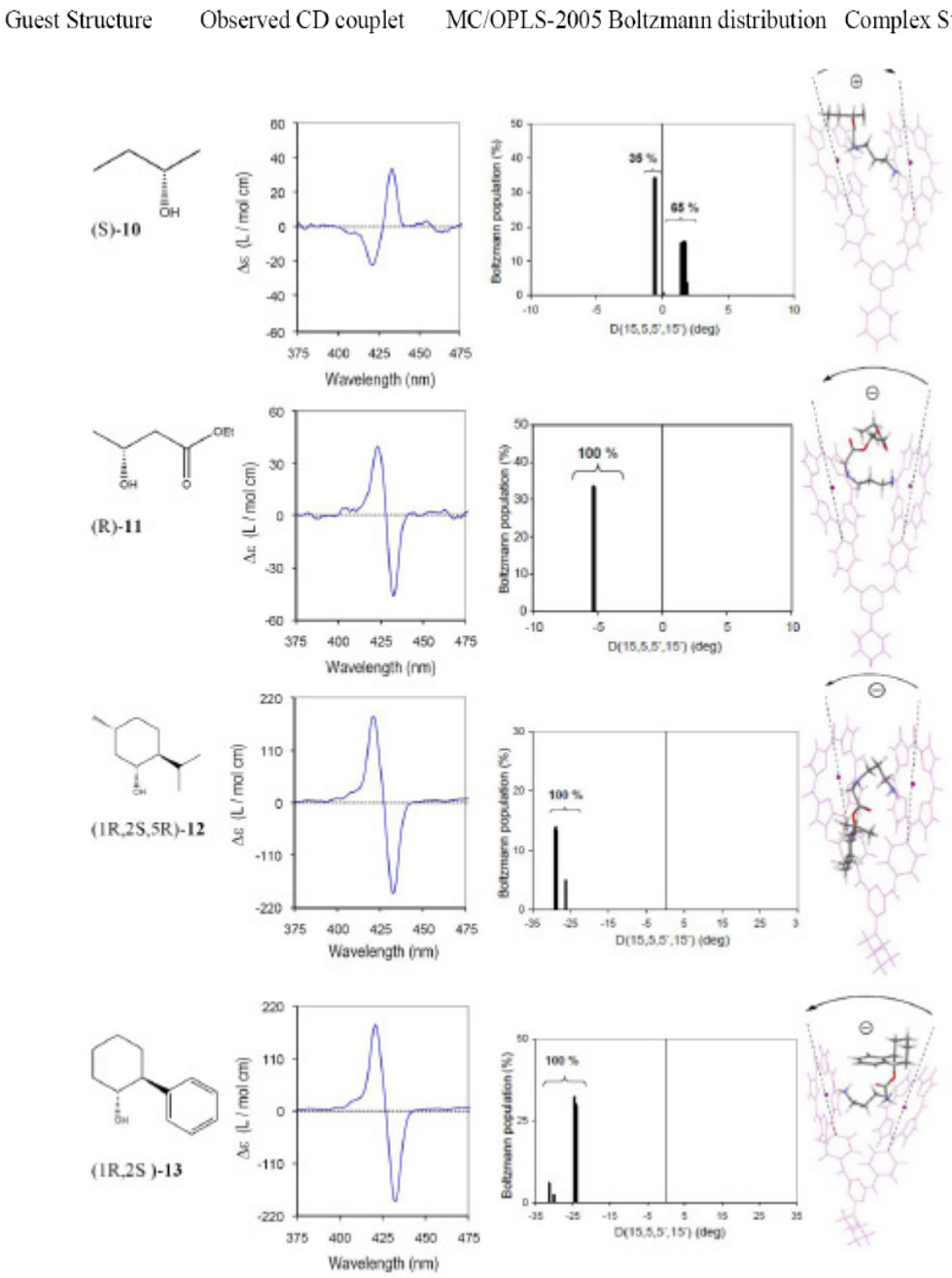

Figure 2.13: starting from the left: structures of underivatized guests, and CD data, Boltzmann distribution, and schematic representation of supramolecular complex of their conjugates with carrier **18**.

This investigation provides agreement between the sign of the interporphyrin helicity and the observed CD couplet for the four monoalcohol derivatives-**B/TT** complexes. Moreover, hydrogen-bonded forms of **12'** and **13'** in the tweezer display a larger interporphyrin helicity, which is associated with the higher CD amplitude. Therefore, we assume that the folded, rather than open conformations of **12'** and **13'** prevail within the **B/TT** host in solution.

2.2.4 α-Amino Alcohols

As can be seen from Table 2.3, formation of the host/guest complex between the **B/TT** tweezer and each of the derivatized amino alcohols yielded observable CD exciton couplets which are diagnostic of the existence of preferential stereodifferentiation of porphyrins in the presence of this family of guest.

Structure of the Underivatized Guest	Solvent	Guest equivalents	λ/Δε (nm/L·mol^{-1}·cm^{-1})	A_{CD} amplitude observed (L·mol^{-1}·cm^{-1})	CD couplet *predicted*
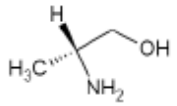 (*R*)-2-amino-1-propanol / (*R*)-**19**	n-hexane	60 eq.	431 nm - 41 422 nm + 41	- 82	
	methylcyclohexane	150 eq.	431 nm - 44 422 nm + 40	- 84	negative
	dichloromethane	70 eq.	432 nm - 15 422 nm + 15	- 30	
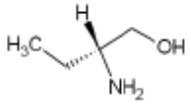 (*R*)-2-amino-1-butanol / (*R*)-**20**	n-hexane	10 eq.	427 nm - 13 416 nm + 12	- 25	
	methylcyclohexane	30 eq.	434 nm - 28 425 nm + 17	- 45	negative
	dichloromethane		No distinctive CD		
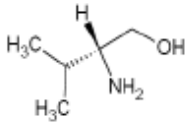 (R)-2-amino-3-methyl-1-butanol / (R)- **21**	n-hexane	200 eq.	430 nm - 22 421 nm + 20	- 42	
	methylcyclohexane	200 eq.	431 nm - 29 422 nm + 25	- 54	negative
	dichloromethane	200 eq.	430 nm - 7 423 nm + 10	- 17	
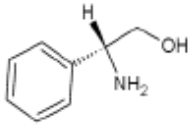 (*R*)-2-amino-2-phenylethanol / (*R*)- **22**	n-hexane	200 eq.	433 nm - 63 423 nm + 66	-129	
	methylcyclohexane	200 eq.	435 nm - 14 425 nm + 40	- 54	negative
	dichloromethane		No distinctive CD		
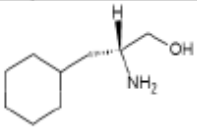 (*S*)-2-amino-3-cyclohexyl-1-propanol / (*S*)- **23**	n-hexane	100 eq.	430 nm + 74 421 nm -32	+ 106	
	methylcyclohexane	100 eq.	431 nm + 58 421 nm - 30	+88	positive
	dichloromethane		No distinctive CD		

Table 2.3: summary of CD responses for derivatized amino alcohols.

With a closer look at the table, one can observe consistent trends: (*R*)-configured guests result in a negative CD couplet, while (*S*)-configured guest exhibits a positive CD

couplet. While measurements of the CD spectra upon complexation in three solvent environments (*n*-hexane, methylcyclohexane, and dichloromethane) provided varying amplitudes, they all gave the same CD sign. The lack of solvent dependence on the sign of the CD response is an important outcome since molecular modeling investigations which are used for interpreting the CD data are performed in vacuum. Indeed, the potential change in sign of the observed CD would signal the need for performing molecular modeling studies in solvent environment, which would considerably hamper the efficiency in applying the tweezer methodology. The general observation regarding uniformity in the sign of CD exciton couplet exhibited by the **B/TT** tweezer is one of the advantages that it has over some previously applied tweezers. Nevertheless, since hexane predominantly gave the most discernable signal and in particular the highest amplitude at the smallest number of equivalences, we can establish that it represents the best solvent for determining the AC of amino alcohols with the **B/TT** tweezer.

The absolute configuration of the selected chiral amino alcohols is known, yet previous studies suggest that the prevailing interporphyrin helicity can be influenced by steric-size factors, conformational factors (H-bonding, π-π stacking) as well as by variation in preferred coordination sites between the Zn^{II} of the porphyrins and available nucleophiles of the chiral guest. As it can be seen from Table 2.3, each of the five amino alcohols resulted in the optimal correspondence between the sign of the CD exciton couplet and the sign of the interporphyrin helicity. One of the key advantages of the **B/TT**-tweezer relative to the **A**-tweezer is the fact that due to its lower conformational flexibility evidenced by it having 6 rather than 12 degrees of freedom (commercial tweezer), the population of low energy conformers uniformly favours one sign of interporphyrin twist.[14,15] In all of the cases examined, ~ 99% of stable conformers result in the same sign of the interporphyrin helicity. This consistency in the sign is significant because it removes any possibility for an ambiguous AC assignment. Figure 2.14 illustrates a theoretical model associated with the most stable conformation for each of the five host/guest complexes considered before.

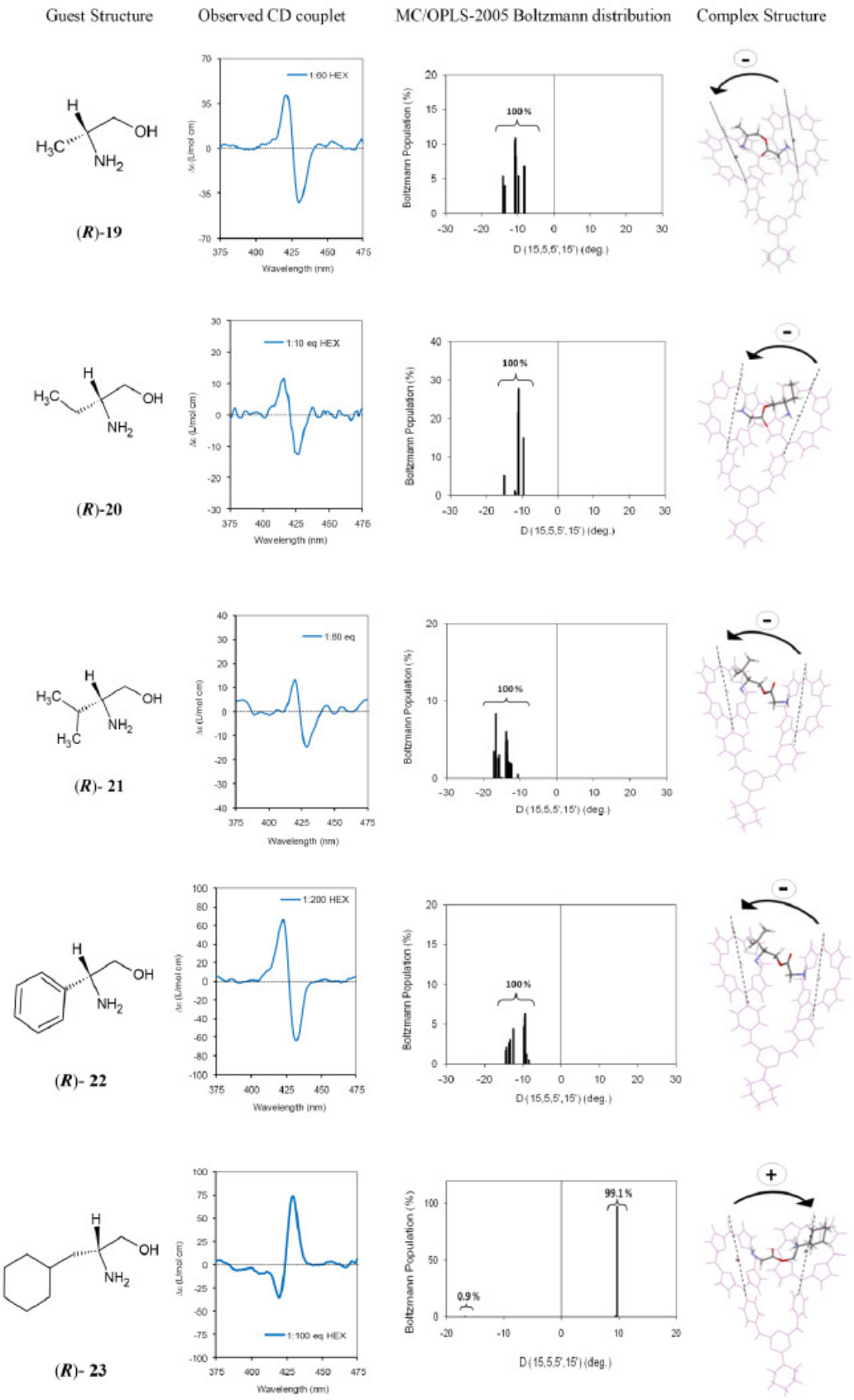

Figure 2.14: comparison of the experimental CD responses and prevailing interporphyrin helicity for derivatized amino alcohols with carrier **18**.

Besides establishing if the **B/TT** can be used as a reliable AC reporter of derivatized amino alcohols, one of the appealing challenges behind investigating the amino alcohols is to determine if **B/TT** could provide a diagnostic CD for this family of guests even without derivatisation. Previous reports on the commercial tweezer indicate that its complexation with the selected amino alcohols requires derivatisation in order to provide a CD response. As it can be seen from Table 2.4, underivatized amino alcohols complexed with the **B/TT** do provide CD exciton couplet responses with the exception of amino alcohol **22**.

Underivatized Guest	Solvent	Guest equivalents	$\lambda/\Delta\varepsilon$ ($nm/L \cdot mol^{-1} \cdot cm^{-1}$)	A_{CD} amplitude observed ($L \cdot mol^{-1} \cdot cm^{-1}$)	CD couplet observed in n-hexane
	n-hexane	40 eq.	432 nm + 42 422 nm - 35	+ 77	
(*R*)-19	methylcyclohexane	10 eq.	431 nm + 25 424 nm - 9.0	+ 34	
	dichloromethane	200 eq.	428 nm + 7.4 422 nm - 6.5	+ 14	
	n-hexane	100 eq.	431 nm - 8.2 425 nm + 20	- 29	
(*R*)-20	methylcyclohexane	100 eq.	433 nm - 8.4 424 nm + 9.9	- 18	
	dichloromethane		No distinctive CD		
	n-hexane	60 eq.	433 nm - 41 423 nm + 58	- 99	
(*R*)- 21	methylcyclohexane	60 eq.	434 nm - 23 425 nm + 39	- 63	
	dichloromethane		No distinctive CD		
	n-hexane				
(*R*)- 22	methylcyclohexane		No distinctive CD		
	dichloromethane				
	n-hexane	60 eq.	432 nm + 48 424 nm - 12	+ 60	
(*S*)- 23	methylcyclohexane	100 eq.	433 nm + 43 426 nm - 11	+ 54	
	dichloromethane		No distinctive CD		

Table 2.4: summary of CD responses for underivatized amino alcohols.

Binding of the amino alcohol **22** is most likely sterically hindered due to presence of the bulky phenyl moiety, which is only one atom away from the coordinating amino group. It is important to note that underivatized amino alcohols **20**, **21**, **23** do provide the same sign of the CD couplet as their derivatized analogues, therefore suggesting that these CD responses are diagnostic of the AC for these chiral guests. Surprisingly, however, amino alcohol **19** exhibits a positive CD couplet which is opposite in sign of the negative CD couplet obtained for the underivatized analogue. The molecular modeling studies of the 1:1 complex between the **B/TT** and the underivatized **19** display a prevalence of the negative interporphyrin helicity, which does not agree with the observed CD response. The apparent sign reversal between the derivatized and underivatized amino alcohol **19** could be justified as the result of deviation from 1:1 host/guest complexation. Specifically, previously published studies of amino alcohols have provided a word of caution due to a notable difference in the binding affinity of alcohols and amines with zincated porphyrins. According to Borhan and coworkers,[2] the large difference in binding affinity of the two groups could disrupt 1:1 complex with increasing equivalence of amino alcohols added. The resulting 2:1 complex is not expected to be CD active. The fact that amino alcohol **19** does provide the CD couplet could indicate an even more intricate complexation mechanism, which will be the subject for future investigations.

Although the **B/TT** does provide optimism in terms of being able to respond to the chirality of small chiral guests such as underivatized amino alcohols considered herein, it seems that the lack of derivatisation would only be applicable for those guests that intrinsically have two nucleophiles with the same binding affinities (diamines and possibly dialcohols). Therefore, for now we promote the use of **B/TT** as a reliable AC reporter for the derivatized amino alcohols.

REFERENCES

[1] Huang, X.; Rickman. B.H.; Borhan. B.; Berova, N.; Nakanishi, K., *J. Am. Chem. Soc.*, **1998**, *120*, 6185. (b) Huang, X.; Borhan. B.; Rickman. B.H.; Nakanishi, K.; Berova, N., *Chem. Eur. J.*, **2000**, *6*, 216. (c) Kurtan, T.; Nesnas, N.; Li, Y.Q.; Huang, X.F.; Nakanishi, K.; Berova, N., *J. Am. Chem. Soc.*, **2001**, *123*, 5962. (d) Proni, G.; Pescitelli, G.; Huang, X.F.; Nakanishi, K.; Berova, N., J. Am. Chem. Soc., **2003**, *125*, 12914.

[2] Tanasova, M.; Vasileiou, C.; Olumolade, O., O.; Borhan, B., *Chirality*, **2009**, *21*, 374.

[3] Borovkov, V.V.; Hembury, G.A.; Inoue, Y., *Acc. Chem. Res.*, **2004**, *37*, 449.

[4] Fazio, M.A.; Lee, O.P.; Schuster, D.I., *Org. Lett.,* **2008**, *10*, 4979.

[5] Carofiglio, T.; Lubian, E.; Menegazzo, I.; Saielli, G.; Varotto, A., *J. Org. Chem.*, **2009**, *74*, 9034.

[6] Gans, P.; Sabatini, A.; Vacca, A., *Talanta*, **1996**, *43*, 1739.

[7] Packer, M. J.; Zonta, C.; Hunter, C. A., *J. Magn. Reson.*, **2003**, *162*, 102.

[8] Gomila, R.M.; Garau, C.; Frontera, A.; Quinonero, D.; Ballester, P.; Costa, A.; Deyà, P.M., *Tetrahedron Lett.*, **2004**, *45*, 9387.

[9] Bagno, A.; Saielli, G., *Theor. Chem. Acc.*, **2007**, *117*, 603.

[10] Mohamadi, F.; Richards, N.G.J.; Guida, W.C.; Liskamp, R.; Lipton, M.; Caufield, C.; Chang, G.; Hendrickson, T.; Still, W.C., *J. Comput. Chem.*, **1990**, *11*, 440.

[11] Petrovic, A.; Chen, Y.; Pescitelli, G.; Berova, N.; Proni, G., *Chirality*, **2010**, *22*, 129.

[12] Chen, Y.; Petrovic, A.; Roje, M.; Pescitelli, G.; Kayser, M.M.; Yang, Y.; Berova, N.; Proni, G., *Chirality*, **2010**, *22*, 140.

[13] Berova, N.; Pescitelli, G.; Petrovic, A., G.; Proni, G., *Chem. Comm.*, **2009**, 5958.

[14] Kurtàn, T.; Nesnas, N.; Li, Y.-Q.; Huang, X.; Nakanishi, K.; Berova, N., *J. Am. Chem. Soc.* **2001,** *123,* 5962.

[15] Kurtàn, T.; Nesnas, N.; Koehn, F.E; Li, Y.-Q.; Nakanishi, K.; Berova, N., *J. Am. Chem. Soc.* **2001,** *123,* 5974.

EXPERIMENTAL SECTION

3.1 Materials and Reagents

Tetraphenyl porphyrin **TPP** was purchased from EGA-CHEMIE, Germany. 5-(4-aminophenyl)-10,15,20-(3,5-tert-butylphenyl)porphyrin, **T**, was prepared according to the literature procedures.[xx] Other reagents and solvents (Sigma-Aldrich, Fluka and Carlo Erba Reagenti) were of the highest grade available and were used without further purification. Solvents employed in the spectroscopic studies are of spectroscopic grade and used as received. Silica gel MN 60 (70–230 Mesh) by Macherey-Nagel and alumina neutral (Brockmann Grade III) were used for column chromatography. Analytical thin layer chromatography (TLC) was performed using a Polygram SilG/UV_{254} TLC plates with fluorescent indicator.

3.2 Instruments

Routine ^{1}H-NMR spectra were recorded with a spectrometer operating at 250 MHz. Two-dimensional NMR spectra were acquired at 298 K, on a 400 MHz spectrometer equipped with a 5 mm multinuclear inverse z-field gradient probe-head. Data processing was performed on a workstation using the TOPSPIN 1.3 software. The proton chemical shifts were referenced to the residual ^{1}H $CDCl_3$ solvent signal (7.26 ppm). Proton resonance assignments were obtained using 2D homonuclear correlation spectroscopy (DQF-COSY for free guest and host, DQF-COSY and TOCSY for the host-guest assignments) with gradient coherence selection. ^{1}H one-dimensional spectra were acquired with 32 transients, 8022.6 Hz spectral width, 16K data points. Double-Quantum Filtered Correlation (DQF-COSY) and Total Correlation Spectroscopy (TOCSY) experiments were recorded using a repetition delay of 2 s; a total of 400 experiments of 32 scans were accumulated; 2K data points were recorded in the acquisition dimension (F2) and the spectral width was 20.05 ppm. Zero-filling in both F1 and F2 multiplication with a gaussian function in F2 and a squared sine function (in DQF-COSY) or a squared cosine function (in TOCSY) in F1, was performed prior to Fourier transformation. In the TOCSY experiments the spin-lock time period was 70 ms. UV-vis spectra were recorded on a spectrophotometer equipped with a thermostated cell holder. Routine UV-vis spectra were recorded in CH_2Cl_2 on a Varian Cary 50 Spectrophotometer equipped with a temperature-controlled cell holder. Mass spectra (ESI-MS) were recorded on a LC-MSD-Trap-SL (Agilent Technologies, Palo

Alto, USA). Samples were dissolved in acetonitrile (~10^{-5} M) and injected in a stream of the same solvent, containing 0.1% of formic acid, at 50 µl min^{-1} (nitrogen nebulizing gas pressure = 20 psi; flow = 5 L min^{-1}; T = 325 °C). CD spectra were measured with a JASCO J-715 spectropolarimeter (Japan) equipped with a nitrogen-controlled quartz cell (path length 1 mm) in a cryostat, at room temperatures. Scanning conditions were as follows: scanning rate 200 nm/min, bandwidth 2 nm, response time 2 s, scanning range 390-460 nm.

3.3 Methods

3.3.1 General procedure for milligram scale preparation of host-guest complexes for measurement of CD

In a typical experiment, a 1 µM tweezer solution is prepared by the addition of a 35 µL aliquot of tweezer (0.1 mM in anhydrous CH_2Cl_2) to 3 mL of CH_2Cl_2. The exact concentration of the diluted tweezer solution is determined by UV from the known ε value of the Soret band in CH_2Cl_2 (ε = 1'055'830 L mol^{-1} cm^{-1}). This tweezer solution is purple. The free amine solution of conjugate (0.3 mg, 1.03 µmol) is prepared from its TFA salt after the addition of 0.5 mL of MeOH and 1 mL of CH_2Cl_2, followed by solid Na_2CO_3 (10 mg). The solvent is then dried under a stream of argon followed by placement under a high vacuum (0.2 Torr) for 20 min. Anhydrous CH_2Cl_2 (1 mL) is then added to yield the free amine solution of conjugate (1.03 mM). An aliquot of 4 µL of the latter solution (*ca.* 5 equivalents) is added to 0.8 mL of the prepared porphyrin tweezer solution to afford tweezer/conjugate host-guest complex. The UV-vis and CD spectra are recorded at 25 °C and corrected for background. In the UV spectra, the red shift of the tweezer Soret band indicates that complexation actually takes place. Analogously, we observed that the colour of the tweezer solution transitions from purple to green, as the guest is added.

Fives amino alcohols **19-23** were selected for current investigation and each of them has undergone the same derivatisation procedure. The synthesis was carried in three steps: Boc protection of amino groups in amino alcohols, amino alcohol derivatisation using glycine and the removal of the Boc group.

3.3.2 General procedure for the determination of the binding constants by UV-vis spectroscopy

For the determination of the binding constants, a micromolar solution of **B/TT** in CH_2Cl_2 was introduced in a UV-vis cuvette (optical path: 1 cm) and titrated by adding aliquots of a guest stock solution in CH_2Cl_2 by using a 10 μL gas-tight microsyringe. After any addition the solution was equilibrated for 5 minutes inside the cell-holder (temperature set at 298 K) of the UV-vis spectrophotometer then the corresponding UV-vis spectrum was acquired in the range 380÷700 nm. All the data were corrected by a dilution factor and background subtraction of the solvents. The addition was continued until the recorded spectrum was super-imposable to the previous one. All the spectra were imported into the program HYPERQUAD program,[1] a suite of programs designed for analyzing chemical equilibria using the nonlinear least-squares curve-fitting based on a desired host:guest model (in our case a 1:1 dimer:diamine model).

3.3.3 Computational details for NMR shielding theoretical calculations

NMR shielding calculations require high level DFT methods[2] using the ADF software package.[3] In Particular, the BLYP functional[4] and an all-electron, triple-ζ, double polarization, Slater-type basis set (TZ2P) were employed. Considering the size of the tweezer, a high computational effort is required, especially if relativistic effect have to be considered. However, we have previously reported[5] for analogous tweezers that relativistic effects can be safely ignored. Indeed, relativistic proton chemical shifts, even for the NH_2 protons (*i.e.* the closest to the heavy atoms) differ only by less than 0.1 ppm from the non-relativistic results. Chemical shifts were calculated as $\delta = \sigma_{ref} - \sigma$ where σ_{ref} is the shielding constant of TMS (σ_H = 31.21 ppm) and σ the shielding constants of interest. Chemical shifts of magnetically equivalent protons were obtained after averaging of the single resonances. In order to take into account the conformational properties of the molecule, the NMR shielding calculations were carried out starting from three different conformers of similar energy. These conformers resulted from Monte Carlo (MC) conformational search algorithm and OPLS-2005 force field (*vide infra*).

3.3.4 Molecular Modeling Protocol

In addition to the derivatisation and empirical CD measurements of the subsequently formed host/guest complexes, a Molecular Modeling (MM) computational approach was

used to predict the prevailing host/guest structure. This approach was used in previous studies and provided a valid method to relate inter-porphyrin twist and the AC of the guest. The molecular modeling approach is broadly applicable as it simultaneously takes into account conformational, electronic and steric factors. It allows the identification of the most probable host-guest complex structures and provides an insight in host guest coordination sites. The implementation of molecular modeling to elucidate the chirality of tweezer complexes, has overcomed the limitation of the relative steric-size approach. Herein, molecular modeling investigations were carried out with the support of Monte Carlo (MC) conformational search algorithm and OPLS-2005 force field.[6] The use of OPLS-2005 allows for a more meaningful consideration of the relatives energies and Boltzmann populations of conformations obtained via MC searches, which opens a window for a more detailed structural analysis of tweezer complexes.[6]

The overall theoretical approach has been carried out using Macro Model v9.5 applet within the Schrödinger suite software. The conformational space of the complex was first sampled using two separate tracks: the first one used a hybrid Monte Carlo Stochastic Dynamics (MC/SD) search followed by a MC algorithm; the second one used only a MC algorithm yet with multiple initial conformations of the guest "seeded" within the tweezer host with 0º interporphyrin helicity. The first track, MC/SD algorithm was used because it performs an extensive survey of the potential energy surface in order to identify the low energy host/guest conformation and therefore find those that are stable. The MC/SD search was performed using as condition a simulation temperature of 300 K, a time step of 1fs, an equilibrium time of 1ps and a simulation time of 1ns. All runs were performed using OPLS-2005 as force field and no solvent. The number of minimization steps was set to 10000, by setting coordination constrains of 2.2 Å ± 0.5 Å for N-Zn distance and a force constant equal to 100. The theoretical conformational search has yielded a pool of most stable conformers within 10 kJ/mol energy window whose Boltzmann weighted distribution of interporphyrin helicities was subsequently compared with the sight of the observed CD couplet.

3.4 Synthesis of Compounds

3.4.1 Synthesis of 5-(4-aminophenyl)-10,15,20-tris-(3,5-di-*tert*-butylphenyl) porphyrin, T

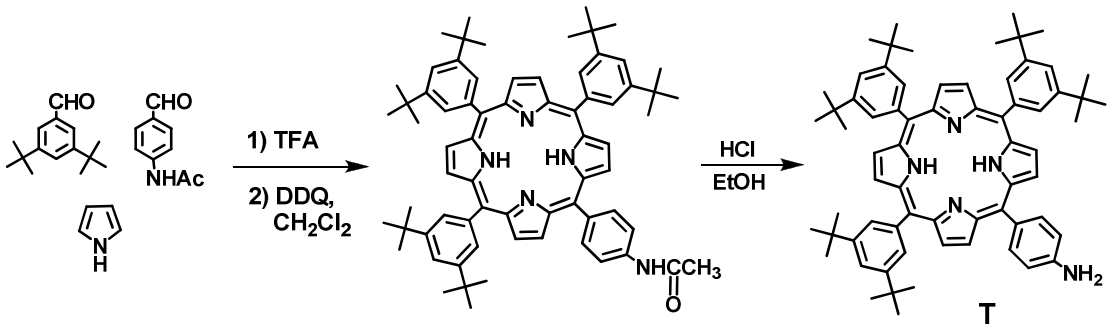

Following a literature method,[7] (1.637 g, 7.5 mmol) and *p*-acetamidobenzaldehyde (0.410 g, 2.5 mmol) were dissolved in 1 L of CH_2Cl_2 contained in a 2 L three-necks flask. The flask was covered with aluminium foil and purged with N_2 for 10 min before freshly-distilled pyrrole (700 μL, 10 mmol) was injected. The reaction was stirred for another 10 min, and the reaction was initiated by the injection of TFA (1.4 mL, 20 mmol). After stirring at room temperature for 1 h, DDQ (1.70 g, 7.5 mmol) was added. The reaction was stirred additionally for 1 h at room temperature and was then neutralized with triethylamine (2.8 mL, 20 mmol). The crude mixture was purified with silica gel flash chromatography; elution with CH_2Cl_2 was able to remove tetraphenyl porphyrin, and then with 20% EtOAc in CH_2Cl_2 to collect the desired mono-porphyrin product. Solvent was removed under vacuum, affording a purple solid in a yield of ~18 %. ^{1}H-NMR ($CDCl_3$, 250 MHz) δ: 8.8 ppm (m, 6H, βH), 8.5 ppm (d, 2H, βH), 8.0 ppm (m, 6H, Ar-*meta*-H), 7.9 ppm (d, 2H, ArH), 7.7 ppm (m, 3H, Ar-*para*-H), 7.4 ppm (d, 2H, ArH), 7.1 ppm (s, 1H, NH), 2.0 ppm (s, 3H, CH_3), 1.4 ppm (s, 54H, *tert*-BuH), -2.8 ppm (s, 2H, pyrrole H). ESI-MS $C_{70}H_{81}N_5O$ (CH_3CN + 1% HCOOH as eluent) m/z: obsd 1007.9 $[MH]^+$ (calcd 1008.64), obsd 504.2 $[MH_2]^{2+}$ (calcd 504.82). UV-vis (CH_2Cl_2, nm): 421, 513, 548, 592, 647.

A solution of porphyrin-amide (0.2067 g, 0.2 mmol) was dissolved in 60 mL EtOH in a 250 mL flask. Concentrated HCl (40 mL, 6 M) was added to the reaction mixture, which was heated at reflux for 13 h. The crude mixture was cooled, diluted with water and extracted with CH_2Cl_2 six times. The organic layer was washed with H_2O three times and

with saturated $NaHCO_3$ solution twice. The pooled organic layer was dried over Na_2SO_4 and filtered. The solvent was removed under vacuum and flash chromatography with silica gel and CH_2Cl_2 afforded the desired porphyrin in quantitative yield. ^{1}H-NMR ($CDCl_3$, 250 MHz) δ: 8.8 ppm (m, 8H, βH), 8.0 ppm (m, 6H, Ar-*meta*-H), 7.9 ppm (d, 2H, ArH), 7.7 ppm (m, 3H, Ar-*para*-H), 6.9 ppm (d, 2H, ArH), 3.9 ppm (s, 2H, NH2), 1.4 ppm (d, 54H, *tert*-BuH), -2.7 ppm (s, 2H, pyrrole H). ESI-MS $C_{68}H_{79}N_5$ (CH_3CN + 1% HCOOH as eluent) m/z: obsd 966.8 $[MH]^+$ (calcd 966.63), obsd 483.5 $[MH_2]^{2+}$ (calcd 483.82). UV-vis (CH_2Cl_2, nm): 422, 515, 550, 593, 649.

3.4.2 Synthesis of Bis(3,5-di-*tert*-Butylphenyl-Porphyrin-Zn^{II}) Homodimer, B/TT

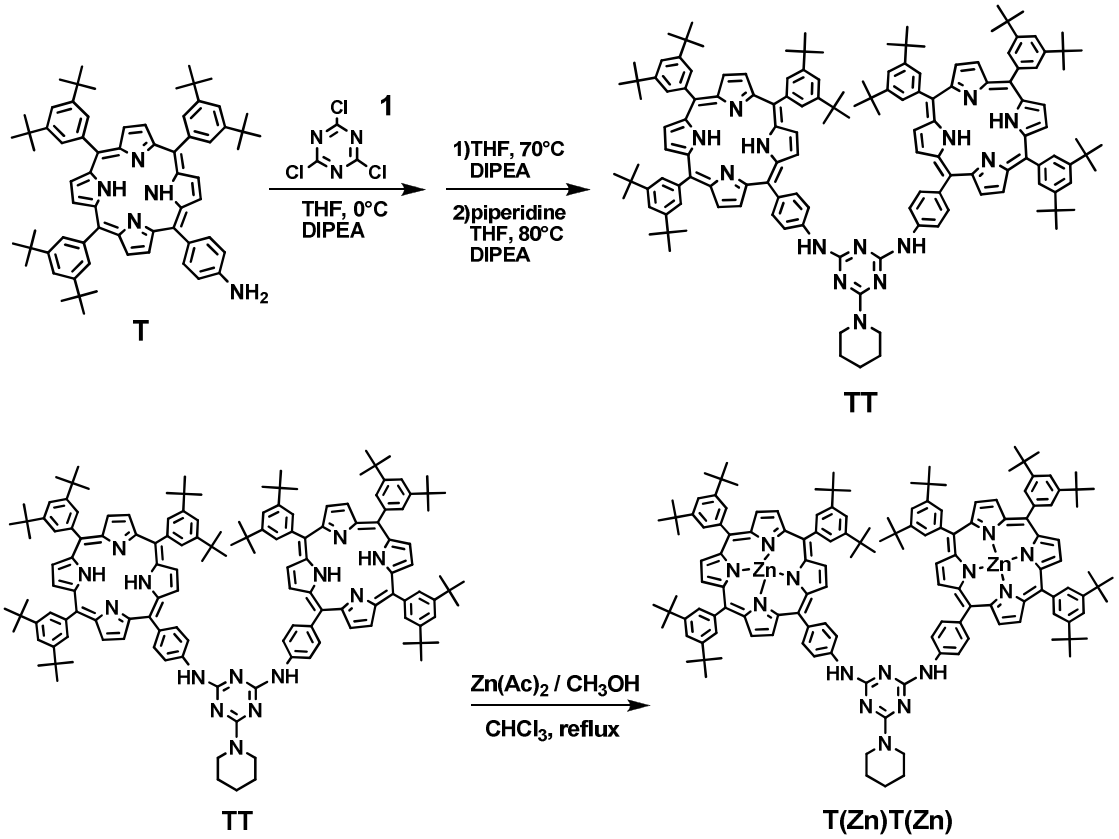

Following the one-pot protocol,[8] to a solution of porphyrin **T** (19.1 mg, 20 μmol) in THF (1.0 mL) cooled at 0 °C, a THF solution of cyanuric chloride **1** (3.7 mg, 20 μmol) and DIPEA (3 mg, 24 μmol) was added. After stirring for 10 min at 0 °C, the solution was left to reach room temperature. The reaction was complete, as resulting from TLC analysis (silica gel, petroleum ether/ethyl acetate 3:2 v/v) showing the disappearance of porphyrin **T** (R_f = 0.31) and the formation of a new spot at R_f = 0.63 corresponding to the **T**-cyanuric

chloride mono-adduct. A second equivalent of porphyrin **T** (19.1 mg, 20 μmol) was then added together with 1.2 equiv of DIPEA and the reaction was stirred at 70 °C for 24 h. After observing the almost complete formation of the bis-adduct (R_f = 0.73), an excess of piperidine (5.0 mg, 60 μmol) was added together with 1.2 equiv of DIPEA and the mixture was stirred at 80 °C for 3 h so leading to the **B/TT** derivative. After removal of the solvent, the residue was purified by flash chromatography (silica gel, eluent: petroleum ether/ethyl acetate 3:2 v/v) affording 70 mg (82%) of **B/TT** derivative (R_f = 0.78). ^{1}H-NMR ($CDCl_3$, 250 MHz) δ: 9.09 (d, 4H, β-pyrrole), 9.02 (m, broad 12H,β-pyrrole), 8.04 (d, 4H, phenyl aromatic protons near triazine ring), 8.10-7.78 (m, 14H, phenyl aromatic protons) 7.19 (br s, 2H, NH), 3.99 (br s, 4H, piperidine), 1.74-1.68 (br s, 6H, piperidine), -2.46 (s, 4H, pyrrole NH). ESI-MS $C_{144}H_{166}N_{14}$ (CH_3CN + 1% HCOOH as eluent) m/z: obsd 2093.4 $[MH]^+$ (calcd 2093.95), obsd 1047.5 $[MH_2]^{2+}$ (calcd 1047.48), obsd 698.7 $[MH_3]^{3+}$ (calcd 698.65), obsd 524.4 $[MH_4]^{4+}$ (calcd. 524.24). UV-vis (CH_2Cl_2, nm): 421, 517, 551, 594, 649.

For the preparation of the corresponding Zn^{II} complex, to a solution of **B/TT** (40 mg, 19 μmol) in 5 mL of $CHCl_3$ was added a saturated solution of zinc acetate (0.5 mL) in CH_3OH and refluxed for 1 h. The solvent was evaporated. The residue was dissolved with CH_2Cl_2 and washed with water in order to remove the excess of zinc acetate. The organic phases were combined, dried over Na_2SO_4, filtered and concentrated under reduced pressure to give a purple solid (96% yield, R_f = 0.75 (silica gel, eluent: petroleum ether/ethyl acetate 3:2 v/v). ^{1}H-NMR ($CDCl_3$, 250 MHz) δ: 9.09 (d, 4H, β-pyrrole), 9.02 (m, broad 12H, β-pyrrole), 8.04 (d, 4H, phenyl aromatic protons near triazine ring), 8.10-7.78 (m, 14H, phenyl aromatic protons) 7.19 (br s, 2H, NH), 3.99 (br s, 4H, piperidine), 1.74-1.68 (br s, 6H, piperidine) 1.53 (s, 108H, *t*-butyl protons). UV-vis (CH_2Cl_2, nm): 425 (Soret band, ε = 1'055'830 $M^{-1}cm^{-1}$), 553, 596.

3.4.3 Synthesis of L-lysine derivatives 8 and 9

The synthesis of L-lysine methyl amine is performed in two steps from the N,N-di-Boc-L-lysine which is linked to the methyl amine in the presence of 1-(3-dimethyl-aminopropyl)-3-ethylcarbodiimide (EDC) and 4-(dimethyl-amino)pyridine (DMAP).

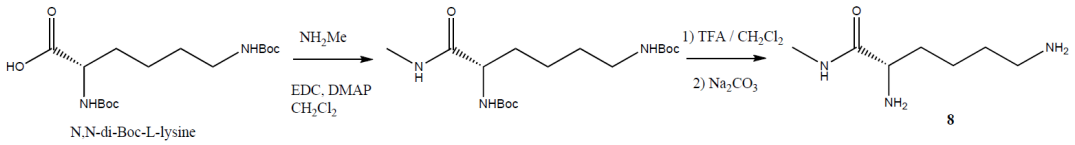

The obtained amide is deprotected with 10% TFA in dichloromethane to afford the TFA salt of L-lysine methyl amide **8**. The same synthesis is used for L-lysine benzyl amide **9**.

3.4.4 Boc protection of amino groups in amino alcohols

To a solution of amino alcohol in dry THF (3 mL), triethylamine (100 µL) and di-*t*-butyl carbonate (1.2 eq) were added. After stirred overnight in argon atmosphere at room temperature, the solvent was evaporated and CH_2Cl_2 (10 mL) was added. The solution was then washed with NH_4Cl aqueous solution (10 mL) and dried with Na_2SO_4. The mixture was filtrated and analyzed by TLC, ESI-MS and ^{1}H-NMR.

3.4.5 Amino alcohol derivatisation

To a solution of N-boc-amino alcohol in CH_2Cl_2 (1 mL), N-boc-glycine (1.2 eq), EDC (1.5 eq) and DMAP (0.2 eq) were added. The solution was stirred overnight at room temperature and the mixture separated by column chromatography.

3.4.6 Removal of the Boc groups

The compound was dissolved in 10% TFA in CH_2Cl_2 (1 mL). After stirred overnight at room temperature, the solution was evaporated to give the product.

REFERENCES

[1] Gans, P.; Sabatini, A.; Vacca, A., *Talanta*, **1996**, *43*, 1739.

[2] Bagno, A.; Saielli, G., *Theor. Chem. Acc.*, **2007**, *117*, 603.

[3] Huang, X.; Rickman, B.H.; Borhan, B.; Berova, N.; Nakanishi, K., *J. Am. Chem. Soc.*, **1998**, *120*, 6185.

[4] Huang, X.; Borhan, B.; Rickman, B.H.; Nakanishi, K.; Berova, N., *Chem. Eur. J.*, **2000**, *6*, 216.

[5] (a) Kurtàn, T.; Nesnas, N.; Li, Y.-Q.; Huang, X.; Nakanishi, K.; Berova, N., *J. Am. Chem. Soc.* **2001,** *123,* 5962. (b) Kurtàn, T.; Nesnas, N.; Koehn, F.E; Li, Y.-Q.; Nakanishi, K.; Berova, N., *J. Am. Chem. Soc.* **2001,** *123,* 5974.

[6] (a) Petrovic, A.; Chen, Y.; Pescitelli, G.; Berova, N.; Proni, G., *Chirality*, **2010**, *22*, 129. (b) Chen, Y.; Petrovic, A.; Roje, M.; Pescitelli, G.; Kayser, M.M.; Yang, Y.; Berova, N.; Proni, G., *Chirality*, **2010**, *22*, 140.

[7] Fazio, M.A.; Lee, O.P.; Schuster, D.I., *Org. Lett.,* **2008**, *10*, 4979.

[8] Carofiglio, T.; Lubian, E.; Menegazzo, I.; Saielli, G.; Varotto, A., *J. Org. Chem.*, **2009**, *74*, 9034.

Chapter III

Supramolecular Self-Assembly of Porphyrin Derivatives onto Conductors and Semiconductors Surfaces

INTRODUCTION

1.1 Self-Assembly: What does it means?

Over the past decades, self-assembly has attracted a lot of research attention and transformed the relations between chemistry, materials science and biology. In general, self-assembly is considered as a strategy for nanofabrication that involves designing molecules and supramolecular entities. Sometimes, chemists in their publications explain this concept using the metaphor of the car: *put the different parts of a car in a big box, and shake the whole, will you get a car?* This is what self-assembly can achieve.[1]

In molecular self-assembly, molecules (or parts of molecules) or ions spontaneously and in reversible way, form more complex and ordered supramolecular entities involving noncovalent interactions and with no human intervention.[2] These spontaneous association phenomena, initially found in biological systems, are not necessarily limited to the bulk solution, in which the phenomenon is called three-dimensional self-assembly, and can also occur at two-dimensional systems such as surfaces and interfaces between different phases.

The conventional method that a chemist employs to synthesize new compounds in the laboratory relies on the sequential formation of covalent bonds, using tedious and repetitive process. In all stage of synthetic pathway, more and more product is lost, even in relatively high-yielding steps. Furthermore, this approach is limited when it comes to constructing large or complex entities (*e.g.*, a cell). Synthetic chemists have met tremendous challenges in making natural products with procedures that can involve upwards of 30 steps.[3] Mistakes could not easily be corrected because of the comparatively high energy required to break and reform covalent bonds.

Nature circumvents these limitations by creating relatively simple building blocks that spontaneously assemble into high structured systems for specific functions, including the transfer and storage of genetic information in nucleic acids,[4] the organization of lipids into protective cell membranes that serve as molecular receptors for the cell, and the hierarchical structure of spider silk, still one of the strongest known fibrous materials yet flexible enough to absorb the impact energy of an unlucky fly.[5]

Self-assembly can today be found in a variety of fields, from biology to materials science and electronics and is an important tool for the development of new advanced technological materials.

1.1.1 Concepts and Classifications

Jean-Marie Lehn has considered self-assembly as one of the core concepts of supramolecular chemistry and has introduced three distinctive terms: *templating*, *self-assembly* and *self-organisation*. Together, these terms cover the processes that enable preorganized molecular components to come together spontaneously, in a well-defined way, to give entities presenting order in one, two or three dimensions.[6,7,8] Templating consists in interactions between the components and regular features in their environment that determine the structures that form. Crystallization on surfaces that determine the morphology of the crystal is one example (Figure 1.1A).[9,10] Self-assembly (or *static* self-assembly) is due to the minimization of free energy in a closed system and it leads to an equilibrium state. The formation of the ordered structure may require energy (*e.g.*, in the form of stirring) but once it is formed, it is stable. For instance, molecular crystals and phospholipids with hydrophobic and hydrophilic ends placed in aqueous solution spontaneously form a stable structure or the assemblies of peptide in nanofibers (Figure 1.1B).[11,12] Self-organization (or *dynamic* self-assembly) only occurs far from equilibrium, in open systems, as it requires external energy source. It is a local phenomenon with production of order out of irreversible process with energy dissipation.[13,14] A more complex example is the assembly of a biological cell (Figure 1.1C).

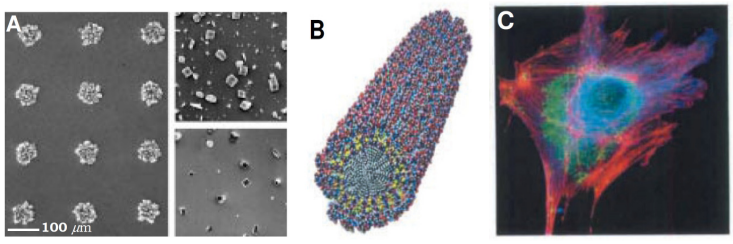

Figure 1.1: self-assemblies examples of A) Templating, sample patterned surface-printed circles of $HS(CH_2)_{15}CO_2H$ in a background of $HS(CH_2)_{15}CH_3$ supported on Ag(111) with calcite crystals. B) Static self-assembled peptide amphiphile nanofibers. C) Dynamic, an optical micrograph of a cell with fluorescently labeled cytoskeleton and nucleus; microtubules (~24 nm in diameter) are coloured red.

In 1991, Lindsey introduced a wide ranging classification scheme built upon the works on the tobacco mosaic virus (TMV) and the enzyme ribonuclease.[15] This definitive scheme is broken up into seven broad, overlapping, classes.

Class 1. Strict Self-Assembly

Strict self-assemblies form spontaneously in particular conditions of concentration, pH, temperature and pressure. The product formation is fully reversible and represents the global thermodynamic minimum for the system. Sometimes an additive or a template is needed to boost the efficiency of the assembly. This basic concept is not true for all proteins, some of which are assembled by entities such as chemical helper.[16,17,18]

Class 2. Irreversible Self-Assembly

This class is the counterpart of the strict self-assembly. Irreversible reactions are involved and bring to a formation of product through irreversible bond-forming steps under kinetic control. The correct structure of product must arise without any error, because there is no margin in self-correction for the final product.[19] Tandem, cascade or domino reactions are examples of irreversible self-assembly that are important in organic synthesis, but not so significant for supramolecular chemistry.[20,21]

Class 3. Precursor Modification Followed by Self-Assembly

Self-assembly takes place only if the precursor undergoes chemically modification before reacting. Biological example is the synthesis of collagen, the fibrous proteins that form the major component of skin and bone. The assembly of such structures within a cell would be fatal.[22] Collagen precursor, procollagen, prevents this by endcapping amino acid chains (propeptides). Once synthesized, procollagen is secreted out of the cell, where proteolytic enzymes remove the propeptides. The resulting collagen molecules are less soluble than their precursors, and self-assembly of fibrils are rapidly started.

Class 4. Self-Assembly with Post-Modification

In this case the final product undergoes modification after the self-assembly processes. One of the classical biological examples is the synthesis of insulin; other examples in supramolecular chemistry are catenanes, rotaxanes and knots.

Class 5. Assisted Self-Assembly

In assisted self-assembly process an external agent is required for the final assembly. This concept becomes important with the recognition of the role played by molecular chaperones in protein folding. Molecular chaperons are a group of molecules that mediated assembly and are not present in the final structure. They inhibit the formation of intermediate species leading to non-functional components and do not affect the thermodynamic of the assembly process. Chaperones help in folding nascent polypeptide chains by preventing aggregation of peptide sequences, and they modulate refolding of denatured proteins, only influencing the kinetics of the process.[23]

Class 6. Directed Self-Assembly

Directed self-assembly involves a template molecule that participate to the assembly processes but does not appear in the final products. The external participant promotes the formation of the desired product by thermodynamic stabilization of the association of building blocks or destabilization of undesired aggregates. Template could also play a kinetical key role in directing self-assembly along preferential pathway reactions. An example from biology is the scaffolding protein directed assembly of viral capsids;[24] from chemistry is the use of vesicles, liquids, and foams to direct biomimetic mineralization and polymerization.[25,26]

Class 7. Self-Assembly with Intermittent Processing

This last class represents combinations of all the above classes and involve complex processes in which there are sequential alternations of self-assembly and covalent or irreversible modifications resulting in highly-controlled process. In general such processes are only found in biology and the best understood examples are ribosome biogenesis[27,28] and bacteriophage assembly.[29,30,31]

Self-assembly that is associated with large building units, covers a broad range of length scale from Angstrom to centimeter, different dimensions, and different sources of origins (Figure 1.2).

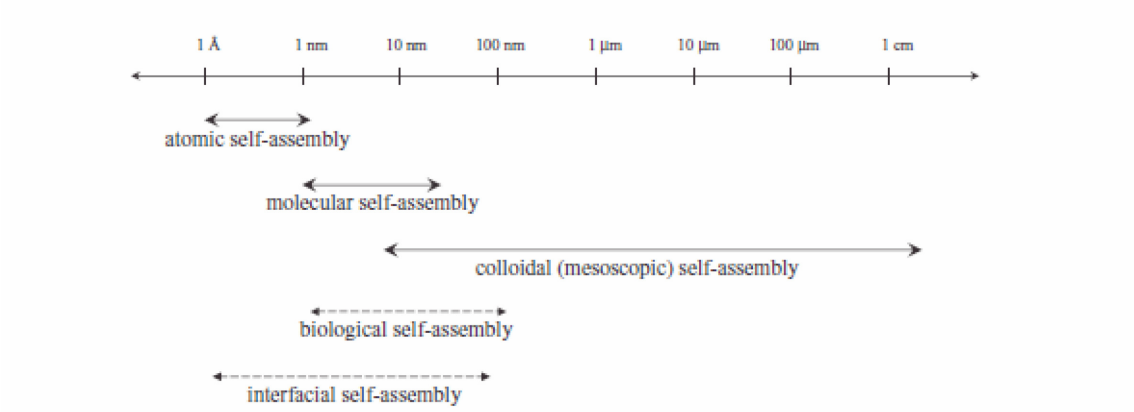

Figure 1.2: classification of self-assemblies based on the size/nature of building units and on the system where the self-assembly occurs.

Typical ranges of sizes for which self-assembly is relevant are molecular, nanoscale (colloids, nanowires and nanospheres, and related structures), and meso- to macroscopic components (objects with dimensions from microns to centimeters). The rules for self-assembly in each of these ranges are similar but not identical. New types of aggregates, especially those with potential applications in microelectronics,[32,33] photonics,[34,35] near-field optics,[36] and the youngest field of nanoscience,[37,38,39] have become increasingly important from technological point of view. There are many opportunities for fabrication of useful structures of nano and macroscale components using self-assembly.[12]

1.1.2 What drives Self-Assembly?

In the self-assembly process, whether it occurs at an atomic- molecular- or colloidal- length scale, weak and long-range forces compared with the chemical forces take important roles. There are three representative groups: (1) the driving forces that bring the self-assembly units together, (2) the opposing forces that balance with the driving forces, and (3) the forces that determine the directionality and functionality of self-assembled aggregates.

Self-assembly processes are mainly controlled by attractive driving forces and repulsive opposition forces that drive often self-assembly in the nondirectional way. Nevertheless, there are other forces that are directly responsible for the directionality. These are hydrogen bonding, coordination and π-π interactions, but much weaker forces, like steric repulsion, are also commonly found. These forces can be a part of a driving or

opposition force during the self-assembly process, but sometimes act almost uniquely as directional force.[40]

However, self-assembly results not only from equilibrium in the directional and/or nondirectional forces. Indeed, in these conditions thermodynamic products in which free energy is maximized will be favoured. Consequently, entropic and enthalpic effects must be considered. Synthesis of discrete, ordered structures from a set of subunits seems to be only enthalpically driven process due to that new favourable interactions formation. However, this happens also at the cost of losing translational, vibrational, and rotational degrees of freedom. In addition, it is important to consider that many other effects occur to contribute to the self-assembly. For instance, hydrophobic effect, which drives amphiphilic subunits to assemble into micelles and lipid bilayer structures such as liposomes, and this is largely an entropic phenomenon.[41]

1.2 Three-Dimensional (3D) and Two-Dimensional (2D) Self-Assembly

Most of the studies on self-assembly, particularly in the early stages of research, focused on solution-based systems, which revealed the fundamental concepts of this exciting field. It the beginning, the biological field was more investigated due to the amazing quantity of complex structures that form by self-assembly. Cell contains a great range of these structures such as lipid membranes, folded proteins, structured nucleic acids, protein aggregates, molecular machines, and many others (Figure 1.3).[42] In aqueous solution, phospholipids aggregate to form larger micellar and membranous structures due to their solubility properties in water. Molecular crystals,[43,44] liquid crystals,[45] colloids,[46] lipid bilayers[47] and phase separated polymers,[48,49] are all examples of molecular self-assembly, as are the folding of polypeptide chains into proteins,[50] the folding of nucleic acids into their functional forms[51] or the association of a ligand with a receptor.[52]

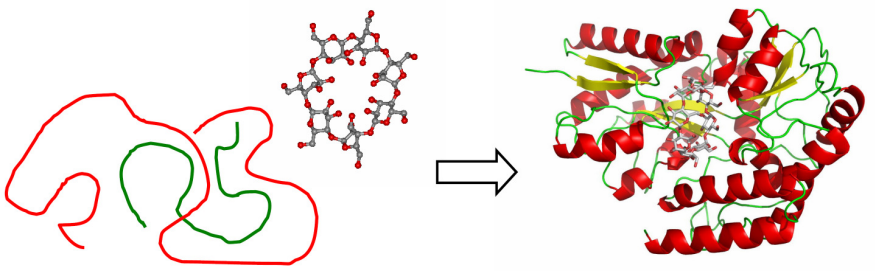

Figure 1.3: example of three-dimensional self-assembly: protein folding in the presence of β-cyclodextrin.

On the other hand, the self-assembly process for their formation in solution often can generate not well-defined, or sometimes infinite- size self-assembled structures, due to the highly stepwise mechanism (molecule-by-molecule-wise or monomer-by-monomer-wise) and the highly external energy input.[53]

To overcome these restrictions, the use of a surface in which molecules can be precisely accommodated at the single-molecule level is one of the most promising approaches. Fabrication of surface self-assembly, commonly called two-dimensional (2D) self-assembly can follow two strategies:

- the *top-down* strategy that use tools to whittle away undesired material to leave the final product. Examples include: fashioning an arrowhead from a rock, building a table from lumber, assembling a car, and fabricating a microchip;[54]
- the *bottom-up* strategy constructs the desired features from fundamental building blocks, usually spontaneously self-assembling. This approach is most used and offers considerable advantages over any other strategy for the construction of ordered structures with nanometer precision over an extended scale.[54]

The equilibrium between the constituents and the final product, along with the reversibility of the systems towards multistable nanostructured materials, contributes to the self-rearrangement of the components within the assembled structure and thus to the formation of long-range ordered and defect-free systems barely accessible through conventional covalent synthesis.[55]

Surface self-assembly is so unique, compared with bulk self-assembly, due to the inevitable interactions between the building units and the interfaces where the self-assembly takes place. The strength of this interaction can vary but is usually comparable to the intermolecular forces among the building units. This intrinsic factor yields three typical characteristics of surface self-assembly[56] that are significantly differentiated from bulk ones:

1. bulk self-assembly always has to be amphiphilic character encoded into each building unit to ensure the proper force balance. However, for surface self-assembly, this is not necessarily a prerequisite. Whether the building units are amphiphilic or not, once they are attracted onto the given solid substrate, the force interplay among themselves in many cases is enough to induce self-assembly;

2. interactions of the building units with the solid interface can alter the intermolecular forces among the building units themselves. For example, even non-polar molecules can have dipole moments when they are adsorbed onto the interfaces and their symmetry break-ups;

3. in the two-dimensional self-assembly, the aggregates always exist in a state of confinement (or attachment) on the surface. Thus arises in significantly different physical and chemical properties from those analogues in bulk self-assembly. For instance, the magnetism of metal nanoparticles assembled at solid surfaces can be greatly changed from that of those formed in bulk solution.

1.3 Deposition of Molecular Nanostructures on Surface

The fabrication of complex supramolecular structures by self-assembly of specifically designed molecular functional building blocks and their control at the single-molecule level remains a challenge of particular interest in materials science due to their potential use for applications in energy, catalysis and molecular nanoelectronics.[57,58]

Molecular nanostructures are attractive due to the tunability of their properties by selectively modifying specific functional groups while leaving the rest of the molecule unchanged. Noncovalent interactions play an important role in the definition of the final structure. Specifically, dispersion and van der Waals forces,[59] dipole-dipole and donor-acceptor interactions,[60,61] hydrogen bonds,[62,63] or metal complexation[64] allow for good molecular mobility on the surface and, as a consequence, promote the formation of target structures under equilibrium conditions, which provide the apt environment for the necessary self-correction of defects, ultimately resulting in well-developed long-range order. Complex two-dimensional nanonetworks have been obtained by deposition of organic molecules whose self-assembly is driven by the equilibria between weak and reversible lateral (intermolecular) and vertical (molecule-substrate) interactions.[65]

To build up molecular nanomaterials, the chemist needs a toolkit containing a variety of pieces which can be incorporated into the final object (Figure 1.4), and which must be arranged with the help of appropriate noncovalent interactions in the solid state.

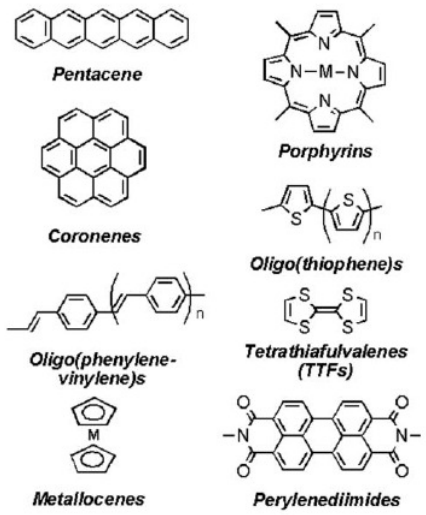

Figure 1.4: molecular units used frequently for the preparation of functional nanostructures.

There are different deposition methods for the preparation of molecular nanostructures important in surface science which many of these are illustrated in Figure 1.5.[55]

In *self-assembled monolayers* (SAMs, Fig. 1.5a), molecules have a chemical functionality with specific affinity for a solid surface with which can form covalent bonds or weak interactions that drives the formation of the monolayer. SAMs can be done either in solution or under high vacuum. *Langmuir films* consist of amphiphilic molecules spread on a liquid surface, typically water (Fig. 1.5b). The hydrophilic headgroup of the amphiphile has an affinity to the water while the hydrophobic endgroup sticks out of the interphase between layer and water.[66] *Langmuir-Blodgett* films (LB) are prepared by transferring Langmuir films onto a solid substrate by vertical or horizontal lifting. Multilayers are obtained by repeated dipping (Fig. 1.5c).

Solvent evaporation techniques are based on a controlled solvent evaporation. Relevant examples of this type of technique are *drop casting* (Fig. 1.5d), spin coating (Fig. 1.5e) and *zone casting* (Fig. 1.5f).[67,68] Drop casting consists in allowing a small volume of solution of compound to fall onto the substrate surface and leaving it to dry either in air or in an atmosphere of the solvent (*dewetting* phenomena) to ensure slower evaporation. Another similar deposition method is *soaking* in which the substrate is dipped into the solution for a certain period of time (minutes) and then extracted and left to dry in air. In spin coating the solution of functional molecules is applied on the substrate, which is then rotated on a spinning wheel at high speed. The centrifugal forces push the excess solution

over the edge of the substrate and a residue remains thanks to surface tensions (*e.g.*, polymers, thin films and nanostructures of small molecules). Zone casting is a method for preparation of oriented, anisotropic layers of soluble molecular materials on substrates that have not been pre-oriented. The material in solution is continuously supplied through a nozzle onto a moving substrate and the solvent evaporation takes place from the surface of the meniscus formed between a special flat nozzle and the substrate.

Others more recent deposition methodologies are based on the use of functional molecules as ink on a rubber. Basically, the stamp is pressed into the ink (either the pure molecule or a solution of it) and is then removed and pressed onto a surface (*Stamping* method, Fig 1.5g). *Dip Pen Nanolithography* (DPN, Fig.1.5h) is a scanning probe lithography technique where an atomic force microscope tip is used to transfer molecules to a surface via a solvent meniscus. This technique allows surface patterning on scales of under 100 nanometers. These two methods have a very wide variety of guises within the field of soft lithography and printing, with microcontact printing being particularly popular, since it allows patterning over relatively large areas.[69]

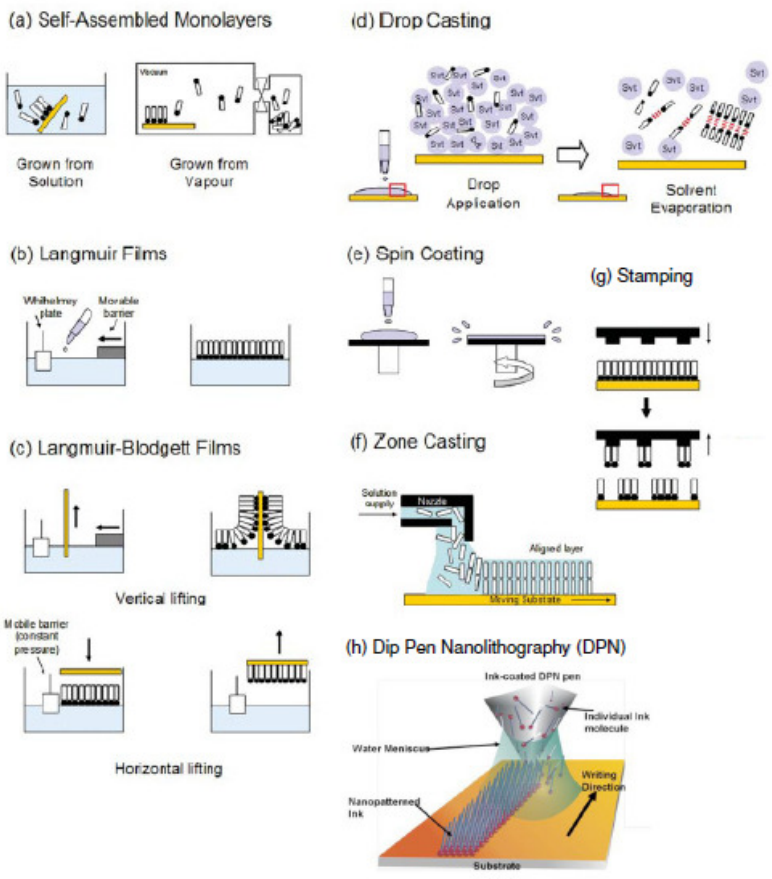

Figure 1.5: overview of the various preparation routes for the deposition of molecular nanostructures on surfaces.

1.4 Self-Assembly of Porphyrins Derivatives

Porphyrinic units attached by covalent bonds are not supramolecular assemblies by themselves. Nevertheless, these compounds are often used as components of supramolecular systems. Some separate molecules can self-organize to form more complex supramolecular structures sustained by noncovalent interactions between different parts of the molecule.

Interactions between individual porphyrinic segments in multiporphyrinic systems give rise to new properties inherent to the assembly that are not the sum of components. Electronic interaction of the π-systems of oligoporphyrins depends on the relative positioning, geometry, rigidity, and type of bonds connecting porphyrinic cycles.[70,71] Expanded π-conjugation allows the preparation of materials possessing non-linear optical properties,[72] molecular wires,[73,74] photon tunnels,[75] multispin molecules with magnetic properties,[76,77] and devices for information storage.[78]

1.4.1 Gas Sensing Applications

The broad technological potential of porphyrin-based systems is mainly ascribable to their peculiar chemico-physical properties, synthetic design flexibility, and to their spontaneous self-assembling due to π–π interactions between the porphyrin central rings.[79] Thanks to these interactions, in cooperation with ancillary recognition units introduced *ad hoc* by decorating the macrocycle with proper exocyclic substituents (*i.e.*, hydrogen bond donors/acceptors, coordination centres, and so forth), remarkably ordered nanostructures could be obtained.[80] However, it should be pointed out that the degree of order required is application-dependent. In particular, for gas sensing applications, a *meso* rather than a *nano* scale order is mandatory to obtain an homogeneous substrate coverage and adhesion, together with a tailored thickness, porosity and gas permeability of the sensitive layer.[81] In the case of porphyrin systems, such mesoscale order can be achieved very conveniently by self-assembly exploiting nondirectional dispersion forces and directional hydrogen bonding between the porphyrin molecules.

The interaction of the porphyrins with the substrate surface can also play an important role. Sensors based on free-base and metalated porphyrin thin films[82,83] have been synthesized by various self-assembly preparation strategies such as drop-casting,[84]

soaking,[85] dipping[69] and spin-coating[86] controlling the substrate surface chemistry and properly selecting the deposition solvent. Such methods have a lot of advantages over other approaches exploiting covalent interactions, such as: i) facile preparation of different systems, whose morphology can be tuned even at a molecular level; ii) use of very mild synthesis conditions; iii) obtainment of stable materials.[87,88]

1.4.2 Solar Energy Applications

At present, self-assembly of organic molecules on different substrates is one of the most studied approaches in order to obtain surface supported supramolecular nanostructures with controlled dimensions and innovative properties. This *bottom-up* strategy can potentially become a simple, versatile, and effective approach to obtain predetermined and defect-free nanostructured two dimensional (2D) macroscopic materials. Its success depends on the capacity to build "smart" molecular building units, able to organize themselves in a predetermined pattern by a careful exploitation of molecule-molecule and molecule-substrate interactions. To this end, only a detailed study of the physicochemical properties at the atomic and molecular scale of the self-organizing interfacial systems can provide the necessary know-how to build increasingly complex and chemically stable 2D functional nanosystems in a reproducible way.[2,89]

The supramolecular bidimensional ordering of [60]fullerene and its derivatives with organic counterparts self-assembled on suitable metal or semiconductor single-crystal surfaces is a topic of rapidly growing interest in the nanoscience community.[54,90,91] A promising potential for applications in many different fields such as sensing, catalysis, nanoelectronics, and photochemical conversion of solar energy is foreseen, although the state-of-the-art research efforts in this area are still focused on fundamental issues concerning the often complex relationships between molecular structure and functionalization, surface structure, and intermolecular versus molecule/substrate interactions on one side, and the resulting supramolecular architectures on the other. The strategy pursued to produce the multicomponent arrays usually consists of a two-step approach:

a. surface self-organization of a molecular species able to interact with itself and with fullerene and its derivatives. Typically dispersion, dipolar, noncovalent directional

(*e.g.*, hydrogen bonds), host-guest, and/or electron donor-acceptor (D-A) interactions are exploited, or a combination of two or more;

b. subsequent fullerene dosage on the ordered organic layer acting as a template. Thermal treatment is sometimes used to improve the order.

Calix-[8]-arene[92] and corannulene[93] are examples of templating layers that have been used or proposed for C_{60} ordering through host-guest interactions.

However, the most promising results to date are obtained when D-A interactions are exploited between porphyrins-based templating layers (D) and fullerene (A), as recently reviewed by Bonifazi et al.,[90] although direct charge transfer from/to the substrate might complicate this schematic picture. The rather strong D-A interactions between fullerenes and porphyrins[94] prevent, at least in a certain temperature range, one of the most common obstacles in Multicomponent Self-Assembly (MSA), namely, the phase separation of the two species to form surface-supported single-component islands. In fact, the rather strong tendency of fullerene to arrange in hexagonal or distorted hexagonal close-packed islands on most substrates has to be overcome if MSA has to be attained. Such a tendency is based on the 1.30 eV/molecule intermolecular interaction energy,[95] mostly van der Waals type, with dipolar contributions arising from the uneven charge density distribution on single and double C-C bonds.[96,97] In addition, the modified surface energetics arising from the presence of the porphyrin network on the surface allows for efficient avoidance of the often found surface reconstructions promoted by the presence of fullerene when deposited on the bare substrate.[98,99,100] Finally, the extreme versatility given by organic functionalization of the porphyrin macrocycle provides a powerful degree of freedom in designing and fine-tuning the "pitch" of the templating layer, by which the geometry of the MSA and the mutual distance between fullerene units within ordered arrays can be effectively controlled.

Often such noncovalently interacting organic networks are flexible and able to respond to the presence of guest molecules by adapting their conformation to optimize the host-guest interactions. The resulting ordered MSA networks may additionally involve long-range, substrate-mediated interguest interactions that are ultimately responsible for the dimensions of the ordered domains.[101,102] As a matter of fact, the extent of the long-range order is a key issue for potential applications of surface-supported MSA systems because a very high degree of coherence in the orientation, alignment, and packing of the

building units is necessary as a basis for large-scale uniformity and coordination in the operations of functional materials. Long-range ordered MSA arrays can be produced only if several conditions are simultaneously fulfilled:

- high diffusion coefficients of all the molecular species involved in the process at the given growth temperature;

- an optimal balance between lateral intermolecular versus vertical molecule-substrate interactions;

- the careful design of intermolecular recognition through preferential noncovalent interactions between the different components of the assembly to avoid phase separation.

In the few examples concerning C_{60}/porphyrin MSAs so far reported in the literature,[2] Ag(110) has been mainly used as the substrate because it meets the first two requirements mentioned above.

REFERENCES

[1] Drexler, *Engines of Creation*, p. 2 ; Richard Jones, **2004**, p. 91-93.

[2] Whitesides, G. M.; Grzybowski, B., *Science*, **2002**, *295*, 2418.

[3] Nicolaou, K.C.; Yang: Z.; La , J.J.; Ueno, H.; Nantermet, P.G.; Guy, R.K.; Claiborne, C.F.; Renaud, J.; Couladouros, E.A.; Paulvannan. K.; Sorenson, E.J., *Nature*, **1994**, *367*, 630.

[4] Lawrence, D.S.; Jiang, T.; Levett, M., *Chem. Rev.*, **1995**, *95*, 2229.

[5] Smith, B.L.; Schaffer, T.E.; Vian, M.; Thompson, J.B.; Frederick, N.A.; Kindt. J.; Belcher, A.; Stucky, G.D.; Morse, D.E.; Hansma, P.K., *Nature*, **1999**, *399*, 761.

[6] J.-M. Lehn, *Science*, **2002**, *295*, 2400.

[7] J.-M. Lehn, *Supramolecular Chemistry*, VCH, Weinheim, **1995**.

[8] Vogtle, F., *Supramolecular Chemistry*, John Wiley & Sons, Chichester, **1993**.

[9] Aizenberg, J.; Black, A. J.; Whitesides, G. M., *Nature*, **1999**, *398*, 495.

[10] van Blaaderen, A.; Ruel, R.; Wiltzius, P., *Nature*, **1997**, *385*, 321.

[11] Desiraju, G.R.; *Crystal Engineering: The Design of Organic Solids*, Elsevier, New York, **1989**.

[12] Isaacs, L.; Chin, D.N.; Bowden, N.; Xia, Y.; Whitesides, G.M., in *Supramolecular Technology*, D.N. Reinhoudt, Ed. Wiley, New York, **1999**, pp. 1-46.

[13] Jakubith, S.; Rotermund, H.H.; Engel, W.; von Oertzen, A.; Ertl, G., *Phys. Rev. Lett.*, **1990**, *65*, 3013.

[14] Hess, B., *Naturwissenschaften*, **2000**, *87*, 199.

[15] Lindsey, J.S., *New J. Chem.*, **1991**, *15*, 153.

[16] Templated Organic Syntliesis: Diederich, F.; Stang. P.J., Eds. Wiley-VCH, Weinheim, **2000**.

[17] Busch, D.H.J., Incl. Phenom. Mol. Recognit. Chem., **1992**, 12, 389.

[18] Lindsey, J.S., *New J. Chem.*, **1992**, *12*, 153.

[19] Atwood, J.L.; Steed, J.W., *Encyclopedia of Supramolecular Chemistry*, Taylor & Francis Group, **2001**.

[20] McCarroll, A.J.; Walton, J.C., *Angew. Chem.*, **2001**, *40*, 2225.

[21] Gibb, C.L.D.; Stevens, E.D.; Gibb, B.C., *Chem. Comm.*, **2000**, 363.

[22] Fuller, M.T.; Kings, J., *Biophys. J.*, **1980**, *32*, 381.

[23] Ellis, R. J.; Hemmingsen, S. M., *Trends Biochem. Sci.*, **1989**, *14*, 339.

[24] Dokland, T.; McKenna, R.; Ilag, L.L.; Bowman, B.R.; Incardona, K.L.; Fane, B.A.; Rossmann, M.G., *Nature*, **1997**, *389*, 308.

[25] Mann, S.J., *Chem. Soc. Dalton Trans.*, **1994**, 3953.

[26] Rotello, V.M., Ed. Tetrahedron. Symposium in Print Special Edition, **2002**: Vol. 48, 621-844.

[27] Nomura, M., *Science*, **1973**, *179*, 864.

[28] Anderson, R.G.W., *Cell Biology: A Comprehensive Treatise*, Vol. 4, Prescott D. M., Goldstein L., Eds., Academic, New York, **1980**, pp. 393-441.

[29] Wood, W.B., *Genetic Mechanisms of Development*, Ruddle F.H., Ed., Academic, New York, **1973**, pp. 29-46.

[30] King, J., *Biological Regulation and Development*, Vol. 2, *Molecular Organization and Cell Function*, Goldberg R. F., Ed., Plenum, New York, **1980**, pp. 101-132.

[31] Thompson, R.L.; Goel, N.S., *BioSystems*, **1985**, *18*, 23.

[32] Sirringhaus, H., Kawase, T., Friend, R.H., Shimoda, T., Inbasekaran, M., Wu, W.; Woo, E.P., *Science*, **2000**, *290*, 2123.

[33] Rogers, J.A., Bao, Z., Baldwin, K., Dodabalapur, A., Crone, B., Raju, V.R., Kuck, V., Katz, H., Amundson, K., Ewing, J.; Drzaic, P., *Proc. Natl. Acad. Sci. USA*, **2001**, *98*, 4835.

[34] Jenekhe, S.A.; Chen, L.X., Science, **1999**, *283*, 372.

[35] Xia, Y., Gates, B., Yin, Y.; Lu, Y., *Adv. Mater.*, **2000**, *12*, 693.

[36] Wu, M.H.; Whitesides, G.M., *Appl. Phys. Lett.*, **2001**, *78*, 2273.

[37] Lieber, C.M., *Sci. Am.*, **2001**, *285*, 58.

[38] Klimov, V.I., Mikhailovski, A.A., Xu, S., Malko, A., Hollingsworth, J.A., Leatherdale, C.A., Eisler, H.-J.; Bawendi, M.G., *Science*, **2000**, *290*, 314.

[39] Sun, S.H., Murray, C.B., Weller, D., Folks, L.; Moser, A., Science, **2000**, *287*, 1989.

[40] Lee, Y.S., *Self-Assembly and Nanotechnology A force balance Approach*, John Wiley & Sons, Inc, **2008**.

[41] Tanford, C., *The Hydrophobic Effect*, John Wiley and Sons, New York, **1973**.

[42] Alberts, B., Bray, D., Lewis, J., Raff, M., Roberts, K., Watson, J.D., *Molecular Biology of the Cell*, Garland, New York, **1994**.

[43] Desiraju, G.R., *Crystal Engineering: The Design of Organic Solids*, Elsevier, New York, **1989**.

[44] Schwiebert, K.E., Chin, D.N., MacDonald, J.C., Whitesides, G.M., *J. Am. Chem. Soc.*, **1996**, *118*, 4018.

[45] Schmidt-Mende, L.; Fechtenkotter, A.; Mullen, K.; Moons, E.; Friend, R.H.; MacKenzie, J.D., *Science*, **2001**, *293*, 1119.

[46] Evans, D.F.; Wennerstrom, H., *The Colloidal Domain: Where Physics, Chemistry, Biology, and Technology Meet*, Wiley, New York, **1999**.

[47] Jones, M.N.; Chapman, D., *Micelles, Monolayers, and Biomembranes*, Wiley–Liss, New York, **1995**.

[48] (a) Thomas, E.L., *Science*, **1999**, *286*, 1307. (b) Kumar, A.; Abbott, N.A.; Kim, E.; Biebuyck, H.A.; Whitesides, G.M.; *Acc. Chem. Res.*, **1995**, *28*, 219.

[49] (a) De Rosa, C.; Park, C.; Thomas, E.L.; Lotz, B., *Nature (London)*, **2000**, *405*, 433. (b) Miyashita, N.; Kurth, D.G., *J. Mater. Chem.*, **2008**, *18*, 2636.

[50] Grantcharova, V.; Alm, E.J.; Baker, D.; Horwich, A.L., *Curr. Opin. Struct. Biol.*, **2001**, *11*, 70.

[51] Neidle, S., *Handbook of Nucleic Acid Structure*, Oxford Univ. Press, Oxford, U.K., **1999**.

[52] Bongrand, P., *Rep. Prog. Phys.*, **1999**, 62, 921.

[53] Kohnle, A., *Curr. Opin. Colloid Interface Sci.*, **2009**, *14*, 157.

[54] Bonifazi, D.; Enger, O.; Diederich, F., *Chem. Soc. Rev.*, **2007**, *36*, 390.

[55] Gomar-Nadal, E.; Puigmart-Luis, J.; Amabilino, D.B., *Chem. Soc. Rev.*, **2008**, *37*, 490.

[56] (a) Ma, X.; Yang, Y.; Deng, K.; Zeng, Q.; Zhao, K.; Wang C.; Bai, C.; *J. Mater. Chem.*, **2008**, *18*, 2074. (b) Cicoira, F.; Santato, C.; Rosei, F., *Top. Curr. Chem.*, **2008**, *271*, 203. (c) Special issue *Supramolecular Chemistry Anniversary: Chem. Soc. Rev.*, **2007**, *36*, 125.

[57] Joachim, C.; Gimzewski, J.K.; Aviram, A., *Nature (London)* **2000**, *408*, 541.

[58] (a) Barth, J.V., *Annu. Rev. Phys. Chem.* **2007**, *58*, 375. (b) Barth, J.V.; Costantini, G.; Kern, K., *Nature (London)* **2005**, *437*, 671.

[59] (a) Silly, F.; Shaw, A.Q.; Porfyrakis, K.; Briggs, G.A.D.; Castell, M.R., *Appl. Phys. Lett.*, **2007**, *91*, 253109. (b) Silly, F.; Shaw, A.Q.; Briggs, G.A.D.; Castell, M.R., *Appl. Phys. Lett.* **2008**, *92*, 023102. (c) Silly, F.; Shaw, A.Q.; Castell, M.R.; Briggs, G.A.D., *Chem. Commun.*, **2008**, *16*, 1907.

[60] (a) Stepanow, S.; Lingenfelder, M.; Dmitriev, A.; Spillmann, H.; Delvigne, E.; Lin, N.; Deng, X.; Cai, C.; Barth, J. V.; Kern, K., *Nat. Mater.*, **2004**, *3*, 229. (b) Langner, A.; Tait, S.L.; Lin, N.; Rajadurai, C.; Ruben, M.; Kern, K., *Proc. Natl. Acad. Sci. U.S.A.* **2007**, *104*, 17927. (c) Schlickum, U.; Decker, R.; Klappenberger, F.; Zoppellaro, G.; Klyatskaya, S.; Ruben, M.; Silanes, I.; Arnau, A.; Kern, K.; Brune, H.; Barth, J.V., *Nano Lett.*, **2007**, *7*, 3813. (d) Decker, R.; Schlickum, U.; Klappenberger, F.; Zoppellaro, G.; Klyatskaya, S.; Ruben, M.; Barth, J.V.; Brune, H., *Appl. Phys. Lett.* **2008**, *93*, 243102. (e) Gambardella, P.; Stepanow, S.; Dmitriev, A.; Honolka, J.; de Groot, F. M.F.; Lingenfelder, M.; Gupta, S.S.; Sarma, D.D.; Bencok, P.; Stanescu, S.; Clair, S.; Pons, S.; Lin, N.; Seitsonen, A.P.; Brune, H.; Barth, J.V.; Kern, K., *Nat. Mater.*, **2009**, *8*, 189.

[61] (a) Grill, L.; Dyer, M.; Lafferentz, L.; Persson, M.; Peters, M.V.; Hecht, S., *Nat. Nanotechnol.*, **2007**, *2*, 687. (b) Matena, M.; Riehm, T.; Stohr, M.; Jung, T.A.; Gade, L.H., *Angew. Chem., Int. Ed.*, **2008**, *47*, 2414. (c) Treier, M.; Richardson, N.V.; Fasel, R., *J. Am. Chem. Soc.*, **2008**, *130*, 14054. (d) Treier, M.; Fasel, R.; Champness, N.R.; Argent, S.; Richardson, N.V., *Phys. Chem. Chem. Phys.*, **2009**, *11*, 1209.

[62] (a) Cavallini, M.; Biscarini, F., *Nano Lett.* **2003**, *3*, 1269. (b) Cavallini, M.; Stoliar, P.; Moulin, J. F.; Surin, M.; Leclère, P.; Lazzaroni, R.; Breiby, D.W.; Andreasen, J.W.; Nielsen, M.M.; Sonar, P.; Grimsdale, A.C.; Mullen, K.; Biscarini, F., *Nano Lett.*, **2005**, *5*, 2422.

[63] Sakai, M.; Iizuka, M.; Nakamura M.; Kudo, K., *Synth. Met.*, **2005**, *153*, 293.

[64] Last, J.A.; Hillier, A.C.; Hooks, D.E.; Maxson J.B.; Ward, M.D., *Chem. Mater.*, **1998**, *10*, 422.

[65] (a) Theobald, J.A.; Oxtoby, N.S.; Phillips, M.A.; Champness, N.R.; Beton, P.H., *Nature (London)*, **2003**, *424*, 1029. (b) Theobald, J.A.; Oxtoby, N.S.; Champness, N.R.; Beton, P.H.; Dennis, T.J.S., *Langmuir*, **2005**, *21*, 2038. (c) Perdigao, L.M.A.; Perkins, E.W.; Ma, J.; Staniec, P.A.; Rogers, B.L.; Champness, N.R.; Beton, P.H., *J. Phys. Chem. B*, **2006**, *110*, 12539. (d) Staniec, P.A.; Perdigao, L.M.A.; Saywell, A.; Champness, N.R.; Beton, P.H., *Chem. Phys. Chem.*, **2007**, *8*, 2177.

[66] Talham, D.R., *Chem. Rev.*, **2004**, *104*, 5479.

[67] Palermo, V.; Morelli, S.; Simpson, C.; Mullen K.; Samorì, P., *J. Mater. Chem.*, **2006**, *16*, 266.

[68] Tracz, A.; Pakula, T.; Jeska, J.K., *Mater. Sci-Poland*, **2004**, *22*, 415.

[69] Gates, B.D.; Xu, Q.; Stewart, M.; Ryan, D.; Willson C.G.; Whitesides, G.M., *Chem. Rev.*, **2005**, *105*, 1171.

[70] Harvey, P.D., in *The Porphyrin Handbook*; Kadish, K.M., Smith, K.M., Guilard, R., Eds.; Academic Press: San Diego, CA, **2003**; Vol. 18.

[71] Balaban, T.S. in *Encyclopedia of Nanoscience and Nanotechnology*; Nalwa, H.S., Ed.; American Scientific Publishers: Stevenson Ranch, CA, **2004**.

[72] Anderson, H.L.; Martin, S.J.; Bradley, D.D.C.; *Angew. Chem., Int. Ed.*, **1994**, *33*, 655.

[73] Marvaud, V.; Launay, J.-P., *Inorg. Chem.*, **1993**, *32*, 1376.

[74] Wagner, R.W.; Lindsey, J.S.; Seth, J.; Palaniappan, V.; Bocian, D.F., *J. Am. Chem. Soc.*, **1996**, *118*, 3996.

[75] Prathapan, S.; Johnson, T.E.; Lindsey, J.S., *J. Am. Chem. Soc.*, **1993**, *115*, 7519.

[76] (a) Miller, J.S.; Calabrese, J.C.; McLean, R.S.; Epstein, A.J., *Adv. Mater.*, **1992**, *4*, 498. (b) Wynn, C.M.; Girtu, M.A.; Sugiura, K.-I.; Brandon, E.J.; Manson, J.L.; Miller, J.S.; Epstein, A.J., *Synth. Mater.*, **1997**, *85*, 1695.

[77] (a) Brandon, E.J.; Rogers, R.D.; Burkhart, B.M.; Miller, J.S., *Chem. Eur. J.*, **1998**, *4*, 1938. (b) Shultz, D.A.; Lee, H.; Gwaltney, K.P., *J. Org. Chem.*, **1998**, *63*, 7584.

[78] Hopfield, J.J.; Onuchic, J.N.; Beratan, D.N., *J. Phys. Chem.*, **1989**, 6350.

[79] De Napoli, M.; Nardis, S.; Paolesse, R.; Graça M.; Vicente, H.; Lauceri, R.; Purrello, R., *J. Am. Chem. Soc.*, 2004, *126*, 5934.

[80] Iengo, E.; Zangrando, E.; Alessio, E., *Acc. Chem. Res.*, **2006**, *39*, 841.

[81] D'Amico, A.; Di Natale, C.; Paolesse, R.; Macagnano, A.; Mantini, A., *Sens. Actuators, B*, **2000**, *65*, 209.

[82] (a) Hasobe, T.; Kamat, P.V.; Troiani, V.; Solladié, N.T.; Ahn, K.; Kim, S.K.; Kim, D.; Kongkanand, A.; Kuwabata, S.; Fukuzumi, S., *J. Phys. Chem. B*, **2005**, *109*, 19. (b) Paolesse, R.; Monti, D.; La Monica, L.; Venanzi, M.; Froio, A.; Nardis, S.; Di Natale, C.; Martinelli, E.; D'Amico, A., *Chem. Eur. J.*, **2002**, *8*, 2476. (c) Bazzan, G.; Smith, W.; Francesconi, L.C.; Drain, C.M., *Langmuir*, **2008**, *24*, 3244.

[83] (a) Herve, G.; Quanmin, G., *Thin Solid Films*, **2009**, *517*, 2651. (b) Elmans, J.A.A.W.; van Hameren, R.; Nolte, R.J.M.; Rowan, A.E., *Adv. Mater.*, 2006, *18*, 1251. (c) Oncel, N.; Bernasek, S. L., *Appl. Phys. Lett.*, **2008**, *92*, 133305.

[84] (a) Treossi, E.; Liscio, A.; Feng, X.; Palermo, V.; Müllen, K.; Samorì, P., *Small*, **2009**, *5*, 112. (b) Iavicoli, P.; Linares, M.; del Pino, A.P.; Lazzaroni, R.; Amabilino, D.B., *Superlattices Microst.*, **2008**, *44*, 556. (c) Simikiene, I.; Sabataityte, J.; Barbonas, G.J.; Reza, A.; Beinoras, J., *Mater. Sci. Eng. C*, **2006**, *26*, 1007. (d) Hill, J.P.; Wakayama, Y.; Akada, M.; Ariga, K., *J. Phys. Chem. C*, **2007**, *111*, 16174. (e) Koepf, M.; Bucher, J.A.; Weiss, J., *J. Am. Chem. Soc.*, 2008, *130*, 9994.

[85] (a) Sivanesan, A.; John, S.A., *Langmuir*, **2008**, *24*, 2186. (b) Smith, A.R.G.; Ruggles, J.L.; Yu, A.; Gentle, I.R., *Langmuir*, **2009**, *25*, 9873.

[86] Garg, K.; Singh, A.; Debnath, A.K.; Nayak, S.K.; Chattopadhyay, S.; Aswal, D.K.; Hayakawa, Y.; Gupta, S.K.; Yakhmi, J.V., *Chem. Phys. Lett.*, **2010**, *488*, 27.

[87] (a) Bhosale, S.V.; Bissett, M.A.; Forsyth, C.; Langford, S.J.; Neville, S.M.; Shapter, J.G.; Weeks, L.; Woodward, C.P., *Org. Lett.*, **2008**, *10*, 2943. (b) George, H.; Guo, Q., *Thin Solid Films*, **2009**, *517*, 2651.

[88] Dini, F. Martinelli, E. Pomarico, G. Paolesse, R. Monti, D. Filippini, D. D'Amico, A. Lundström, I. Di Natale, C. *Nanothecnology*, **2009**, *20*, 055502.

[89] (a) Barth, J.V.; Costantini, G.; Kern, K., *Nature*, **2005**, *437*, 671. (b) Elemans, J.A.A.W.; Lei, S.; De Feyter, S., *Angew. Chem., Int. Ed.*, **2009**, *48*, 7298.

[90] (a) Bonifazi, D.; Mohnani, S.; Llanes-Pallas, A.; *Chem. Eur. J.*, **2009**, *15*, 7004. (b) Bonifazi, D.; Kiebele, A.; Stohr, M.; Cheng, F.; Jung, T.; Diederich, F.; Spillmann, H., *Adv. Funct. Mater.*, **2007**, *17*, 1051.

[91] Sanchez, L.; Otero, R.; Gallego, J.M.; Miranda, R.; Martın, N., *Chem. Rev.*, **2009**, *109*, 2081.

[92] Pan, G.-B.; Liu, J.-M-; Zhang, H.-M.; Wan, L.-J.; Zheng, Q.-Y.; Bai, Ch.-L., *Angew. Chem., Int. Ed.*, **2003**, *42*, 2747.

[93] Parschau, M.; Fasel, R.; Ernst, K.-H.; Groning, O.; Brandenberger, L.; Schillinger, R.; Greber, T.; Seitsonen, A.P.; Wu, Y.-T.; Siegel, J.S., *Angew. Chem., Int. Ed.*, **2007**, *46*, 8258.

(d) Bhattacharya, S.; Nayak, S.K.; Chattopadhyay, S.; Manerjee, M., *Spectrochim. Acta, Part A*, **2007**, *66*, 243.

[94] (a) Olmstead, M.M.; Costa, D.A.; Maitra, K.; Noll, B.C.; Phillips, S.L.; van Calcar, P.M.; Balch, A.L., *J. Am. Chem. Soc.*, **1999**, *121*, 7090. (b) Boyd, P.D.W.; Hodgson, M.C.; Rickard, C.E.F.; Oliver, A.G.; Chaker, L.; Brothers, P.J.; Bolskar, R.D.; Tham, F.S.; Reed, C.A., *J. Am. Chem. Soc.*, **1999**, *121*, 10487. (c) Basiuk, V.A., *J. Phys. Chem. A*, **2005**, *109*, 3704.

[95] Nakamura, J.; Nakayama, T.; Watanabe, S.; Aono, M., *Phys. Rev. Lett.*, **2001**, *87*, 048301.

[96] Hou, J.G.; Jinlong, Y.; Haiqian, W.; Qunxiang, L.; Changgan, Z.; Langfeng, Y.; Bing, W.; Chen, D.M.; Qinshi, Z., *Nature*, **2001**, *409*, 304.

[97] Gritsch, T.; Coulman, D.; Behm, R.J.; Ertl, G., *Phys. Rev. Lett.*, **1989**, *63*, 1086.

[98] Murray, P.W.; Pedersen, M.O.; Lægsgaard, E.; Stensgaard, I.; Besenbacher, F., *Phys. Rev. B*, **1997**, *55*, 9360.

[99] Pedio, M.; Felici, R.; Torrelles, X.; Rudolf, P.; Capozi, M.; Rius, J.; Ferrer, S., *Phys. Rev. Lett.*, **2000**, *85*, 1040.

[100] Weckesser, J.; Cepek, C.; Fasel, R.; Barth, J.V.; Baumberger, F.; Greber, T.; Kern, K., *J. Chem. Phys.*, **2001**, *115*, 9001.

[101] Kiebele, A.; Bonifazi, D.; Cheng, F.; Stohr, M.; Diederich, F.; Jung, T.; Spillmann, H., *Chem. Phys. Chem.*, **2006**, *7*, 1462.

[102] Sykes, E.C.H.; Mantooth, B.A.; Han, P.; Donhauser, Z.J.; Weiss, P.S., *J. Am. Chem. Soc.*, **2005**, *127*, 7255.

RESULTS AND DISCUSSION

2.1 Self-Assembly Studies

As previously reported, porphyrin-based supported systems offer potential technological applications in many fields thanks to their peculiar chemical-physical properties. In this research project, we took in account the possibility to apply these features to create sophisticated supported materials for gas sensing and photovoltaic applications. In the former case, we consider the deposition of melamine-bridged bis(porphyrin) dyad, **P(H_2)P(H_2)**, and the corresponding Zn^{II} metalated complex, **P(Zn)P(Zn)** on Si(100) substrate. In the second case, we choose to study the molecular deposition of single porphyrin molecules, like **TPP**, **TPPNH_2**, and **trans-TPP(NH_2)$_2$** on conductor material, as Ag(110).

2.1.1 Surface-Driven Porphyrin Self-Assembly on Pre-Activated Si Surfaces

Self-assembly of melamine-bridged bis(porphyrin) dyads, such as **P(H_2)P(H_2)**, and **P(Zn)P(Zn)** are investigated on Si(100) substrate (Figure 2.1).[1] Their peculiar molecular structures allow to anticipate interesting self-assembly capabilities tailored by adjacent ring π-π interactions and by the hydrogen bonding acceptor-donor pattern typical of melamine unit.[2]

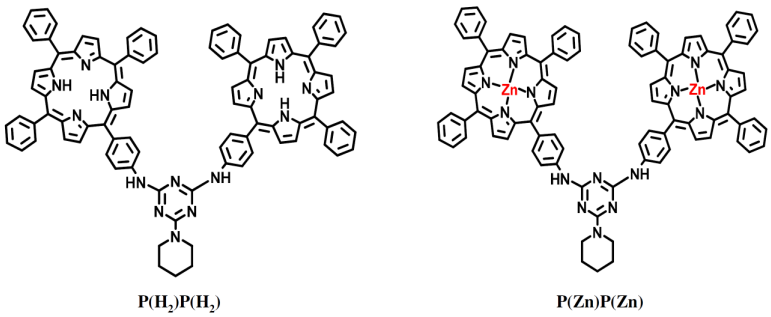

Figure 2.1: molecular structures of free-base and metalated porphyrin dyads.

In order to study the influence of the substrate coating protocol on the morphology of the resulting self-assembled films, a preliminary comparison of drop-casting *vs*. soaking procedure was performed. In both cases, a 0.1 mM solution of **P(H$_2$)P(H$_2$)** in tetrahydrofuran (THF) was used to deposit the porphyrin dimer on clean Si(100) substrates. Preliminary tests with a porphyrin concentration either higher (1 mM) or lower (0.01 mM) than 0.1 mM were also performed in order to investigate the effect of concentration on the self-assembly process. While in the former case a strongly unhomogeneous deposit was observed reasonably due to marked intermolecular aggregation phenomena in solution, in the latter, limited substrate coverage was detected due to the low porphyrin concentration. As a consequence, the 0.1 mM concentration was used for all the samples discussed in this Thesis project. The surface coverage of the resulting film was investigated by FE-SEM (Field Emission-Scanning Electron Microscopy) and AFM (Atomic Force Microscopy) techniques.

Drop casting consists of letting a small volume of solution of compound fall onto the substrate surface and leaving it to dry either in air or in an atmosphere of the solvent to ensure slower evaporation. The molecular self-assembly at the surface is highly influenced by the dewetting phenomena (or rupture of the thin solvent liquid film on the substrate), which depends on the solvent, the solution concentration and the substrate nature. A likely deposition methodology is soaking. Here, the substrate is dipped into the solution for a certain period of time (minutes or longer) and then extracted and left to dry in air.[3] Under these conditions, both preparation methods failed to produce a homogeneous substrate coverage as is showed in SEM micrographs below (Figure 2.2).

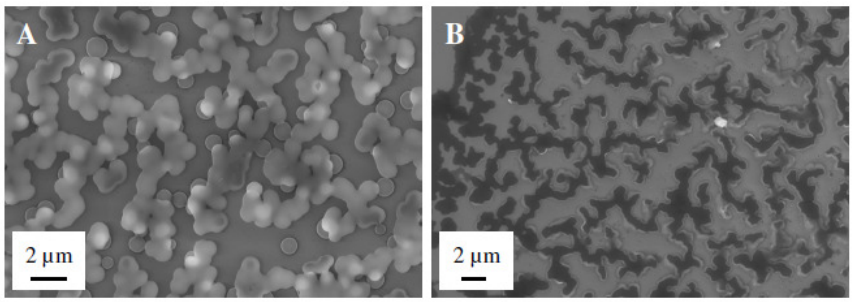

Figure 2.2: plane-view FE-SEM images of self-assembled **P(H$_2$)P(H$_2$)** films obtained from a 0.1 mM THF solution on non-activated Si substrates by: A) drop-casting; B) soaking. Bright areas represent the sample.

In particular, while the drop-casted specimen was characterized by the presence of interconnected globular aggregates with a typical size of *ca.* 1 μm (Fig. 2.2A), a relatively flat island-like deposit was obtained by soaking procedure (Fig. 2.2B). To this regard, it is worthwhile noting that the morphology of Fig. 2.2B was observed only in some restricted regions of the substrate, while the remaining areas were completely uncovered. The morphological differences between the two samples can be likely ascribed to the influence of the preparation route on the formation mechanism of such large-scale aggregates. In particular, in the drop-casting methodology the solvent evaporation rate seems to have an important effect on intermolecular aggregation phenomena.[4,5,6]

Based on our results, it seems that the THF evaporation rate was too high with respect to the porphyrin capability of interacting with the silicon substrate. On the other hand, in the case of soaking, the substrate immersion in the porphyrin solution for a definite period of time (8 h in the present case) favoured a surface-driven self-assembly process, dominated by intermolecular forces between the organic molecules and the substrate itself.[9] The adopted silicon substrates were covered by a *ca.* 2 nm thick native SiO_2 layer characterized by an appreciable amount of surface -OH groups.[7] As a consequence, the formation of the island-like structures evidenced in Fig. 2.2B could have been driven, at least during the first steps of the self-assembly process, by the existence of hydrogen bonding interactions between the melamine-bridge of the porphyrin dimers and the surface hydroxyl groups.

In order to further validate these hypothesis and to improve the coverage characteristics of the **P(H_2)P(H_2)** molecular films, we decided to perform a controlled surface activation procedure consisting in the immersion of the silicon supports in a *piranha* solution (H_2SO_4/H_2O_2 7:3) thus increasing the concentration of surface -OH groups.[8] Furthermore, **P(H_2)P(H_2)** depositions on these substrates were performed from 0.1 mM THF and chloroform ($CHCl_3$) solutions, in order to investigate whether the aggregation of the porphyrin dyad was not only affected by the substrate pre-treatment but also by interactions with the solvent molecules.[4,5,9] Since the soaking protocol allowed a better morphological control than drop-casting, only the latter deposition methodology was used. SEM images of the **P(H_2)P(H_2)** self-assembled porphyrin on activated Si substrates as a function of the used solvent are displayed in Figure 2.3.

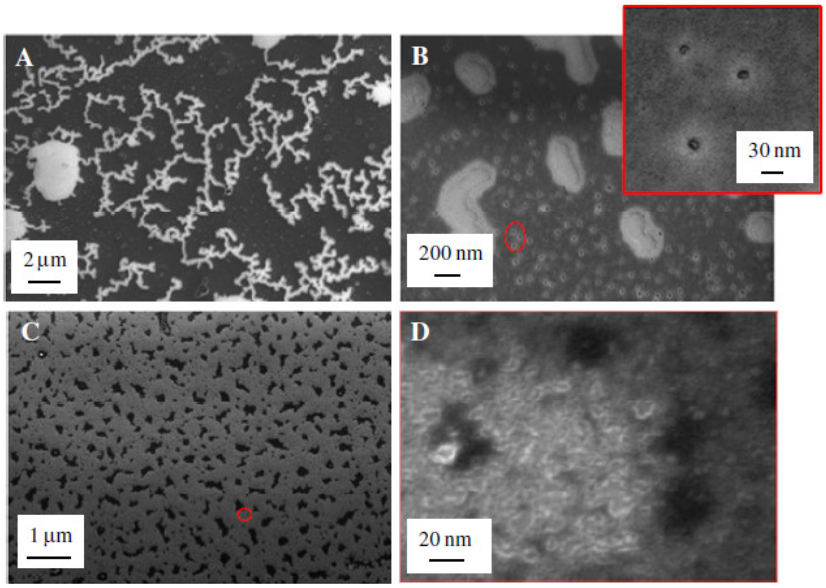

Figure 2.3: plane-view FE-SEM micrographs of self-assembled films obtained by immersion of activated Si substrates in: A), B) a **P(H_2)P(H_2)** in THF solution; C), D) a **P(H_2)P(H_2)** in $CHCl_3$ solution.

As regards, the specimen obtained from the THF solution, here after **P(H_2)P(H_2)-THF**, a worm-like morphology was evidenced at low magnification levels (Fig. 2.3A). In addition, a careful image inspection (Fig. 2.3B) revealed also the presence of small islands between worm-like structures, with a typical size of 200-500 nm, and some globular aggregates *ca.* 30 nm in size. As a whole, a substrate coverage close to 40% of the whole Si(100) surface was measured, confirming that the *piranha* solution treatment effectively enhanced the amount of -OH groups on the silicon surface, beneficially affecting the overall self-assembling process as well as the deposit homogeneity. On the other hand, the use of chloroform as solvent strongly improved the characteristics of the self-assembled film (sample **P(H_2)P(H_2)-$CHCl_3$**, Fig. 2.3C-D). In fact, the measured substrate coverage reached the 85%, resulting much more extended than in the THF case (compare Fig. 2.3C with Fig. 2.3A) and, correspondingly, the morphology of the covered regions was more regular and uniform (compare Fig. 2.3D with Fig. 2.3B). These results suggested that $CHCl_3$ increased the effectiveness of -OH groups on the oxidized silicon substrate to interact via hydrogen-bonding with porphyrin dimers, thus promoting the first step of the self-assembling process.

In order to further confirm that intermolecular association is a function of the used solvent and to evaluate the size distribution of molecular assemblies, AFM measurements were also carried out on the two last samples (Figure 2.4).

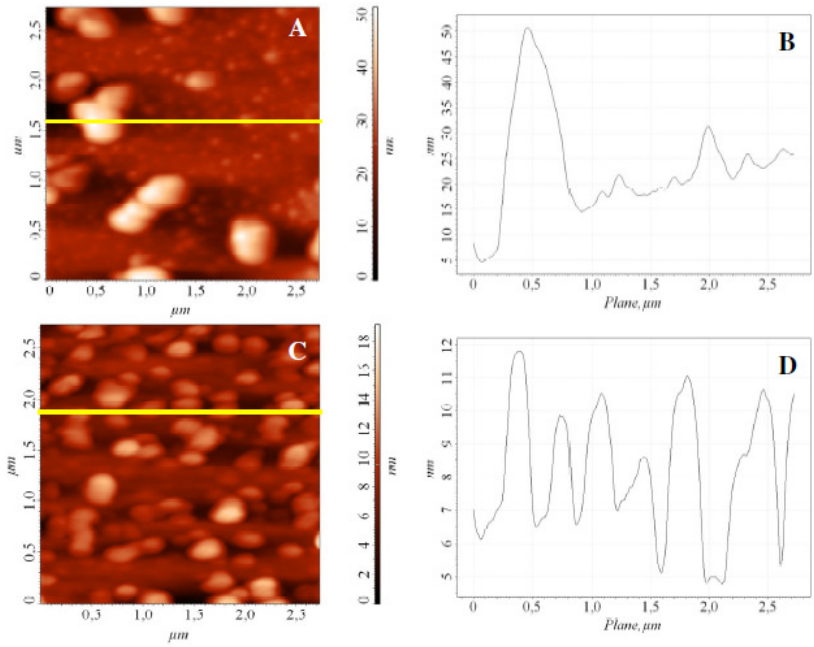

Figure 2.4: AFM micrographs and line depth profiles of: A), B) **P(H$_2$)P(H$_2$) -THF**; C), D) **P(H$_2$)P(H$_2$) -CHCl$_3$**.

Fig. 2.4A displays the AFM micrograph of sample **P(H$_2$)P(H$_2$)-THF** together with the corresponding line-scan profile (Fig. 2.4B). In agreement with FE-SEM data, the formation of an heterogeneous deposit was evidenced. In particular, the presence of large and small aggregates with a lateral size of *ca.* 300-500 nm and 40-80 nm, respectively and heights varying from 30 to 80 nm, was detected and mainly attributed to a solvent-driven assembly process rather than to surface-promoted phenomena. Conversely, sample **P(H$_2$)P(H$_2$)-CHCl$_3$** (Fig. 2.4C-D) was characterized by a more uniform substrate coverage and by a homogeneous distribution of rounded particles with a lateral size of 50-100 nm and *ca.* 10 nm high. As a whole, the above results further confirmed that both the substrate activation and the deposition solvent played a crucial role for the obtainment of uniform molecular films. In particular, the present findings suggest that chloroform, possessing a scarce affinity for surface -OH groups and a negligible coordinating capacity toward porphyrin with respect to THF, favoured the first steps of the self-assembly process through hydrogen bonds between the porphyrin molecules and the -OH groups on the silicon surface (Figure 2.5).[10] After the formation of the first molecular layer, π–π stacking interactions between the porphyrin rings drive the subsequent aggregation stages, leading to an uniform organic deposit. Conversely, in the case of THF, a quite strong hydrogen-

bonding acceptor, the π–π stacking of aromatic systems in the solution was favoured, reducing the effectiveness of silicon surface activation.[9]

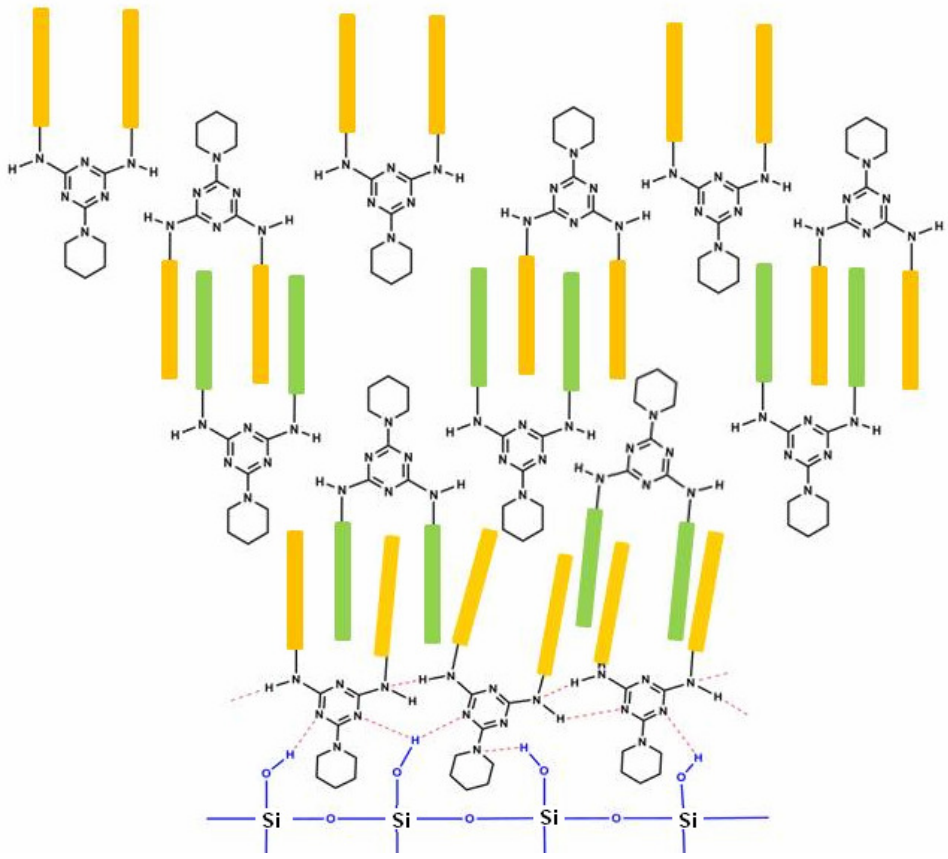

Figure 2.5: molecular self-assembly scheme of **P(H_2)P(H_2)-$CHCl_3$** on the activated Si substrate.

Based on the above results, the attention was subsequently devoted to the deposition of the Zn-metalated porphyrin **P(Zn)P(Zn)** on activated Si substrate by a chloroform solution. Interestingly, FE-SEM investigations on sample **P(Zn)P(Zn)-$CHCl_3$** (Fig. 2.6) revealed the formation of a self-assembled molecular film smoother than that obtained from the corresponding free-base porphyrin (compare Fig. 2.3C). Specifically, Fig. 2.6A displays a substrate coverage of 92% which is a value even larger than that of specimen **P(H_2)P(H_2)-$CHCl_3$**. Furthermore, the FE-SEM picture of Fig. 2.6B, recorded at higher magnification level, evidenced the formation of a flat deposit, where the globular features characteristic of **P(H_2)P(H_2)-$CHCl_3$** were less evident. To support this affirmation, the AFM micrograph of the same sample together with the corresponding line-scan profile is also reported.

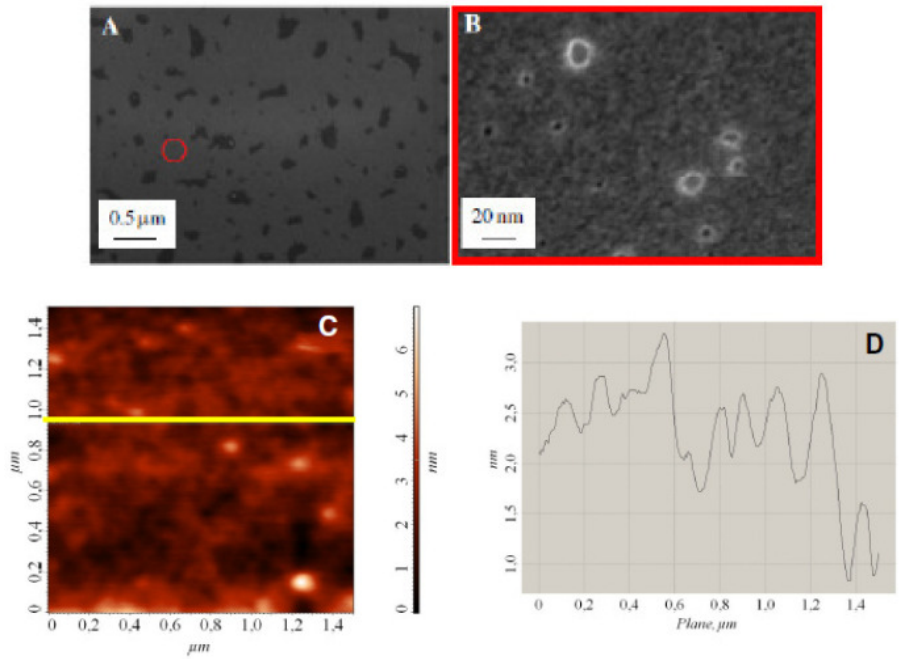

Figure 2.6: A), B) plane-view FE-SEM micrographs of a self-assembled film obtained by immersion of an activated Si substrate in a chloroform solution of **P(Zn)P(Zn)**. C), D) AFM micrographs and line depth profiles of **P(Zn)P(Zn) - $CHCl_3$**.

These different morphologies could be tentatively explained by considering that, in the case of sample **P(Zn)P(Zn)-$CHCl_3$**, the presence of the Zn^{II} ions in the porphyrin nucleus disfavoured solution pre-aggregation phenomena enhancing, on the other hand, the substrate-driven self-assembly process through the coordination of the metal centre to surface hydroxyls. In other words, the obtainment of a homogeneous self-assembled molecular film depends on a global balance between porphyrin solvent, porphyrin-porphyrin and porphyrin-substrate interactions.

The chemical composition of the most uniform films, *e.g.*, **P(H_2)P(H_2)-$CHCl_3$** and **P(Zn)P(Zn)-$CHCl_3$**, was also investigated by the XPS (X-ray Photoelectron Spectroscopy) technique. The survey spectrum of sample **P(Zn)P(Zn)-$CHCl_3$** (Figure 2.7) was characterized only by Zn, N, C, O and Si signals, indicating that the adopted synthetic procedure yielded pure molecular systems, free from undesired contaminants. The same considerations also hold for specimen **P(H_2)P(H_2)-$CHCl_3$** apart from the obvious absence of the zinc photopeaks. In both cases, the appearance of the silicon signals could be related to the formation of organic porphyrin films leaving uncovered some substrate surface, as evidenced by AFM and FE-SEM analyses.

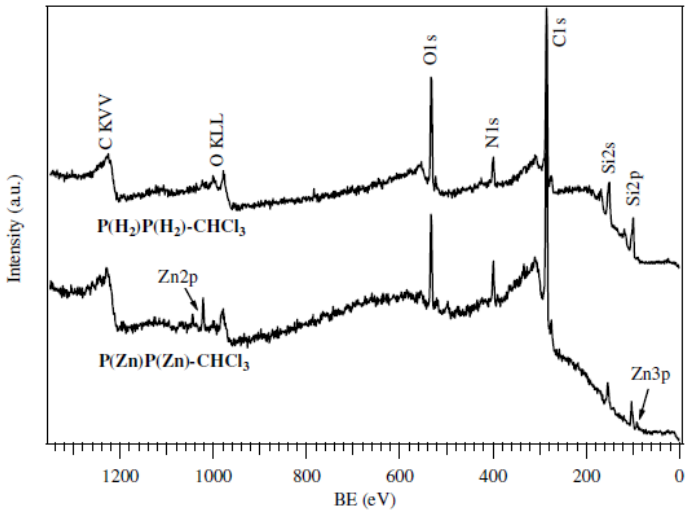

Figure 7: XPS spectra of samples **P(H$_2$)P(H$_2$)-CHCl$_3$** and **P(Zn)P(Zn)-CHCl$_3$**.

For the two samples the Si 2p peak (not reported) was characterized by two contributing bands located at binding energy (BE) values of 99.5 and 102.8 eV. While the first signal can be attributed to Si(0) from the silicon substrate, the high BE component is in agreement with the presence of an hydroxylated silica surface layer, as also evidenced by the O 1s peak centred at a BE of 532.5 eV.[11] If the formation of a thin SiO_2 layer is commonly observed on silicon because of atmospheric oxidation, the presence of hydroxyl groups, reasonably enhanced by the substrate pre-treatment with the *piranha* solution, played an important role for the surface grafting of the porphyrin-dimer molecules. It is also worthwhile observing that the Si surface percentage decreased from *ca.* 15 to 6% on going from **P(H$_2$)P(H$_2$)-CHCl$_3$** to **P(Zn)P(Zn)-CHCl$_3$**. This result is indicative of better substrate coverage on the latter sample, as already evidenced by AFM and FE-SEM results.

Concerning the C 1s peak (Fig. 2.8A), the strong component at 284.8 eV accounted for the presence of the different aromatic and aliphatic carbon atoms in the dimer-porphyrin molecules.[12] It is also worthwhile observing that the measured C/N ratio (~9) was always higher than the expected stoichiometric value (6.86). Such a result evidenced that also adventitious carbon arising from atmospheric contamination partially contributed to the band located at 284.8 eV.[38] Finally, the weak tailing at ~287.0 eV is typical of porphyrinic systems.[12,13]

The N 1s signal (Fig. 2.8B) is often regarded as the most sensitive probe to describe the charge distribution in porphyrins.[12,14,15] Nevertheless, in the current case data

interpretation was not straightforward due to the presence of several non-equivalent nitrogen atoms. To this regard, the N 1s peak can be considered as the resultant of two partially overlapped bands, one centred at ~398.5 eV (I), and the second one at ~400.0 eV (II), both contributed from several species.

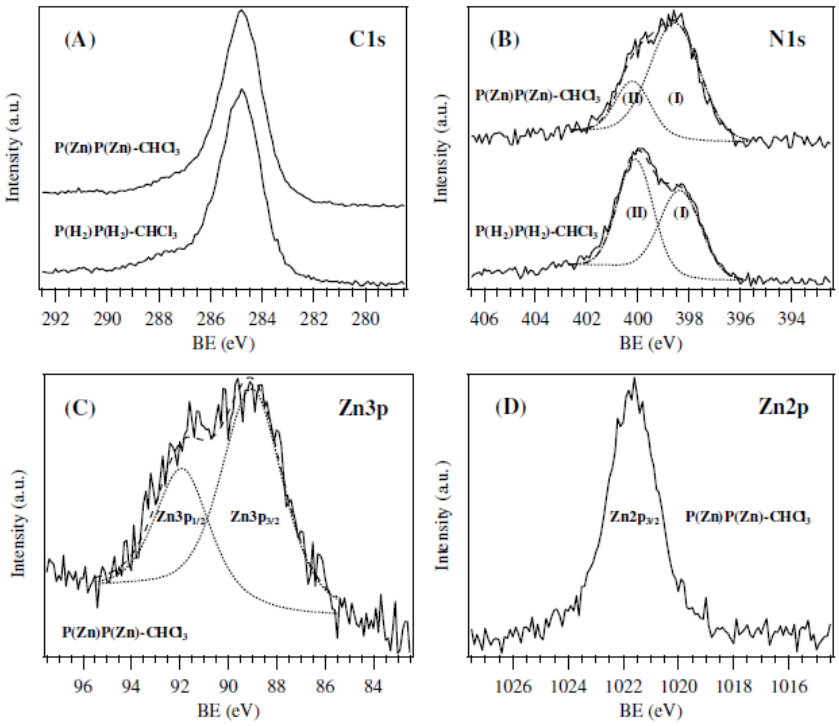

Figure 2.8: detailed C 1s (A), N 1s (B), Zn 3p (C) and Zn 2p (D) XPS regions for **$P(H_2)P(H_2)$-$CHCl_3$** and **P(Zn)P(Zn)-$CHCl_3$**.

While for sample **P(Zn)P(Zn)-$CHCl_3$** the low binding energy (BE) component was more intense than the higher BE, the opposite situation was detected for **$P(H_2)P(H_2)$-$CHCl_3$**. On these bases, it is reasonable to suppose that:

i) for **$P(H_2)P(H_2)$-$CHCl_3$** the 398.5 eV contribution arises from four non-protonated pyrrolic nitrogen atoms of the porphyrin moiety, together with other three atoms of the triazine ring. On the other hand, the more intense contribution centred at 400.0 eV could be traced back to four protonated pyrrolic nitrogen atoms in the porphyrinic ring, as well as to the three remaining nitrogen atoms covalently bonded to the triazine moiety (melaminic nitrogens);[12,15,16]

ii) upon Zn coordination the porphyrin nitrogen atoms are expected to become equivalent and to present a BE value relatively close to the non-protonated pyrrolic nitrogens.[13,14,16,17] Therefore, the signal centred at 398.5 eV accounts for eight Zn-coordinated nitrogen atoms plus the contribution of the triazinic nitrogens. Conversely, the high BE component can be traced back to the three remaining "extra-porphyrin" melaminic nitrogen atoms. In other words, upon Zn coordination, the low BE N 1s component grows at expenses of the high BE one.

Also, in the case of **P(Zn)P(Zn)-$CHCl_3$** the shape of both Zn 3p and Zn 2p peaks (Fig. 2.8C-D) indicated the presence of a single type of equivalent Zn atoms. Furthermore, the Zn 2p3/2 peak position (BE = 1021.6 eV) was in agreement with the BE values reported in the literature for similar systems,[18] supporting the coordination of Zn^{II} to the porphyrinic ring. To this regard, the N:Zn ratio (*ca.* 9:1) was in rather good agreement with the presence of two Zn ions for each porphyrin dyad (expected value: 7:1).

2.1.1.1 Gas Sensing Properties of Thin Films

According to the above results and considering the ever higher importance of porphyrin molecular systems in detection of various gases and volatile compounds, the gas sensing properties of the most promising organic films were preliminary investigated. The exposure of porphyrin systems to oxidizing or reducing gases causes a charge–transfer between the gas and the delocalized molecular π-system. This mechanism significantly modifies the optical absorbance spectrum as well as the electrical conductance of the films, providing the bases for gas sensing measurements.[19,20] In particular, attention was mainly devoted to sample **P(Zn)P(Zn)-$CHCl_3$**.

The conductance of the **P(Zn)P(Zn)-$CHCl_3$** layer in synthetic air at different humidity levels was measured to control the stability of this material under room conditions. The graph reported in Figure 2.9 shows the conductance value as a function of the relative humidity (RH) in the range 0-50% RH. As it can be seen, the conductance value were quite reproducible (average value $1.45e^{-6}$ S with a standard deviation of $1e^{-7}$ S) despite tests were performed at room temperature. These results pointed out the low system reactivity towards water, an important feature for the detection of several analytes in the presence of aqueous moisture.

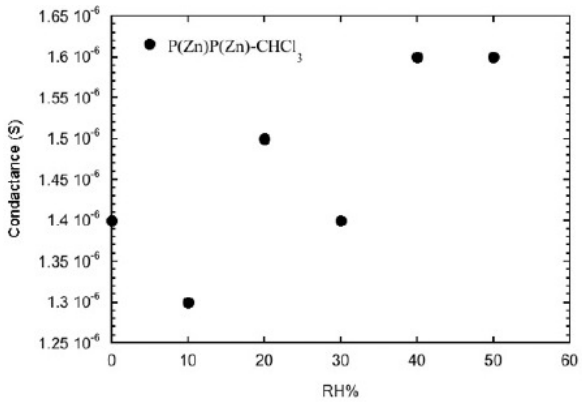

Figure 2.9: conductance values of sample **P(Zn)P(Zn)-CHCl$_3$** as a function of the relative humidity (RH).

Subsequently, the gas sensing properties of sample **P(Zn)P(Zn)-CHCl$_3$** were investigated towards ammonia detection at two different humidity levels (RH 10% and 50%). Current variation of the supported organic porphyrin film introduced into the test chamber was determinated (Figure 2.10). The observed current decreasing, as ammonia interacts with the layer, can be ascribed to the coordination of NH_3 to the Zn metallic center, which alters the electronic structure of porphyrin dyads, thus resulting in a conductance change.[19]

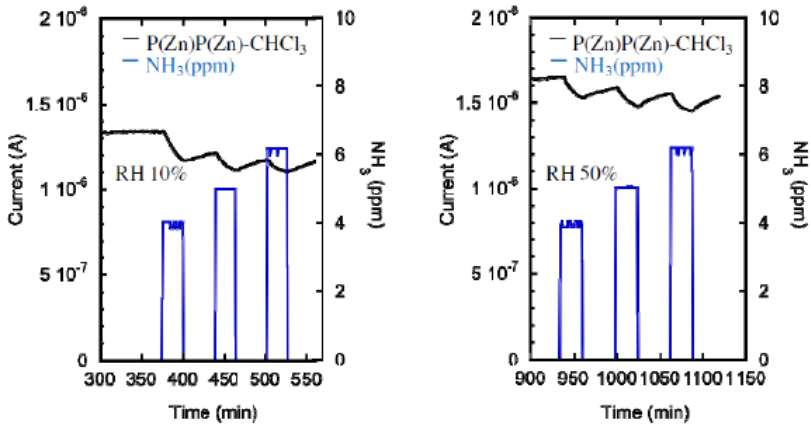

Figure 2.10: current variation of sample **P(Zn)P(Zn)-CHCl$_3$** as a function of different ammonia concentration at two different humidity levels.

It is also worthwhile observing that no current variation was registered when the system was exposed to ethanol (100-500 ppm) and acetone (10-100 ppm), indicating that the obtained porphyrin film is highly selective to ammonia. Notably, the present system performances are better than those of other bis(porphyrin) molecules, deposited by spin-

coating on glass substrates, which showed negligible responses towards H_2S, NH_3 and NO_2. [19]

2.1.2 Fullerene/Porphyrin Multicomponent Nanostructures on Ag(110): from Supramolecular Self-Assembly to Extended Copolymers

Chromophoric molecules such as fullerenes and porphyrins are appealing π-conjugated modules for the construction of functional molecular materials possessing exceptional electrochemical and photophysical properties.[21,22] One of the most interesting aspects of C_{60} and porphyrins is that they spontaneously attract each other mainly through dispersion and donor–acceptor interactions, as experimentally determined both in solution and in the solid state.[23,24,25] Taking advantage of the fullerene–porphyrin affinities it is possible to selectively engineer supramolecular assemblies on surfaces with a large periodicity. Characterizing these assemblies by scanning probe methods, such as scanning tunneling microscopy (STM), provides a detailed insight into the structures at the molecular and atomic levels.[26] A limited number of studies has been undertaken to elucidate the supramolecular behavior of single porphyrin molecules on surfaces.[27,28] In particular, their assembly with other redox- and/or photoactive molecular species, such as fullerenes, on surfaces has not been fully investigated.[29]

In this Thesis project, the *bottom-up* fabrication of organic nanopatterned surfaces based on 2D supramolecular assemblies composed of porphyrins and C_{60} on Ag(110) was investigated. In particular, three types of porphyrin are considered: simple tetraphenyl porphyrin (**TPP**), 5-(4-aminophenyl)-10,15,20-triphenyl porphyrin (**TPPNH$_2$**), where one phenyl group has been substituted by a *p*-amino phenyl group, and **TPP(NH$_2$)$_2$**, where two *trans*-phenyl groups have been substituted by two *p*-amino phenyl groups. In the general acronym **TPP** collectively indicates all three tetraphenyl porphyrin species when no ambiguity arises from this usage.

The central and bottom rows of Figure 2.11 show STM images and molecular models, respectively, of **TPP**, **TPPNH$_2$**, and **TPP(NH$_2$)$_2$** monolayer islands deposited on Ag(110) at room temperature. For symmetry reasons, each molecular species self-organizes in two equivalent domains rotated by 59° from each other. All overlayers form simply commensurate superstructures (integer matrix elements in matrix notation at the

bottom), which indicates that all molecules in each overlayer occupy equivalent adsorption sites.

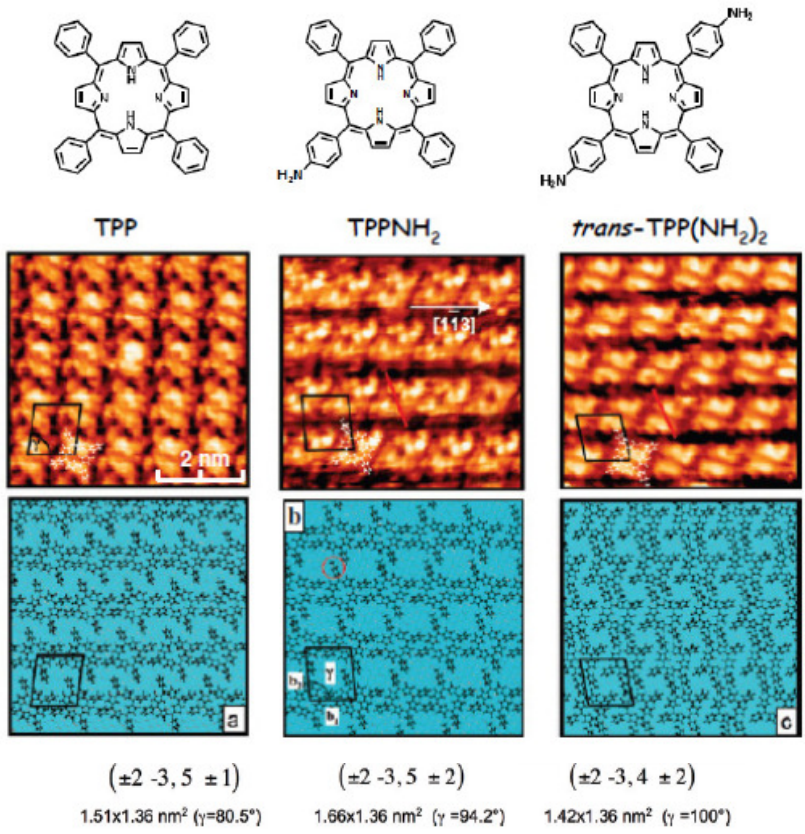

Figure 2.11: single molecule models (top), high resolution STM images (center), and related superstructure models (bottom) of three different **TPPs** on Ag(110): (a) **TPP** (7x7 nm^2, *V*=0.53 V, I=3.2 nA); (b) **TPPNH$_2$** (7x7 nm^2, *V*=0.03 V, I=0.03 nA) and (c) **TPP(NH$_2$)$_2$** (7x7 nm^2, *V*=0.22 V, I=2.27 nA). The Ag(110) substrate atoms are shown as light blue circles in the bottom-most row. Unit cells are drawn in black. For every unit cell, the matrix notation with respect to the substrate and unit cell dimensions (unit vector lengths and angle γ between unit vectors) are reported. Red lines in panels b and c highlight the most probable direction of alignment of aminophenyl rings.

Changing the number and the position of aminophenyl rings, the molecular stripe direction and the **TPP-TPP** nearest neighbours (NN) distance along the horizontal-oriented stripes do not change (which is reflected in the invariance of the first row in matrix notations for the three superstructures), whereas the interstripe separation is modified, giving rise to different surface densities for the three phases. This is an indication that the aminophenyl rings of **TPPNH$_2$** and **TPP(NH$_2$)$_2$** point to adjacent stripes rather than to nearest neighbour molecules within each aligned stripe (*i.e.*, the aminophenyl groups are

aligned along the red lines in the STM images of Figure 2.11). Intrastripe orientation of aminophenyl rings is unlikely also for steric reasons.[30]

Codeposition of **TPP** and C_{60} submonolayers on the Ag(110) substrate held at room temperature has been optimized in order to obtain an approximately 1:1 ratio between the two components which leads to the formation of a short-range ordered bicomponent nanostructure organized in small islands. After extensive annealing (~ 400 min) at 410 K, molecules self-assemble in a very large 2D long-range ordered and commensurate nanostructure, resulting from the equilibrium between weak reversible lateral **TPP**-C_{60} and vertical molecules-substrate interactions. Figure 2.12 displays STM results concerning **$TPPNH_2$** and **$TPP(NH_2)_2$**.

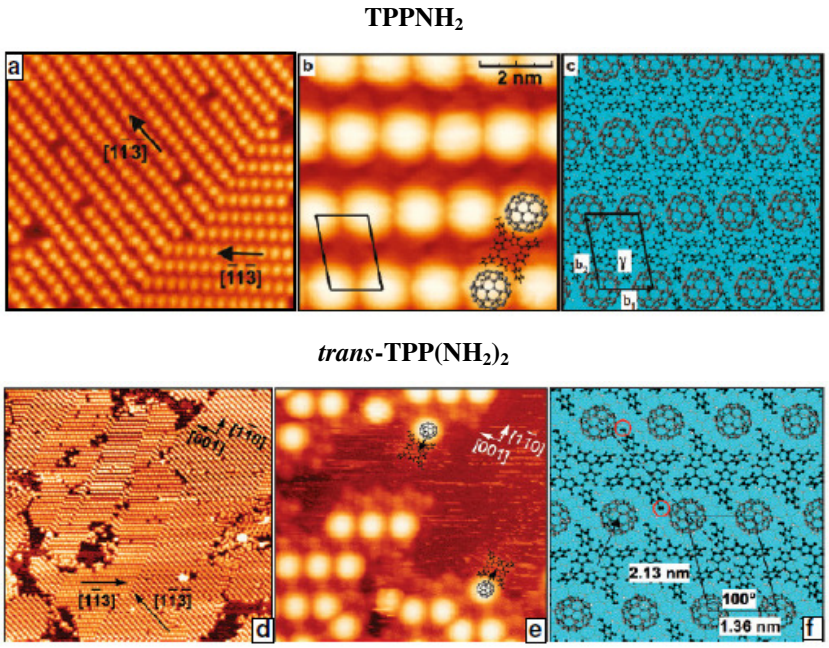

Figure 2.12: top. (a) large-scale STM image of the multicomponent **$TPPNH_2$**/C_{60} self-assembly on Ag(110) obtained at 410 K and measured at RT (90x90 nm^2, *V*=-1.0 V, I=1.0 nA); (b) STM image (7x7nm^2,*V*=1.0V, I=1.0 nA) and (c) molecular model of the (2 -3, 6 3) domain, drawn to scale with (b). Bottom. (d) bicomponent **$TPP(NH_2)_2$**/C_{60} self-assembled nanostructure on Ag(110) obtained by annealing the system at 410 K and measured at RT (140x140 nm^2, *V*=0.4 V, I=4.0 nA); (e) High resolution STM image (15x15 nm^2, *V*=0.3 V, I=0.2 nA) of a defective domain boundary; (f) molecular model of the bicomponent nanostructure. The superstructure unit cell is shown. Red circles highlight NH_2 groups on a **$TPP(NH_2)_2$** molecule.

The large scale STM image reported in Fig. 2.12a and 2.12d shows very extended, long-range ordered and low defectivity islands (two domains rotated by 59° from each

other form for symmetry reasons), wherein island areas are in the range 3000-7000 nm^2 with a defectivity, mainly in the form of C_{60} vacancies, that is lower than 1%.26 These complex nanostructures are strictly equivalent and characterized by alternating stripes of C_{60} and amino **TPPs** aligned along the two and equivalent substrate directions (see big black arrow Fig. 2.12a and d) forming the commensurate unit cell sketched in Figure 2c and 2f, where the two species appear in a 1:1 ratio and are both in direct contact with the substrate. The C_{60}-C_{60} NN distance along a stripe is 1.4 - 0.1 nm, that is, it mirrors the intrastripe NN intermolecular distance found in the pure porphyrin phase and is substantially larger than the NN interfullerene distance (1.0 nm) in the close-packed c(4 x 4) phase produced by fullerene alone on Ag (110).27 The same bicomponent superstructure has been obtained by self-assembling C_{60} with the tetraphenyl porphyrin, **TPP**. This means that the weak interactions responsible for the self-organization of these supramolecular structures are not influenced by the presence and the number of peripheral amino groups on the **TPP** molecules, at least in the range that has been explored in this Thesis work.

Furthermore, from high resolution STM images collected at the borders of ordered domains, where several isolated C_{60}-**TPP** couples can be singled out, it is possible to infer the orientation of this weak interaction. As it can also seen in Fig. 2.12e, two C_{60} and two **TPP(NH_2)$_2$** molecules have been evidenced in order to indicate that every **TPP(NH_2)$_2$** unit "captures" a C_{60} molecule (marked with black arrows) by laterally coordinating it, possibly through a couple of adjacent peripheral phenyl rings linked to the porphyrin macrocycle. Time-lapsed STM imaging confirms the reversibility of such supramolecular interactions at the borders of the already formed bicomponent islands.

As evidenced by red circles in Fig. 2.12f, the two aminophenyl rings of each **TPP(NH_2)$_2$** molecules point toward NN C_{60} molecules rather than toward the NN **TPP(NH_2)$_2$** units belonging to the same **TPP** stripe. Such an arrangement is required for steric reasons,[30] and it is also deduced by comparing the unit cells of the different single component porphyrin ordered phases on Ag(110), reported in Figure 2.11, to the unit cell of the bicomponent phase: as already remarked, the superstructure unit cell parameter along the horizontal-substrate direction is preserved (1.4 nm) on going from the single component overlayers to the bicomponent supramolecular network.

To this point, the behavior of the three different **TPP** molecules with respect to C_{60} is exactly the same when the sample is annealed at 410 K. However, the thermal stability of this common superstructure is very high when **TPP(NH_2)$_2$** is used as a building unit in

the bicomponent self-assembly, while it is definitely lower when either **TPP** or **TPPNH$_2$** are employed. The left columns of each image in Figure 2.13 show the common nanostructure obtained using the three different porphyrins by means of a long annealing treatment (150 min) at 410 K, whereas the right column reports images of the resulting surface morphology after an additional annealing treatment of 30 min at 640 K. It appears that when one starts from **TPP** and **TPPNH$_2$** the bicomponent ordered network is disrupted upon high temperature annealing. Phase separation occurs and consequently most C_{60} molecules segregate in close packed c(4 x 4) domains, while porphyrin molecules form a disordered phase.[30,31,32]

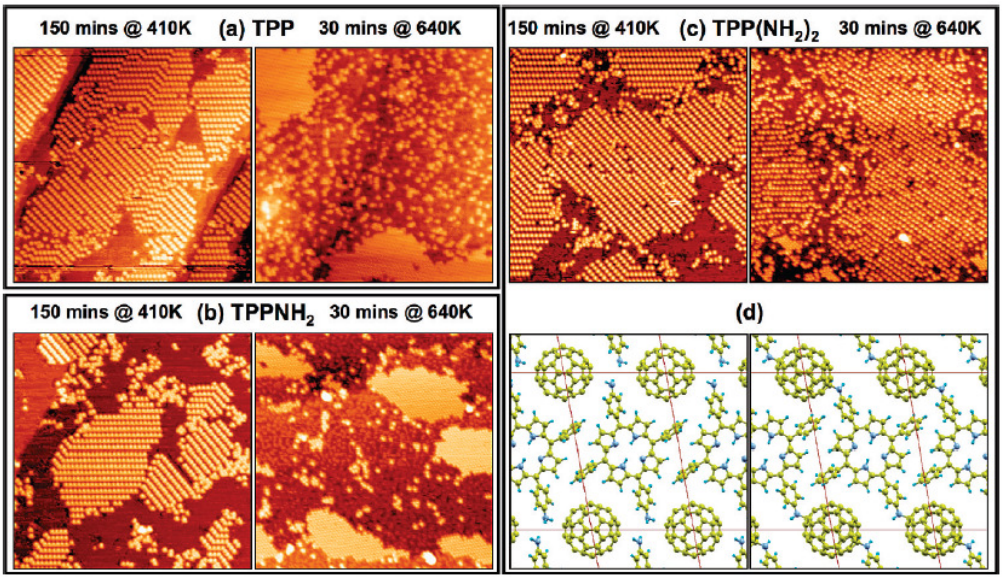

Figure 2.13: different thermal stability of binary self-assembled nanostructures starting from C_{60} and (a) **TPP** (left) *V*=0.8 V, I=1.0 nA; (right) *V*=0.7 V, I=1.0 nA); (b) **TPPNH$_2$**, (left) *V*=0.5 V, I=0.9 nA; (right) *V*=0.8 V, I=1.9 nA), (c) **TPP(NH$_2$)$_2$** (left) *V*=0.5 V, I=0.3 nA; (right) *V*=0.5 V, I=0.4 nA). All STM images are 85x85 nm^2 in size. Annealing temperatures and times are indicated. (d) Molecular model of the supramolecular network (left) and a hypothetic model of the covalently linked structure (right).

On the other hand, the self-assembled nanostructure starting from **TPP(NH$_2$)$_2$** resists to the thermal treatment: the local order and the dimensions of the ordered islands remain approximately unaltered. The observed high thermal stability is in line with the behavior of other covalent organic frameworks[33,34] and its high temperature limit seems to be determined by the onset of **TPP** degradation at about 680 K, as obtained from thermogravimetric analysis (see Experimental Section, Appendix III).

It is evident that the different responses to the high temperature thermal treatment strictly depend on the presence and number of amino groups on **TTP** molecules. The ability of amines to react with C_{60} both in self-assembled monolayers in solution[35,36,37] and in the solid state is well established: this property has been exploited for the production of fullerene polymers, as recently reviewed.[38] The model sketched in Fig. 2.13d shows that the two *trans* amino phenyl groups on each **TPP(NH$_2$)$_2$** molecule are very close to two C_{60} units positioned on adjacent stripes: with a few degrees of anticlockwise rotation and/or with a little shift of **TPP(NH$_2$)$_2$** monomers, the two amino groups can be positioned at a covalent bonding distance with respect to both adjacent C_{60} molecules, resulting in the copolymer chains along the longer diagonal of the superstructure unit cell. On the basis of the available STM data, is impossible to exclude the other possibility, namely the clockwise rotation of **TPP(NH$_2$)$_2$** monomers in order to bind along the shorter diagonal of the oblique unit cell. It is worth noting that if the two bonding schemes were energetically roughly degenerate, a randomly linked 2D covalent network would occur. Quantum chemistry calculations explicitly including the interactions of both molecular species with the substrate are needed to address this interesting issue.

In summary, the peculiar high thermal stability of the binary nanostructure containing **TPP(NH$_2$)$_2$** molecules can be explained by the fact that both amino groups on each *trans*-amino porphyrin unit react with nearby C_{60} molecules in the preorganized supramolecular network forming covalently bonded (TPP-NH-$C_{60}H_2$-NH-)$_n$ copolymer chains. Very similar water-soluble main-chain fullerene polymers with a molecular weight up to 20.0 kg/mol, wherein C_{60} units are linked through aromatic diamines, have been also reported in literature to form in solution.[39]

To substantiate the hypothesis of covalent bonding between the molecular building units, the thermal stability of the three **TPP** molecules has been investigated in order to exclude that a different thermal behavior of **TPP**, **TPPNH$_2$**, and **TPP(NH$_2$)$_2$**-C_{60} bicomponent nanostructures is due to an intrinsically higher thermal stability of **TPP(NH$_2$)$_2$** on Ag(110).

Each **TPPs** has been deposited on Ag(110) held at room temperature (RT). Three similar single component ordered phases (Figure 2.14, top) have been obtained and then annealed at increasing temperature, following the same thermal treatment used for the bicomponent systems (Figure 2.14, bottom).

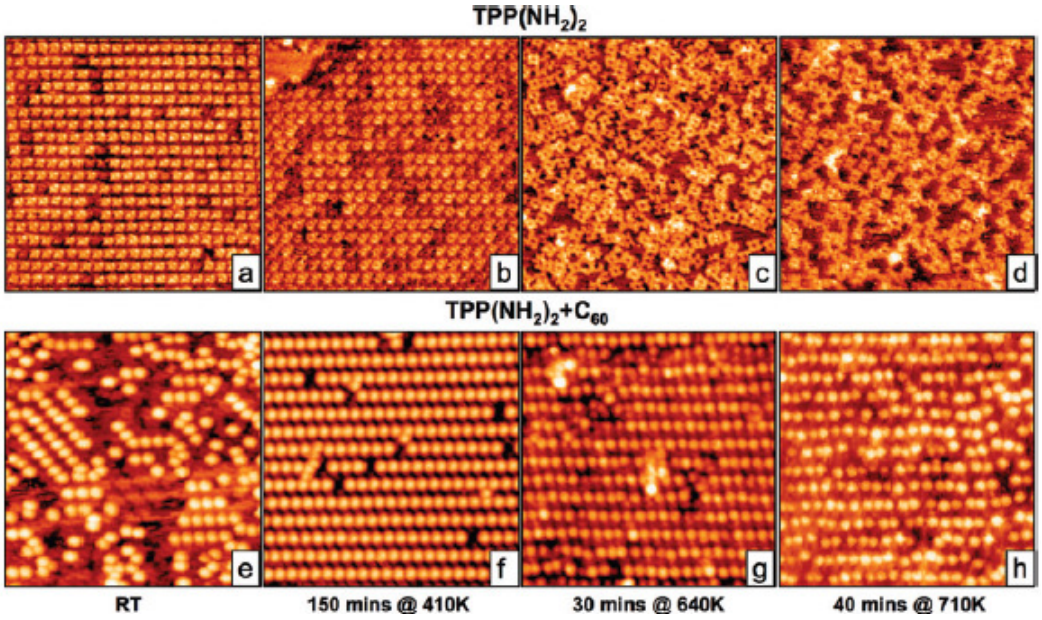

Figure 2.14: thermal stability of the single component **TPP(NH$_2$)$_2$** self-assembly (a-d, top) compared to the thermal stability of the bicomponent **TPP(NH$_2$)$_2$** - C_{60} system (e-h, bottom): (a) *V*=0.4 V, I=3.0 nA; (b) *V*=0.65 V, I=10.0 nA; (c) *V*=0.24 V, I=3.0 nA; (d) *V*=0.53 V, I=15.0 nA; (e) *V*=1.0 V, I=1.0 nA; (f) *V*=0.55 V, I=0.35 nA; (g) *V*=1.0 V, I=2.6 nA; (h) *V*=0.20 V, I=1.6 nA. All STM images are 15x15 nm^2 in size. Annealing temperatures and times are indicated for each column.

The resulting single component nanostructures at different annealing conditions demonstrated that the higher stability of the **TPP(NH$_2$)$_2$** - C_{60} bicomponent system is not related to a higher intrinsic stability of *trans*-amino porphyrin with respect to the silver substrate. This is a further indication that the binary nanostructure containing **TPP(NH$_2$)$_2$** is stabilized through an extended network of covalent bonds. The notable effect of annealing between RT and 410 K is the development of large ordered domains from small supramolecular islands (Fig. 2.14e and f). Increasing the annealing temperature to 640 K (Fig. 2.14g) only causes a partial loss of registry of the overlayer rows with respect to the substrate, which can be attributed to small conformational adjustment of the covalently linked chains due to torsional degrees of freedom activated by the thermal treatment. The higher degree of disorder at 710 K (Fig. 2.14h) indicates an incipient decomposition of the overlayer. These observations could indicate that (a) the **TPP(NH$_2$)$_2$** - C_{60} lateral interactions in the supramolecular network are weaker and less directionally specific than the C_{60}-C_{60} direct van der Waals interactions in fullerene clusters and closepacked C_{60} ad-islands; (b) at 410 K only a tiny minority of fullerene molecules reacts with **TPP(NH$_2$)$_2$**

even after extended annealing times, thus setting a lower temperature limit for the occurrence of the covalent bonds formation.

In-situ spectroscopic evidence for the occurrence of the polymerization reaction at 640 K is also provided by X-ray photoelectron spectroscopy (XPS). Figure 2.15 shows the N 1s XP spectrum of **TPP(NH$_2$)$_2$** molecules belonging to the **TPP(NH$_2$)$_2$**/C$_{60}$ bicomponent network on Ag(110) after annealing at the two relevant temperatures. The N 1s region shows characteristic changes in the course of the reaction, which are in agreement with the proposed bonding scheme.

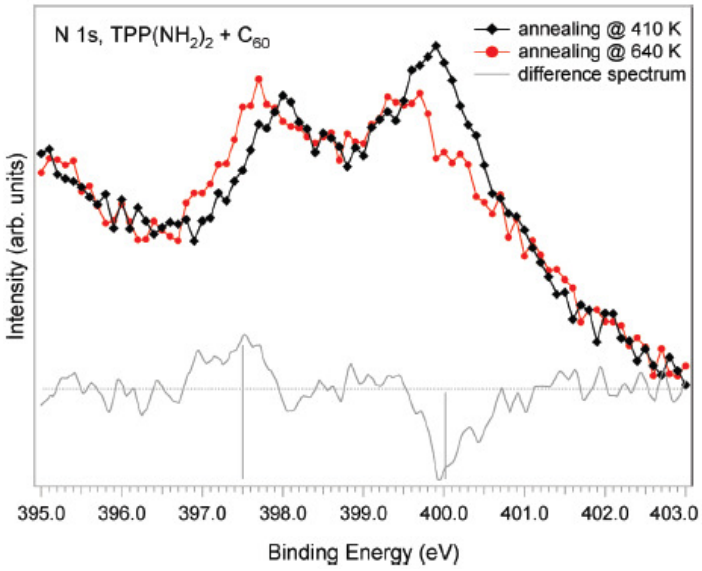

Figure 2.15: Al Kα-excited N 1s XP spectrum of the **TPP(NH$_2$)$_2$**/C$_{60}$ bicomponent network after annealing at 410 K (black squares) and at 640 K (red circles). The difference spectrum is also shown.

The spectrum after the thermal treatment at 410 K consists of two components at 400.1 and 398.2 eV with different relatively intensity ratio, while in pristine **TPP** (spectrum not shown) the two components have the same intensity, reflecting the equal number of nitrogen atoms within the two types of molecules.[40,41]

In **TPP(NH$_2$)$_2$** the high binding energy (BE = 400.0 eV) component is more intense, since the contribution of the two primary amino groups cannot be resolved from the pyrrolic contribution.[37] After annealing at 640 K, the high BE component decreases, while a new component appears at 397.5 eV, whose intensity roughly equals the intensity decrease around 400.0 eV (see the difference spectrum in Figure 2.15). In literature, almost the same binding energy shift is observed when surface grafted primary alkylamines react

with C_{60} to form R-NH-C_{60}H adducts.[37] The XPS spectra of the N 1s region provide a fingerprint for the occurrence of the polymerization reaction. The obtained covalently linked network is particularly robust and is resistant to air and water exposure.

To better understand the occurrence of the fullerene-aminoporphyrin reaction, equimolar amounts of **TPPNH$_2$** and C_{60} have been mechanically blended with a pestle in an agate mortar. The solid mixture was then heated for 1 h at 85 °C. TLC analysis (petroleum ether/ethyl acetate 3:2 v/v) showed the complete disappearance of the porphyrin (R_f = 0.56) and the formation of a new product (R_f = 0.79). Both UV-vis and ^{13}C-NMR analysis confirmed that this new product contained the spectroscopic signatures of the porphyrin and the fullerene units and were different from those obtained for a 1:1 mixture of the two compounds (Figure 2.16). These results show that the addition reaction between **TPPNH$_2$** and C_{60} takes place smoothly even at low temperatures.

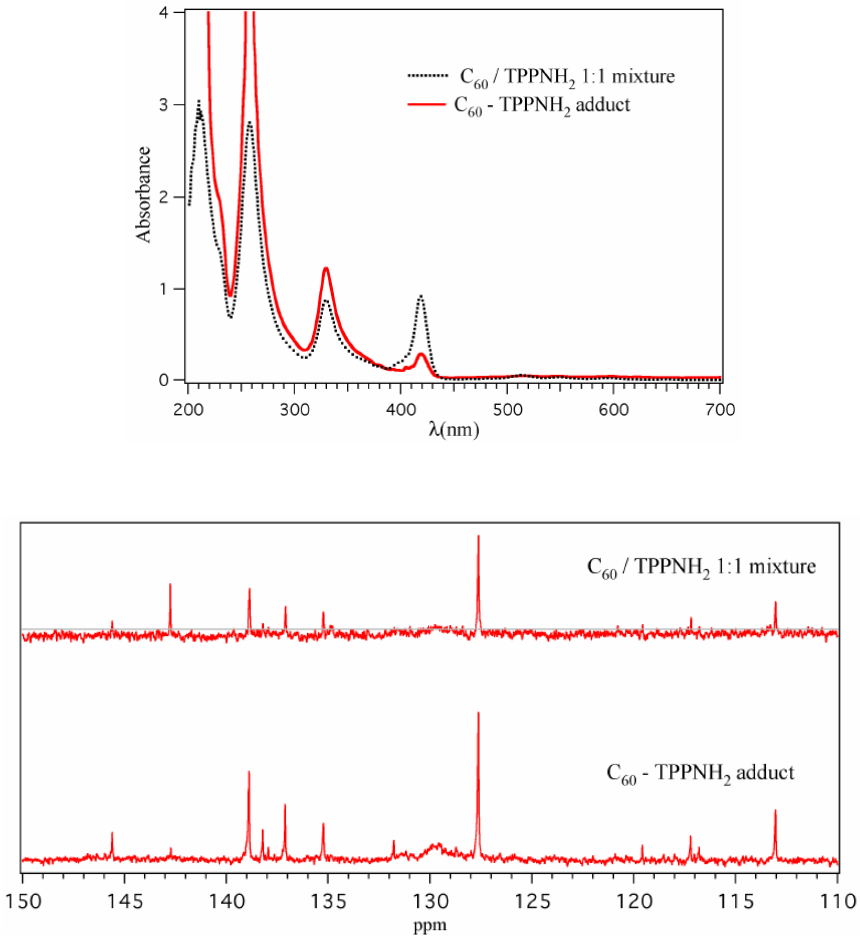

Figure 2.16: top. UV-vis spectra in cyclohexane of the **TPPNH$_2$** - C_{60} adduct in comparison with a 1:1 mixture of the two components. Bottom. ^{13}C-NMR of the **TPPNH$_2$** - C_{60} adduct in comparison with a 1:1 mixture of the two components (solvent: CS_2-$CDCl_3$ 4:1 v/v).

As shown here, a substantially higher temperature is required to trigger the reaction in the surface-supported supramolecular aggregate, which is a key for the successful two step synthesis of the covalently linked nanostructures. A higher reaction temperature on the surface with respect to solution and solid state may be traced back to a substantially reduced entropic term due to frozen orientational degrees of freedom in the supramolecular network, possibly coupled to an active role of the substrate in the form of charge transfer from Ag to C_{60}, which is expected to partially hinder the nucleophilic attack of the amino-groups to fullerene.[42,43]

In conclusion, the extended, ordered, and covalently linked bicomponent molecular superstructure can be obtained by thermal triggering of covalent bonds formation in a preorganized supramolecular network of C_{60} and **TPP(NH_2)$_2$**. These results show promising potential for the synthesis of highly ordered networks of surface-supported functional copolymers for energy applications. In particular, they point to a possible route for the simple and effective one-pot synthesis of extended regular networks of covalently bonded donor-acceptor (D-A) arrays for efficient charge separation through the choice of properly functionalized D and A building units.

REFERENCES

[1] (a) Carofiglio, T.; Varotto, A.; Tonnellato, U., *J. Org. Chem.*, **2004**, *69*, 8121. (b) Carofiglio, T.; Lubian, E.; Menegazzo, I.; Saielli, G.; Varotto, A., *J. Org. Chem.*, **2009**, *74*, 9034.

[2] Seto, C.T.; Whitesides, G.M., *J. Am. Chem. Soc.*, **1990**, *112*, 6409.

[3] Nadal, E.G.; Luis, J.P.; Amabilino, D.B., *Chem. Soc. Rev.*, **2008**, *37*, 490

[4] Koepf, M.; Bucher, J.A.; Weiss, J., *J. Am. Chem. Soc.*, **2008**, *130*, 9994.

[5] George, H.; Guo, Q., *Thin Solid Films*, **2009**, *517*, 2651.

[6] Milic, T. ; Garno, J.C. ; Batteas, J.D. ; Smeureanu, G.; Drain, M., *Langmuir*, **2004**, *20*, 3974.

[7] Bekermann, D.; Gasparotto, A.; Barreca, D.; Bovo, L.; Devi, A.; Fischer, R.A.; Lebedev, O.I.; Maccato, C.; Tondello, E.; van Tendeloo, G., *Cryst. Growth Des*., **2010**, *10*, 2011.

[8] (a) Szunerits, S.; Boukherroub, R., *Langmuir*, **2006**, *22*, 1660. (b) McIntire, T.M. Smalley, S.R. Newberg, J.T.; Lea, A.S.; Hemminger, J.C.; Finlayson-Pitts, B.J., *Langmuir*, **2006**, *22*, 5617. (c) Bertin, A.; Schlaad, H., *Chem. Mater.*, **2009**, *21*, 5698.

[9] (a) Treossi, E.; Liscio, A.; Feng, X.; Palermo, V.; Müllen, K.; Samorì, P., *Small*, **2009**, *5*, 112. (b) Iavicoli, P.; Linares, M.; del Pino, A.P.; Lazzaroni, R.; Amabilino, D.B., *Superlattices Microst.*, **2008**, *44*, 556.

[10] De Luca, G. Liscio, A. Maccagnani, P. Noldem, F. Palermo, V. Müllen, K. Samorì, P., *Adv. Func. Mater.*, **2007**, *17*, 3791.

[11] (a) Moulder, J.F.; Stickle, W.F.; Sobol, P.W.; Bomben, K.D., *Handbook of X-ray Photoelectron Spectroscopy*, Perkin-Elmer, Eden Prairie, MN, **1992**. (b) Dieckhoff, S. Schlett, V.; Possart, W.; Henneman, O.-D.; Günster, J.; Kempter, V., *Appl. Surf. Sci.*, **1996**, *103*, 221. (c) Barreca, D.; Gasparotto, A.; Maccato, C.; Tondello, E.; Rossetto, G.; *Thin Solid Films*, **2008**, *516*, 7393.

[12] Silipigni, L.; De Luca, G.; Quattrone, T.; Monsù Scolaro, L.; Salvato, G.; Grasso, V., *J. Phys. Condens. Matter*, **2006**, *18*, 5759.

[13] Gulino, A.; Mineo, P.; Fragalà, I., *Inorg. Chim. Acta*, **2008**, *361*, 3877.

[14] Liu, H.; Duclairoir, F. ; Fleury, B.; Dubois, L.; Chenavier, Y.; Marchon, J.-C., *Dalton Trans.*, **2009**, 3793.

[15] Klappenberger, F.; Weber-Bargioni, A.; Auwärter, W.; Marshall, M.; Scriffin, A.; Barth, J.V., *J. Phys. Chem.*, **2008**, *129*, 214802.

[16] (a) Watcharinyanon, S.; Puglia, C.; Göthelid, E.; Bäckvall, J.-E.; Moons, E.; Johansson, L.S.O., *Surf. Sci.*, **2009**, *603*, 1026. (b) Zanoni, R.; Aurora, A.; Cattaruzza, F.; Decker, F.; Fastiggi, P.; Menichetti, V.; Tagliatesta, P.; Capodilupo, A.-L.; Lembo, A., *Mater. Sci. Eng. C*, **2007**, *27*, 1351. (c) Khabashesku, V.N.; Zimmerman, J.L.; Margrave, J.L., *Chem. Mater.*, **2000**, 12, 3264.

[17] (a) Krasnikov, S.A.; Sergeeva, N.N.; Brzhezinskaya, M.M.; Preobrajenski, A.B.; Sergeeva, Y.N.; Vinogradov, N.A.; Cafolla, A.A.; Senge, M.O.; Vinogradov, A.S., *J. Phys. Condens. Matter.*, **2008**, *20*, 235207. (b) Sugiura, K. I. Iwasaki, K. Umishita, K. Hino, S. Ogata, H. Miyajima, S. Sakata, Y., *Chem. Lett.*, **1999**, 841.

[18] Zhang, Z.; Hu, R.; Liu, Z., *Langmuir*, **2000**, 16, 1158.

[19] Garg, K.; Singh, A.; Debnath, A.K.; Nayak, S.K.; Chattopadhyay, S.; Aswal, D.K.; Hayakawa, Y.; Gupta, S.K.; Yakhmi, J.V., *Chem. Phys. Lett.*, **2010**, *488*, 27.

[20] Biesaga, M.; Pyrinska, K.; Trojanoweiz, M., *Talanta*, **2000**, *51*, 209.

[21] Garcia, R.; Martinez, R.V.; Martinez, J., *Chem. Soc. Rev.*, **2006**, *35*, 29.

[22] Credi, A.; *Aust. J. Chem.*, **2006**, *59*, 157.

[23] Wang, Y.-B.; Lin, Z., *J. Am. Chem. Soc.*, **2003**, *125*, 6072.

[24] Bonifazi, D.; Accorsi, G.; Armaroli, N.; Song, F.; Palkar, A.; Echegoyen, L.; Scholl, M.; Seiler, P.; Jaun, B.; Diederich, F., *Helv. Chim. Acta*, **2005**, *88*, 1839.

[25] Boyd, P.D.W.; Reed, C.A., *Acc. Chem. Res.*, **2005**, *38*, 235.

[26] (a) Schneider, W.-D., *Phys. Status Solidi A*, **2001**, *187*, 125. (b) De Feyter, S.; Gesquiere, A.; Abdel-Mottaleb, M.M.; Grim, P.C.M.; De Schryver, F.C.; Meiners, C.; Sieffert, M.; Valiyaveettil, S.; Mullen, K., *Acc. Chem. Res.* **2000**, *33*, 520.

[27] (a) Otsuki, J.; Nagamine, E.; Kondo, T.; Iwasaki, K.; Asakawa, M.; Miyake, K., *J. Am. Chem. Soc.*, **2005**, *127*, 10 400. (b) Yoshimoto, S.; Yokoo, N.; Fukuda, T.; Kobayashi, N.; Itaya, K., *Chem. Commun.* **2006**, 500. (c) Yoshimoto, S.; Sugawara, S.; Itaya, K., *Electrochemistry* **2006**, *74*, 175.

[28] (a) Ma, H. ; Yang, L.-Y.O. ; Pan, N.; Yau, S.-L.; Jiang, J.; Itaya, K.; *Langmuir* **2006**, *22*, 2105. (b) Elemans, J. A. A. W. van Hameren, R.. Nolte, R. J. M Rowan, A. E., *Adv. Mater.*, **2006**, *18*, 1251.

[29] (a) Yoshimoto, S.; Higa, N.; Itaya, K., *J. Am. Chem. Soc.* **2004**, *126*, 8540. (b) Yoshimoto, S.; Honda, Y.; Murata, Y.; Murata, M.; Komatsu, K.; Ito, O.; Itaya, K., *J. Phys. Chem. B*, **2005**, *109*, 8547.

[30] Di Marino, M.; Sedona, F.; Sambi, M.; Carofiglio, T.; Lubian, E.; Casarin, M.; Tondello, E., *Langmuir* **2010**, *26*, 2466.

[31] David, T.; Gimzewski, J. K.; Purdie, D.; Reihl, B.; Schlitter, R., *Phys. Rev. B* **1994**, *50*, 5810–5813.

[32] More precisely, the thermal stability of the nanostructure self-assembled starting either from **TPP** or **$TPPNH_2$** is even lower: after annealing for several tens of minutes at 470 K, a new porous superstructure appears,[30] which is characterized by a 3:1 C_{60}:TPP ratio. If the temperature of the thermal treatment is increased to 520 K the c(4 x 4) C_{60} single component islands phase-separate, as reported in Figure 2.12.

[33] Zwaneveld, N. A. A.; Pawlak, R.; Abel, M.; Catalin, D.; Gigmes, D.; Bertin, D.; Porte, L., *J. Am. Chem. Soc.* **2008**, *130*, 6678.

[34] Bieri, M.; Treier, M.; Cai, J.; Aıt-Mansour, K.; Ruffieux, P.; Groning, O.; Groning, P.; Kastler, M.; Rieger, R.; Feng, X.; Mullen, K.; Fasel, R., *Chem. Commun.* **2009**, 6919.

[35] Backer, S. A.; Suez, I.; Fresco, Z. M.; Rolandi, M.; Fréchet, J. M. J., *Langmuir* **2007**, *23*, 2297.

[36] Chen, K.; Caldwell, W. B.; Mirkin, C. A., *J. Am. Chem. Soc.* **1993**, *115*, 1193.

[37] Zhang, X; Teplyakov, A. V., *Langmuir* **2008**, *24*, 810.

[38] Giacalone, F.; Martin, N., *Chem. Rev.* **2006**, *106*, 5136.

[39] Samal, S.; Choi, B.-J.; Geckeler, K. E., *Chem. Commun.* **2000**, 1373.

[40] (a) Gottfried, J. M.; Flechtner, K.; Kretschmann, A.; Lukasczyk, T.; Steinruck, H.-P., *J. Am. Chem. Soc.* **2006**, *128*, 5644. (b) Flechtner, K.; Kretschmann, A.; Bradshaw, L. R.; Walz, M.-M.; Steinru¨ ck, H.-P.; Gottfried, J. M., *J. Phys. Chem. C* **2007**, *111*, 5821.

[41] (a) Shubina, T. E.; Marbach, H.; Flechtner, K.; Kretschmann, A.; Jux, N.; Buchner, F.; Steinruck, H.-P.; Clark, T.; Gottfried, J. M., *J. Am. Chem. Soc.* **2007**, *129*, 9476. (b) Buchner, F.; Flechtner, K.; Bai, Y.; Zillner, E.; Kellner, I.; Steinruck, H.-P.; Marbach, H.; Gottfried, J. M., *J. Phys. Chem. C* **2008**, *112*, 15458.

[42] Magnano, E.; Vandré, S.; Cepek, C.; Goldoni, A.; Laine, A. D.; Currò, G. M.; Santaniello, A.; Sancrotti, M., *Surf. Sci.* **1997**, *377-379*, 1066.

[43] Goldoni, A.; Cepek, C.; Magnano, E.; Laine, A. D.; Vandré, S., *Phys. Rev. B* **1998**, *58*, 2228.

EXPERIMENTAL SECTION

3.1 Materials and Reagents

[60]fullerene was purchased from Bucky USA (99.5%). Tetraphenyl porphyrin **TPP** was purchased from EGA-CHEMIE, Germany. Other reagents and solvents (Sigma-Aldrich, Fluka and Carlo Erba Reagenti) were of the highest grade available and were used without further purification. Solvents employed in the spectroscopic studies are of spectroscopic grade and used as received. Silica gel MN 60 (70–230 Mesh) by Macherey-Nagel and neutral alumina (Brockmann Grade III) were used for column chromatography. Analytical thin layer chromatography (TLC) was performed using a Polygram SilG/UV254 (TLC plates).

3.2 Instruments

^{13}C-NMR spectra for characterization of compounds were recorded with a spectrometer Bruker Avance-300 MHz, using $CDCl_3$ as solvent. Chemical shifts were referenced to the residual proton resonance in $CDCl_3$ (δ 7.26 ppm). Routine UV-vis spectra were recorded in CH_2Cl_2 on a Varian Cary 50 Spectrophotometer. Field Emission-Scanning Electron Microscopy (FE-SEM) measurements were carried out by means of a Field Emission Zeiss SUPRA 40VP instrument. Plane-view micrographs were acquired using an accelerating voltage of 10 kV. Substrate coverage was calculated by means of ImageJ software package. Silicon (100) wafers were purchased from MEMC®, Merano, Italy. AFM images were obtained using a NT–MDT SPM Solver P47H–PRO instrument operating in tapping mode and in air. XPS spectra were recorded on a Perkin Elmer F 5600ci spectrometer using a non monochromatized Al Kα excitation source (1486.6 eV). The Binding Energy (BE) shifts were corrected assigning to the C1s line of adventitious carbon a value of 284.8 eV. The estimated standard deviation for BEs was ± 0.2 eV. The atomic compositions were evaluated using sensitivity factors provided by F V5.4A software. STM measurements were performed with an Omicron scanning tunneling microscope (VTSTM) operating in ultra high vacuum (UHV) at a base pressure of 2 x10^{-10} mbar, at room temperature, in constant current mode, using a Pt-Ir tip. HPLC analysis of fullerene-amino porphyrin adduct was carried out on a Shimadzu

LC-10AD VP instrument, equipped with a Jasco UV-275 UV detector at 340 nm, using a Cosmosil Buckyprep column (Nacalai Tesque, 4.6 × 250 mm). Differential scanning

calorimetry and thermogravimetric analysis were performed with TA instruments SDT 2960. The heating ramp is from room temperature to 1500 °C in the rate range of 0.1-100 °C/min, in air or nitrogen atmosphere. Both the crucibles, one for reference and one for the sample, are made of ceramic.

3.3 Methods

3.3.1 Sample Preparation for SEM and Gas Sensing Experiments

Substrate cleaning. Si(100) wafers were cleaned, without removing the native SiO_2 layer[1] by the following stepwise procedure: i) sonication in methanol at room temperature (15 min); ii) iterative (ten-fold) immersion in water/sulphonic detergent, water, acetone, isopropanol; iii) drying under nitrogen flow. The substrates were subsequently stored in a desiccator over molecular sieves. After this procedure, the Si(100) substrates were covered by an amorphous silica layer *ca.* 2-3 nm thick characterized by a Root Mean Square (RMS) roughness as low as 0.2 nm and a carbon surface contamination limited to a few at.%, as evidenced by Atomic Force Microscopy (AFM) and X-ray Photoelectron Spectroscopy (XPS), respectively.

Substrate activation. Substrates cleaned according to the above procedure were immersed in a *piranha* solution (70% H_2SO_4 / 30% H_2O_2) at 50 °C for 1 h followed by a careful rinsing with water (Milli-Q pure) and isopropanol and stored into a desiccator over molecular sieves overnight. Besides removing surface organic contaminants, such a procedure has been reported to efficiently increase the content of surface –OH groups.[2,3,4]

Substrate coating. *Drop-casting procedure*: the substrates were washed with the solvent used to prepare the porphyrin dimer solution (*e.g.*, THF or $CHCl_3$) and dried under nitrogen flow. Then, a drop of 0.1 mM solution of **P(H$_2$)P(H$_2$)** or **P(Zn)P(Zn)** was deposited on the substrate and the sample was left to dry in a desiccator overnight. *Soaking procedure:* the substrates were washed with the solvent used to prepare the porphyrin dimer solution (*e.g.*, THF or $CHCl_3$) and dried under nitrogen flow. Then, the substrates were immersed at room temperature into a 0.1 mM solution of **P(H$_2$)P(H$_2$)** or **P(Zn)P(Zn)** for 8 h. After this time, the coated silicon wafers were removed from the solution and put into a desiccator overnight.

Gas sensing tests. Platinum contacts (500 nm thick) were sputtered on the sample surface at a distance of 3 mm between each other. Electrical characterization was carried out by the voltamperometric technique at a constant bias of 1 V, and a picoammeter measured the current flowing between the two contacts. The flow-through technique was used to determine the gas sensing properties of the molecular deposit. A constant flow of synthetic air (0.3 L/min), mixed with the desired amount of gaseous species (*e.g.*, water, ammonia, diethyl amine, ethanol and acetone) flowed through a stabilized sealed chamber maintained at 20 °C, atmospheric pressure and controlled humidity. All sensing tests were performed at room temperature.

3.3.2 Sample Preparation for STM Measurements

Sample Preparation in UHV. The Ag(110) crystal was cleaned by repeated cycles of 1 keV Ar^+ sputtering and annealing at 820 K until a clean surface with sufficiently large terraces was confirmed by STM imaging. The three different **TPP** molecules were deposited from a PBN crucible held at temperatures between 500 and 590 K, whereas C_{60} (99% purity) was sublimed at temperatures between 850 and 890 K from a tungsten crucible. The Ag specimen was kept at room temperature during sublimations. Both crucibles were outgassed for a long time to avoid impurities during the depositions onto the substrate.

Scanning Tunneling Microscopy (STM). The experiments were performed with an Omicron scanning tunneling microscope (VTSTM) operating in UHV at a base pressure of 2×10^{-10} mbar. The STM measurements were carried out at RT in constant current mode, using a Pt-Ir tip. The sample bias voltage (*V*) and the tunneling current (*I*) are indicated for all STM images. STM images were analyzed with the WSxM software.[5]

X-ray Photoelectron Spectroscopy (XPS). Measurements were performed *in situ* at room temperature by means of a Scienta M-780 Al Kα (1486.6 eV) monochromatic X-ray source and a Scienta SES-100 photoelectron analyzer fitted to the STM preparation chamber. The overall instrumental resolution measured at the Fermi edge of the clean Ag sample was 0.3 eV. The binding energies are referenced to the Fermi edge (BE = 0).

3.4 Synthesis of Compounds

3.4.1 Synthesis of 5-(4-aminophenyl)-10,15,20-triphenyl porphyrin, $TPPNH_2$

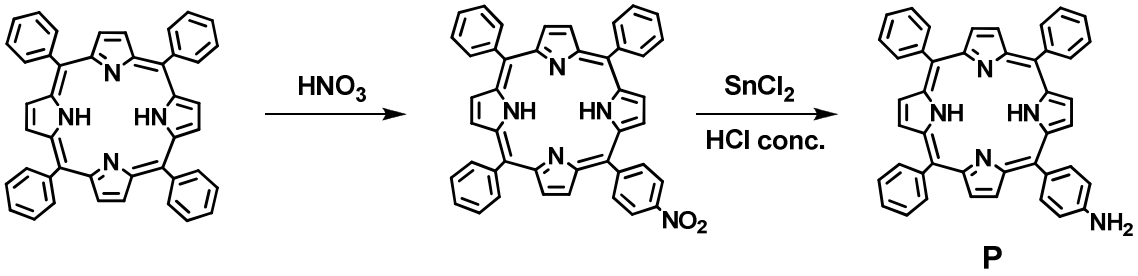

Following a general procedure,[6] tetraphenyl porphyrin (4 g, 6.51 mmol) was dissolved in 600 ml of pentene-stabilized chloroform under nitrogen. Red fuming nitric acid (6.8 g, 108 mmol) was added to the stirred solution of porphyrin at 0-5 °C through a pressure-equalizing dropping funnel over a 2 h period. The reaction was monitored at intervals by TLC to insure total conversion of starting material (R_f = 0.88) to product (R_f = 0.78) by using chloroform/hexane (3:1) on silica plates. The dark green solution was extracted with 5 x 300 mL portions of water, dried over magnesium sulphate and sodium carbonate, filtered and concentrated under reduce pressure to give 4.5 g of nitro mixture. The reduction of nitro compound was conducted according to a modification of Hasegawa's procedure.[7] Raw material (2.5 g, 3.79 mmol) was dissolved in 80 mL of concentrated hydrochloric acid under nitrogen. Tin(II) chloride dehydrate (2.6 g, 11.5 mmol) was added to the solution and the reaction was heated to 65 °C for 1 h. The porphyrin solution was cooled and added to 300 mL of cold water and was adjusted to pH 8 with concentrated ammonium hydroxide. The aqueous phase was extracted with 6 x 300 mL portions of chloroform, which were combined and dried over sodium sulphate. The organic phase was concentrated and this solution was separated on silica column with methylene chloride as an eluent. The product was obtained in 70% yield. ^{1}H-NMR ($CDCl_3$, 250 MHz) δ: 8.95 (d, 2H, β-pyrrole), 8.84 (d, 2H, β-pyrrole), 8.22 (m, 6H, *ortho* triphenyl), 8.00 (d, 2H, 4-aminophenyl), 7.76 (m, 9H, *meta\para* triphenyl), 7.06 (d, 2H, 4-aminophenyl), 4.02 (s, 2H, amino), -2.75 (s, 4H, pyrrole NH). ESI-MS $C_{44}H_{31}N_5$ (CH_3CN + 1% HCOOH as eluent) m/z: obsd 630.7 $[MH]^+$ (calcd 630.75), obsd 315.9 $[MH_2]^{2+}$ (calcd 315.88). UV-vis (CH_2Cl_2, nm): 419 (Soret band, ε = 337'000 $M^{-1}cm^{-1}$), 516 (ε = 9'300 $M^{-1}cm^{-1}$), 553 (ε = 5'300 $M^{-1}cm^{-1}$), 592 (ε = 3'000 $M^{-1}cm^{-1}$), 648 (ε = 2'800 $M^{-1}cm^{-1}$).

3.4.2 Synthesis of 5,15-bis(4-aminophenyl)-10,20-diphenylporphyrin, *trans*-TPP(NH_2)$_2$

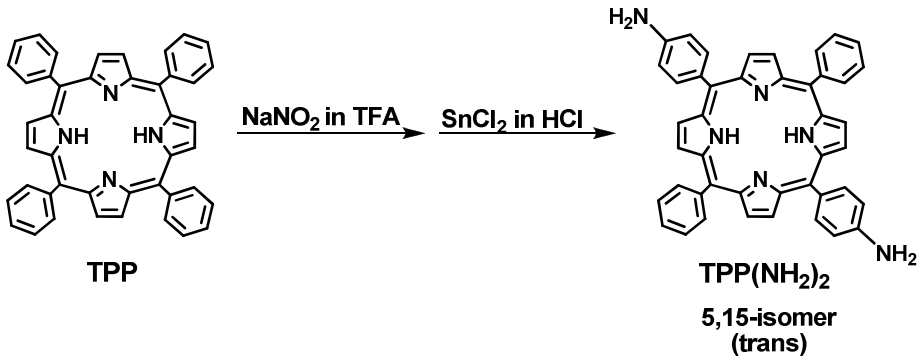

Following a literature procedure,[8] to a solution of **TPP** (200 mg, 0.326 mmol) in TFA (10 mL) was added sodium nitrite (183 mg, 2.65 mmol). After 90 seconds stirring at room temperature, the reaction was poured into 100 mL of water and extracted with DCM (6x25 mL). The organic layers were washed once with saturated aqueous $NaHCO_3$ and once with water before being dried over anhydrous Na_2SO_4. The organic solution was filtered and the solvent was removed under vacuum. The residue was purified on a plug of silica gel, eluting with dichloromethane. After evaporation of the solvent, the residue was dissolved in 50 mL of concentrated hydrochloric acid and, while stirring, tin(II) chloride (0.8 g, 3.55 mmol) was carefully added. The final mixture was heated to 65 °C for 1 h under nitrogen before being poured into cold water (100 mL). The aqueous solution was neutralized with ammonium hydroxide until pH 8. The aqueous solution was extracted with dichloromethane until colourless. The organic layer was then concentrated under vacuum and the residue was purified on a plug of alumina, using CH_2Cl_2/petroleum ether 8:2 v/v for elution. The final residue was recrystallized from methanol, yielding 20 mg (30%) of the 5,15-isomer. ^{1}H-NMR (CD_2Cl_2, 250 MHz) δ: 8.84 (m, 4H, β-pyrrole), 8.94-8.82 (m, 8H, β-pyrrole), 8.60-8.20 (m, 8H, phenyl aromatic protons), 7.77-7.74 (m, 8H, phenyl amino), 4.02 (br, s, 4H, -NH_2), -2.74 (s, 2H, inner protons pyrrole porphyrin). ESI-MS $C_{44}H_{32}N_6$ (CH_3CN + 1% HCOOH as eluent) m/z: obsd 645.8 $[MH]^+$ (calcd 645.77), obsd 323.7 $[MH_2]^{2+}$ (calcd 323.38). UV-vis ($CHCl_3$, nm): 419 (ε = 278'000), 514 (ε = 13'500), 549 (ε = 9'570), 595 (ε = 4'600), 650 (ε = 4'300). Elem. Anal. calcd for $C_{44}H_{32}N_6 \cdot 1.5\ H_2O$: C, 78.66; H, 5.25; N, 12.52. Found: C, 78.25; H, 5.00; N, 12.22.

3.4.3 Synthesis of C_{60}-TPPNH$_2$ Adduct

A solid mixture of 5-(4-aminophenyl)-10,15,20-triphenyl porphyrin, **TPPNH$_2$**, and C_{60} in 1:1 molar ratio was heated at 85 °C. After 1 h, TLC analysis (silica gel, eluent petroleum ether/ethyl acetate 3:2 v/v) confirmed the complete disappearance of **TPPNH$_2$** (R_f = 0.56) and the formation of a new product (R_f = 0.79) containing both the features of porphyrin and C_{60}. This confirmed the formation of poliadducts between fullerene and porphyrin after thermal treatment, as shown in ^{13}C-NMR, UV-visible, XPS spectra and HPLC chromatogram. ^{13}C-NMR (CS_2/$CDCl_3$ 4:1 v/v, 75.5 MHz) δ: 192.97, 148.38, 143.50, 139.66, 138.98, 137.89, 136.01, 132.55, 130.72, 130.65, 128.41, 120.36, 117.98, 117.57, 113.82, 22.35. UV-vis (cyclohexane, nm): 329, 419, 515, 547, 597, 651.

REFERENCES

[1] Bekermann, D.; Gasparotto, A.; Barreca, D.; Bovo, L.; Devi, A.; Fischer, R.A.; Lebedev, O. I.; Maccato, C.; Tondello, E.; Van Tendeloo, G., *Cryst. Growth Des.*, **2010**, *10*, 2011.

[2] Szunerits, S.; Boukherroub, R., *Langmuir*, **2006**, *22*, 1660.

[3] McIntire, T. M.; Smalley, S.R.; Newberg, J.T.; Lea, A.S.; Hemminger, J.C.; Finlayson-Pitts, B.J., *Langmuir*, **2006**, *22*, 5617.

[4] Bertin, A.; Schlaad, H., *Chem. Mater.*, **2009**, *21*, 5698.

[5] Horcas, I.; Fernandez, R.; Gomez-Rodriguez, J. M.; Colchero, J.; Gomez-Herrero, J.; Baro, A. M., *Rev. Sci. Instrum.*, **2007**, *78*, 13705.

[6] Kruper, W. J.; Chamberlin, T. A.; Kochanny, M.; Lang, K. *J. Org. Chem*. **1989**, *54*, 2753.

[7] (a)Hasegawa, E., et al, *Eur.Poly.J.* **1978**, *14*,123. b)Tsuchida, E., *J.Macromol.Sci.***1979**, *(4)*, 545.

[8] Luguya, R.; Jaquinod, L.; Fronczek, F.R.;Graca, M.; Vicente, H.; Smith, K.M., *Tetrahedron*, **2004**, *60*, 2757.